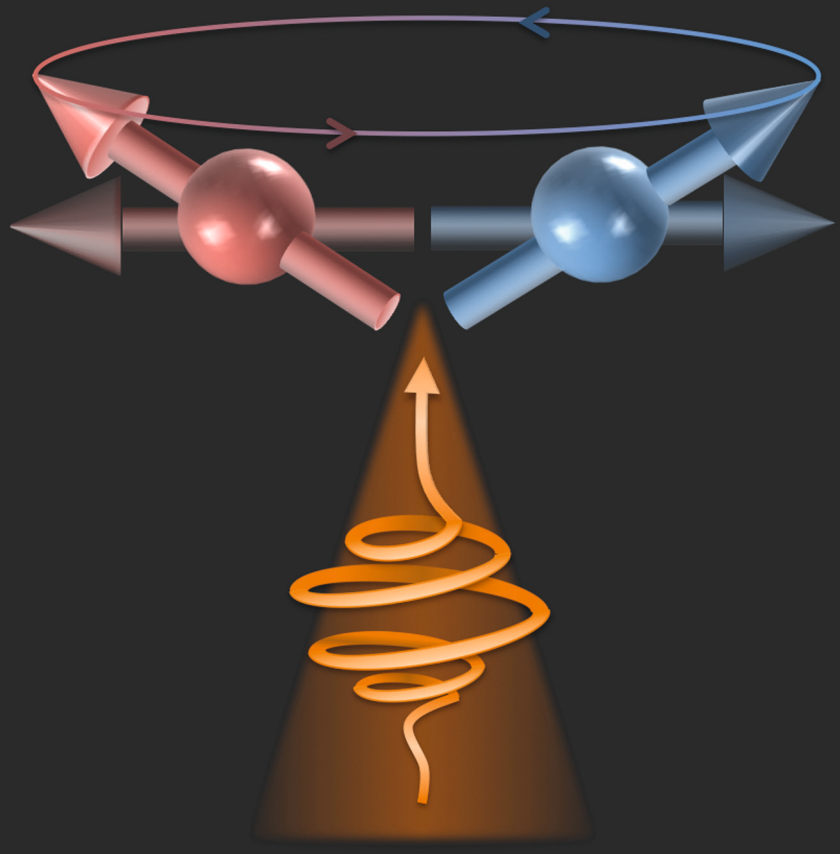

Microscopic description of the inverse Faraday effect at subpicosecond time scales

Darya Popova

Member of the Helmholtz Association

JÜLICH
FORSCHUNGSZENTRUM

Schriften des Forschungszentrums Jülich
Reihe Schlüsseltechnologien / Key Technologies Band / Volume 83

Forschungszentrum Jülich GmbH
Peter Grünberg Institute (PGI)
Quantum Theory of Materials (PGI-1/IAS-1)

Microscopic description of the inverse Faraday effect at subpicosecond time scales

Darya Popova

Schriften des Forschungszentrums Jülich
Reihe Schlüsseltechnologien / Key Technologies Band / Volume 83

ISSN 1866-1807 ISBN 978-3-89336-962-1

Bibliographic information published by the Deutsche Nationalbibliothek.
The Deutsche Nationalbibliothek lists this publication in the Deutsche Nationalbibliografie; detailed bibliographic data are available in the Internet at http://dnb.d-nb.de.

Publisher and Distributor: Forschungszentrum Jülich GmbH
Zentralbibliothek
52425 Jülich
Tel: +49 2461 61-5368
Fax: +49 2461 61-6103
Email: zb-publikation@fz-juelich.de
www.fz-juelich.de/zb

Cover Design: Grafische Medien, Forschungszentrum Jülich GmbH

Printer: Grafische Medien, Forschungszentrum Jülich GmbH

Schriften des Forschungszentrums Jülich
Reihe Schlüsseltechnologien / Key Technologies, Band / Volume 83

D 82 (Diss.,RWTH Aachen University, 2013)

ISSN 1866-1807
ISBN 978-3-89336-962-1

The complete volume is freely available on the Internet on the Jülicher Open Access Server (JUWEL) at www.fz-juelich.de/zb/juwel

Abstract

This Thesis is devoted to the microscopic study of the inverse Faraday effect at subpicosecond time scales. The inverse Faraday effect (IFE) is a magneto-optical process, which leads to the generation of magnetization by circular polarized light. Ultrafast manipulation of spin dynamics is of highly importance for the development of novel concepts of information processing and data storage. Therefore, the IFE, which provides the possibility to non-thermally and coherently induce and control magnetization dynamics at femtosecond time scales, gained much significance in recent years. However, despite its relevance for technological applications, the origin of this effect is still poorly understood.

A theoretical description for the IFE induced by stationary laser light was developed in 1960'ies considering the experimental conditions available at that time. However, the laser technology moved forward dramatically in the last fifty years. Magneto-optical experiments nowadays are performed by laser pulses of several tens of femtoseconds duration, which is five orders of magnitude faster than that half century ago. This leads to principally new physics of laser induced magnetic processes, which requires novel theoretical approaches for their interpretation.

It is shown here in detail that the mechanisms of magnetization changes due to the IFE triggered by ultrashort laser pulses is quite different from that by stationary excitation. A new theoretical approach based on the solution of the time-dependent Schrödinger equation is provided in this Thesis. It allows to describe magnetization time evolution triggered by circularly-polarized laser pulses at subpicosecond time scales. It is shown that the ultrafast IFE consists of two processes: the stimulated Raman scattering, which leads to the change of a system's magnetic state, and the excitation of magnetization precession due to the deviation of the magnetic vector from its ground state.

The study of the electron structure, which defines the selection rules for light-induced transitions, is necessary for the investigation of the magneto-optical effects in crystals. The microscopic considerations are especially rel-

evant for the investigation of ultrafast magnetic processes induced by laser pulses, the spectral width of which is of the same order as the electron interactions energies. A detailed study of the role of various electron interactions, especially that of the spin-orbit coupling, is performed here in detail. The dependence of the value of the IFE on ultrafast laser pulse properties is studied.

In view of technological applications, it is not only important to know the mechanism of the magnetization dynamics excitation, but also to be able to manipulate the induced dynamics. Therefore, it is useful to know how the optical process affects total angular momentum components individually. The Heisenberg picture for the ultrafast IFE is derived from the Schrödinger picture for this purpose. The operator describing the perturbation of a system by an electric field will be substituted by a time-dependent operator expressed in terms of momentum operators. The operator allows to separate the action of light on a magnetic system from that of other possible magnetic interactions. The equations of motion of magnetic components during the excitation are derived from this operator.

This approach is first applied to investigate spin dynamics driven by a common action of the IFE and an external magnetic field. It is demonstrated that the spin dynamics during the excitation is considerably affected by the magnetic field even if the period of the induced Larmor oscillation is several tens times higher than the laser pulse duration. Finally, the laser induced dynamics of an easy plane antiferromagnet is described. The equations of motion, which determine the time evolution of the magnetic vectors of the magnetic sub-lattices, are derived. It is shown the ultrafast IFE induces a net magnetic moment in this system.

Zusammenfassung

Diese Arbeit ist der mikroskopischen Untersuchung des inversen Faraday Effekts (IFE) auf subpikosekunden Zeitskalen gewidmet. Der IFE ist ein magneto-optischer Prozess, bei dem zirkular polarisiertes Licht Magnetisierung in Materialien erzeugt. Ultraschnelle Manipulation der Spindynamik hat große Bedeutung für die Entwicklung neuartiger Konzepte der Informationsverarbeitung und Datenspeicherung. Der IFE bietet eine Möglichkeit für nichtthermische, kohärente Erzeugung und Kontrolle von Magnetisierung in Femtosekundenintervallen und hat in den letzten Jahren viel an Bedeutung gewonnen. Trotz seiner Relevanz für technologische Anwendungen, ist der Ursprung dieses Effektes noch schlecht verstanden.

Eine theoretische Beschreibung des IFE, induziert durch stationäres Laserlicht, wurde in sechziger Jahren entwickelt, wobei die zu diesem Zeitpunkt verfügbaren experimentellen Bedingungen berücksichtigt wurden. Doch die Lasertechnologie sich in den letzten fünfzig Jahren weiter entwickelt. Magnetooptische Experimente werden heutzutage mit Laserimpulsen von wenigen Zehntel Femtosekunden Dauer, fünf Größenordnungen kürzer als die vor ein halben Jahrhundert, durchgeführt. Das führt zu grundsätzlich neuer Physik und neue theoretische Ansätze zur Interpretation laser-induzierter magnetischen Prozesse sind erforderlich.

Es wird hier im Detail gezeigt, dass die Mechanismen der Magnetisierungsveränderungen durch den IFE, ausgelöst von ultrakurzen Laserimpulsen, ganz anderes sind als bei stationärer Anregung. Ein neuer Ansatz, basierend auf Lösung der zeitabhängigen Schrödinger Gleichung, wird in dieser Arbeit entwickelt. Er erlaubt die Zeitentwicklung der Magnetisierung zu beschreiben, die durch zirkular-polarisierte Laserimpulse unter einer Pikosekunde Dauer verursacht wird. Es wird gezeigt, dass der ultraschnelle IFE aus zwei Prozessen besteht: die stimulierte Raman-Streuung, die zu einer Veränderung eines magnetischen Systemzustandes führt, und die Anregung der Magnetisierungspräzession aufgrund der Abweichung des magnetischen Vektors von seinem Grundzustand.

Die Kenntniss der Elektronenstruktur, die die Auswahlregeln für lichtinduzierte Übergänge bestimmt, ist notwendig für die Untersuchung magnetooptischer Effekte in Kristallen. Diese mikroskopischen Überlegungen sind besonderes relevant für die Untersuchung von ultraschnellen magnetischen Prozessen induziert durch Laserimpulse, deren spektrale Breite von der gleichen Größenordnung wie Elektronenwechselwirkungsenergie ist. Eine detaillierte Studie der Rolle der verschiedenen Elektronenwechselwirkungen, vor allem, der Spinbahnwechselwirkung, wird hier im Detail durchgeführt. Die Abhängigkeit der Stärke des IFE von den Eigenschaften der Laserimpulse wird untersucht.

Im Hinblick auf technische Anwendungen reicht es nicht den Mechanismus der Anregung der Magnetisierungsdynamik zu kennen, sondern man muss in der Lage sein die induzierte Dynamik zu manipulieren. Daher ist es notwendig zu wissen, wie der optische Prozess unmittelbar auf die Drehimpulskomponenten wirkt. Hierzu wird das Heisenbergbild zur Beschreibung des ultraschnellen IFE aus dem Schrödinger Bild hergeleitet. Die Störung eines Systems durch ein elektrisches Lichtfeld kann dann durch eine zeitabhängige Kombination von Drehimpulsoperatoren ausgedrückt werden. Mit dieser Operatorbeschreibung kann man die Wirkung von Licht auf ein magnetisches System von anderen magnetischen Wechselwirkungen trennen. Die Bewegungsgleichungen von magnetischen Komponenten während der Anregung werden aus dieser Operatorbeschreibung abgeleitet.

Mit diesen Bewegungsgleichungen wird zunächst Spindynamik erzeugt durch das Zusammenspiel von IFE und externem Magnetfeld, untersucht. Es wird gezeigt, dass die Spindynamik während der Anregung durch das Magnetfeld wesentlich beeinflusst wird, auch wenn die Schwingungsperiode der induzierten Larmorpräzession um ein zehnfaches größer als die Laserpulsdauer ist. Schließlich wird die laserinduzierte Dynamik eines Antiferromagneten mit leichter Ebene beschrieben. Die Bewegungsgleichungen, die die zeitliche Entwicklung der magnetischen Vektoren der magnetischen Teilgitter bestimmen, werden abgeleitet. Es wird gezeigt, dass der ultraschnelle IFE ein magnetisches Moment in diesem System erzeugt.

Contents

Conventions

The following conventions are used throughout this Thesis.

Notations

Expectation values of operators are written without brackets. For example, if $\hat{A}$ is an operator, then

$$A = \langle \hat{A} \rangle$$

Partial derivatives with respect to time are expressed by a prime. For example, if $B(t)$ is a time-dependent function, then

$$B' = \frac{\partial B}{\partial t}$$

Units

All equations in the thesis are written in Hartree atomic units [1, 2]. Table 1 contains the fundamental quantities, which are set to one in atomic units. Table 2 contains derived quantities, which are equal to one in atomic units, and their values in SI units.

Quantity	Symbol	Value in SI units
Electron mass	m_e	$9.10938291(40) \times 10^{-31}$ kg
Elementary charge	e	$1.602176565(35) \times 10^{-19}$ C
Reduced Planck's constant	$\hbar$	$1.054571726(47) \times 10^{-34}$ J s
Coulomb force constant	$1/(4\pi\epsilon_0)$	$8.9875517873681 \times 10^{9}$ N m^2 C^{-2}

Table 1: Fundamental constants of atomic units and their values in SI units.

Quantity	Definition	Value in SI units
Length	Bohr radius $a_0 = \hbar^2/(m_e c\alpha)$	$5.2917720859(36)\times10^{-11}$ m
Energy	Hartree energy $E_h = \alpha^2 m_e c^2$	$4.35974417(75)\times10^{-18}$ J
Time	$\hbar/E_h$	$2.418884326505(16)\times10^{-17}$ s
Velocity	$a_0 E_h/\hbar = \alpha c$	$2.1876912633(73)\times10^{6}$ m/s
Force	E_h/a_0	$8.2387225(14)\times10^{-8}$ N
Temperature	E_h/k_B	$3.1577464(55)\times10^{5}$ K
Pressure	E_h/a_0^3	$2.9421912(19)\times10^{13}$ Pa
Electric field	$E_h/(ea_0)$	$5.14220652(11)\times10^{11}$ V/m
Magnetic induction	$\hbar/(ea_0^2)$	$2.35051742(20)\times10^{5}$ T

Table 2: Derived atomic units and their values in SI units. α is the fine structure constant: $\alpha = e^2/(4\pi\epsilon_0\hbar c) \approx 1/137$.

Chapter 1

Introduction

1.1 Ultrafast optical manipulation of magnetic order

Ultrafast optical control of magnetization dynamics is a rapidly developing field of research [3, 4]. This topic attracts much attention due to the potential usefulness for technological applications in spintronics, data storage and manipulation, and quantum information processing. At the same time, it puts fundamental questions about spin and orbital dynamics on time scales τ corresponding to the energy of electron interactions ($E_{\text{el.int.}} \sim 1/\tau$).

The subpicosecond optical manipulation techniques are highly promising for the dramatical decrease of the magnetic recording speed. Since several years it was believed that the magnetization reversal via the magnetic field-induced precessional motion was the fastest method to record a bit. However, it was shown that the speed of the precessional magnetic switching is limited to several picoseconds [5]. This barrier is overcome by the laser driven magnetization reversal, which can take place on subpicosecond time scales [6].

One of the pioneering experiments, which demonstrated that laser pulses can excite ultrafast magnetization dynamics, was done by Beaurepaire *et al.* in 1996, when they showed that laser pulses can induce demagnetization in a ferromagnetic nickel film on femtosecond time scales [7]. These results raised much interest and led to further investigations of laser driven subpicosecond magnetization dynamics, which developed gradually into a new field of research [4]. It was shown that the excitation by ultrafast laser pulses can lead not only to demagnetization, but to other effects on magnetization, such as generation of coherent magnetic precession [8–10], spin reorientation [11] and modification of magnetic structure [12].

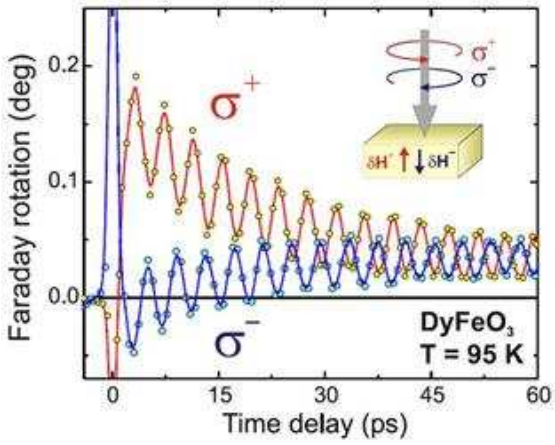

Figure 1.1: The figure is taken from Ref. [9]. Magnetic precessions in $DyFeO_3$ measured by the Faraday effect. σ_+ and σ_- refer to right-handed and left-handed circularly polarized laser pulses, respectively. The inset represents the effective fields $\delta\mathbf{H}^+$ and $\delta\mathbf{H}^-$ induced by σ_+ and σ_- pulses.

Although much experimental [13–18] and theoretical [19–23] work has been done towards understanding of the processes responsible for these effects, they are still unclear and remain a matter of hard debates [24–28]. The problem to reveal the underlaying mechanisms of laser driven magnetization dynamics is that it is hard to distinguish different processes triggered by a laser pulse and determine the contribution of various electron spin interactions to the spin dynamics. There are also difficulties associated with interpretations of the measurements performed by techniques based on magneto-optical response, since they are designed to probe a medium being in equilibrium [29–31]. Thus, effects due to subpicosecond laser excitations of magnetic states of a medium open new insight on the spin dynamics and put many fundamental and intriguing questions. Together with potential technological usefulness, this makes the study of the topic very attractive.

This thesis is devoted to the theoretical investigation of *the inverse Faraday effect* (IFE), one of the optically driven magnetization processes, which can take place on femtosecond time scales. According to its classical definition, the IFE is the generation of magnetization in a non-absorbing medium by circularly polarized laser pulses [32,33]. It will be shown below that this effect has a central role for the induced magnetization dynamics by ultrafast lasers.

In 2005, it was demonstrated by Kimel *et al.* that femtosecond laser pulses can induce and coherently control the spin dynamics in magnetic materials *non-thermally* [9]. Circularly polarized laser pulses, called pump pulses, of 200 fs duration irradiated the rare-earth orthoferrite $DyFeO_3$. The Fe spins in this compound are coupled antiferromagnetically and are slightly canted due to the Dzialoshinsky-Moriya interaction, thus $DyFeO_3$ is a weak ferromagnet. Laser pulses, called probe pulses, were used for the measurement of the magnetization of the samples via the (direct) Faraday effect, which is the rotation of the polarization plane of light transmitted through a magnetic medium [33]. It is called Faraday rotation and is proportional to magnetization of the medium.

The authors showed that the pump pulses excite the oscillations of the Fe spins around their equilibrium direction (see Fig. 1.1). The phase of the oscillations depends on the helicity of the laser pulse and was opposite for laser pulses of opposite helicities. These phenomena were attributed to the inverse Faraday effect (IFE).

This work introduced a new relevant approach to realize the ultrafast all-optical control of magnetization. The method to non-thermally manipulate magnetization dynamics is of high importance for possible applications in magnetic recording. This approach helps to avoid the problems caused by material heating: the required cooling time limits the repetition frequency and heat diffusion puts limits on the recording density [34]. At the same time, this process can be used in combination with other laser-induced mechanisms to observe versatile effects on magnetization dynamics. Thus, the inverse Faraday effect known since the 1960's [32, 35, 36] started to attract much attention in recent years.

Later on, the IFE triggered by ultrashort circularly polarized laser pulses was shown in other rare-earth orthoferrites. It caused the excitation of antiferromagnetic resonances in $TmFeO_3$ [37], quasiferromagnetic resonance in $ErFeO_3$ [38], and was used to observe the novel mechanism of "inertia-driven spin switching" (see Ref. [39] for details) in $HoFeO_3$. All these compounds are weak ferromagnets as is typical for rare-earth orthoferrites. However, the demonstrations of the ultrafast IFE are not limited to the orthoferrites. It was shown that the process caused the excitation of coherent magnons in easy-plane weak ferromagnet $FeBO_3$ [10], the precession of magnetization of rare-earth paramagnet $Dy_3Al_5O_{12}$ in an external magnetic field [40], and magnetization changes in paramagnetic $NaTb(WO_4)_2$ crystals [41] and in a ionic liquid 1-butyl-3-methylimidazolium tetrachloroferrate, which is paramagnetic [42].

The inverse Faraday effect in an compensated antiferromagnet was observed by Satoh *et al* for the first time. Circularly polarized laser pulses of 120 fs

duration excited out-of-plane and in-plane modes of antiferromagnetic spin oscillations in NiO with the frequency of 1.07 THz and 140 GHz (the period of 900 fs and 7 ps) correspondingly [43, 44]. This finding is quite interesting, because there is no net magnetization in this material as opposed to canted antiferromagnets, which were used in the experiments demonstrating the IFE before. In addition, it is relevant for the study of the terahertz radiation from NiO, which attracts much attention due to the simple structure and room temperature antiferromagnetism of this material [45–49].

Reid *et al.* demonstrated that the ultrafast IFE led to an unusual magnetic behavior in lutetium iron garnet $[Lu_{1.69}Y_{0.65}Bi_{0.66}](Fe_{3.85}Ga_{1.15})O_{12}$ [50]. There are two kind of sites in this compound, where magnetic Fe ions are situated: a tetrahedral-coordinated site and an octahedral-coordinated site. The sites of different symmetry are antiferromagnetically coupled, thereby the ones of the same symmetry are ferromagnetically coupled forming two ferromagnetic sublattices. The ratio of tetrahedral sites to octahedral sites is 3 to 2, therefore the compound is ferrimagnetically ordered. The magneto-optical properties of the sites of different symmetry are inequivalent [51]. The authors showed that this diversity led to a distinct response of the sublattices to the excitation by circularly polarized laser pulses. Thus, the IFE acted locally on each sublattice, which caused the canting between them. The precession of the canted Fe moments was attributed to the excitation of a magnetic-dipole forbidden exchange resonance[1], which had not been observed previously. Its frequency provided the value of the exchange interaction between the magnetic sublattices. This study demonstrated that the action of the IFE goes beyond its classical interpretation as an effective magnetic field produced by circularly polarized laser light, since it influences sublattices differently in contrast to a magnetic field.

The joint action of the IFE with other ultrafast laser-induced magneto-optical effects can also lead to striking results on magnetization dynamics. It was shown in Refs. [52, 53] that the combination of the ultrafast IFE and the non-thermal effect of optically induced magnetic anisotropy [11] could be used to control magnetization in magnetic garnet films. Femtosecond laser pulses were used to coherently prepare a new long-lived magnetic state in $Lu_{3-x-y}Y_xBi_yFe_{5-z}Ga_zO_{12}$ ferrimagnetic garnet films and to rotate magnetization in it during 100 femtoseconds via the IFE.

Makino *et al.* observed magnetization precession in ferromagnetic EuO

[1]The two sublattices have equal gyromagnetic ratios, which are both determined by Fe ions. Thus, there is no torque, which can be exerted by a magnetic field, and the mode is forbidden.

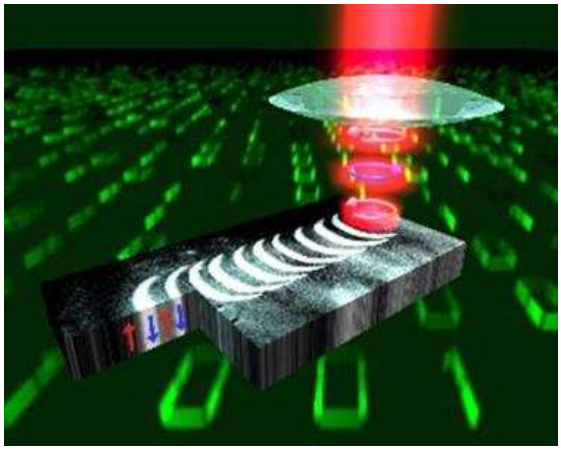

Figure 1.2: The figure is taken from Ref. [56]. The all-optical recording of magnetic bits in GdFeCo. A circularly polarized laser beam is scanned across the sample. Depending on the desired direction of magnetization, the polarization of the beam is switched between left and right circular.

films, which depended on the helicity of circularly-polarized laser pulses of 100 fs duration [54]. The observation was explained by the combined action of the ultrafast IFE with the novel effect of optically induced magnetization enhancement[2].

Despite of the advantage of the IFE that it is a non-thermal process, the action of this effect together with thermal processes started to attract much interest since remarkable results had been demonstrated by Stanciu *et al* [56]. They showed that a single circularly polarized pulse of 40 fs duration triggered a full magnetization reversal in an amorphous ferrimagnetic alloy GdFeCo. The magnetization reversal was the result of both laser heating and the ultrafast IFE. The authors could switch the magnetization and write bits, controlling this process by changing the light helicity (see Fig. 1.2). This results were of high importance for technological applications, since it was the first observation of magnetization reversal by a subpicosecond stimulus [57]. Therefore, this finding motivated a plenty of investigations of the magnetization reversal mechanism in GdFeCo [58–65]. However, it was demonstrated later that the laser induced heating, *i. e.* the absorption of photons from a linearly polar-

[2]The effect of optically induced magnetization enhancement in EuO is attributed to the optical transition from the $4f$ to the $5d$ state, see Ref. [55] for the details.

ized subpicosecond laser pulse, could be sufficient to switch magnetization in GdFeCo [65].

A further intriguing result due to an involved interplay of the IFE effect with the effect of laser heating was observed by Jong *et al* [66]. The authors demonstrated that the action of a single 60 fs circularly polarized laser pulse can cause a creation of a magnetic domain in rare-earth orthoferrite $(SmPr)FeO_3$ on a picosecond time scale. The magnetization of the domains was determined by the helicity of the laser pulse. The heating by the laser pulse mediated a spin reorientation phase transition in the material several tens of picoseconds after the excitation. At much shorter time scales, the IFE excited a coherent low-amplitude spin precession. Thereby, a laser pulse helicity determined the magnetic state of a domain at the time, when the phase transition started to take place. That provided a desired direction for resulting domain magnetization after the phase transition. This observation demonstrated that the IFE can control a magnetic phase transition and creation of magnetic domains without application of an external magnetic field.

Another potential application of the IFE was suggested by Terui *et al.* [67]. The authors used the IFE to induce two-dimensional spin wave propagation in Bi-doped rare-earth iron garnet, introducing a new method, which is relevant for the field of magnonics[3]. Very recently, this finding was implemented by Satoh *et al.* in Ref. [69] to realize a direction control of spin-wave emission by circularly polarized laser pulses spatially shaped into an ellipse. This is a very important achievement with the potential for fast and arbitrary synthesis of spin-wave patterns, which was not possible before.

Summing up, the ultrafast IFE has a very high significance for the field of ultrashort laser induced magnetization. The coherent excitation of spin waves on ultrashort time scales, which can be triggered by the IFE, is of high importance for the field of spintronics, magnetic storage technology and quantum computation (the latter will be discussed in the next Section). Complicated dynamics induced by the IFE can provide an access to a new information on the elementary interactions in materials as was shown by Reid *et al.* [50]. A skillful combination of the IFE with other effects induced by ultrafast laser pulses can significantly influence magnetic states of a medium, demonstrating remarkable and untrivial results.

The theory describing the IFE introduced by Pitaevskii [32] and developed

[3]Magnonincs is the field of research, by which one tries to use spin waves to store, carry and process information in nanostructure elements. For instance, spin wave packets can be used to carry information on much longer distances than by electric currents (see, for example, Ref. [68]).

further by Pershan *et al.* [35] about 50 years ago can be referred to as the classical theory of the IFE. At that time, typical laser excitation times were several tens of nanoseconds, and the theory was derived for a medium in thermal equilibrium. The condition of thermal equilibrium allowed to interpret the action of circularly polarized light as the creation of an effective magnetic field. However, this assumption cannot be applied for the magnetization processes taking place on femtosecond time scales, which are shorter than any relaxation time of a system. Therefore, the classical theory becomes unvalid, when characteristic times of the magnetization dynamics reduce to the subpicosecond region.

A comprehensive experimental study, which proved that the thermodynamic model of the inverse Faraday effect is not applicable at femtosecond time scales, was performed by Reid *et al.* in Ref. [40]. The authors came to the conclusion that the ultrafast IFE instead should be described microscopically. The same idea has been provided by Satoh *et al*., who showed that treatment of the IFE as an effective magnetic field is not applicable to describe magnetization dynamics at subpicosecond time region [43]. However, the classical theory is still being used to describe the IFE on femtosecond time scales.

This thesis presents a new approach to study the IFE, which can be applied at femtosecond time scales. For this aim, a thorough study of the microscopical mechanisms responsible for the IFE on the subpicosecond time scale is performed. It will be shown how the presented theory is connected with the classical one, and what are the limitations of the latter.

There are several fundamental questions about the mechanisms of ultrafast spin excitations, which are very important for the field of ultrafast laser induced magnetization dynamics, since the answers to them provide the idea about the mechanisms and, as a result, about the time limits of magnetic processes. The first question is about the time evolution of angular momentum and the role of the spin-orbit coupling for the optical generation of magnetization [16, 70–72]. The other one is about the coupling of laser light with electron interactions, especially if their energies correspond to the time scales of laser excitation: $E_{\text{el.int.}} \sim 1/\tau$ (Ref. [4] and the references therein). These issues are addressed in this thesis in detail. I present the analysis of the function of the spin-orbit coupling for the IFE and its effect on the time evolution of a spin during the excitation. The subpicosecond laser driven magnetization precessions due to the interplay of different interactions of various magnitudes is studied and compared, thereby the contributions of the exchange, spin-orbit, crystal field and Zeeman interactions are considered.

Techniques to manipulate magnetization vector motion, which would follow an arbitrarily multidimensional trajectory are essential for the field of spintronics. Therefore, the coherent control of magnetization precession by laser pulses attracts much attention (see, for instance, Ref. [47]). The theoretical model of magnetization precessions induced by femtosecond circularly polarized light provided here is necessary for the design of techniques to coherently control such dynamics. The study of the dependencies of magnetization precessions on properties of a single laser pulse, which is also done in this thesis, can be very useful for realizations of all-optical control of magnetization.

Finally, the spin-flip stimulated Raman scattering process, which is the optical process responsible for the IFE [35], and thus thoroughly studied here, is the essential mechanism for coherent optical control of a qubit state. The role of this process for the quantum information processing is discussed in the next Section.

1.2 Ultrafast optical control of spin based qubits

The ability to completely control the state of a qubit is the basis for quantum information processing. One of the most promising realizations of the control of a qubit is based on the optical manipulation of a spin state [73, 74]. A single qubit operation for spin based qubits is an arbitrary coherent rotation of a qubit spin. The rotations can be performed by laser driven transitions, which bring the system in a new spin state. The main attractiveness of these kind of methods is that the operation time can be dramatically decreased due to the possibility to perform the optical control over a spin state on picosecond or even femtosecond time scales, which are much shorter than the spin decoherence time[4].

These schemes are typically applied to electron or hole spins in charged quantum dots formed in direct band gap III-V compounds (see Fig. 1.3a). An electron (or hole) in such systems can be considered as a single particle due to the large band gaps, which suppress elementary excitations [76]. Controllable optical properties, discrete energy levels and large dipole moments of quantum dots also make them promising candidates for optically controlled qubit systems.

[4]Electron spin decoherence can be due to hyperfine interaction with nuclear spins, local magnetic field fluctuations, phonon scattering via spin-orbit coupling *etc.* Spin coherence time in quantum dots can be several microseconds [75].

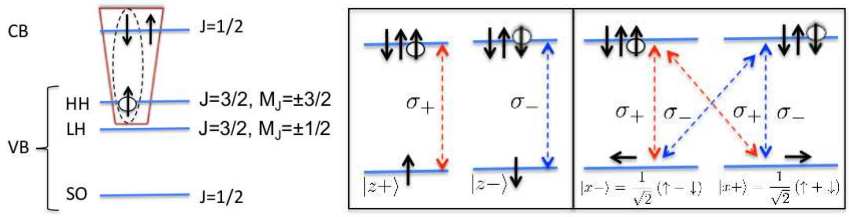

(a) (b)

Figure 1.3: (a) The energy level scheme of a trion state in electron charged III-V quantum dots. The arrow in a circle designates a hole spin, the other two arrows stay for electron spins. The dotted oval represents an exciton formed by the hole and the electron. The red trapezoid represents the trion. CB and VB are the conduction and valence bands, HH and LH are the heavy and light hole states, SO is the split-off hole band. (b) Optical selection rules for the electron-trion transitions by left- (σ_+) or right-circularly (σ_-) polarized light. In the left square: Spin is aligned parallel to the light propagation direction. In the right square: Spin is aligned perpendicular to the light propagation direction.

The energy levels of electron charged III-V quantum dots are depicted on the Fig. 1.3a. The top of the valence band and the bottom of the conduction band have p and s characters correspondingly. The states in the valence band are split due to a large spin-orbit coupling. The top of the valence band has $J = 3/2$, being split by energy about 20-30 meV into two bands with the projection $M_J = \pm 3/2$, called heavy hole states, and $M_J = \pm 1/2$, called light hole states. The state with $J = 1/2$ is called split-off hole band and is about 0.1-0.5 eV lower than the top of the valence band. Excitation by light leads to a creation of an exciton, *i. e.* a hole and an electron, thereby the latter forms a singlet with the resident electron (see Fig. 1.3a). The quasi-particle, which consists of the exciton and the additional electron is called a trion. Optical spin rotation involves the Raman process, which incorporates the creation of a trion by the absorption of a circularly polarized photon and recombination back to a single electron state by the emission of a photon. If spin is initially perpendicular to the propagation direction of a circularly polarized laser pulse, optical selection rules allow the Raman scattering to the single spin state with the opposite spin (see Fig. 1.3b).

A quantum computation scheme based on the optical manipulation of electron spin in quantum dots via the stimulated Raman scattering has been first

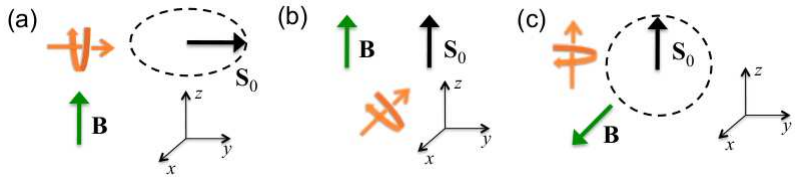

Figure 1.4: Schemes representing the geometries of the experiments of (a) Berezovsky *et al.*, (b) Press *et al.* and (c) Greilich *et al.* The green arrows show the directions of the applied magnetic fields denoted as **B**, the yellow arrows correspond to the light propagation directions, and the bold black arrows show the directions, in which the spins were initialized, denoted as $\mathbf{S}_0$. The dotted lines show the trajectories of the spin Larmor precessions before the (first) arrival of the laser pulses: (a) in the xy plane, (b) no precession and (c) in the yz plane.

proposed in 1999 by Imamoglu *et al.* [77]. Since then, much theoretical [78–82] and experimental [83–90] effort has been done before the full control over a single electron spin state became possible. Up to the present time, the schemes for the ultrafast optical control over a qubit are being intensively searched for and many successful implementations of optical qubit manipulations have been suggested [91–97], some of them are described further.

One of the first achievements of the coherent optical arbitrary rotation of a spin was demonstrated by Berezovsky *et al.* in Ref. [91]. The system they used was charged GaAs interface quantum dots embedded in an optical cavity [90]. Its ground state is formed by a single electron in the lowest conduction band level (see Fig. 1.3a). The measurement of a spin state of the system was performed by the magneto-optical Kerr effect with a probe pulse, which provided the value of the projection of the spin on the y-axis (see Fig. 1.4a).

The first step for the control was to initialize the electron spin in one direction. This was completed by optical pumping [98] using a circularly polarized pump pulse propagating along the y axis. The pump pulse excited spin-polarized electrons and holes into the continuum of states above the quantum dot, thereby some of them relaxed back to the ground state with the spin pointing in the y direction. The magnetic field of 0.7 T, which was applied in the z direction, caused the spin precession around the z axis after the accomplishment of optical pumping.

At some time t_c after the pump pulse, the control pulse[5] arrived. The

[5]A pulse, which is used to manipulate a spin state, is called control pulse. Sometimes, it

control pulse was circularly polarized propagating in the y direction and of 30 ps duration, corresponding to the spectral width of 0.2 meV. This pulse excited the lowest-energy interband transition to the trion state, consisting of two electrons in a singlet state and a heavy hole (see Fig. 1.3a). The detuning of the control pulse from the resonance was chosen in the range between approximately 1.5 and 5 meV, so that the transitions could drive the system back to the ground state leaving the excited states not populated. Although the electron was brought back to the ground state after the transitions had taken place, its spin state was changed. This phenomenon was described by the authors as the generation of the effective magnetic field along the y axis during the presence of the pulse due to the optical Stark effect. Namely, as the rotation of the spin around the total magnetic field, which is the sum of the effective field and the applied field, during the excitation. Although the effect of the control pulse was described in terms of the optical Stark effect[6], the authors commented that the phenomenon is practically the stimulated Raman scattering.

Thus, the spin operation was performed as follows. First, the initialized spin precessed around the magnetic field for the time t_c. Thus, t_c determined the position of the spin at the moment, when the control pulse arrived. The control pulse changed the spin orientation, thereby the modified spin position depended on the spin orientation at the time t_c. After the action of the control pulse, the spin continued the Larmor precession. Therefore, the phase of the final spin precession could be controlled by changing the time t_c. The next demonstration of the capability of the spin control was performed with the control pulse always arriving at the same time $t_c = 1.3$ ns. The probe pulse measured the spin position at the time $t_{probe} = 2.5$ ns. It was shown that this position was determined by the detuning from the resonance and the intensity of the control pulse.

Thereby, the authors were able to achieve the coherent electron spin rotations through arbitrary angles up to π radians at nanosecond time scales. This was attained by changing the time of the control pulse arrival or varying its detuning and intensity. However, only at most 200 spin operations during the coherence time could be performed using the set-up and samples applied in the experiment.

is called tipping or rotation pulse.

[6]Optical Stark effect is a light-induced shift of energy levels. In some references, the effect of Raman transitions, resulting in the change of a spin state, are explained by the optical Stark effect. However, according to my opinion, *spin-flip stimulated Raman scattering* is more suitable definition, since it reveals the mechanism of the process.

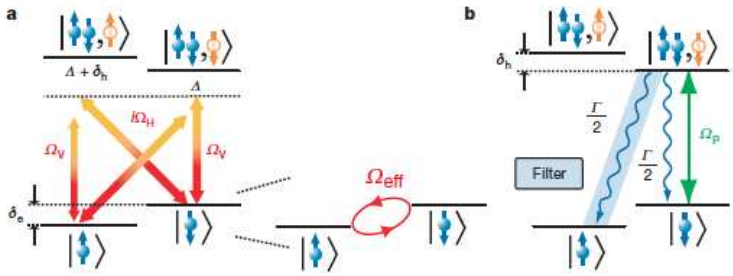

Figure 1.5: The figure is taken from Ref. [92]. The schemes used by Press *et al.* to initialize, control and measure the spin. (a) The four-level system and the spin rotation scheme. (b) The spin initialization and measurement scheme performed by optical pumping. A laser excites a transition between the $|\downarrow\rangle$ and $|\uparrow\downarrow\Downarrow\rangle$ states. The spontaneous emission, allowed to both states $|\downarrow\rangle$ and $|\uparrow\rangle$, leads to the initialization of the $|\uparrow\rangle$ state (see Refs. [98, 99] for details). The measurement is performed by the detection of the spontaneous emission to the $|\uparrow\rangle$ state after the optical pumping from the $|\downarrow\rangle$ to the $|\uparrow\downarrow\Downarrow\rangle$ state. Ω_H and Ω_V are the Rabi frequencies driven by the orthogonal linear polarizations of electric field $\pi/2$ out of phase with each other, denoted as H and V. Ω_{eff} is the effective Rabi frequency between the states $|\downarrow\rangle$ and $|\uparrow\rangle$. Γ is trion's total spontaneous emission rate, Ω_p is the transition rate between $|\downarrow\rangle$ and $|\uparrow\downarrow\Downarrow\rangle$.

The next successful experiment demonstrating the complete coherent control over an initialized electron spin state was implemented by Press *et al.* in Ref. [92]. This scheme was applied to the spin in doped InGaAs quantum dots [100]. The external magnetic field $B = 7$ T in their geometry was directed along the z axis, causing the Zeeman splitting of the ground electron spin states denoted as $|\uparrow\rangle$ and $|\downarrow\rangle$ of approximately 1 meV (Fig. 1.5,a). Two trion states were used as the intermediate states in the spin manipulation scheme. These states denoted as $|\uparrow\downarrow\Downarrow\rangle$ and $|\uparrow\downarrow\Uparrow\rangle$ consisted of a pair of electrons and an unpaired heavy hole and were the lowest energy interband states (Fig. 1.3a). The initialization and measurement of the spin state were achieved by optical pumping (Fig. 1.5,b).

The ground state was manipulated by a single circularly polarized control pulse, propagating in the x direction perpendicular to the magnetic field (Fig. 1.4b). The pulse was of 4 ps duration (corresponding to the spectral width of 0.5 meV) and had the large detuning Δ (approximately 1 meV) from the excited states. The action of the control pulse triggered the stimulated Ra-

man scattering process, which coherently changed the spin between $|\uparrow\rangle$ and $|\downarrow\rangle$, remaining the trion states unpopulated. The Rabi oscillation between the $|\uparrow\rangle$ and $|\downarrow\rangle$ states was equal to the spin rotation around the x axis. Up to six Rabi oscillations could be observed in the experiment increasing the power of the control pulse.

In order to obtain the complete SU(2) control[7] over the qubit state, three rotations around x, z and x axes were applied. The two rotations around the x axis by desired angles were obtained by adjusting the intensity of two control pulses, which were applied with a time delay between each other. The rotation around the z axis by arbitrary angles was accomplished by enabling the Larmor precession during the time delay, which could be tuned. This optical manipulation scheme allowed to accomplish a single-qubit gate operation within a single Larmor period of 38 ps. Thus, it was estimated that 10^5 operations were possible during the coherence time.

The first difference of the set-up of Press *et al.* compared to that of Berezovsky *et al.* was that much higher magnetic field was applied. This led to the faster spin dynamics due to the Larmor precession, however, considerably affecting the spin rotation during the action of the control pulses. The next difference was that two pulses instead of one were used, and the Larmor precession was prompted only after the rotation of the spin by the first pulse.

Later, the same method as implemented by Press *et al.* in Ref. [92] was applied by Greve *et al.* to manipulate a quantum dot hole qubit, showing the robustness of hole spins for ultrafast optical control techniques [96]. The authors demonstrated the reduced hyperfine interaction of quantum dot hole spins with nuclear spins, which limits the coherence times of electron spin qubits.

Greilich *et al.* in Ref. [94] realized the ultrafast optical control of the spins in the ensemble of $(\mathrm{In,Ga})\mathrm{As}$ quantum dots, each containing a single electron on average [101]. The ensemble of quantum dots was chosen to increase the optical coupling compared to that of a single quantum dot. Previously, it was demonstrated that the spin ensemble confined in singly charged quantum dots can be driven into a single mode of precession about a low magnetic field (<0.6 T) [102]. Therefore, the total spin of the ensemble can be treated equally to a single spin, if the external magnetic field does not exceed 0.6 T. In the experiment by Greilich *et al*, the amplitude of the applied magnetic field was 0.3 T (corresponding to the Zeeman splitting of 0.04 meV). The relatively low amplitude of the field also helped to minimize the effect of the Larmor precession during the presence of the control pulse.

[7]Single qubit transformations are described by SU(2) matrices.

Circularly polarized laser pulses of 1.5 ps duration (≈1.5 meV spectral width) propagating in the z direction were used to control the spin state. The pulses were tuned in the vicinity of the trion $|\uparrow\downarrow\Uparrow\rangle$ resonance. Thus, the optical manipulation scheme effectively included only three levels: the ground state with the spin split by the magnetic field in the x direction and the excited trion state $|\uparrow\downarrow\Uparrow\rangle$. The spins were initialized in the z direction perpendicular to the applied magnetic field using the optical pumping to the trion state. The spin polarization along the z axis was measured by the ellipticity of a probe pulse.

Due to the resonance excitation, the conditions had to be found, when the excited level remained unpopulated, but the transitions through the excited state back to the ground state had taken place. For this goal, the intensity of the control laser pulse was varied and the time evolution of the z projection of the total spin of the ensemble was measured. The intensity of the pulse, which gave the maximal amplitude of the spin precessions, was chosen.

Since the spin was initialized in the z direction, which was perpendicular to the magnetic field, it started to precess in the y-z plane (see Fig. 1.4c). First, the authors were applying the control pulse with zero detuning at different times t_c after the spin initialization. They showed that this resulted in the spin rotation by π degrees every time except when the spin was aligned parallel to the control pulse propagation direction at the time t_c.

The next demonstration was with the control pulse arriving at the moment when initialized spin was rotated to the $-y$ direction by the magnetic field. Thereby, the maximal effect on the spin state could be gained since the spin orientation was perpendicular to the control pulse propagation direction. The rotations around the z-axis by any angles from π to 0 were achieved by the detuning from the resonance from 0 to 3.08 meV as theoretically calculated by Refs. 78, 79.

And finally, they could observe the following effect. If a pulse applied at time t_c rotated spins by an angle π, the increase of the signal from the spin was observed around the time $2t_c$. This phenomenon is called a spin echo [103] and is due to the refocusing of inhomogeneously precessing spins. The spin echo effect allows to increase the dephasing time of a spin. Later, Press *et al.* implemented the optically driven spin-echo effect to a single electron spin [8] in InAs quantum dot, which suppressed the nuclear spin noise, and increased the decoherence time from nanoseconds to microseconds [104].

Electron and hole spins in quantum dots are not the only systems considered for implementations of ultrafast optical qubit control. The other sys-

[8]The dephasing of a single electron spin is due to nuclear spins.

tems include electron spins in quantum wells [105–107], magnetic dopants in QDs [108, 109] and nitrogen-vacancy centers in diamond [110, 111].

The next step towards the creation of a quantum processor is the realization of quantum entanglement between several qubits. Much effort is being done now to design multi-spin entangled states and achieve the control over them [74]. Ultrafast optical techniques make it possible to address a single quantum dot and provide the opportunities to manipulate interacting spin systems individually [112–115].

Although much progress has been made towards the ultrafast optical qubit control, the main obstacle is the short coherence times of a single spin or spin system, which limit the number of gate operations. Usually, picosecond laser pulses are used to perform spin state manipulations. The application of even shorter laser pulses may improve the situation, but it's implementation requires the understanding of the light-matter interactions at femtosecond time scales.

The theoretical investigation of ultrafast optical manipulation of a qubit is not the main topic of this thesis, however the results presented here are also relevant for this field. The thesis is mainly concentrated on the study of the stimulated Raman scattering process at femtosecond time scales, which is the origin of the inverse Faraday effect [35]. At the same time, this process is used for the ultrafast qubit control in the most optical manipulation schemes. The conclusions concerning the interaction of femtosecond laser light with a magnetic state of a medium via the stimulated Raman scattering process presented in this work are meaningful for implementing faster qubit optical manipulation schemes. The insight to the coupling of electron interactions to the femtosecond laser light can be also helpful for the developing of new ideas of ultrafast optical control of entanglement between several spins.

1.3 Scope of the thesis

Chapter 2 of the thesis starts with the introduction to the classical theory of the inverse Faraday effect. This theory will be reviewed in view of subpicosecond laser excitation. It will be shown which assumptions of the theory cannot be applied to describe magnetization dynamics at ultrafast time scales. Further, the introduction to our approach to describe the time evolution of magnetization without approximations on the pulse duration using the time-dependent Schrödinger equation is given. The detailed comparison of this approach with the classical theory is performed, demonstrating the discrepancies produced by the latter at the regime of subpicosecond excitation. Chapter 3 discusses the optical mechanism responsible for the ultrafast IFE and the spin-flip stimu-

lated Raman scattering. The role of spin-orbit coupling is studied, particularly in the regime when its value is on the order of the spectral width of excitation. The dependence of the value of the effect on laser pulse properties is investigated. The Chapter 4 introduces a momentum operator, which provides the equations of motion of magnetic vector components, which change in time due to the stimulated Raman process. The laser driven launching of a spin Larmor precession due to an external magnetic field is studied in Chapter 5. It is shown that the spin dynamics during the excitation determines the final magnetic state after it. Chapter 6 discusses the influence of a crystal field interaction on the value of IFE. A method to model subpicosecond magnetization dynamics induced by the ultrafast IFE in magnetic crystals is provided. The mechanism of the creation of a magnetic moment in an antiferromagnet is explained.

Chapter 2

The theory of the inverse Faraday effect

2.1 The phenomenological theory of the inverse Faraday effect

The IFE was first theoretically predicted by Pitaevskii in 1960 [32] from a pure phenomenological ansatz on the basis of a thermodynamic potential describing the internal energy of a system. Pitaevskii considered a nonmagnetic medium placed in a strong constant magnetic field $\mathbf{H}$ and a weak electric field $\mathbf{E}$ varying with a frequency ω_0 at which the medium is transparent. The author showed that if the entropy and the temperature of a medium are constant, then the variation of the free energy $\delta\mathcal{F}$ is given by the integral over the volume V

$$\delta\mathcal{F} = \int \left(\delta F(E=0,\mathbf{H}) - \frac{1}{16\pi} E^*_{0k} E_{0l} \delta\epsilon_{kl} \right) dV, \tag{2.1}$$

where $F(\mathbf{E},\mathbf{H})$ is the density of the free energy, k and l are x, y or z. $\mathbf{E}_0$ is the amplitude of the electric field:

$$\mathbf{E} = \frac{1}{2}\left(\mathbf{E}_0 e^{-i\omega_0 t} + \mathbf{E}^*_0 e^{i\omega_0 t}\right). \tag{2.2}$$

ϵ is the dielectric tensor, which in the absence of absorption obtains the form [116]

$$\epsilon = \epsilon_1 + \epsilon_2 + \epsilon_3, \tag{2.3}$$

where

$$\epsilon_1 = \begin{pmatrix} \epsilon_{01} & 0 & 0 \\ 0 & \epsilon_{01} & 0 \\ 0 & 0 & \epsilon_{01} \end{pmatrix}, \ \epsilon_2 = \epsilon_{02} \begin{pmatrix} H_x^2 & H_x H_y & H_x H_z \\ H_x H_y & H_y^2 & H_y H_z \\ H_x H_z & H_y H_z & H_z^2 \end{pmatrix}, \tag{2.4}$$
$$\epsilon_3 = i\epsilon_{03} \begin{pmatrix} 0 & H_z & -H_y \\ -H_z & 0 & H_x \\ H_y & -H_x & 0 \end{pmatrix},$$

H_x, H_y and H_z are the components of an external magnetic field, $\epsilon_{01(2,3)}$ are constants, which depend on the laser frequency and the amplitude of the external field.

Applying the thermodynamic equation

$$\mathbf{B} = 4\pi \frac{\partial F}{\partial \mathbf{H}}, \tag{2.5}$$

together with the relations

$$4\pi \frac{\partial F_0}{\partial \mathbf{H}} = \mathbf{H}, \quad F(0, \mathbf{H}) = F(0, 0) + \frac{H^2}{8\pi} \tag{2.6}$$

the author obtained

$$\mathbf{B} = \mathbf{H} + \frac{1}{4} E_{0k}^* E_{0l} \frac{\partial \epsilon_{kl}}{\partial \mathbf{H}}. \tag{2.7}$$

The induced magnetic field $\mathbf{B}$ is nonzero even if an external magnetic field $\mathbf{H}$ is absent

$$\mathbf{B}(\mathbf{H} = 0) = \frac{1}{4} E_{0k}^* E_{0l} \left. \frac{\partial \epsilon_{kl}}{\partial \mathbf{H}} \right|_{\mathbf{H}=0}, \tag{2.8}$$

since the third part of the dielectric tensor gives a contribution into $\mathbf{B}$ at zero external magnetic field

$$\frac{\partial \epsilon_1}{\partial \mathbf{H}} = 0, \ \left. \frac{\partial \epsilon_2}{\partial \mathbf{H}} \right|_{\mathbf{H}=0} = 0, \ \left. \frac{\partial \epsilon_3}{\partial \mathbf{H}} \right|_{\mathbf{H}=0} \neq 0. \tag{2.9}$$

Multiplying $\partial \epsilon_{3kl} / \partial \mathbf{H}$ by the components of the electric field, one obtains

$$\begin{aligned} B_x &= \frac{i\epsilon_{03}}{4} E_{0k}^* E_{0l} \frac{\partial \epsilon_{3kl}}{\partial H_x} = \frac{i\epsilon_{03}}{4} (E_{0y}^* E_{0z} - E_{0z}^* E_{0y}) \\ B_y &= \frac{i\epsilon_{03}}{4} E_{0k}^* E_{0l} \frac{\partial \epsilon_{3kl}}{\partial H_y} = \frac{i\epsilon_{03}}{4} (E_{0z}^* E_{0x} - E_{0x}^* E_{0z}) \\ B_z &= \frac{i\epsilon_{03}}{4} E_{0k}^* E_{0l} \frac{\partial \epsilon_{3kl}}{\partial H_z} = \frac{i\epsilon_{03}}{4} (E_{0x}^* E_{0y} - E_{0y}^* E_{0x}), \end{aligned} \tag{2.10}$$

which results in a well-known classical equation of the inverse Faraday effect

$$\mathbf{M}(\mathbf{H}=0)=\frac{\mathbf{B}}{4\pi}=\frac{i\epsilon_{03}}{16\pi}\mathbf{E}_0^*\times\mathbf{E}_0 \tag{2.11}$$

Thus, Pitaevskii showed that a varying electric field, which is not linearly polarized, can create in a medium an average magnetic moment proportional to the intensity (see Eq. (B.4)) of the electric field E^2. There are two essential points in these considerations. First, the induced magnetic moment can be present only during the action of the electric field, otherwise $\mathbf{B}=\mathbf{H}$ (since the medium is considered to be nonmagnetic). Second, the expression for the free energy (2.1) and, thus, the relations that followed are correct, if the medium is in thermodynamic equilibrium.

Pershan in Ref. [117] in 1962 also made a conclusion that magnetization can be produced by a circularly polarized optical field. Pershan derived the induced magnetization from a potential function[1], which he obtained using the similar considerations as in Ref. [32]. He introduced the potential function in the case of the electric field propagating in the z direction as

$$F=\chi H_z(E_R E_R^*-E_L E_L^*)=i\chi H_z(E_{0x}E_{0y}^*-E_{0y}E_{0x}^*), \tag{2.12}$$

$E_{R(L)}=(E_{0x}\mp iE_{0y})/\sqrt{2}$ are the amplitudes of right (left) circularly polarized components of light, χ is a constant characteristic of the material. It directly follows that the effect is maximal for circularly polarized light, and is zero, when $|E_R|^2=|E_L|^2$, *i. e.* if light is linearly polarized.

The authors showed that the same function is responsible for the change of optical dielectric constants for right and left circularly polarized light (denoted as $\Delta\epsilon_R$ and $\Delta\epsilon_L$ respectively) via the derivatives

$$\begin{aligned}\Delta\epsilon_R&=-\frac{\partial^2 F}{\partial E_R\partial E_R^*}=-\chi H_z,\\ \Delta\epsilon_L&=-\frac{\partial^2 F}{\partial E_L\partial E_L^*}=\chi H_z,\end{aligned} \tag{2.13}$$

which results in the (direct) Faraday effect.

The relation between the Faraday effect and the IFE was explicitly discussed by van der Ziel *et al.* in Ref. [36][2]. The Faraday effect, which is the rotation of polarization of linearly polarized light, which propagates through

[1] Pitaevskii used the term "free energy density" for the same function.

[2] As far as I know, the term "inverse Faraday effect" was first used by van der Ziel *et al.* in Ref. [36].

a magnetic medium, is given by an angle $\theta/d = \mathcal{V}/H$, d is the propagation length. $\mathcal{V}$ is called "Verdet constant", and is related to the constant χ from Eq. (2.12) by

$$\mathcal{V} = -\frac{4\pi^2\chi}{n_0\lambda_0}, \tag{2.14}$$

n_0 is the refraction index in the absence of an external field, λ_0 is the wavelength of the light in the vacuum. The induced magnetization due to the IFE in zero applied magnetic field, which is given by the relation[3]

$$M_z = -\frac{\partial F}{\partial H_z} = -\chi(E_R E_R^* - E_L E_L^*), \tag{2.15}$$

can be expressed by

$$M_z = \frac{\lambda_0\mathcal{V}}{4\pi^2}(E_R E_R^* - E_L E_L^*). \tag{2.16}$$

Thereby, the induced magnetization by circularly polarized light and the Faraday rotation are determined by the same constant $\mathcal{V}$. Thus, the two effects were related to each other. The Eqs. (2.7) and (2.15) can be generalized by the expression

$$\mathbf{M} = -i\chi\mathbf{E}_0^* \times \mathbf{E}_0. \tag{2.17}$$

In the same article, van der Ziel *et al.* [36] reported the first experimental observation of the effect. The experiments were done with several types of samples: $Eu^{+2} : CaF_2$ crystals, diamagnetic glasses, and organic and inorganic liquids. The samples were irradiated by a Q-switched ruby laser with the energy 0.1 J and peak laser intensity 10^7 W/cm^2. The pulses were circularly polarized and had 30 nanoseconds duration at the full width at half-maximum (FWHM). The measurements were done at zero applied magnetic field.

The authors showed that the magnetization was induced in the samples during the action of circularly polarized light. It was proportional to the light intensity and changed the sign, when the light polarization switched from right to left circular. Furthermore, they demonstrated that the Verdet constant obtained by Eq. (2.16) obeys the general relation $\mathcal{V} = C_0 + C_1/T$ (C_0 and C_1 are constants, and T is a sample temperature), which was derived for the Faraday effect [118].

[3]Note that constants entering the expressions for the induced magnetization derived by Pitaevskii (Eq. 2.11) and Pershan *et al.* are related by $\chi = -\epsilon_{03}/(16\pi)$.

2.2 Quantum mechanical description of the inverse Faraday effect at long time scales

The quantum mechanical description of the IFE was provided by Pershan *et al.* in Ref. [35]. They considered the perturbation by light $\hat{V}(t) = -\mathbf{d}\cdot\mathbf{E} = \mathbf{d}\cdot\mathbf{A}'/c$, where $\mathbf{d}$ is the dipole moment of the system, which can be represented as

$$\hat{V}(t) = v(t)e^{i\omega_0 t} + v^*(t)e^{-i\omega_0 t}, \tag{2.18}$$

where ω_0 is the frequency of the optical field. The wave function of the system due to the action of the electric field $\mathbf{E}(t)$ was found with the time-dependent Schödinger equation

$$i\frac{\partial\Psi(t)}{\partial t} = [\mathcal{H}_0 + \hat{V}(t)]\Psi(t), \tag{2.19}$$

the general solution of which is (see Appendix A)

$$\begin{aligned}\Psi(t) =& e^{-i\mathcal{H}_0 t}\left(\Psi_0 - i\int_{-\infty}^{t} dt'\, e^{i\mathcal{H}_0 t'}\hat{V}e^{-i\mathcal{H}_0 t'}\Psi_0\right. \\ &\left. - \int_{-\infty}^{t} dt'\, e^{i\mathcal{H}_0 t'}\hat{V}e^{-i\mathcal{H}_0 t'}\int_{-\infty}^{t'} dt''\, e^{i\mathcal{H}_0 t''}\hat{V}e^{-i\mathcal{H}_0 t''}\Psi_0 + \ldots\right).\end{aligned} \tag{2.20}$$

$\mathcal{H}_0$ is the Hamiltonian of the system in the absence of the optical field

$$\mathcal{H}_0 = \sum_\alpha \mathbf{p}_\alpha^2/2 + \mathcal{V}_{\text{int}}. \tag{2.21}$$

$\mathbf{p}_\alpha$ is the momentum of an electron, $\mathcal{V}_{\text{int}}$ is the sum of the kinetic energy of nuclei, the interaction energy between electrons and nuclei and mutual Coulomb energy of the electrons and nuclei. The interactions, which are important for effects on the spin of the electrons, such as the spin-orbit- and Zeeman interactions, must be also included to $\mathcal{V}_{\text{int}}$. The summation is over all electrons in the system.

Pershan introduced an effective Hamiltonian $\mathcal{H}_{\text{eff}}(t)$, which connects the eigenstates $|i\rangle$ and $|f\rangle$ belonging to the same ground state manifold, by the relation

$$\begin{aligned}\langle i|1 - i\int_{-\infty}^{t}\mathcal{H}_{\text{eff}}(t')dt'|f\rangle =& \\ = \langle i|1 - i\int_{-\infty}^{t}\overline{V}(t')dt' - \int_{-\infty}^{t}\overline{V}(t')dt'\int_{-\infty}^{t'}\overline{V}(t'')dt''|f\rangle,&\end{aligned} \tag{2.22}$$

where $\overline{V}(t) = e^{i\mathcal{H}_0 t}\hat{V}(t)e^{-i\mathcal{H}_0 t}$. The term "ground state manifold" refers to a system's ground state, which is energetically split by magnetic excitations into levels having different magnetic signatures. The perturbation is of the first order of the inverse light velocity $1/c$: $\hat{V}(t) = -\mathbf{d}\cdot\mathbf{E} = \mathbf{d}\cdot\mathbf{A}'/c$, where $\mathbf{A}$ is the vector potential. Taking the terms up to the second order of $1/c$ in the expansion (2.20) and with $\langle i|\overline{V}(t)|f\rangle = 0$, the authors obtained

$$\begin{aligned}\mathcal{H}_{\text{eff}}(t)_{if} = \langle f|\mathcal{H}_{\text{eff}}(t)|i\rangle &= -i\sum_j \langle f|\overline{V}(t)|j\rangle \int_{-\infty}^{t} \langle j|\overline{V}(t')|i\rangle\, dt', \\ &= -i\sum_j e^{i\omega_{jf}t}\langle f|V(t)|j\rangle \int_{-\infty}^{t} dt' e^{i\omega_{ij}t'}\langle j|V(t')|i\rangle\end{aligned} \tag{2.23}$$

where the summation is over all possible excited states j, $\omega_{mn} = \varepsilon_n - \varepsilon_m$, where $\varepsilon_{m(n)}$ is the energy of a state $m(n)$. Thus, the effective Hamiltonian $\mathcal{H}_{\text{eff}}(t)_{if}$ is defined by the transition amplitudes of Raman scattering from an initial state i to final states f.

At this point, the authors made an assumption that the amplitude of the perturbation, $v(t)$, varies on a characteristic time scale T that is much larger then the inverse of the detuning $1/|\omega_0 \pm \omega_{ij}| = 1/\Delta\omega$. For laser pulses of several tens of nanosecond duration, this assumption is quite reasonable, since $1/T$ in energy units is of the order of $10^{-2}\ \mu eV$. Therefore, the approximation

$$\int_{-\infty}^{t} v(t')e^{i(\omega_{ij}\pm\omega_0)t'}dt' \approx v(t)\frac{e^{i(\omega_{ij}\pm\omega_0)t}}{i(\omega_{ij}\pm\omega_0)} \tag{2.24}$$

becomes valid except for resonant transitions $\pm\omega_0 \approx \omega_{ij}$. This leads to

$$\int_{-\infty}^{t} e^{i\omega_{ij}t'}V(t')dt' = v(t)\frac{e^{i(\omega_{ij}+\omega_0)t}}{i(\omega_{ij}+\omega_0)} + v^*(t)\frac{e^{i(\omega_{ij}-\omega_0)t}}{i(\omega_{ij}-\omega_0)}. \tag{2.25}$$

Substituting Eq. (2.25) to (2.23), the authors found that the effective Hamiltonian can be expressed as

$$\mathcal{H}_{\text{eff}}(t)_{if} = -i\sum_j \left[\frac{v_{ij}(t)v^*_{jf}(t)}{\omega_{ij}+\omega_0} + \frac{v_{jf}(t)v^*_{ij}(t)}{\omega_{ij}-\omega_0}\right] e^{i\omega_{if}t}, \tag{2.26}$$

where $v_{nm}(t) = \langle m|v(t)|n\rangle$. The terms $v_{ij}v_{jf}e^{i(\pm 2\omega_0+\omega_{if})t}$ were omitted here, since they correspond to a second harmonic process. They connect an initial state to final states which are energetically widely separated from the initial state and need not to be considered here.

If $v(t) = -\mathbf{d} \cdot \mathbf{E}_0$, then it is easy to show that the effective Hamiltonian becomes

$$\mathcal{H}_{\text{eff}}(t)_{if} = -\sum_{kl} e^{i\omega_{if}t} \chi_{if}^{kl} E_{0k}^* E_{0l}, \tag{2.27}$$

where k and l stay for x, y or z, and χ_{if}^{kl} is the polarizability tensor [119]

$$\chi_{if}^{kl} = \sum_j \left[\frac{(d_l)_{ij}(d_k)_{jf}^*}{\omega_{ij} + \omega_0} + \frac{(d_k)_{ij}^*(d_l)_{jf}}{\omega_{ij} - \omega_0} \right], \tag{2.28}$$

$(d_{k(l)})_{mn}$ is the dipole matrix element between states m and n for a $k(l)$ vector component of the electric field: $(d_{k(l)})_{mn} = \langle n|d_{k(l)}|m\rangle$. The polarizability tensor is connected with the dielectric tensor ϵ_{kl} by the density matrix ρ_{if} of the electron system

$$\frac{(\epsilon - 1)_{kl}}{4\pi} = \sum_{if} \chi_{if}^{kl} \rho_{if}. \tag{2.29}$$

The density matrix assures that the transitions from a state i to a state f occur with the same probability as from f to i [120]. At the same time (see Eq. 2.13),

$$\frac{(\epsilon - 1)_{kl}}{4\pi} = -\frac{\partial F}{\partial E_{0k}^* \partial E_{0l}}. \tag{2.30}$$

The effective Hamiltonian $\mathcal{H}_{\text{eff}}(t)_{if}$ can now be related to the potential function (2.12) by

$$F = \sum_{if} e^{-i\omega_{if}t} \mathcal{H}_{\text{eff}}(t)_{if} \rho_{if}, \tag{2.31}$$

$$= \sum_{if,kl} \chi_{if}^{kl} E_{0k}(t)^* E_{0l}(t) \rho_{if}. \tag{2.32}$$

The meaning of Eq. (2.31) is the following. The effective Hamiltonian describes the transitions in a system triggered by the laser light. Namely, the ones from the initial ground state i via the virtual excited states j to final states f belonging to the ground state multiplet. The potential function is the thermal average of the effective Hamiltonian $\mathcal{H}_{\text{eff}}$. It characterizes the free energy produced in the system by light. That means, the potential function F describes a new thermal equilibrium, which is produced by the laser excitation, which constantly brings the system to a new state.

Finally, the induced magnetization $\mathbf{M}(t)$ is connected to the effective Hamiltonian $\mathcal{H}_{\text{eff}}$ by the thermodynamic relation $\mathbf{M} = -\partial F/\partial \mathbf{H}$ (Eq. 2.15)

$$\mathbf{M}(t) = \sum_{kl} \frac{E_{0k}^*(t) E_{0l}(t)}{4\pi} \frac{\partial \epsilon_{kl}}{\partial \mathbf{H}}. \tag{2.33}$$

Pershan *et al.* underlined that in order to apply the thermodynamic relation (2.15) to the induced magnetization, it should be satisfied that $E_0(t)E_0^*(t)$ changes slowly compared to any relaxation times of the system. Thus, Eq. (2.15) describes the magnetization in the new equilibrium, which is created during the presence of a slowly varying laser excitation.

To sum up, four conditions have to be satisfied for the validity of Eq. 2.33:

1) the intensity of the electric field varies slowly compared to any thermal relaxation times of the system. In this case, the system has enough time to relax to the new conditions produced by an optical field. A new quasi stationary magnetic state is created due to the interaction with the laser light;

2) the intensity of the electric field varies on a characteristic time scale that is much larger than the inverse of the detuning from a resonance (in time units);

3) the frequency of the excitation is far from any resonance in the system;

4) Eq. 2.33 is derived for the magnetization induced during the presence of light.

2.3 The theory of the inverse Faraday effect at subpicosecond time scales

The results of this Section are published in Ref. [121] and are reused with the permission from Daria Popova, Andreas Bringer and Stefan Blügel.

2.3.1 The stationary and ultrafast inverse Faraday effect

With the advent of ultrafast pump-probe experiments the experimental conditions today became quite different from the ones realized in the past. First, the time scales are totaly different. The duration of the laser pulses used in the experiment of van der Ziel *et al.* [36] were 30 nanoseconds. Thereby, laser pulses used in modern experiments are of several tens of femtoseconds duration. That is about six orders of magnitude shorter than in 1965. Laser fluences of pulses applied today are also much higher. In the experiment of Kimel *et al.* [9] the fluence (see Eq. (B.3)) was about 10^{11} W/cm^2, which is four orders of magnitude higher than that in Ref. [36]. Another essential difference lies in the observation of the magnetization dynamics. Ziel *et al.* [36] measured the magnetization during the time the pulses were present and the variation of magnetization was zero after the action of the pulse. However,

the magnetization dynamics after the action of a laser field is of interest and requires an interpretation nowadays, which is opposite to the essence of the studies in 1960-ies.

Nevertheless, the relation $\mathbf{M} = -i\chi \mathbf{E}_0^* \times \mathbf{E}_0$ is still applied to describe the magnetization dynamics induced by ultrafast laser pulses. However, let me revise the criteria of this equation (listed above) for an excitation by a laser pulse of 100 fs duration:

Criteria 1) is not satisfied. Moreover, for such pulse duration, an opposite extreme case is valid: the pulse duration is much shorter than thermal relaxation times;

2) is not satisfied. $1/T$ in energy units is about 10 meV, which is on the order of or even larger than a detuning $\Delta\omega$;

3) is satisfied in some experiments (but not necessarily). However, the condition $\Delta\omega \gtrsim 1/T$ instead of $\Delta\omega \gg 1/T$ is fulfilled even for off-resonance excitations;

4) is not satisfied for magnetization dynamics after the excitation, which is usually studied nowadays.

Thus, the assumptions used to derive the effective Hamiltonian and induced magnetization in Refs. [32,35,36,117] are not valid for the novel experimental conditions. This means, that the mechanisms of the generation of magnetization *during* the presence of a *stationary* electric field are different from that responsible for the modern experimental observations of coherent magnetic precessions *after* the excitation by *subpicosecond* intense laser pulses. I will refer to the former process as "the stationary IFE", and to the latter one as "the ultrafast IFE".

An experimental evidence that magnetization dynamics predicted by the thermodynamical treatment of the IFE disagrees with that observed on subpicosecond time scales was provided by Reid *et al.* [40]. They compared the initial amplitudes of the observed oscillations, excited by a light pulse of 50 femtosecond length, with static measurements of the materials Verdet constant, which is proportional to χ, over a range of temperatures and found that the two have very different temperature dependencies. They also obtained that the frequency of the oscillations are 30 times higher than that expected for magnetization precessing due to an action of an effective magnetic field, generated by a laser pulse.

This experiment demonstrated that the thermodynamic approach which works at the nanosecond region is not valid for the description of magnetization dynamics at subpicosecond time scales. Therefore, an interpretation different from the classical one is required to explain the novel experiments on the

ultrafast IFE. The aim of this work is to reconsider the theory of Pershan *et al.* in Ref. [35] and provide an extension of the theory, which can be applicable for magnetization dynamics at subpicosecond time scales. The understanding of the ultrafast mechanisms, which are responsible for the ultrafast IFE, is essential for the ability to manipulate spin precessions, which arise after the action of circularly-polarized light pulse on a system.

It will be shown further in this Chapter which assumptions used to derive the induced magnetization due to the stationary IFE lead to incorrect results if applied to magnetization dynamics induced by subpicosecond excitation. A new approach applicable for the description of the ultrafast IFE, which does not rely on these assumptions, will be provided. It will be discussed that the ultrafast IFE should be interpreted as the induced dynamics of a system brought to a new magnetic state by optical transitions.

2.3.2 Effective Hamiltonian

Let me first consider the condition of the validity of the classical relations of the IFE that the intensity of the electric field varies on a characteristic time scale that is much larger than the inverse of the detuning from a resonance (in time units): $T \gg 1/|\omega_{ij} - \omega_0|$. It means that the laser field can be considered as stationary, which was the condition considered by Pershan *et al.* [35]. This assumption resulted in approximation (2.24). However, the ultrafast magnetization experiments are carried out with laser pulses of femtosecond duration, and this means that $T \sim 1/|\omega_{ij} - \omega_0|$. The change of a pulse amplitude in time cannot be considered as constant for such pulses.

This difference can be illustrated taking the perturbation by a circularly polarized Gaussian-shaped pulse, $v(t) = -\mathbf{d} \cdot \mathbf{n}\, \mathcal{E}\, e^{-t^2/T^2}$. $\mathcal{E}$ is the time independent part of the amplitude of the electric field, $\mathbf{n}$ is the vector perpendicular to the direction of propagation ($\mathbf{E}_0 = \mathbf{n}\, \mathcal{E}\, e^{-t^2/T^2}$). The left plot on Fig. 2.1 exhibits the shape of a pulse for which the approximation (2.24) holds. During the time considered, the amplitude of $v(t)$ does not change significantly and the time integral over the field is determined by the periodic function $e^{\pm i\omega_0 t}$. In the right plot, the constant T that characterizes the pulse width is 20 times shorter and the variation of $v(t)$ is important. When integrating over the pulse, the factor e^{-t^2/T^2} cannot be omitted.

The exact solution of the integral in Eq. (2.25) for the Gaussian-shaped

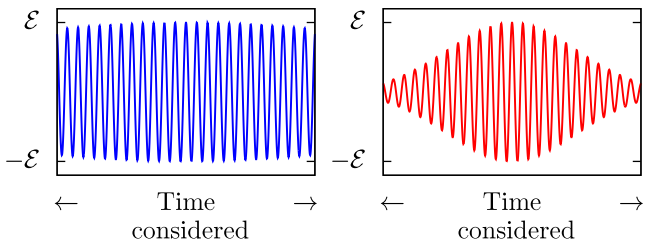

Figure 2.1: Left: Pulse with amplitude that does not change noticeably in time. Right: Gaussian-shaped pulse. Time T characterizing the pulse duration is a factor 20 times shorter for the right pulse as compared to the left pulse.

laser pulse is given by (see Appendix A)

$$\int_{-\infty}^{t} e^{i\omega_{ij}t'}\bar{V}(t')dt' = -\mathbf{d}\cdot\mathbf{n}\,\mathcal{E}\,\frac{T\sqrt{\pi}}{2}\times \tag{2.34}$$
$$\times\left[e^{-\frac{\left(T\left(\omega_{ij}+\omega_0\right)\right)^2}{4}}\left(1+\mathrm{erf}\left(\frac{t}{T}-\frac{i}{2}T\left(\omega_{ij}+\omega_0\right)\right)\right)\right.$$
$$\left.+\,e^{-\frac{\left(T\left(\omega_{ij}-\omega_0\right)\right)^2}{4}}\left(1+\mathrm{erf}\left(\frac{t}{T}-\frac{i}{2}T\left(\omega_{ij}-\omega_0\right)\right)\right)\right].$$

Therefore, the exact expression (*i. e.* not applying the assumption (2.25)) for the effective Hamiltonian according to Eq. (2.23) is

$$\langle f|\mathcal{H}_{\mathrm{eff}}(t)|i\rangle = -\,i\sqrt{\pi}\mathcal{E}^2T\sum_j d_{ij}d_{jf}e^{-\frac{t^2}{T^2}}e^{i\omega_{jf}t}\cos\omega_0 t\times$$
$$\times\left[e^{-\frac{\left(T\left(\omega_{ij}+\omega_0\right)\right)^2}{4}}\,\mathrm{erfc}\left(\frac{i}{2}T\left(\omega_{ij}+\omega_0\right)-\frac{t}{T}\right)+\right. \tag{2.35}$$
$$\left.e^{-\frac{\left(T\left(\omega_{ij}-\omega_0\right)\right)^2}{4}}\,\mathrm{erfc}\left(\frac{i}{2}T\left(\omega_{ij}-\omega_0\right)-\frac{t}{T}\right)\right].$$

The function $\mathrm{erfc}(z)$ ($z=|z|\,e^{i\theta}$ is a complex number) approaches asymptotically $e^{-z^2}/\sqrt{\pi}z$ for large complex arguments, $|z|\to\infty$, and a polar angle $|\theta|<3\pi/4$ [126]. Substituting this asymptote into Eq. (2.35) one obtains exactly Eq. (2.26). Thus, the range of the validity of Eq. (2.26) can be determined precisely. From the condition $|\theta|<3\pi/4$ it follows that $T|\omega_{ij}\pm\omega_0|>2t/T$, and the condition $T\cdot|\omega_{ij}\pm\omega_0|\gg 1$ is necessary for $|z|\to\infty$. Therefore, Eq. (2.26) is certainly applicable to the experiments of Ziel *et al.* [36], when the pulse

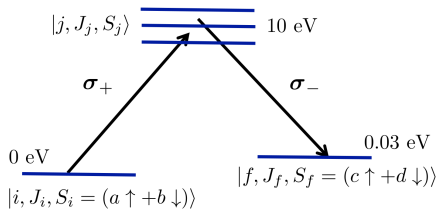

Figure 2.2: The three-level system investigated. The laser pulse causes transitions from the initial state $|i\rangle$ to the intermediate $|j\rangle$ and then to the final one $|f\rangle$, with a magnetic state different from the one of the initial state. Due to the spin-orbit coupling of $|j\rangle$, spin is influenced. The sign σ_+ represents the absorption of left-polarized photons, σ_- denotes the emission of left-polarized photons.

durations were nanoseconds. But it is not valid for pulses of subpicosecond duration and times larger than the pulse duration.

In order to obtain the effective Hamiltonian for a system, the transition amplitudes between the initial, intermediate, and final states should be calculated and summed. Thus, the simplest possible system, for which the effective Hamiltonian can be calculated is a three-level system as depicted in Fig. 2.2.

Due to some internal or external magnetic field all spins in the system are aligned in one direction. In order to produce magnetic changes in the system, it should be excited with circularly-polarized light propagating in a direction, not parallel to the initial spins alignment. If the light propagation direction is chosen as the axis of quantization, the ground state is a mixture of spin-up and -down states. The intermediate states of the system mix the orbital momentum and spin, which results in final states having different magnetic quantum numbers from the initial ones. This means that the spin-orbit coupling split the excited states with different combinations of $|M_L + 1, \uparrow\rangle$ and $|M_L + 1, \downarrow\rangle$ (M_L is the projection of the orbital moment of the initial state). Selection rules and dipole matrix elements for the transition with circularly-polarized light to the excited state are different for each spin component [35]. Thereby, the spin of the electron is influenced by the virtual state. After the emission of a photon, the electron arrives to a state with spin components different from the initial ones. This mechanism will be discussed in detail in the next Chapter.

This three-level system will be used to demonstrate the discrepancies in describing the subpicosecond laser excitation to obtain the effective Hamiltonian and to derive the induced magnetization. Although, the system is far from

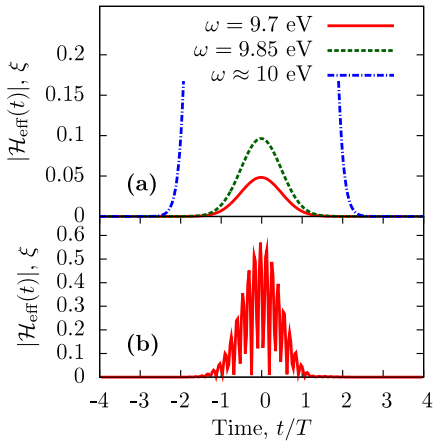

Figure 2.3: (a) Time evolution of the amplitude of the effective Hamiltonian (2.26) at different laser frequencies. (b) The time evolution of the amplitude of the effective Hamiltonian (2.35) at the laser frequency $\omega_0 = 9.7$ eV.

a realistic one, the results of such comparison are general, and the temporal behavior of the functions presented further would be similar for a many levels system.

First, the time evolutions of the amplitudes of both effective Hamiltonians (2.26) and (2.35) are calculated for the excitation by a Gaussian-shaped laser pulse that is 100 fs long ($T = 10^{-13}$ sec). The results are plotted in Fig. 2.3(a) and (b), respectively, in units of energy $\xi = \mathcal{E}^2 d_{ij} d_{jf} T$. The amplitude can be estimated with the following reasonable assumptions: if the dipole matrix elements are of the order of 1 a.u. (≈ 53 pm) and the electric field amplitude is about 10^7 V/m, which is a typical value for laser fluences of 10^{11} W/cm^2, then $\xi \approx 10^{-4}$ eV.

When the excitation frequency is off-resonance, Fig. 2.3(a) shows that the amplitudes of function (2.26) reproduce the typical behavior of transition amplitudes. The maximum increases, when the excitation frequency is closer to the resonance. At resonance the function (2.26) simply diverges. It is indicated in Fig. 2.3(a) by a curve taken with a small detuning off resonance: $\omega_0 - \omega_{ij} = 10^{-6}$ eV. This divergence is a manifestation of the importance of the assumption of Pershan *et al.*'s [35] that the excitation frequency must be significantly away from resonances, $|\omega_0 \pm \omega_{ij}| \gg 1/T$.

In Fig. 2.3(b) we depicted the action of the effective Hamiltonian (2.35) only for one excitation frequency namely $\omega_0 = 9.7$ eV, because plots of close-

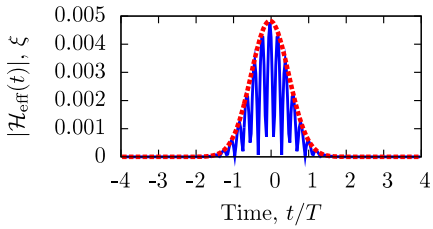

Figure 2.4: Time evolutions of the amplitude of both effective Hamiltonians (2.26) (dashed red) and (2.35) (solid blue) at $T = 10^{-12}$ sec and at the laser frequency $\omega_0 = 9.7$ eV. On this plot the unit ξ is rescaled according to the increased T.

by frequencies overlap in a way that cannot be graphically resolved. The functions at the frequencies $\omega_0 = 9.85$ eV and $\omega_0 = 10$ eV are very similar, the height of the maximum almost does not change, only the positions of the local maxima are different. The amplitudes of Eq. (2.35) are oscillating functions consistent with the presence of the term $\cos \omega_0 t$.

From the plots one can see that at the frequency $\omega_0 = 9.7$ eV the amplitude of the function (2.26) is one order of magnitude smaller than the one of (2.35). Furthermore, the former function is smooth, while the latter is oscillating. The completely different behavior of both functions arises from the fact that the validity condition of the approximation (2.24) is not satisfied for the considered laser pulse, since $T(\omega_{ij} - \omega_0) \approx 10$ for the off-resonance pulses and $\approx 10^{-4}$ for the resonance pulse. The maximum of the function (2.35) is approximately proportional to T, while the one of (2.26) is determined by $2\omega_0/|\omega_{ij}^2 - \omega_0^2|$, leading to the factor of 10 difference between the amplitudes.

Though both functions differ significantly under the chosen conditions, they approach each other with the increase of T. Fig. 2.4 shows both functions for $\omega_0 = 9.7$ eV, when T is one order of magnitude larger. The oscillations of the function (2.35) still remain, because the terms $v_{ij}v_{jf}e^{i(\pm 2\omega_0 + \omega_{if})t}$ were not eliminated in Eq. (2.35).

2.3.3 Induced magnetization

Pershan *et al.* [35] connected the induced magnetization to the effective Hamiltonian via the derivative of the potential function (2.31) with respect to an

external magnetic field H (see Eq. 2.15). Thus,

$$M(t) = -\frac{\partial F}{\partial H} = \sum_{if} \frac{\partial \left(e^{-i\omega_{if}t}\mathcal{H}_{\text{eff}}(t)_{if}\rho_{if}\right)}{\partial H} \propto \sum_{kl} E^*_{0k}(t)E_{0l}(t) \tag{2.36}$$

These equations describe the magnetization induced during the action of the excitation *i.e.* when $\mathbf{E}_0(t)$ and $\mathcal{H}^{if}_{\text{eff}}(t)$ are nonzero. According to relation (2.36), the magnetization is zero after the action of the pulse. The formalism to connect the effective Hamiltonian to the potential function, which would provide the induced magnetization, is correct only if a medium is in thermodynamic equilibrium. It is satisfied if $\mathcal{H}_{\text{eff}}$, and consequently $E^*_{0k}(t)E_{0l}(t)$, change slowly compared to thermal relaxation times of the system.

The situation is very different in the modern experiments demonstrating the ultrafast IFE, where the changes in magnetization are observed after the action pulse. Moreover, the condition of a thermodynamical equilibrium cannot be considered in the ultrafast magnetization experiments, where intensities are very high and the time scales are shorter than any relaxation time of the system. Therefore, the description (2.36) is certainly not applicable to the observations of magnetization dynamics in the recent experiments.

In order to study the time dependence of the magnetization after the action of a fast laser pulse we suggest to calculate the second order wave function $\Psi_2(t)$, which is the third term of the expansion in Eq. (2.20)

$$\Psi_2(t) = \int_{-\infty}^{t} dt'\, e^{i\mathcal{H}_0 t'}\hat{V}e^{-i\mathcal{H}_0 t'} \int_{-\infty}^{t'} dt''\, e^{i\mathcal{H}_0 t''}\hat{V}e^{-i\mathcal{H}_0 t''}\Psi_0. \tag{2.37}$$

Ψ_2 is the wave function, which describes the transitions from the initial state via the excited states to final states. For the three-level system, when the transitions via the intermediate state j result in the final state f with a different magnetic signature from that of i, $\Psi_2(t)$ provides the probability of the change of the magnetic state of the system.

The induced magnetization $M_\alpha(t)$ can be derived from this function with the help of the momentum operators $\hat{j}_\alpha$ (α stays for x, y, z) as follows. If the wave-function of an atomic system is $\widetilde{\Psi}$, then the α component of its magnetization is given by $-\mu_B g_J \cdot \langle\widetilde{\Psi}|\hat{j}_\alpha|\widetilde{\Psi}\rangle/|\widetilde{\Psi}|^2$. The final state f belongs to the same ground state manifold as the initial one, i. Therefore, the total influence of i and the state f on the magnetization should be accounted: $\widetilde{\Psi} = \Psi_0 + \Psi_2$. The induced magnetization is obtained after the subtraction of the

initial magnetization

$$\begin{aligned} M_\alpha(t) =& -\mu_B g_J \left(\frac{\langle \Psi_0 + \Psi_2 | \hat{j}_\alpha | \Psi_0 + \Psi_2 \rangle}{\|\Psi_0 + \Psi_2\|^2} - \frac{\langle \Psi_0 | \hat{j}_\alpha | \Psi_0 \rangle}{\|\Psi_0\|^2} \right) \\ =& -\mu_B g_J \left(\frac{\left(\langle \Psi_0 | \hat{j}_\alpha | \Psi_2 \rangle - \langle \Psi_0 | \Psi_2 \rangle \langle \Psi_0 | \hat{j}_\alpha | \Psi_0 \rangle \right) + c.c.}{\|\Psi_0 + \Psi_2\|^2} \right. \\ &\left. + \frac{\langle \Psi_2 | \hat{j}_\alpha | \Psi_2 \rangle - |\Psi_2|^2 \langle \Psi_0 | \hat{j}_\alpha | \Psi_0 \rangle}{\|\Psi_0 + \Psi_2\|^2} \right). \end{aligned} \tag{2.38}$$

Note that the impact of the $\Psi_1(t)$ to the magnetization was ignored. The magnetization was normalized by the factor $\|\Psi_0 + \Psi_2\|^2$, but not by $\|\Psi_0 + \Psi_2\|^2 + \|\Psi_1(t)\|^2$. This is because the IFE experiments are typically done at frequencies corresponding to the transparency region of a material, where the absorption is very weak[4]. Therefore, the intermediate states can be considered as virtually excited, and the effect of the first order wave function is not taken into account.

Let us now examine the expression for the induced magnetization (2.38). The second order wave function is proportional to $w = \xi T = \mathcal{E}^2 d_{ij} d_{jf} T^2$, and therefore is proportional to the peak intensity of a laser pulse $I_0 \propto \mathcal{E}^2$. Thus, the induced magnetization contains terms of different orders of I_0, starting from the linear one. If the terms higher than the first order are ignored, the induced magnetization can be represented as

$$M_\alpha(t) \approx -\mu_B g_J \left[\left(\langle \Psi_0 | \hat{j}_\alpha | \Psi_2 \rangle - \langle \Psi_0 | \Psi_2 \rangle \langle \Psi_0 | \hat{j}_\alpha | \Psi_0 \rangle \right) + c.c. \right]. \tag{2.39}$$

Thus, $M(t)$ depends linearly on the *peak* intensity. This results from the interference between the initial and final state, which belongs to the same ground state manifold. The same dependence is observed in experiments [3, 4, and the references therein].

However, the time evolution of $M(t)$ does not follow that of the pulse intensity. It is related to the second order wave function $\Psi_2(t)$ instead. The latter is connected to the effective Hamiltonian by the integral

$$\Psi_2(t) = -i \int_{-\infty}^{t} \mathcal{H}_{\text{eff}}(t') dt'. \tag{2.40}$$

Again, the different approaches to calculate the second order wave function are compared considering an excitation by a Gaussian-shaped laser pulse of 100 fs

[4]See, for instance, Ref. [127] and [128] for the optical spectra of orthoferrites and NiO respectively.

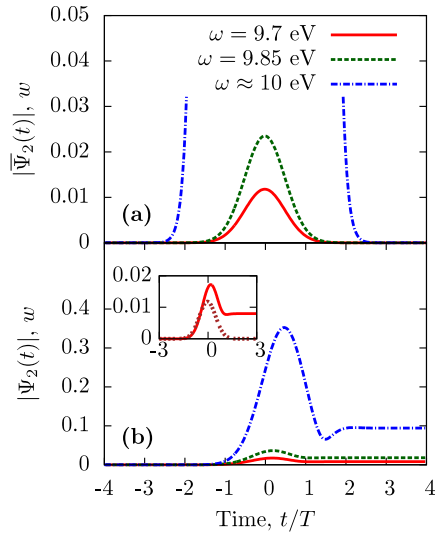

Figure 2.5: (a) The time evolution of the second order wave function $|\overline{\Psi}_2(t)|$ applying the approximation (2.24). (b) The time evolution of the second order wave function $|\Psi_2(t)|$ according to the effective Hamiltonian (2.35). Inset: $|\Psi_2(t)|$ (solid red) and $|\overline{\Psi}_2(t)|$ (dashed brown) at $\omega_0 = 9.7$ eV.

duration. Ψ_2 is calculated for the three-level system using both Hamiltonians (2.26) and (2.35), respectively. The solution resulting from Hamiltonian (2.26) is denoted as $\overline{\Psi}_2$. For its calculation, the approximation (2.24) was applied, which is consistent with the derivation of Hamiltonian (2.26).

The time evolutions of $|\overline{\Psi}_2|$ and $|\Psi_2|$ are plotted in Figs. 2.5(a) and (b), respectively, in the dimensionless units $w = \xi T$. The evolution of $\overline{\Psi}_2$ is proportional to the effective Hamiltonian (Fig. 2.5(a)) and thus it has the same functional dependence as the potential function in Eq. (2.31). This confirms that the functional F can be used to calculate the magnetization under the conditions, when assumption (2.24) is applicable. $\overline{\Psi}_2$ goes to zero after the excitation is finished, and so is the induced magnetization, which is compatible with Eq. (2.31).

Except at resonance, the functions $|\overline{\Psi}_2|$ and $|\Psi_2|$ exhibit the same behavior during the first half of the pulse (see the inset of Fig. 2.5(b)), but the key difference is that the function $|\Psi_2|$ is nonzero after the action of the pulse. This means that the system remains in an altered state, *i.e.* with an altered magnetization, after the laser pulse has faded away. Therefore, $\Psi_2(t)$ is able

to describe the magnetization dynamics after the excitation in the ultrafast magnetization experiments.

In order to calculate $\Psi_2(t)$ and $M(t)$ in a solid state correctly, the wave functions, which describe all transitions over excited levels j and final states f, which would effect the spin, should be summarized $\Psi_2(t) = \sum_{jf} \Psi_2^{jf}(t)$. It means that the excited states should be accurately investigated in a real material, and the transition amplitudes to any possible final states of the ground state manifold should be calculated. However, the simple system presented here does not influence the conclusions on the temporal behavior of the effective Hamiltonian and magnetization, which is the main concern of this Chapter.

The main result concerning the time-dependence of the magnetization is that it is determined by the function $\Psi_2(t)$ and has the similar behavior, as depicted on the Fig. 2.5. The magnetization changes during the action of the pulse, and remains altered after the action. The time evolution of $\mathbf{M}(t)$ in the ultrafast regime is completely different from that expected from the relation $-i\chi\mathbf{E}^*(t) \times \mathbf{E}(t)$, but approaches it with increasing T (see the discussion of Eq. (2.35)). However, the induced magnetization $M(t)$ depends still linearly on the light fluence/*peak* intensity.

It also can be concluded that, since the function $\Psi_2(t)$ depends strongly on the ultrashort laser pulse properties (such as shape or frequency) in the ultrafast regime, the same should be true for the induced magnetization. This statement is supported by the observation of Iida *et al.* in Ref. [122]. They obtained that the initial phase and amplitude of the probe pulse polarization oscillation, which is proportional to the induced magnetization, depends on the pump wavelength. This result opens large opportunities for tuning spin dynamics by adjusting laser properties.

To sum up, the approximations used to develop the theory of the IFE in Refs. [32,35,36,117] are not applicable to the recent ultrafast experiments. The induced magnetization due to the IFE cannot be extracted from the potential function (2.31) in the regime of a subpicosecond excitation ($T \sim 1/\Delta\omega$). Under these circumstances, the effective Hamiltonian must be integrated over time to obtain the wave function describing the transitions, which cause the change of the magnetic state. Thus, the change of magnetization after the action of an ultrashort laser pulse can be obtained solving the time-dependent Schrödinger equation up to the second order of $1/c$ without further approximations.

The interpretation of the IFE as the generation of an effective magnetic field does not hold for the ultrafast excitation. Instead, it should be interpreted as a system coherently brought to a new magnetic state by laser induced transitions:

from the initial to the intermediate state and from the intermediate to the final state with different magnetic state from the initial one. The system remains in this non-equilibrium state, which results in the precession of magnetization and relaxation processes observed after the excitation.

Similar considerations concerning the validity of classical interpretations can be applied to other magneto-optical effects (such as the magneto-optical Kerr effect, the Faraday effect, *etc*). Most of relations to describe these effects are derived from thermodynamical functionals. However it is demonstrated here that magnetization dynamics should be treated differently in (sub-)picosecond and nanosecond time regions. Thus, the relations for the magneto-optical effects should be reconsidered in view of different experimental conditions.

2.4 The IFE-1 and IFE-2 processes

The inverse Faraday effect was predicted by Pitaevskii [32] and was defined by him as "magnetization of a transparent medium induced by oscillating electric field". It was derived by differentiation of the thermodynamical potential with respect to an external magnetic field. The quantum mechanical description was provided by Pershan *et al.* in Ref. [35]. It is based on an effective Hamiltonian derived from the time-dependent Schrödinger equation up to the second order. The effective Hamiltonian describes the interaction of light with a transparent medium. Since the assumption that the laser intensity "changes slowly compared to thermal relaxation times of the system" was meaningful for the experimental conditions at that times [36], it was possible to derive a potential function from this Hamiltonian. Pershan *et al.* showed that the induced magnetization is a derivative of this potential. Their formulation of the effect was "the IFE consists of a magnetization induced by circularly polarized light in a nonabsorbing material". Therefore, the IFE according to Pitaevskii and Pershan *et al.*'s formalisms consist of two processes, which come together: (IFE-1) interaction of light with a transparent magnetic medium; (IFE-2) this interaction produces a quasi-stationary relaxed state, which leads to the creation of magnetization in the sample.

The IFE-2 takes place, if the intensity "changes slowly compared to thermal relaxation times of the system". In this case the interaction of light with a medium leads to a new thermal equilibrium, because IFE-1 keeps changing the magnetic state of the system and the system has enough time to relax according to the new conditions. This quasi-stationary state exists only during the presence of the excitation. The IFE-2 process does not take place in the

ultrafast magnetization experiments, because the action of the laser pulses is shorter than any relaxation times of a system, and the effects observed in the modern experiments do not represent the IFE according to its classical definition.

However, a kind of the IFE-2 valid for the ultrafast dynamics would be the IFE-2uf process. The IFE-2uf takes place because the system is brought away from its ground magnetic state by transitions induced by circularly-polarized laser light. The system has to react to being in this new state, thus a magnetic precession starts. There are also some decay processes observed in the next several tens of picoseconds due to relaxation or damping processes. The term "ultrafast IFE" should be meant by the combination of the IFE-1 and IFE-2uf processes.

Magnetization dynamics after the excitation, *i.e.* IFE-2uf process, is straightforwardly accessed in the experiments. Magnetic precessions are the usual target for the problem of all-optical manipulation of magnetic order [4, and the references therein]. However, these effects are determined by the action of a laser light on the system, *i.e.* by the IFE-1 process. Therefore, it is essential to get insight into and characterize the IFE-1 in order to control the subsequent dynamics.

The IFE-1 process incorporates coherent spin excitations due to the stimulated Raman scattering process. The next Chapter is concentrated on the study of the mechanism of a change of a spin state via optically induced transitions.

Chapter 3

Mechanism of the ultrafast IFE due to the spin-orbit coupling

3.1 Introduction

In this Chapter, a detailed insight into the mechanism of the change of a magnetic state due to the stimulated Raman scattering process triggered by a circularly polarized laser pulse is given. In this process a laser pulse stimulates an optical transition from the ground state to a virtual excited state. Via the transition to the virtual state, the magnetic state of the electron brought back to the ground state is changed. This process is simulated at the femtosecond time scale and the mechanism of optically induced magnetic state changes due to circularly polarized light is investigated.

The spin dynamics, which accompanies this process, and its dependence on system and laser pulse properties are studied. It is shown in this Chapter that a system is brought to a new magnetic state after the action of an ultrashort laser pulse. The magnetization dynamics after the excitation by a laser is caused by the fact that the system is not in the initial state anymore.

It was shown in Chapter 2 that the standard expression $\mathbf{M}(t) \propto \mathbf{E}^*(t) \times \mathbf{E}(t)$, which connects the induced magnetization $\mathbf{M}(t)$ with the generating electric field $\mathbf{E}(t)$ is not applicable for subpicosecond pulses. Therefore, the time-dependence of the induced magnetization requires much deeper understanding for the interpretation of the experiments done at subpicosecond time scale. In this Chapter, the time evolution of $\mathbf{M}(t)$ for atomic systems during and after the presence of an ultrafast laser pulse is calculated, and its dependence on laser pulse properties is studied. It is shown that the magnetization is nonzero after the excitation, as observed in experiments.

The role of spin-orbit coupling (SOC) for the ultrafast IFE is discussed. It is commonly accepted that SOC is necessary for magneto-optical effects [33]. However, it is unclear what is the exact function of this interaction for the process. It is also open to question what happens when the spectral width of a laser pulse is of the order of SOC and whether it limits the pulse duration required for the effect. To answer these questions, a detailed study of the laser-induced spin dynamics in a system with SOC is performed. A simple model, in which SOC is the only spin-dependent interaction, allows to reveal the pure contribution of this interaction.

Throughout this Chapter, the action of a laser pulse with an electric field $\mathbf{E}$ varying with a frequency ω_0:

$$\mathbf{E} = -\mathbf{n}\mathcal{E} f(t/T - \mathbf{r}/(cT)) \sin(\omega_0 t), \tag{3.1}$$

on electronic systems with spatial extend much smaller than the wavelength $\lambda_0 = c/\omega_0$ is considered, therefore, the spatial dependence of the laser pulse is ignored. $\mathcal{E}$ is the time-independent part of the amplitude of the electric field, $\mathbf{n}$ is perpendicular to the direction of propagation and the function $f(t/T - \mathbf{r}/(cT))$ describes the time and spatial dependence of the amplitude of the electric field. A Gaussian-shaped laser pulse is chosen: $f(t/T) = e^{-t^2/T^2}/\sqrt{\pi^3}$ (3D-normalized). The laser pulse considered is circularly left-polarized, propagating in the z direction, *i.e.* $\mathbf{n} = (\mathbf{n}_x + i\mathbf{n}_y)/\sqrt{2}$, $\mathbf{n}_x$ and $\mathbf{n}_y$ are the unit vectors in the x and y directions. Therefore,

$$\mathbf{E} = -(\mathbf{n}_x + i\mathbf{n}_y)\mathcal{E} e^{-t^2/T^2} \sin(\omega_0 t)/\sqrt{2\pi^3}. \tag{3.2}$$

The factor T equal to 100 fs ($T = 10^{-13}$ s) and laser fluence $E_{\text{fl}} \approx 2$ mJ/cm^2 are taken, if not otherwise declared. The former parameter corresponds to the pulse duration at FWHM of the electric field amplitude of approximately 170 fs and the pulse duration at FWHM of the pulse intensity of 117 fs. The latter is typically referred to as simply "the pulse duration". The spectral width at FWHM of the spectral density (see Eq. (B.5)) is ≈ 15 meV. The amplitude $\mathcal{E}$ is $\approx 10^9$ V/m and peak intensity $I_0 \approx 5 \times 10^9$ W/cm^2 at the chosen values of the pulse fluence and duration.

Most of results of this Chapter are published in Ref. [129] and are reused with the permission from Daria Popova, Andreas Bringer and Stefan Blügel.

3.2 Magnetization via the stimulated Raman scattering process

3.2.1 The action of a laser field on an electronic system

Let me briefly recall the approach to describe the action of the electric field **E** on the system, which is introduced in Chapter 2. The electric field is related to the vector potential [130]

$$\mathbf{E} = -\frac{1}{c}\mathbf{A}'. \tag{3.3}$$

The vector potential obeys the wave equation

$$\Delta\mathbf{A} = \left(\frac{\partial}{c\partial t}\right)^2 \mathbf{A} = \frac{1}{c^2}\mathbf{A}'' \quad ; \quad \nabla\mathbf{A} = 0. \tag{3.4}$$

This equation is fulfilled, when the spatial extent of the wave train, cT is large compared to the wavelength λ_0.

An unpertubed electronic system is described by the Hamiltonian $\mathcal{H}_0$

$$\mathcal{H}_0 = \sum_\alpha \mathbf{p}_\alpha^2/2 + \mathcal{V}_{\text{int}}. \tag{3.5}$$

$\mathbf{p}_\alpha$ is the momentum of an electron, $\mathcal{V}_{\text{int}}$ is the sum of the kinetic energy of nuclei, the interaction energy between electrons and nuclei and mutual Coulomb energy of the electrons and nuclei. The interactions, which are important for effects on the spin of the electrons, such as the spin-orbit- and Zeeman interactions, must be also included to $\mathcal{V}_{\text{int}}$. The summation is over all electrons in the system, the mass and charge of an electron and Planck's constant are set to 1 (atomic units).

Wave functions of a perturbed electronic system are found by the solution of the time-dependent Schrödinger equation. The momentum operator is replaced by $\mathbf{p} - \mathbf{A}/c$ and the equation of motion for an electronic wave function Ψ is

$$i\frac{\partial\Psi}{\partial t} = \left[\sum_\alpha \left(\mathbf{p}_\alpha - \mathbf{A}(\mathbf{r}_\alpha, t)/c\right)^2/2 + \mathcal{V}_{\text{int}}\right]\Psi \tag{3.6}$$

The solution is the expansion

$$\Psi(t) = e^{-i\mathcal{H}_0 t}\left(\Psi_0 + \Psi_1(t) + \Psi_2(t) + \cdots\right). \tag{3.7}$$

The Raman process, which is of interest, is of the second order in the inverse speed of light $1/c$. Therefore, the terms up to the third one in the expansion

(3.7) are important. They are derived in Appendix A.3.1 for a Gaussian-shaped laser pulse.

It is shown in Appendix A.2 that, in the case of a discrete spectrum, the first order wave function describes one photon transitions from the initial state i of a system to all possible final states j. It can be expressed as a summation over the j states

$$\Psi_1(t) = \sum_j d_{ij}\Gamma_j^{(1)}(t)|\phi_j\rangle, \tag{3.8}$$

$d_{ij} = \langle\phi_j|\mathbf{n}\cdot\sum_\alpha \mathbf{r}_\alpha|\Psi_0\rangle$ is the dipole matrix element of the transition from the ground state i to a final state j, ϕ_j is the wave function of the j state, the time-dependence of $\Psi_1(t)$ is introduced by the function $\Gamma_j^{(1)}(t)$.

The second order wave function, which would provide the induced magnetization due the ultrafast IFE, is the summation over all possible intermediate j and final f states, to which the transitions are allowed

$$\Psi_2(t) = \sum_{jf} d_{ij}d_{jf}\Gamma_{jf}^{(2)}(t)|\phi_f\rangle. \tag{3.9}$$

The time-dependent function $\Gamma_{jf}^{(2)}(t)$ for the excitation by a Gaussian-shaped laser pulse is derived in Appendix A.3.1

$$\begin{aligned}\Gamma_{jf}^{(2)}(t) =& \frac{2(\varepsilon_f-\varepsilon_j)(\varepsilon_j-\varepsilon_i)}{\sqrt{\pi}}\left(\frac{\mathcal{E}T}{2\pi\omega_0}\right)^2 \\ &\times\int_{-\infty}^{t}dt'\Bigg[e^{i(\varepsilon_f-\varepsilon_j)t'}\cos(\omega_0 t')e^{-t'^2/T^2} \\ &\times\Bigg[e^{-\frac{\left(T\left(\omega_{ij}+\omega_0\right)\right)^2}{4}}\operatorname{erfc}\left(\frac{i}{2}T\left(\omega_{ij}+\omega_0\right)-\frac{t'}{T}\right) \\ &+e^{-\frac{\left(T\left(\omega_{ij}-\omega_0\right)\right)^2}{4}}\operatorname{erfc}\left(\frac{i}{2}T\left(\omega_{ij}-\omega_0\right)-\frac{t'}{T}\right)\Bigg]\Bigg],\end{aligned} \tag{3.10}$$

ε_i, ε_j and ε_f are the energies of the initial i, an intermediate j and a final state f, $\omega_{kl} = \varepsilon_l - \varepsilon_k$.

3.2.2 Laser induced magnetization

It is shown in Chapter 2 (see Eq. 2.38) that the laser induced magnetization $\mathbf{M}(t)$ via the stimulated Raman scattering transitions is related to the second order wave function $\Psi_2(t)$ as

$$\Delta\mathbf{M}(t) \propto \frac{\langle\Psi_0+\Psi_2(t)|\boldsymbol{\sigma}|\Psi_0+\Psi_2(t)\rangle}{|\Psi_0+\Psi_2(t)|^2} - \langle\Psi_0|\boldsymbol{\sigma}|\Psi_0\rangle, \tag{3.11}$$

where $\Psi_2(t)$ includes the summation over the final states f belonging to the ground state multiplet (see Eq. (3.9)). $\boldsymbol{\sigma}$ denotes Pauli matrices:

$$\sigma_x = \begin{pmatrix} 0 & 1 \\ 1 & 0 \end{pmatrix}, \quad \sigma_y = \begin{pmatrix} 0 & -i \\ i & 0 \end{pmatrix}, \quad \sigma_z = \begin{pmatrix} 1 & 0 \\ 0 & -1 \end{pmatrix} \tag{3.12}$$

Nonzero $\Delta\mathbf{M}(t)$ is provided by the condition $\Psi_0 \not\propto \Psi_2(t)$. Thus, an interaction, which lifts the degeneracy of spin components regarding the excitation, is required for magnetization to change. This is provided by the spin-orbit coupling (SOC), which mixes spin and orbital momentum during the transitions, as will be shown below.

3.2.3 Spin-orbit coupling

SOC is the interaction of a particle motion with its spin. For an electron, it is the coupling between the electron spin and orbital momentum. The SOC is a relativistic effect, thus it is provided by the Hamiltonian

$$\mathcal{H}_0 = c\boldsymbol{\alpha}(\mathbf{p} - \frac{1}{c}\widetilde{\mathbf{A}}) + \beta c^2 + \widetilde{\phi} \tag{3.13}$$

$\widetilde{\mathbf{A}}$ and $\widetilde{\phi}$ are the vector and scalar potentials of the electric field of an electron. $\beta = \begin{pmatrix} \mathbf{1} & 0 \\ 0 & \mathbf{-1} \end{pmatrix}$, $\mathbf{1} = \begin{pmatrix} 1 & 0 \\ 0 & 1 \end{pmatrix}$, $\boldsymbol{\alpha} = \begin{pmatrix} \boldsymbol{\sigma} & 0 \\ 0 & \boldsymbol{\sigma} \end{pmatrix}$. Ignoring the part of the Hamiltonian describing positrons, Eq. (3.13) becomes

$$\mathcal{H}_0 = \left[c^2 + \frac{1}{2}\left(\mathbf{p} - \frac{\widetilde{\mathbf{A}}}{c}\right) - \frac{p^4}{8c^2}\right] + \widetilde{\phi} - \frac{1}{2c}\boldsymbol{\sigma}\cdot\widetilde{\mathbf{H}} - \frac{1}{8c^2}\nabla\cdot\mathbf{E} + \mathcal{H}_{\mathrm{SOC}}, \tag{3.14}$$

$$\mathcal{H}_{\mathrm{soc}} = \left[-\frac{i}{8c^2}\boldsymbol{\sigma}\cdot\nabla\times\widetilde{\mathbf{E}} - \frac{1}{4c^2}\boldsymbol{\sigma}\cdot\widetilde{\mathbf{E}}\times\mathbf{p}\right], \tag{3.15}$$

$\widetilde{\mathbf{E}}$ and $\widetilde{\mathbf{H}}$ are electric and magnetic internal fields. If electric field $\widetilde{\mathbf{E}}$ is center-symmetric, then $\nabla\times\widetilde{\mathbf{E}} = 0$ and $\widetilde{\mathbf{E}} = -(\mathbf{r}/r)(\partial V/\partial r)$, leading to

$$\mathcal{H}_{\mathrm{soc}} = \frac{1}{4c^2 r}\frac{\partial V}{\partial r}\boldsymbol{\sigma}\cdot\mathbf{r}\times\mathbf{p} = \frac{1}{4c^2 r}\frac{\partial V}{\partial r}\boldsymbol{\sigma}\cdot\mathbf{L} = -\zeta_{\mathrm{soc}}\mathbf{S}\cdot\mathbf{L} \tag{3.16}$$

The role of SOC for the ultrafast IFE will be studied further. It will be shown that this interaction is necessary for the effect.

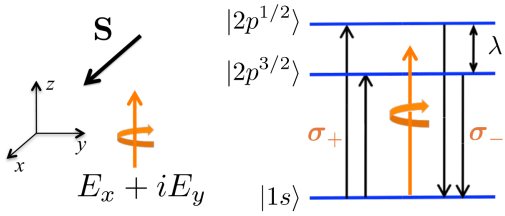

Figure 3.1: The single spin system excited by a circularly left polarized pulse in the Voigt geometry. The process designated as $\boldsymbol{\sigma}_+$ is the absorption of a left-polarized photon. $\boldsymbol{\sigma}_-$ is the emission of a left-polarized photon.

3.3 Single spin system excited by polarized laser light

The study starts with the most simple system, which will provide an insight into the optical process leading to magnetic state changes. The system consists of one electron excited by circularly polarized light. The role of only one interaction, SOC, for the ultrafast IFE will be first considered. This will provide a clear basis for the study of the mechanism leading to optically induced magnetization changes. The systems will become more complicated and the other electron interactions will be gradually included in the course of the thesis.

Let us consider a single spin system (hydrogen atom-like model) excited by the laser pulse with the electric field (3.2) (see Section 3.1). The system is initially in the ground $1s$ state with the spin $\mathbf{s}_0$ aligned initially in the x direction ($s_{0x} = 1/2$), which is perpendicular to the laser pulse propagation direction.

The action of the laser pulse on the system magnetic state is given by the second order wave function $\Psi_2(t)$. This function is determined by laser pulse and system properties. The calculation of $\Psi_2(t)$ requires the knowledge of dipole matrix elements of the transitions from the initial state to possible intermediate states and from the intermediate states to the final states, as well as the energies of the excited states and ground states should be calculated (see Eqs. (3.9) and (3.10)). Thus, the unperturbed Hamiltonians of both ground state multiplet and excited states should be diagonalized to derive the induced magnetization via the stimulated Raman scattering process.

If the quantization axis is chosen in the light propagation direction, then

the wave function of the initial state is

$$\Psi_0 = Y_{00} R_{1s} \begin{pmatrix} \frac{1}{\sqrt{2}} \\ \frac{1}{\sqrt{2}} \end{pmatrix}, \tag{3.17}$$

Y_{00} and R_{1s} are the radial and spherical part of the $1s$ state wave-function. It is assumed that the laser frequency ω_0 is close to the resonance frequency between $1s$ and $2p$ states, and the contribution from the transitions to the other p states can be ignored. The circularly polarized pulse excites the Raman transition from the $1s$ state via the $2p$ state, back to the $1s$, thereby, the spin state in the $1s$ should be changed (Fig. 3.1). A noticeable spin-orbit coupling (SOC), which is about two orders of magnitude higher than in a real hydrogen atom, is included to the excited state.

It is shown in the Appendix C.1 that in the presence of the SOC, the $2p$ state is split into two levels, $2p^{3/2}$ and $2p^{1/2}$ with the total magnetic momentum $J = 3/2$ and $J = 1/2$, repectively, where $\mathbf{J} = \mathbf{S} + \mathbf{L}$. The energy of splitting λ equals to $(3/2)\zeta_{\text{soc}}$. The level $2p^{3/2}$ is below the position of $2p$ and has the energy $\varepsilon_{2p^{3/2}} = \varepsilon_{2p} - (1/3)\lambda$. The level $2p^{1/2}$ is above $2p$ and has the energy $\varepsilon_{2p^{1/2}} = \varepsilon_{2p} + (2/3)\lambda$. The energy of $2p$ is chosen equal to that of a real hydrogen atom. If not otherwise stated, $\lambda = 27.2$ meV is taken.

3.3.1 The second order wave function

$\Psi_2(t)$ due to the excitation by the circularly polarized laser pulse is derived in Appendix C.1

$$\Psi_2(t) = \left(\frac{\mathcal{E} d_0 T}{2\pi}\right)^2 \frac{1}{\sqrt{2}} \begin{pmatrix} \Gamma^{(2)}_{3/2}(t) \\ \frac{1}{3}\,\Gamma^{(2)}_{3/2}(t) + \frac{2}{3}\,\Gamma^{(2)}_{1/2}(t) \end{pmatrix} Y_{00} R_{1s}, \tag{3.18}$$

see Appendix C.1 for the definition of d_0. The functions $\Gamma^{(2)}_{3/2}(t)$ and $\Gamma^{(2)}_{1/2}(t)$ are the time-dependent parts, which enter Eq. (3.9), which describe the transitions involving the intermediate states $2p^{3/2}$ and $2p^{1/2}$, respectively. These functions depend on the energies of initial, intermediate and final states. Since it is assumed that the SOC in the system is considerable, and the $2p$ state is split, $\Gamma^{(2)}_{3/2}(t) \neq \Gamma^{(2)}_{1/2}(t)$.

The second order wave-function (3.18) is a spinor with non-equal time-dependent spin-up and -down parts ($\Gamma^{(2)}_{3/2}(t) \neq \frac{1}{3}\,\Gamma^{(2)}_{3/2}(t) + \frac{2}{3}\,\Gamma^{(2)}_{1/2}(t)$). It means, that the spin does not remain in the x direction (the corresponding spinor would have equal up- and down-parts, see Eq. (3.17)), but performs a rotation. If there were no SOC splitting of the excited state, $\Gamma^{(2)}_{3/2}(t)$ would be equal to

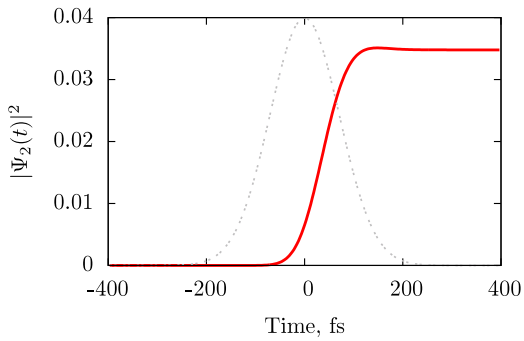

Figure 3.2: The time evolution of the probability of the Raman scattering process at $\lambda \approx 27$ meV. The gray line represents the time evolution of the electric field amplitude.

$\Gamma^{(2)}_{1/2}(t)$, leading to equal spin-up and -down parts of the second order wave function. In this case, the spin would remain in the x direction. Thus, the SOC leads to distinct transition amplitudes for the spin-up and -down components of a spin, thereby the population of a one spin component is transferred to the opposite component after the stimulated Raman scattering process.

The time evolution of the function $|\Psi_2(t)|^2$, which is the probability of the Raman scattering process, is depicted on Fig. 3.2 at laser frequency $\omega_0 = \omega_{1s,2p^{1/2}} - \lambda/2 = \omega_{1s,2p^{3/2}} + \lambda/2$, *i.e.* between the resonance frequency $\omega_{1s,2p^{1/2}} = (\varepsilon_{2p^{1/2}} - \varepsilon_{1s})$ of the $1s$ with the $2p^{1/2}$ state, and the resonance frequency $\omega_{1s,2p^{3/2}} = (\varepsilon_{2p^{3/2}} - \varepsilon_{1s})$ of the $1s$ with the $2p^{3/2}$ state. $|\Psi_2(t)|^2$ is zero before the action of the pulse begins, changes smoothly during the excitation and remains non-zero after the pulse is gone. The time evolution of magnetization follows that of $\Psi_2(t)$, and consequently of $|\Psi_2(t)|^2$, meaning that the spin rotates while the system undergoes the stimulated Raman scattering process. Since $\Psi_2(t)$ is nonzero after the action of the pulse, in the end the spin is rotated relative to the initial position.

Spin rotation by this process is possible, if a system is excited by circularly or elliptically (not linearly) polarized light. It is shown in Appendix C.2 that the second order wave function is proportional to $\begin{pmatrix} \frac{1}{\sqrt{2}} \\ \frac{1}{\sqrt{2}} \end{pmatrix}$ in the case of the excitation by linearly polarized light, which means that the spin is remaining in the x direction. The same condition is necessary for the stationary IFE as well.

Another condition for spin rotation is that the initial alignment of the spin

should be not parallel to the light propagation direction. For example, if the spin is pointing in the $+z$ direction initially, then the wave function of the initial state is $\Psi_0 \propto \binom{1}{0}$. Since the spin-down spinor is not populated, transitions to the spin-down state are not possible and $\Psi_2 \propto \binom{1}{0}$. Thus, transitions from both spin states must take place to transfer the population from one spin state to another, which is possible if spin is not parallel to the propagation direction of a laser pulse, which has unequal left- and right-circularly polarized components[1].

3.3.2 The probability of the spin-flip and induced magnetization

The goal of this subsection is to study the dependence of the efficiency of the ultrafast IFE on the system and laser pulse parameters. A good characteristics would be the probability of the spin-flip, $w_{\text{s-f}}(t)$, that the spin is in the reversed position relative to the initial one. It is given by the projection of the wave function on the $1s$ state with the spinor $\frac{1}{\sqrt{2}}\binom{1}{-1}$, corresponding to a spin in the $-x$ direction,

$$w_{\text{s-f}}(t) = \frac{\left|\langle \Psi_2(t)|1s, \frac{1}{\sqrt{2}}\binom{1}{-1}\rangle\right|^2}{|\Psi_0 + \Psi_2(t)|^2}, \tag{3.19}$$

where it is taken into account that the projection of Ψ_0 onto $|1s, \frac{1}{\sqrt{2}}\binom{1}{-1}\rangle$ are zero.

Let us first study, how $w_{\text{s-f}}(t)$ is related to the induced magnetization. The latter is given by the relation

$$\Delta\mathbf{M}(t) = \mu_S(\mathbf{S}(t) - \mathbf{S}_0), \tag{3.20}$$

where μ_S is the spin magnetic moment, which equals to -1 in atomic units. $\mathbf{S}_0 = (S_{0x}, S_{0y}, S_{0z})$ and $\mathbf{S}(t) = (S_x(t), S_y(t), S_z(t))$, where S_{0x}, S_{0y}, S_{0z} and $S_x(t)$,$S_y(t)$, $S_z(t)$ are the expectation values of $\hat{S}_x$, $\hat{S}_y$ and $\hat{S}_z$ operators in the initial state and during the excitation, respectively. $\mathbf{S}_0$ is simply $(1/2, 0, 0)$. The expectation values during the excitation, $S_\alpha(t)$ (α is x, y and z), are given by

$$S_\alpha(t) = \frac{1}{2}\frac{\langle \Psi_0 + \Psi_2(t)|\sigma_\alpha|\Psi_0 + \Psi_2(t)\rangle}{|\Psi_0 + \Psi_2(t)|^2}, \tag{3.21}$$

where σ_α are the Pauli matrices. $\mathbf{S}(t)$ will be referred to as the "spin vector".

[1]Linearly polarized light can be represented as a sum of equal left- and right-circularly polarized components.

The magnitude of $\Delta\mathbf{M}(t)$ can be found by[2]

$$|\Delta\mathbf{M}(t)| = \sqrt{(S_x(t)-S_{x0})^2+(S_y(t)-S_{y0})^2+(S_z(t)-S_{z0})^2} = \tag{3.22}$$
$$= \sqrt{\left(S_x(t)-\frac{1}{2}\right)^2+S_y^2(t)+S_z^2(t)} = \sqrt{\frac{1}{2}-S_x(t)}.$$

On the other hand, if $\Psi_0+\Psi_2(t)=\begin{pmatrix}\psi_1(t)\\ \psi_2(t)\end{pmatrix}$,

$$w_{\text{s-f}}(t) = \frac{1}{2}\frac{|\psi_1(t)-\psi_2(t)|^2}{|\Psi_0+\Psi_2(t)|^2} = \frac{1}{2}\left(\frac{|\psi_1|^2+|\psi_2|^2}{|\Psi_0+\Psi_2(t)|^2} - \frac{\psi_1^*(t)\psi_2(t)+\psi_1(t)\psi_2^*(t)}{|\Psi_0+\Psi_2(t)|^2}\right)$$
$$= \frac{1}{2}\left(\frac{|\Psi_0+\Psi_2(t)|^2}{|\Psi_0+\Psi_2(t)|^2} - \frac{\langle\begin{pmatrix}\psi_1(t)\\ \psi_2(t)\end{pmatrix}|\sigma_x|\begin{pmatrix}\psi_1(t)\\ \psi_2(t)\end{pmatrix}\rangle}{|\Psi_0+\Psi_2(t)|^2}\right) = \frac{1}{2}-S_x(t). \tag{3.23}$$

Thus, the spin-flip probability for the current system is related to the magnitude of the induced magnetization by $w_{\text{s-f}}(t)=|\Delta\mathbf{M}(t)|^2$.

Both spin-flip probability and induced magnetization are constant and non-zero at the time τ_{p}, when the action of the pulse finishes ($\mathbf{E}(t>\tau_{\text{p}})=0$). The magnitude of the induced magnetization after the excitation, $|\Delta\mathbf{M}(\tau_{\text{p}})|$, could be chosen as the characteristics of the IFE efficiency. However, it is not a constant value in the case, when oscillations of magnetization are induced. Thus, the final spin-flip probability, $w_{\text{s-f}}(\tau_{\text{p}})$, will be considered. $\tau_{\text{p}}=4T=400$ fs is taken, which corresponds to the time, when the factor e^{-t^2/T^2}, describing the time-dependence of the pulse amplitude, becomes negligible.

Dependence on the spin-orbit coupling

Fig. 3.3 shows $w_{\text{s-f}}(\tau_{\text{p}})$ depending on the excitation frequency at three different values of SOC. It can be seen that the SOC plays a crucial role for $w_{\text{s-f}}(\tau_{\text{p}})$. The spin-flip probability is decreased at low values of the SOC. With the increase of SOC, it becomes larger and two peaks at the frequencies $\omega_0=\omega_{2p^{3/2}}=\varepsilon_{2p}-\lambda/3$ and $\omega_0=\omega_{2p^{1/2}}=\varepsilon_{2p}+2\lambda/3$ develop. If the SOC is very large, then the probability of the effect is quite low for the excitation frequencies between $\omega_{2p^{3/2}}$ and $\omega_{2p^{1/2}}$.

It follows from Eq. (3.18) that if $\lambda=0$, no rotation of the spin would be observed. Zero or negligible SOC means that $\varepsilon_{2p^{3/2}}\approx\varepsilon_{2p^{1/2}}$ and, consequently, $\Gamma^{(2)}_{3/2}(t)\approx\Gamma^{(2)}_{1/2}(t)$. Therefore, at any time t the spin-up and -down parts of the spinor (3.18) would be equal to each other, which is the condition that the

[2]The expression S_α^2 should be understood as $\langle S_\alpha\rangle^2$, but not as $\langle S_\alpha^2\rangle$.

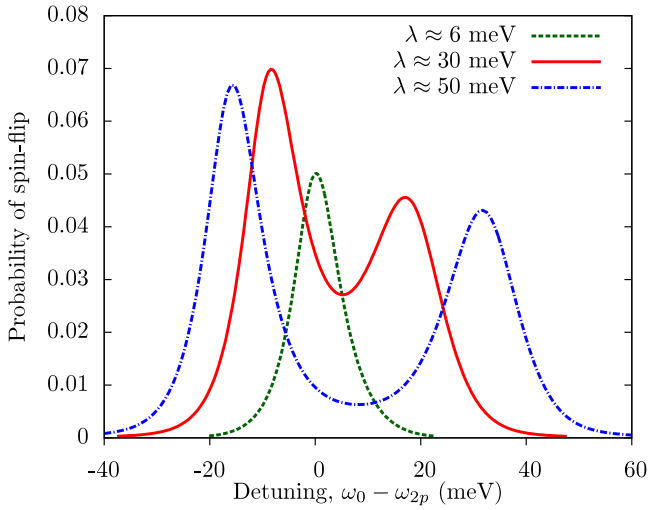

Figure 3.3: The total probability of the spin-flip after the action of the laser pulse depending on the frequency of excitation at different values of λ.

spin is in the x direction, and no rotation would be observed. It explains why if λ is too low, the effect starts to disappear. However, if the SOC is much higher than the pulse spectral width (≈ 15 meV), two peaks become isolated.

Dependence on the laser pulse parameters

It follows from Eq. (3.18) that $\Psi_2(t)$ is proportional to the squared product of the electric field amplitude and the pulse duration, $(\mathcal{E}T_{\rm dr})^2 \propto (\mathcal{E}T)^2$, therefore, the spin-flip probability should be proportional to $(\mathcal{E}T_{\rm dr})^4$ (see Eq. (3.19)). Thus, it can be expected that the variation of the electric field amplitude $\mathcal{E}$ inverse proportionally to the pulse duration $T_{\rm dr}$ yields the similar value of the spin-flip probability. Fig. 3.4a shows the spin-flip probability, $w_{\text{s-f}}(\tau_{\rm p})$, depending on the pulse duration and the detuning. At every value of the pulse duration, the electric field amplitude $\mathcal{E}$ is adjusted so that $\mathcal{E}T_{\rm dr} = \text{const}$. Although $w_{\text{s-f}}(\tau_{\rm p})$ is proportional to $(\mathcal{E}T_{\rm dr})^4$, which is constant, the value of $w_{\text{s-f}}(\tau_{\rm p})$ is quite different at various time durations. It first increases with the increase of the pulse duration from 10 fs to 40 fs, thereby its dependence on the frequency has always one maximum at zero detuning. When the pulse duration increases from 40 fs to 300 fs, two maxima in the frequency dependence develop at $\omega_0 = \omega_{2p^{3/2}}$ and $\omega_0 = \omega_{2p^{1/2}}$. The lines at $\omega_{2p^{3/2}}$ and $\omega_{2p^{1/2}}$ become more

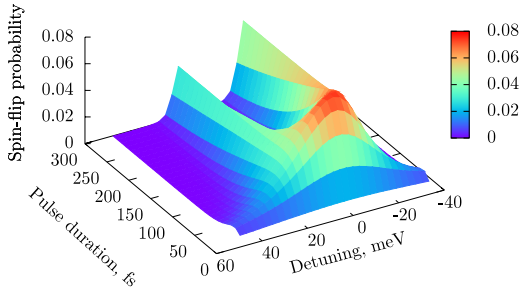

(a)

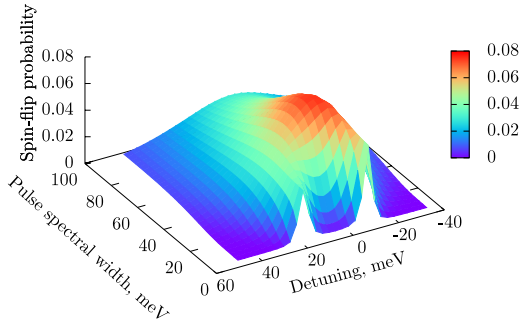

(b)

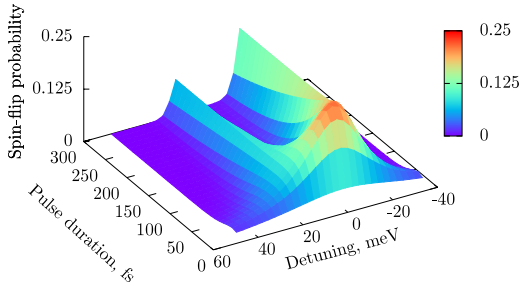

(c)

Figure 3.4: Spin-flip probability depending on the laser pulse frequency and (a) duration, (b) spectral width at constant $\mathcal{E}T_{\mathrm{dr}}$. (c) Spin-flip probability depending on the laser pulse frequency and duration at constant $\mathcal{E}_2 T_{\mathrm{dr}}$, $\mathcal{E}_2 = \sqrt[4]{2}\,\mathcal{E}$. $\lambda = 27.2$ meV.

$\Delta\omega_{\text{sw}}$, meV	Shape	T_{dr}, fs	E_{fl}, mJ/cm^2	I_0, 10^9 W/cm^2
5	Gaus.	364	6.2	0.5
	Rect.	736	5.9	0.3
	Asm. tr.	325	5.5	0.8
15	Gaus.	121	2.1	4.7
	Rect.	245	2.0	2.6
	Asm. tr.	108	1.8	6.7
25	Gaus.	72	1.2	13.4
	Rect.	147	1.2	7.3
	Asm. tr.	65	1.1	18.6

Table 3.1: Properties of the laser pulses used to obtain spin-flip probabilities dependence on Fig. 3.5: spectral widths $\Delta\omega_{\text{sw}}$, shapes, durations T_{dr}, fluences E_{fl}, peak intensities I_0.

narrow, and the probability between these lines decreases rapidly with the increase of the pulse duration from 40 fs to 300 fs.

The effect of the variation of the pulse duration is similar to the variation of the SOC value. This becomes more clear from Fig. 3.4b, which shows the dependence of $w_{\text{s-f}}(\tau_{\text{p}})$ on the pulse central frequency and spectral width, which is inverse proportional to the pulse duration $\Delta\omega_{\text{sw}} \propto 1/T_{\text{dr}}$. If the pulse duration is too short, the spectral width is much larger than the SOC, which leads to $\Gamma^{(2)}_{3/2}(t) \approx \Gamma^{(2)}_{1/2}(t)$. With the increase of the pulse duration, the SOC is effectively increases. Thereby, the two levels, $2p^{3/2}$ and $2p^{1/2}$ interfere, and they together contribute to the effect. With the further increase of the pulse duration, the SOC further effectively increases, which makes the two lines isolated. Both plots have a maximum at the pulse duration of $40 \sim 50$ fs, when the spectral width is about $30 \sim 40$ meV, *i. e.* approximately equal to λ.

The dependence of the spin-flip probability on the laser pulse frequency and duration, when $\mathcal{E}$ is increased by $\sqrt[4]{2}$ times, is shown on Fig. 3.4c. The value of $w_{\text{s-f}}(\tau_{\text{p}})$ is about two times higher at every frequency and pulse duration compared to the previous case. Thus, $w_{\text{s-f}}(\tau_{\text{p}})$ depends linearly on $\mathcal{E}^4$, and therefore, on the peak intensity squared I_0^2. The dependence of the spin-flip probability on the pulse duration is more complicated and relates to the system properties.

It will be shown now that the ultrafast IFE is determined by two laser pulse parameters: the spectral width and the integral of the pulse electric field over time $E_t = \int_{-\infty}^{\infty} |\mathbf{E}(t)| dt$. The effect of three pulses with different shapes

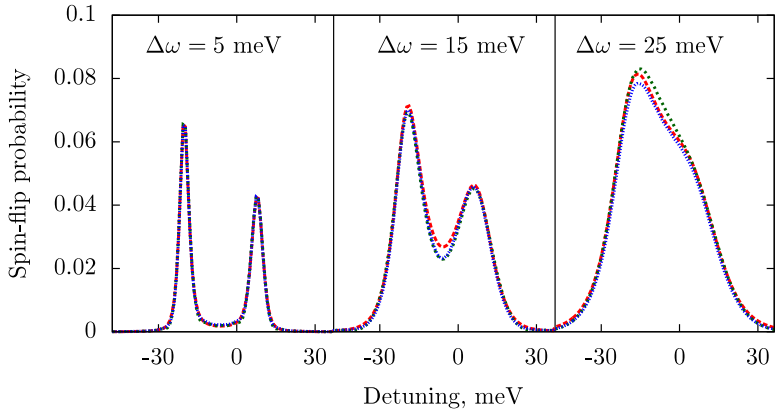

(a)

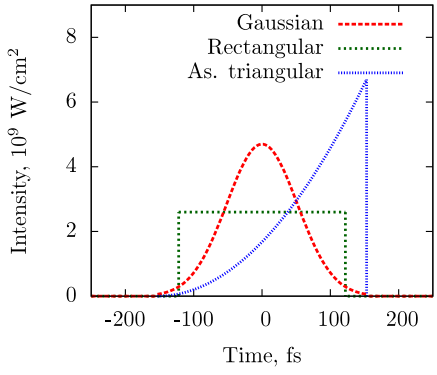

(b)

Figure 3.5: (a) Final spin-flip probabilities due to the excitation by (red) Gaussian-, (blue) rectangular-, (green) asymmetric triangular-shaped pulses, which have equal spectral width of 5, 15 or 25 meV. (b) Intensities of the three pulses with equal spectral widths of 15 meV, which correspond to the middle plot on (a).

on the final spin-flip probability will be compared for this purpose. The pulses with Gaussian, rectangular and asymmetric triangular shape are chosen (see Appendix B).

Fig. 3.5a shows the spin-flip probability dependence on the pulse frequency for pulses with three different shapes and at three different spectral width. The duration and peak intensity of the pulses are tuned in such way that the integral E_t is the same for all pulses and at every spectral width. The dependencies of $w_{\text{s-f}}(\tau_{\text{p}})$ due to pulses with different shapes almost coincide for a given spectral width. The maxima of $w_{\text{s-f}}(\tau_{\text{p}})$ are only slightly different for all pulses.

However, the nine pulses obtain totally different durations and peak intensities due to their different shapes (see Appendix B for details). The pulse fluencies are approximately the same at a given spectral width, but distinguish by several times at different spectral widths. This can be seen from Table 3.1 showing the characteristics of all pulses and Fig. 3.5b showing the intensities of three pulses, which lead to the equivalent effect on the final spin-flip probability.

To sum up, the ultrafast IFE is determined by a pulse spectral width and the integral of the pulse electric field over time. The induced magnetization depends linearly on a peak laser intensity and fluence only if pulse shape and duration are not varied. The pulses with different pulse shapes, but equal spectral widths and fluences provide approximately equal value of the effect.

3.3.3 The influence of the Raman scattering process on the spin orientation

The time dependence of the altered components of the magnetization vector (3.20) are shown on Fig. 3.6a at the laser pulse frequency corresponding to zero detuning from the position of $2p$ ($\omega_0 = \omega_{2p}$). The time evolution of $\Delta\mathbf{M}(t)$ is quite different from that expected from the classical equation $\Delta\mathbf{M}(t) \propto \mathbf{E}^*(t) \times \mathbf{E}(t)$. First, it does not follow the pulse intensity time dependence, but is determined by the time evolution of the second order wave function $\Psi_2(t)$ (see Fig. 3.2), as was discussed in the previous Chapter. Second, $\Delta\mathbf{M}(t)$ remains altered after the action of the pulse, although $\mathbf{E}(\tau_{\text{p}}) = 0$, which explains why the magnetization dynamics can be observed after the excitation by ultrashort laser pulses.

The induced magnetization by the ultrafast IFE also depends on the electric field $\mathbf{E}(t)$ via $\Psi_2(t)$ (see Eq. (3.11)). This dependence is quite complicated in the ultrafast case, but it transfers to the classical relation at long pulse

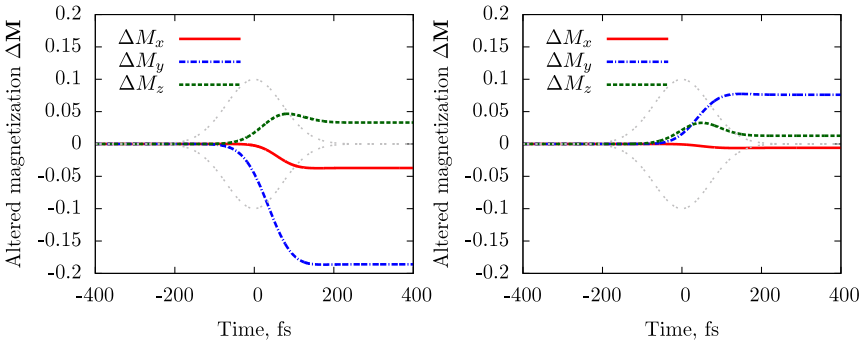

Figure 3.6: The time dependence of the components of the induced magnetization $\Delta M_{x,y,z}$ at $\lambda = 27.2$ meV, when the detuning is: (a) $\omega_0 - \omega_{2p} = 0$ and (b) $\omega_0 - \omega_{2p} = -20$ meV.

durations as shown in Chapter 2. The similarities of the ultrafast IFE to the stationary one are that $\Delta\mathbf{M}(t)$ also depends linearly on the laser pulse *peak* intensity and cannot be induced by linearly polarized light.

It was discussed in the last subsection that the spin-flip probability depends on the laser pulse frequency. The same is also true for $\Delta\mathbf{M}(t)$. Fig. 3.6b shows the time evolutions of $\Delta\mathbf{M}(t)$ components at frequency $\omega_0 = \omega_{2p} + 20$ meV, which is different from that applied for Fig. 3.6a. Comparing Figs. 3.6a and b, it can be seen that both magnitude and orientation of $\Delta\mathbf{M}(t)$ depend on the frequency of excitation. This statement is supported by the observation in Ref. [122], that the initial phase and amplitude of a probe pulse polarization oscillation, which is proportional to the induced magnetization, depends on the pump wavelength.

The dependence of the spin vector orientation on the excitation frequency is studied further in order to explain the observed differences of the time evolutions of $\Delta\mathbf{M}(t)$. The final spin vector orientation $\mathbf{S}(\tau_\mathrm{p}) = \mathbf{M}(\tau_\mathrm{p})/\mu_S = -\mathbf{M}(\tau_\mathrm{p})$ is calculated at different laser frequencies ω_0. ω_0 is varied between $\omega_{1s,2p^{3/2}} - 3\lambda$ and $\omega_{1s,2p^{1/2}} + 3\lambda$, covering the region, when the frequency is close to the resonances ("blue" region "b" on Fig. 3.7(a)) and away from them ("green" region "c" on Fig. 3.7(a)). The frequency dependence of the final spin orientation can be separated into two regimes:

(1) when the excitation frequency is close to the resonances. This case is shown on Fig. 3.7(b). Each blue arrow corresponds to the final spin orientation

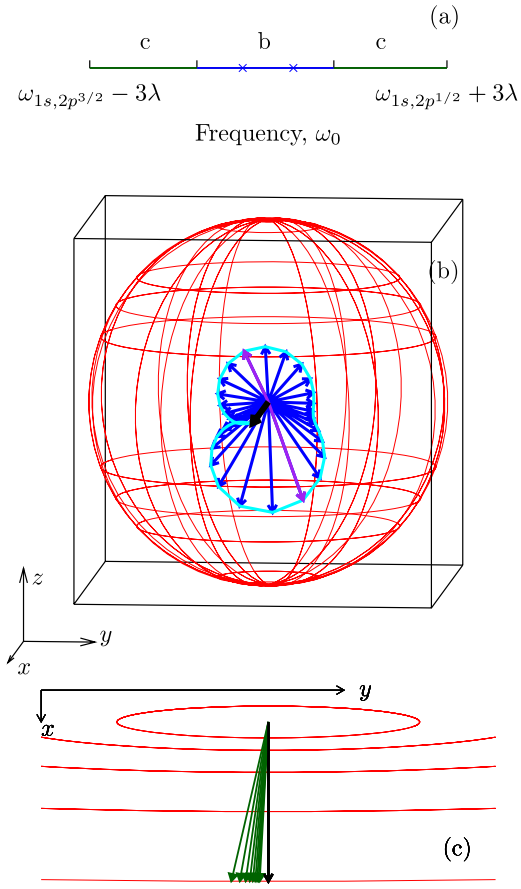

Figure 3.7: (a) The scale within which the laser frequency is varied. "Blue" region "b" corresponds to the plot (b), "green" region "c" corresponds to the plot (c). The blue stars show the exact positions of the resonances (left - $\omega_0 = \omega_{1s,2p^{3/2}}$, right - $\omega_0 = \omega_{1s,2p^{1/2}}$). (b) The final spin vector position, $\mathbf{S}(\tau_\mathrm{p}) = -\mathbf{M}(\tau_\mathrm{p})$, depending on the frequency of excitation in the resonant region "b". It moves clockwise on the plot, when ω_0 increases. The purple arrows correspond to the resonances: lower is at $\omega_0 = \omega_{1s,2p^{3/2}}$, upper is at $\omega_0 = \omega_{1s,2p^{1/2}}$. (c) $\mathbf{S}(\tau_\mathrm{p})$ depending on the frequency of excitation in non-resonant region "c", xy plane, the plot is stretched in the y direction. The initial position of the spin is shown with the black arrow. $\lambda = 27.2$ meV.

at a different laser frequency ω_0, which is varied within the "blue" region "b" on Fig. 3.7(a). When ω_0 is at the "left" boundary of the region "b" the spin orientation is close to the initial one. It moves counterclockwise on the plot with the increase of the frequency and arrives again to the position close to the initial one, when the frequency approaches the "right" boundary. At this regime, first, the effect is quite strong (ΔM is large). Second, the direction of the spin is highly affected by the excitation frequency. Third, the spin alignment is not in the xy plane.

(2) The situation is quite different, when the frequency is away from the resonances. When the frequency is varied within the region "c" on Fig. 3.7(a), the final spin orientation is always in the xy plane, which is depicted on Fig. 3.7(c). The effect is much lower in comparison to the resonance regime (1). The final spin direction still depends on the frequency but much less. The plots are similar for the situations, when the frequency decreases in the "left" region "c", and increases in the "right" region "c". When the frequency goes away from the resonance, the final spin position approaches the initial one from the same "side" in both cases.

3.4 Laser-induced magnetization dynamics in isolated atoms

The next system, for which the ultrafast IFE is investigated, is an atomic gas (isolated atoms). This study is also relevant for materials in which the magnetooptical properties are determined by ions with unfilled f or d shells [51]. In this case, the wave functions of the f and d electrons are localized and can be approximated by the atomic wave functions. The aim of this Section is to demonstrate the mechanism of magnetic state change by circularly polarized light in many-electron systems.

The essential difference of a many-electron system to a one with a spin 1/2 is that its spin is composed of several electron spins according to Hunds rules. Therefore, spin is not a fundamental quantity anymore and the expectation value of the spin orientation cannot be accessed straightforwardly. Thus, the direction of the induced magnetization is obtained by calculation of the expectation values of momentum operators.

The ground state of Co is $3d^7 4s^2$ with the total momentum $J = 9/2$, the orbital momentum $L = 3$ and the spin $S = 3/2$. It is assumed that in the initial state the projection of the total momentum is defined in the x direction: $J_x = 9/2$. The action of the laser pulse described in Section 3.1 is

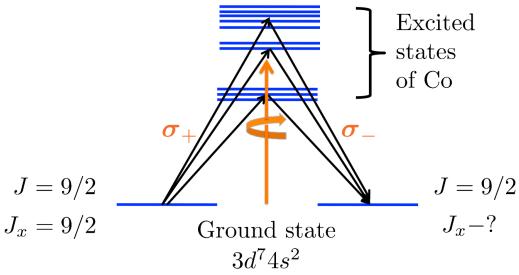

Figure 3.8: Co atom excited by a circularly left polarized pulse.

considered. The pulse direction of propagation is again perpendicular to the initial alignment of the magnetic moment. All excited states to which the laser can cause transitions from the ground state are taken into account (Fig. 3.8).

First, the ground state of the system Ψ_0 has to be found by the solution of the equation

$$\hat{j_x}\Psi_0 = 9/2\,\Psi_0, \tag{3.24}$$

$\hat{j_x}$ is the momentum operator with $(2J+1) \times (2J+1)$ elements. In the z representation, the only nonzero elements of the $\hat{j_x}$ matrix are sub-diagonal and super-diagonal ones:

$$\begin{aligned} \langle m+1|\hat{j_x}|m\rangle &= \frac{1}{2}\sqrt{(J-m)(J+m+1)} \\ \langle m-1|\hat{j_x}|m\rangle &= \frac{1}{2}\sqrt{(J+m)(J-m+1)} \\ \langle q|\hat{j_x}|m\rangle &= 0, \quad q \neq m \pm 1. \end{aligned} \tag{3.25}$$

The resulting ground state wave-function in the J_z representation is

$$\Psi_0 = \begin{pmatrix} \psi_{9/2} \\ \psi_{7/2} \\ \vdots \\ \psi_{-9/2} \end{pmatrix} \tag{3.26}$$

with $2J+1$ elements. It is the superposition of the eigenfunctions of the states with $J_z = m$. For example, $\begin{pmatrix} 0 \\ 1 \\ \vdots \\ 0 \end{pmatrix}$ is the eigenfunction of the state $J_z = 7/2$.

The transitions from the state $\left|n, J, J_z = m\right\rangle$ via an absorption of a left-polarized photon are allowed to the states $\left|\tilde{n}, \tilde{J} = J, J \pm 1, \tilde{J}_z = m+1\right\rangle$. The

reversed process of the stimulated emission leads to the transitions back to $\big|n, J, m\big\rangle$ with a dipole matrix element, which is the conjugate complex of the dipole matrix element of the first transition.

As $\Psi_2^{\tilde{n}\tilde{J}}(t)$ the wave-function, which describes the process with two transitions $|n, J, J_x = 9/2\rangle \rightarrow |\tilde{n}, \tilde{J} = J, J \pm 1, \tilde{J}_x\rangle \rightarrow |n, J, \tilde{\tilde{J}}_x\rangle$, is denoted. Applying the Eq. 3.9, one obtains

$$\Psi_2^{\tilde{n}\tilde{J}}(t) = \begin{pmatrix} |\langle \tilde{n}\tilde{J}\, 11/2|r_+|nJ\, 9/2\rangle|^2 \psi_{9/2} \\ \vdots \\ |\langle \tilde{n}\tilde{J}\, m+1|r_+|nJ\, m\rangle|^2 \psi_m \\ \vdots \\ |\langle \tilde{n}\tilde{J} - 7/2|r_+|nJ - 9/2\rangle|^2 \psi_{-9/2} \end{pmatrix} \Gamma^{(2)}_{\tilde{n}\tilde{J}}(t), \tag{3.27}$$

where $r_+ = (x+iy)/\sqrt{2}$ and $\Gamma^{(2)}_{\tilde{n}\tilde{J}}(t)$ is the time-dependent part, which depends also on the energy difference of the states $\big|n, J\big\rangle$ and $\big|\tilde{n}, \tilde{J}\big\rangle$. The dipole matrix elements $\langle \tilde{J}\, m+1|r_+|J\, m\rangle$ can be found using the relations [131]

$$\begin{aligned} \langle J\, m+1|r_+|J\, m\rangle &= \sqrt{\tfrac{(J-m)(J+m+1)}{J(J+1)(2J+1)}}\, \langle J|r|J\rangle \\ \langle J-1\, m+1|r_+|J\, m\rangle &= \sqrt{\tfrac{(J-m)(J-m-1)}{J(2J-1)(2J+1)}}\, \langle J-1|r|J\rangle \\ \langle J+1\, m+1|r_+|J\, m\rangle &= -\sqrt{\tfrac{(J+m+1)(J+m+2)}{(J+1)(2J+1)(2J+3)}}\, \langle J+1|r|J\rangle. \end{aligned} \tag{3.28}$$

Summing up the contributions from all possible transitions which lead to the Raman processes, the corresponding second order function is obtained

$$\Psi_2^{\mathrm{R}}(t) = \sum_{\tilde{n}\tilde{J}} \Psi_2^{\tilde{n}\tilde{J}}(t) = \begin{pmatrix} \phi_{9/2} \\ \phi_{7/2} \\ \vdots \\ \phi_{-9/2} \end{pmatrix}. \tag{3.29}$$

The resulting wave-function $\begin{pmatrix} \phi_{9/2} \\ \phi_{7/2} \\ \vdots \\ \phi_{-9/2} \end{pmatrix}$ is not proportional to the wave-function of the ground state, $\begin{pmatrix} \psi_{9/2} \\ \psi_{7/2} \\ \vdots \\ \psi_{-9/2} \end{pmatrix}$, because each element of the latter spinor was multiplied by a different factor. Consequently, the spinor of the resulting

wave function does not correspond to the state with $J_x = 9/2$ anymore and the projection of the magnetic momentum of the final state is different from the initial one. Therefore, the magnetic state of the system is altered after experiencing the Raman process.

In order to find out, how the projection of magnetic momentum has changed, the selection rules should be examined. For the J_x component under an excitation by left-circularly polarized light, they are: for the transition to the intermediate level the allowed values of the new x projection $\tilde{J}_x$ are $J_x, J_x \pm 1$ and for ones to the final (ground) state $\tilde{\tilde{J}}_x = J_x, J_x \pm 1, J_x \pm 2$. But $J_x = 9/2$ is the maximum value of the projection of $J = 9/2$ and $\tilde{\tilde{J}}_x = J_x + 1, J_x + 2$ are not possible in this case. Therefore, the possible values of the new magnetic momentum projection are $\tilde{\tilde{J}}_x = 9/2, 7/2, 5/2$ after the excitation.

The new projection of magnetic momentum can take each of that values with a certain probability, which depends on the function $\Psi_2(t)$. The normalized eigenfunction of the state $\left|J = 9/2, J_x = m_x\right\rangle$ is denoted as $\Psi_{0,Jx=m_x}$. Then, the probability, that an electron experiences the stimulated Raman scattering process and comes to the ground state with the projection of the magnetic momentum $J_x = m_x$, is the projection of the function $\Psi_2(t)$ on $\Psi_{0,Jx=m_x}$

$$w_{m_x}(t) = \frac{\left|\langle \Psi_2^{\mathrm{R}}(t) | \Psi_{0,J_x=m_x} \rangle\right|^2}{\left|\Psi_0 + \Psi_1 + \Psi_2\right|^2}, \tag{3.30}$$

$w_{m_x} \neq 0$ for $m_x = 9/2, 7/2, 5/2$. The sum of the functions $w_{m_x}(t)$ is the probability of the Raman process, $w_{5/2}(t) + w_{7/2}(t) + w_{9/2}(t) = |\Psi_2^{\mathrm{R}}|^2$. In order to calculate them, one has to know the energies of the excited states $\left|\tilde{n}\tilde{J}\right\rangle$ of Co and the corresponding dipole matrix elements, $\langle \tilde{n}\tilde{J}|r|nJ\rangle$. This data is taken from the NIST Atomic Spectra Database [132].

The probabilities $w_{5/2}(\tau_{\mathrm{p}})$ and $w_{7/2}(\tau_{\mathrm{p}})$ that the x projection of the magnetic momentum is changed to $5/2$ or $7/2$ after the excitation are depicted on Fig. 3.9 depending on the laser frequency. The probability $w_{9/2}(\tau_{\mathrm{p}})$ is not of interest, since it does not lead to any physical changes in the system. The contribution of every allowed excited level is taken into account for each frequency (see Fig. 3.8). The three strongest lines on Fig. 3.9 correspond to the frequencies of the laser in resonance with the most intense transitions in Co (therefore, the probability of the effect becomes higher at these frequencies). However, other excited states also contribute to the effect. The probabilities that the value of J_x changes to $7/2$ and to $5/2$ after the transitions via excited states are nonzero. It means that the magnetic state of an atom is changed with a certain probability due to transitions caused by laser excitation. Apply-

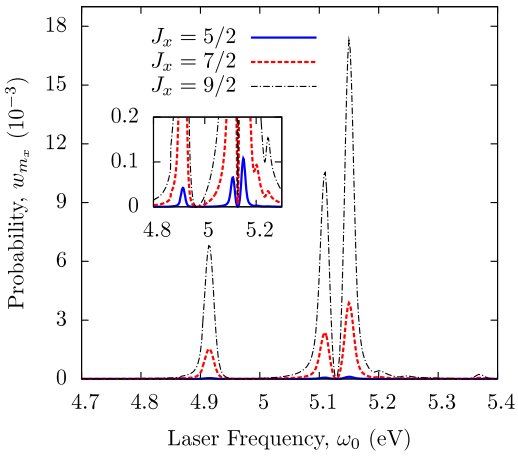

Figure 3.9: The probabilities of possible values of a new magnetic momentum projection J_x after the Raman scattering process in Co atom depending on the frequency of excitation. The inset zooms in the region where $w_{5/2}$ can be discerned.

ing analogous considerations as in the previous Section, it can be easily shown that the effect is present in isolated atoms, only when the laser light is not linearly polarized.

The induced magnetization $\Delta\mathbf{M}(t)$ can be derived by the analogy to Eq. (3.11) using the momentum operators $\hat{j_\alpha}$ (α stays for x, y and z) instead of Pauli matrices σ_α

$$\Delta M_\alpha(t) = -\mu_B g_J \left(\frac{\langle \Psi_0 + \Psi_2(t) | \hat{j_\alpha} | \Psi_0 + \Psi_2(t) \rangle}{|\Psi_0 + \Psi_2(t)|^2} - \langle \Psi_0 | \hat{j_\alpha} | \Psi_0 \rangle \right), \qquad (3.31)$$

μ_B is Bohr magneton and g_J is Landé g-factor, which for the ground state of Co equals to 5/6. The components of $\Delta\mathbf{M}(\tau_\mathrm{p})$ are depicted on the Fig. 3.10 at the time $t = \tau_\mathrm{p}$, *i.e.* after the action of the light, depending on the frequency ω_0 of the excitation. The properties of the excitation are the same as for the previous plot. The x component of $\Delta\mathbf{M}(\tau_\mathrm{p})$ is very weak compared to the other components (the inset of Fig. 3.10). It results from the selection rules, which do not allow J_x to change more than by 2 and be lower than 5/2 in such Raman process.

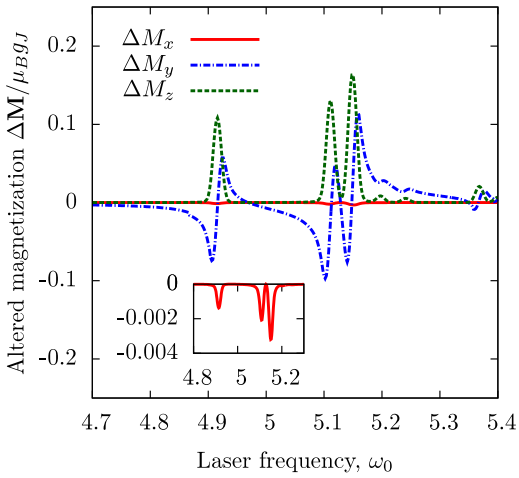

Figure 3.10: The components of altered magnetization $\Delta\mathbf{M}(\tau_\mathrm{p})$ after the Raman scattering process in Co atom depending on the frequency of excitation. The inset zooms in the region where ΔM_x component can be discerned.

3.5 Conclusions

In this Chapter, the optical mechanism of the ultrafast inverse Faraday effect was introduced. It was shown that a laser pulse excites two electron transitions in the systems: from the initial to the intermediate state and from the intermediate to the ground state. Thereby, the magnetic signature of the ground state changes with a certain probability. This is possible due to the SOC, which breaks the spin symmetry for the transitions excited by circularly polarized light.

It was shown that the spin-flip probability and induced magnetization depend strongly on the ultrafast laser pulse properties. Although the spin-flip probability depends on the peak intensity squared, the induced magnetization depends linearly on the peak intensity. However, it was shown that laser pulses with equal spectral width and equal fluence yield equal values of the effect, although their peak intensities may be different.

The time evolution of the induced magnetization does not follow that of the pulse intensity $I(t)$. Therefore, it remains non-zero after the action of the laser pulse, when $I(t) = 0$. The correct time evolution of the induced magnetization can be found by the solution of the time-dependent Schrödinger equation, which provides the dynamics of the wave-functions of involved electrons during

the excitation.

Strictly speaking, the optical mechanism considered in this Chapter is not the stimulated Raman scattering in the case of zero Zeeman splitting. Stimulated Rayleigh scattering may be a proper term providing the scattering takes place on a particle, which is much smaller compared to the light wave length. However, it was always assumed that the spins are initially aligned in a certain direction. This is achieved in experiments by the application of an external magnetic field or taking a magnetically ordered material. Therefore, the magnetic states of a ground state manifold are energetically separated, and the effect is the stimulated Raman scattering. This situation will be considered in the next Chapters. It will be shown that a magnetic precession is excited by a laser pulse in this case.

This Chapter was mostly concentrated on the optical mechanism of the IFE. Thus, only two types of electron interactions were considered in this Chapter: SOC and the electron correlations within a given atom. In the next Chapters, the effects of other interactions acting on both excited and ground states will be studied.

Chapter 4

The ultrafast inverse Faraday effect described by a momentum operator

Kimel *et al.* in Ref. [9] demonstrated the possibility of non-thermal excitation of coherent magnetic precessions by an ultrashort circularly polarized laser pulse. The next step forward to potential applications in spintronics and information processing is the ability to control magnetic oscillations in a material [47, 69]. The task of magnetization dynamics control starts from the determination of the equations of motion of magnetic vector components, and their relation to the laser pulse parameters.

It was discussed in Chapter 2 that magnetization precessions are excited in a material via laser-induced transitions, which bring the system in a non-equilibrium state. A magnetic vector starts to precess due to an external magnetic field, which may be present, or due to internal interactions, such as exchange interaction, or anisotropy fields. If a new non-equilibrium magnetic state of a system is known, then it is straightforward to determine the time evolution of magnetization. For instance, the Landau-Lifschitz-Gilbert equation can be applied for the macroscopic description. The Heisenberg representation can be used for the microscopic description, thereby, the derivative of the expectation value of momentum operators are their commutators with Hamiltonian $\mathcal{H}_0$, which includes the fields acting on the ground state.

A problem arises when one tries to include the effect of a laser pulse into the equations of motion. If the excitation by circularly polarized light is represented by an effective magnetic field, which follows the pulse intensity, then zero induced magnetization after the excitation would be obtained. In some

references [10, 122, 123, 125] the effect of a laser pulse is considered within a sudden approximation, namely, as an action of an ultrashort magnetic pulse with an amplitude proportional to the light intensity multiplied by the Verdet constant. However, there are two disadvantages of this approach. First, the sudden approximation cannot provide the information about the new magnetic state after the excitation. Moreover, it was demonstrated experimentally by [40,133] that the strength of the magneto-optical effects are not determined by the Verdet constant in an ultrafast case. It is shown in the Chapter 3 that the final state due to the ultrafast excitation should be determined by the analysis of selection rules, which is not applied in the sudden approximation.

The second problem of the sudden approximation and other approaches, which consider the action of a laser pulse to be much shorter than the characteristic time of a system, is that the necessary condition for them is not valid in many cases. For instance, they are not applicable to the description of the excitation of terahertz precessions (for example in [43, 50]), when the period of induced oscillations is of several picoseconds. This is just one order of magnitude more than a laser pulse duration. Thus, equations of motion, which can describe the time evolution of a magnetic vector both during and after the action of a laser pulse are necessary.

Equations of motion for microscopic variables are provided by the Heisenberg representation. The goal of this Chapter is to deduce the Heisenberg picture for the ultrafast IFE, which would include only the dynamics of variables relevant for the study. Thus, an operator $\mathcal{H}_J$ which describes the coupling of light to total momentum operators via the ultrafast IFE is derived. It will be shown that it is possible to separate the action of the operator $\mathcal{H}_J$ from that of the Hamiltonian $\mathcal{H}_0$, which includes the stationary internal or external fields acting on the magnetic system apart from light. The first advantage of this approach is that it facilitates the manipulation of magnetic precessions, since it would be known how circularly polarized light influences magnetic components individually. The second benefit is that it can be applied as a link from the microscopic description of the ultrafast IFE provided in this Thesis to a macroscopic one.

4.1 Determination of the momentum operator

The action of circularly polarized light on a magnetic system via the stimulated Raman scattering results in the rotation of a magnetic moment, if it is not parallel to the light propagation direction and the spin symmetry is broken via the SOC. This means that it should be possible to express the action of

light via some operator $\mathcal{H}_J$, which acts on the total angular momentum in the ground state. If such operator exists, then it should obey the Schrödinger equation applied to the wave function of the ground state manifold Ψ_g

$$i\Psi_g' = [\mathcal{H}_0 + \mathcal{H}_J]\Psi_g, \tag{4.1}$$

where $\mathcal{H}_0$ is the Hamiltonian, which includes all internal and external fields apart from light acting on the ground state. The equation of motion of an expectation value of some operator $\hat{D}$ can be found in the Heisenberg representation as

$$iD' = i\langle\Psi'|\hat{D}|\Psi\rangle + i\langle\Psi|\hat{D}|\Psi'\rangle = \langle[\hat{D}, \mathcal{H}_0 + \mathcal{H}_J]\rangle \tag{4.2}$$

The action of the operator $\mathcal{H}_J$ should result in the rotation of J_x, J_y and J_z, therefore, the operators $\hat{J}_x$, $\hat{J}_y$ and $\hat{J}_z$ should not commute with $\mathcal{H}_J$. This means that the operator can be expressed via the $\hat{J}_\alpha$ operators. For instance, the momentum operator in the simplest case of $J = 1/2$ should have the form $\mathcal{H}_J = \begin{pmatrix} a(t) & c(t) \\ c^*(t) & b(t) \end{pmatrix}$. $a(t)$ and $b(t)$ are real functions, because the operator is hermitian.

Thus, the nonlinear operator describing the perturbation by an electric field, $-\mathbf{d}\cdot\mathbf{E}$, will be replaced by a linear time dependent operator $\mathcal{H}_J$ acting on the total angular momentum $\hat{J}$ of a system. In the next Section the elements of the operator $\mathcal{H}_J$ are derived applying the result that the rotation of a magnetic moment is due to different transition amplitudes from and to the states with different J_z projections[1].

4.1.1 The case of zero ground state splitting

The operator is derived in this Subsection first for the case, when there is no field except light acting on the magnetic momentum of a system in the ground state. It was shown in Chapter 2 that the wave function of the ground state manifold of such system perturbed by a laser pulse via the stimulated Raman scattering process is $\Psi_g(t) = \big(\Psi_0 + \Psi_2(t)\big)/|\Psi_0 + \Psi_2(t)|$. Ψ_0 is the wave function of the initial state: $\Psi_g(0) = \Psi_0$; $\Psi_2(t)$ is the second order wave function (see Eq. 2.37). If the total magnetic momentum of the system is equal to J, then the initial wave function Ψ_0 of the system is a spinor, which can be expressed

[1]The action of a circularly polarized laser pulse propagating in the z direction on a magnetic system is considered throughout this chapter.

as

$$\Psi_0 = \begin{pmatrix} P_{01} \\ P_{02} \\ \vdots \\ P_{0n} \end{pmatrix}, \tag{4.3}$$

where $n = 2J+1$ and P_{0k} is the k-th projection of J on the z axis, $\sum_k |P_{0k}|^2 = 1$. It was shown in Chapter 3 that transitions from a ground state $|J, J_z = m_k\rangle$ back only to the state $|J, J_z = m_k\rangle$ are allowed for circularly polarized light propagating in the z direction. It was also shown that the k-th spinor element of the second order wave function Ψ_{02} is proportional to the dipole moments $\langle e|\mathbf{x} \pm i\mathbf{y}|\Psi_{0k}\rangle$, where e is an excited state (see Eqs. 3.18 and 3.27). Thus, the k-th element of Ψ_{02} is proportional to P_{0k} multiplied by some time-dependent factor $A_k(t)e^{i\phi_k(t)}$

$$\Psi_g = \frac{1}{\mathcal{N}(t)} \begin{pmatrix} A_1(t)e^{i\phi_1(t)}P_{01} \\ \vdots \\ A_k(t)e^{i\phi_k(t)}P_{0k} \\ \vdots \end{pmatrix} = \begin{pmatrix} P_1(t) \\ \vdots \\ P_k(t) \\ \vdots \end{pmatrix}, \tag{4.4}$$

$P_{0k} = P_k(0)$, $A_k(0)e^{i\phi(0)} = 1$, $\mathcal{N}^2 = \sum_k |P_{0k}|^2 |A_k|^2$.

It was discussed in Chapter 3 that if the magnetic moment of a system is parallel to the laser pulse propagation direction, then the excitation does not lead to the rotation of magnetic moment. Therefore, if Ψ_0 has a projection only on the z axis, the action of the momentum operator should not result in its rotation. It means that if $\Psi_0 = \begin{pmatrix} 0 \\ \vdots \\ P_{0k} \\ \vdots \end{pmatrix}$, where $|P_{0k}| = 1$, then other magnetic components different from k-th do not become populated due to the action of light: $\Psi_g = \frac{1}{\mathcal{N}(t)} \begin{pmatrix} 0 \\ \vdots \\ A_k(t)e^{i\phi_k(t)}P_{0k} \\ \vdots \end{pmatrix}$. The function Ψ_g is normalized to unity, $|\Psi_g| = 1$, and $\Psi_g = e^{i\phi_k(t)}\Psi_0$. This means, that the momentum operator acts only on the k-th component of the wave function, and is diagonal with elements $(\mathcal{H}_J)_{kk} = -\phi_k'(t)$.

Momentum operator for a single spin

Let us further consider the situation when the spin of a system is not aligned parallel to the light propagation direction. If the operator $\mathcal{H}_J$ was diagonal

in this case, then each spinor component would differ only by a phase from the corresponding initial component, resulting in the rotation of the magnetic momentum only around the z axis. In other words, the $\hat{J}_z$ operator commutes with a diagonal operator, and J_z is not affected by a diagonal operator. However, it was shown in Chapter 3 that it is not necessarily the case. Thus, $\mathcal{H}_J$ should have non-diagonal components, if spin is not aligned parallel to the light propagation direction. The letter condition means that the existence of the non-diagonal components depends on the initial alignment of the magnetic momentum. Thus, the non-diagonal elements should depend on the expectation values of the momentum operators.

First the operator is derived for the simplest case, when $J = S = 1/2$ with the initial wave function $\Psi_0 = \left(\begin{smallmatrix} P_{01} \\ P_{02} \end{smallmatrix}\right)$, $|P_{01}|^2 + |P_{02}|^2 = 1$, and the operator $\mathcal{H}_J$ is a hermitian 2×2 matrix

$$\mathcal{H}_J = \begin{pmatrix} -\phi_1'(t) & c(t) \\ c^*(t) & -\phi_2'(t). \end{pmatrix} \tag{4.5}$$

It is shown in Appendix D that the element c equals to $iP_1P_2^*\left(\nu_1 - \nu_2\right)$ and the momentum operator is

$$\mathcal{H}_J = \begin{pmatrix} -\gamma_1 & iP_1P_2^*\left(\nu_1 - \nu_2\right) \\ iP_1^*P_2\left(\nu_2 - \nu_1\right) & -\gamma_2 \end{pmatrix}, \tag{4.6}$$

where $\nu_{1,2} = \frac{\mathcal{A}_{1,2}'(t)}{\mathcal{A}_{1,2}(t)} = \mathrm{Re}\left(\frac{\mathcal{A}_{1,2}'}{\mathcal{A}_{1,2}}\right)$, $\gamma_{1,2} = \phi_{1,2}'(t) = \mathrm{Im}\left(\frac{\mathcal{A}_{1,2}'}{\mathcal{A}_{1,2}}\right)$. $\mathcal{A}_{1,2}$ are the elements 1 and 2 of a vector $\mathcal{A} = \left(\begin{smallmatrix} A_1(t)e^{i\phi_1(t)} \\ A_2(t)e^{i\phi_2(t)} \end{smallmatrix}\right)$.

The operator can be expressed as a superposition of the spin operators

$$\hat{S}_x + i\hat{S}_y = \begin{pmatrix} 0 & 1 \\ 0 & 0 \end{pmatrix},\ \hat{S}_x - i\hat{S}_y = \begin{pmatrix} 0 & 0 \\ 1 & 0 \end{pmatrix},\ \hat{S}_z = \begin{pmatrix} \frac{1}{2} & 0 \\ 0 & -\frac{1}{2} \end{pmatrix},\ \hat{S}^2 = \begin{pmatrix} \frac{3}{4} & 0 \\ 0 & \frac{3}{4} \end{pmatrix}. \tag{4.7}$$

Applying that $P_1P_2^*$ is the expectation value of the operator $\hat{S}_x - i\hat{S}_y$: $P_1P_2^* = \left\langle \begin{smallmatrix} P_1 \\ P_2 \end{smallmatrix} \right| \left(\begin{smallmatrix} 0 & 0 \\ 1 & 0 \end{smallmatrix} \right) \left| \begin{smallmatrix} P_1 \\ P_2 \end{smallmatrix} \right\rangle$, the convenient form of the operator is obtained

$$\mathcal{H}_J = f(t)\left(S_y\hat{S}_x - S_x\hat{S}_y\right) + g(t)\hat{S}_z + h(t)\hat{S}^2, \tag{4.8}$$

where the functions $f(t)$, $g(t)$ and $h(t)$ are

$$f(t) = 2\left(\nu_2 - \nu_1\right), \quad g(t) = (\gamma_2 - \gamma_1), \quad h(t) = -\frac{2}{3}(\gamma_1 + \gamma_2). \tag{4.9}$$

Thus, the operator $\mathcal{H}_J$ can be separated into three parts. The first one is determined by the function $f(t)$ and describes the quadratic effect. The function $f(t)$ results from the real part of the difference of the transition amplitudes for a spin-up and -down component. The second part determined by $g(t)$ describes the rotation around the z axis. The function $g(t)$ results from the imaginary part of the difference of the transition amplitudes. The third part $h(t)\hat{S}^2$ does not result in spin rotation. The non-zero difference of the transition amplitudes for up and down spin components is necessary for both $f(t)$ and $g(t)$ functions to be non-zero. This is in agreement with the result of Chapter 3, that a mechanism, which breaks a spin symmetry for laser induced transitions is needed for the IFE.

The presence of both linear and quadratic terms of spin components may explain the fact that a single spin is rotated only around the z axis by a laser pulse with a frequency far from a resonance (see Section 3.3.3). The strength of the effect is too weak due to an off-resonance excitation, thus the quadratic terms become negligible and spin motion is determined by the linear component of the momentum operator.

4.1.2 General equations

In this subsection, the momentum operator in the case, when there is some additional field $\mathcal{H}_0$ acting on the magnetic momentum in the ground state, is provided. In this case, the wave function of the ground state is $\Psi_g(t) = \mathcal{U}\big(\Psi_0 + \Psi_2(t)\big)/|\Psi_0 + \Psi_2(t)|$, where $\mathcal{U}$ is the time evolution operator, which obeys the equation $\mathcal{H}_0\mathcal{U} = i\mathcal{U}'$ (see Appendix A.1).

Single spin

In the case of a single spin system, the wave function of the ground state is

$$\Psi_g = \mathcal{U}\left[\frac{1}{\mathcal{N}(t)}\begin{pmatrix} A_1(t)e^{i\phi_1(t)}P_{01} \\ A_2(t)e^{i\phi_2(t)}P_{02}\end{pmatrix}\right] = \begin{pmatrix} P_1(t) \\ P_2(t)\end{pmatrix}. \tag{4.10}$$

The Hamiltonian $\mathcal{H}_g$, acting on the ground state wave function can be separated into two parts

$$\mathcal{H}_g = \mathcal{H}_0 + \mathcal{H}_J, \tag{4.11}$$

the letter is the momentum operator, which has the same form as in the previous case

$$\mathcal{H}_J = f(t)\left(S_y\hat{S}_x - S_x\hat{S}_y\right) + g(t)\hat{S}_z + h(t)\hat{S}^2, \tag{4.12}$$

with $f(t) = 2(\nu_2 - \nu_1)$, $g(t) = (\gamma_2 - \gamma_1)$, $h(t) = -\frac{2}{3}(\gamma_1 + \gamma_2)$. But this time, $\nu_k = \mathrm{Re}(Y_k)$, $\gamma_k = \mathrm{Im}(Y_k)$, $Y_k = [\mathcal{U}\mathcal{A}']_k/[\mathcal{U}\mathcal{A}]_k$, $k = 1, 2$ (see Appendix D.2). The dependence of $\mathcal{H}_J$ on the time evolution operator $\mathcal{U}$ results from the dependence of the second order wave function on the time evolution operator (see Appendix A.1).

Equations for general J

It is shown in Appendix D that the general form of the momentum operator for $J = 2n + 1$ is with diagonal elements $(\mathcal{H}_J)_{kk} = -\phi'_k$, and $(\mathcal{H}_J)_{kl,k\neq l} = iP_kP_l^*(\nu_k - \nu_l)$

$$\mathcal{H}_J = \begin{pmatrix} \ddots & & & & \\ & -\gamma_k & \cdots & iP_kP_l^*(\nu_k - \nu_l) & \cdots \\ & \vdots & \ddots & & \\ & iP_k^*P_l(\nu_l - \nu_k) & & & \\ & \vdots & & & \end{pmatrix}, \tag{4.13}$$

where $\nu_k = \mathrm{Re}(Y_k)$, $\gamma_k = \mathrm{Im}(Y_k)$, $Y_k = [\mathcal{U}\mathcal{A}']_k/[\mathcal{U}\mathcal{A}]_k$, $k = 1 \ldots n$. $\mathcal{A}$ is a vector of the form $\begin{pmatrix} A_1(t)e^{i\phi_1(t)} \\ \vdots \end{pmatrix}$. It can be also expressed as

$$\mathcal{H}_J = -\sum_k^n \gamma_k \hat{N}_k + \frac{1}{2}\sum_{k,l}^n (\nu_k - \nu_l)\left(N_{kl-}\hat{N}_{kl+} - N_{kl+}\hat{N}_{kl-}\right), \tag{4.14}$$

where $\hat{N}_{kl\pm}$ and $\hat{N}_k = \hat{N}_{kk+}$ are momentum operators, the expectation values of which are connected to $P_{k,l}$ by

$$\langle N_{kl+}\rangle = P_kP_l^* + P_k^*P_l \tag{4.15}$$
$$\langle N_{kl-}\rangle = i(P_kP_l^* - P_k^*P_l). \tag{4.16}$$

The operators can be expressed by matrices with elements

$$\begin{aligned} &(N_{kl+})_{kl} = (N_{kl+})_{lk} = 1,\ l \geq k \\ &(N_{kl-})_{kl} = -i, \quad (N_{kl-})_{lk} = i,\ l > k \\ &\hat{N}_k = \hat{N}_{kk+}, \quad (N_{kk+})_{kk} = 1 \\ &(N_{kl\pm})_{mn} = 0, \text{ if } m \neq k,\ m \neq l,\ n \neq k,\ n \neq l \text{ or } l < k. \end{aligned} \tag{4.17}$$

For example, if $J = 3/2$, then

$$\hat{N}_{12+} = \begin{pmatrix} 0 & 1 & 0 & 0 \\ 1 & 0 & 0 & 0 \\ 0 & 0 & 0 & 0 \\ 0 & 0 & 0 & 0 \end{pmatrix}, \quad \hat{N}_{12-} = \begin{pmatrix} 0 & -i & 0 & 0 \\ i & 0 & 0 & 0 \\ 0 & 0 & 0 & 0 \\ 0 & 0 & 0 & 0 \end{pmatrix}, \quad \hat{N}_{1} = \begin{pmatrix} 1 & 0 & 0 & 0 \\ 0 & 0 & 0 & 0 \\ 0 & 0 & 0 & 0 \\ 0 & 0 & 0 & 0 \end{pmatrix}. \tag{4.18}$$

The operators $\hat{N}_{kl\pm}$ and $\hat{N}_k$ can be represented by the combination of $\hat{J}_x$, $\hat{J}_y$, $\hat{J}_z$ and $\hat{J}^2$. For example, if the total momentum $J = 3/2$, the operator $\hat{N}_{12+}$ equals to $\{\{\hat{J}_x, \hat{J}_z\}, 4\hat{J}^2/15 + \hat{J}_z\}/(2\sqrt{3})$, where $\{\}$ designates anti-commutator: $\{\hat{A}, \hat{B}\} = \hat{A}\hat{B} + \hat{B}\hat{A}$.

The operators $\hat{J}_x$, $\hat{J}_y$, $\hat{J}_z$ and $\hat{J}^2$ can be always represented by linear combinations of $\hat{N}_{kl\pm}$ and $\hat{N}_k$ operators: $\hat{J}_x$ - by $\hat{N}_{kl+}$, $\hat{J}_y$ - by $\hat{N}_{kl-}$, and $\hat{J}_z$ and $\hat{J}^2$ - by $\hat{N}_k$. However, if $J > 1/2$, then the operators $\hat{N}_{kl\pm}$ cannot be expressed by linear combinations of $\hat{J}_x$, $\hat{J}_y$, $\hat{J}_z$ and $\hat{J}^2$. Thus, if $J > 1/2$, the light couples via the ultrafast IFE not only to x, y and z magnetic momentum components, but also to magnetic momentum components of a higher order. This means that the value of $J_x^2 + J_y^2 + J_z^2$ is not conserved after the action of light and not only direction, but the length of a magnetic vector is also affected by the IFE.

4.2 Equations of motion

The equations of motion of the expectation values of the $\hat{N}_{kl\pm}$ operators are given by $N'_{kl\pm} = -i\langle[\hat{N}_{kl\pm}, \mathcal{H}]\rangle$ according to the Heisenberg representation, where $\mathcal{H}$ is the Hamiltonian acting on $\hat{N}_{kl\pm}$. If $\mathcal{H} = \mathcal{H}_J$, the general form of the equations of motion is (see Appendix D)

$$N'_{kl\pm} = (\mathcal{F} + \nu_k + \nu_l)N_{kl\pm} \pm (\gamma_k - \gamma_l)N_{kl\mp}, \tag{4.19}$$

where $\mathcal{F} = -2\sum_k \nu_k N_k$. For instance,

$$\begin{aligned} N'_{12+} &= (\mathcal{F} + \nu_1 + \nu_2)N_{12+} + (\gamma_1 - \gamma_2)N_{12-} \\ N'_{12-} &= (\mathcal{F} + \nu_1 + \nu_2)N_{12-} - (\gamma_1 - \gamma_2)N_{12+} \\ N'_{1} &= (\mathcal{F} + 2\nu_1)N_1. \end{aligned} \tag{4.20}$$

It follows from these equations, that if magnetic momentum has a projection only on z axis, then the other components are not populated due to the action of circularly polarized light. For instance, if a wave function has only

q-th non-zero spinor component, then $N_q = 1$ would be the only non-zero expectation value. Thus, all derivatives of $N_{kl\pm}$ and N_k would be zero including that of N_q: $\mathcal{F} = -2\nu_q N_q = -2\nu_q$, $N_q' = (-2\nu_q + 2\nu_q)N_q$.

Now, assume that all elements of $\mathcal{A}$ are equal to each other. This would lead to $\nu_1 = \nu_2 = \ldots = \nu$ and $\gamma_1 = \gamma_2 = \ldots = \gamma$. Thus, any factor $(\gamma_k - \gamma_l)$ entering Eq. 4.19 would de zero. $\mathcal{F} = -2\sum_k \nu_k N_k = -2\nu \sum_k N_k = -2\nu$, since $\sum_k \hat{N}_k = \mathbf{1}$. And any factor $(\mathcal{F} + \nu_k + \nu_l)$ would be also zero: $\mathcal{F} + \nu_k + \nu_l = -2\nu + \nu + \nu = 0$. This means that any $N'_{kl\pm} = 0$ and all variables $N_{kl\pm}$ would not change. Thus, if transitions amplitudes are equal for all magnetic components, rotation of the magnetic moment is not possible. This result is compatible with the discussion of the Chapter 3 that a mechanism which would break the symmetry for transitions of different magnetic components is necessary for the IFE. It was shown that this mechanism is due to the SOC and excitation by a laser pulse, which is not linearly polarized.

4.3 Examples

4.3.1 Equations of motion of a single spin in an external magnetic field

If there is an external magnetic field B, acting on a single spin in the $-x$ direction, then the Hamiltonian acting on the ground state is

$$\mathcal{H}_g = -\omega \hat{S}_x + f(t)\left(S_y \hat{S}_x - S_x \hat{S}_y\right) + g(t)\hat{S}_z + h(t)\hat{S}^2, \tag{4.21}$$

where ω is the Larmor frequency. The time evolution operator $\mathcal{U}$ due to the magnetic field is

$$\mathcal{U} = e^{i\omega \hat{S}_x t} = \begin{pmatrix} \cos(\frac{\omega t}{2}) & -i\sin(\frac{\omega t}{2}) \\ -i\sin(\frac{\omega t}{2}) & \cos(\frac{\omega t}{2}) \end{pmatrix}. \tag{4.22}$$

Acting with this operator on $\mathcal{A}$ and $\mathcal{A}'$ vectors and substituting the result into Y_k, one obtains

$$\begin{aligned} Y_1 &= \frac{V_+' e^{-i\omega t/2} + V_-' e^{i\omega t/2}}{V_+ e^{-i\omega t/2} + V_- e^{i\omega t/2}} \\ Y_2 &= \frac{V_+' e^{-i\omega t/2} - V_-' e^{i\omega t/2}}{V_+ e^{-i\omega t/2} - V_- e^{i\omega t/2}} \\ V_\pm &= \frac{A_1 e^{i\phi_1} \pm A_2 e^{i\phi_2}}{2}, \end{aligned} \tag{4.23}$$

which can be used to determine $f(t)$ and $g(t)$.

For example, if the initial wave function corresponds to the lowest lying state, namely, the spin aligned in the x direction, then $\Psi_0 = \begin{pmatrix} 1/\sqrt{2} \\ 1/\sqrt{2} \end{pmatrix}$. The second order wave function can be expressed as $\Psi_2 = \begin{pmatrix} (1/\sqrt{2})\psi_{21}(t) \\ (1/\sqrt{2})\psi_{22}(t) \end{pmatrix}$. Thus, $V_+ = 1 + (\psi_{21}(t) + \psi_{22}(t))/2$, $V_- = (\psi_{21}(t) - \psi_{22}(t))/2$.

The relation $iS'_\alpha = \langle[\hat{S}_\alpha, \mathcal{H}_g]\rangle$ ($\alpha = x,\ y,\ z$) provides the set of the equations of motion of the spin components S_α due to the laser excitation and the magnetic field

$$\begin{aligned} S'_x &= -f(t)S_xS_z - g(t)S_y \\ S'_y &= -f(t)S_yS_z + g(t)S_x + \omega S_z \\ S'_z &= f(t)(S_x^2 + S_y^2) - \omega S_y. \end{aligned} \tag{4.24}$$

The functions $f(t > \tau_\mathrm{p})$ and $g(t > \tau_\mathrm{p})$ are zero after time τ_p, when the excitation is finished, since $f(t)$ and $g(t)$ are proportional to the components of $\Psi'_2(t)$. It was shown in Chapter 2 that $\Psi_2(t > \tau_\mathrm{p})$ is constant, thus $\Psi'_2(t > \tau_\mathrm{p}) = 0$. Therefore, Eq. (4.24) describes the spin motion due to both laser excitation and magnetic field during the action of a laser pulse. The terms, which determine the spin motion due to the excitation, are smoothly turning off while the excitation is finishing, and the spin motion is determined only by Zeeman interaction after the action of a laser pulse. Thus, the spin motion due to the Zeeman interaction is separated from that due to the ultrafast IFE as desired. This result will be used in the next Chapter for study of the spin dynamics due to the IFE and an external magnetic field.

4.3.2 Equations of motion of magnetic momentum with $J = 3/2$

A system with magnetic momentum $J = 3/2$ excited by circularly polarized light is considered in this example. No other field acting on magnetic moment is assumed ($\mathcal{U} = \mathbf{1}$).

The time evolutions of the expectation values of the momentum operators $\hat{J}_x$, $\hat{J}_y$ and $\hat{J}_z$ are of interest. These operators can be expressed via the

operators $\hat{N}_{kl\pm}$ by

$$\begin{aligned}\hat{J}_x =& \frac{\sqrt{3}}{2}\hat{N}_{12+} + \hat{N}_{23+} + \frac{\sqrt{3}}{2}\hat{N}_{34+}\\ \hat{J}_y =& \frac{\sqrt{3}}{2}\hat{N}_{12-} + \hat{N}_{23-} + \frac{\sqrt{3}}{2}\hat{N}_{34-}\\ \hat{J}_z =& \frac{3}{2}\hat{N}_1 + \frac{1}{2}\hat{N}_2 - \frac{1}{2}\hat{N}_3 - \frac{3}{2}\hat{N}_4.\end{aligned} \tag{4.25}$$

Thus, the expectation values of $\hat{J}_x$, $\hat{J}_y$ and $\hat{J}_z$ and their time derivatives, J_x', J_y' and J_z', can be expressed via $N_{kl\pm}$ and $N_{kl\pm}'$.

The system of first order differential equations for $N_{kl\pm}$ are given by the simple relation (4.19). However, the first order differential equations for J_x, J_y and J_z cannot be represented only in terms of J_x, J_y and J_z. They involve additional variables $N_{kl\pm}$ and N_k. For instance, the equation for J_z' requires at least two additional equations for variables N_k:

$$J_z' = \nu_1 N_1(3-2J_z) + \nu_2 N_2(1-2J_z) - \nu_3 N_3(1+2J_z) - \nu_4 N_4(3+2J_z). \tag{4.26}$$

Thus, there are two approaches to obtain the time evolutions of J_x, J_y and J_z. The first is to solve the systems of first order differential equations for the expectation values of ten involved operators $\hat{N}_{12\pm}$, $\hat{N}_{23\pm}$, $\hat{N}_{34\pm}$, $\hat{N}_1$, $\hat{N}_2$, $\hat{N}_3$ and $\hat{N}_4$. Such equations can be conveniently obtained for $N_{kl\pm}$ applying Eq. (4.19).

$$\begin{aligned}N_1' &= (\mathcal{F} + 2\nu_1)N_1\\ N_2' &= (\mathcal{F} + 2\nu_2)N_2\\ N_3' &= (\mathcal{F} + 2\nu_3)N_3\\ N_4' &= (\mathcal{F} + 2\nu_4)N_4\\ N_{12\pm}' &= (\mathcal{F} + \nu_1 + \nu_2)N_{12\pm} \pm (\gamma_1 - \gamma_2)N_{12\mp}\\ N_{23\pm}' &= (\mathcal{F} + \nu_2 + \nu_3)N_{23\pm} \pm (\gamma_2 - \gamma_3)N_{23\mp}\\ N_{34\pm}' &= (\mathcal{F} + \nu_3 + \nu_4)N_{34\pm} \pm (\gamma_3 - \gamma_4)N_{34\mp},\end{aligned} \tag{4.27}$$

where $\mathcal{F} = -2\left(\nu_1 N_1 + \nu_2 N_2 + \nu_3 N_3 + \nu_4 N_4\right)$. Applying that $\langle \hat{N}_1 + \hat{N}_2 + \hat{N}_3 + \hat{N}_4\rangle = \langle \mathbf{1}\rangle = 1$, the system can be reduced to nine equations. The time evolutions of J_x, J_y and J_z is straightforwardly derived from that of $N_{kl\pm}$ and N_k using the relations (4.25).

The second approach is to reduce the system of nine differential equations of the first order to a system of three differential equations of the third order, which will involve only variables J_x, J_y and J_z. For instance, Eq. (4.26) can be twice differentiated to obtained the expressions for J_z'' and J_z'''. The variables

N_1, N_2, N_3 and N_4 can be first expressed via J_z, J'_z and J''_z and then substituted to the equation for J'''_z. The similar procedure can be applied for J_x and J_y. Thus, the dynamics of J_x, J_y and J_z can be described by a system of three differential equations of the third order, which involve only variables J_x, J_y and J_z.

Note, that a system in the previous example characterized by $S = 1/2$ was described by first order differential equations. It can be shown that the time evolution of J_x, J_y and J_z due to the ultrafast IFE can be described by three differential equations of $2J$-th order, where J is the total momentum.

Let us examine the system of differential equations (4.27). It can be noticed that the equations of motion for the variables N_k include only N_k variables. Thus, N_k are independent from $N_{kl\pm}$ (for $k \neq l$). It means, that since J_z depends only on N_k variables, and J_x and J_y - on $N_{kl\pm}$ (for $k \neq l$), the time evolution of J_z does not depend on the time evolutions of J_x and J_y [2].

This allows the following conclusion. Consider two equal systems, which have initially equal z projections but different x and y projections. If a circularly polarized laser pulse propagating in the z direction excites the systems, then the time evolutions of z components of their magnetic moments will be equal.

Assume now that two equal systems have initially opposite x and y, but equal z magnetic moment projections. The variables entering the differential equations (4.27) for system 1 and 2 are denoted as $N^{(1)}_{kl\pm}$ and $N^{(2)}_{kl\pm}$, correspondingly. The initial conditions for the differential equations (4.27) would be $N^{(1)}_k(0) = N^{(2)}_k(0)$ and $N^{(1)}_{kl\pm}(0) = -N^{(2)}_{kl\pm}(0)$ (for $k \neq l$). The condition $N^{(1)}_k(0) = N^{(2)}_k(0)$ would lead to $N^{(1)}_k(t) = N^{(2)}_k(t)$ and $\mathcal{F}^{(1)}(t) = \mathcal{F}^{(2)}(t)$. It can be easily seen that the latter relation together with the initial condition $N^{(1)}_{kl\pm}(0) = -N^{(2)}_{kl\pm}(0)$ (for $k \neq l$) would result in $N^{(1)}_{kl\pm}(t) = -N^{(2)}_{kl\pm}(t)$. Thus, J_x and J_y would remain opposite for the two systems during and after the action a laser pulse.

Therefore, the following relations are valid for two equal systems excited by a same circularly polarized laser pulse propagating in the z direction. If the systems have equal z components of the magnetic moment, $M_{z1}(0) = M_{z2}(0)$, then these components remain equal $M_{z1}(t) = M_{z2}(t)$ during and after the excitation. If, in addition, they have opposite x and y magnetic vector components, $M_{x1,y1}(0) = -M_{x2,y2}(0)$, then they remain opposite: $M_{x1,y1}(t) = -M_{x2,y2}(t)$. It can be shown that this is true for any J. This result will be applied for the study of the dynamics of an antiferromagnet due to the ultrafast

[2]Note that S'_z depended on $S^2_x + S^2_y$ in the previous example. However, $S^2_x + S^2_y$ can be substituted for $1/4 - S^2_z$, if $S = 1/2$.

IFE in the Chapter 6.

Chapter 5

Larmor precession in an external magnetic field induced by the ultrafast IFE.

Circularly polarized light is able to induce transitions in an electronic system, which would result in a change of the magnetic signature of the ground state manifold. If there is some stationary external magnetic field or an internal field which acts on the magnetic system (such as exchange interaction), the magnetic states of the ground state manifold are energetically separated. In this case, the deviation of a magnetic moment from its ground state due to the action of a circularly polarized light results in the oscillation of a magnetic vector. Therefore, the complete description of the ultrafast IFE requires the investigation of two mechanisms: a laser-induced magnetic state change and triggering of a magnetic precession.

The mechanism of the optical process leading to the change of the magnetic state of a system was discussed in detail in Chapter 3. It was demonstrated in Chapter 4 that the time evolution of a magnetic vector during the excitation is governed by both mechanisms: laser induced transitions into a new magnetic state and the action of a stationary field, which affects the electron magnetic momentum. Therefore, the magnetization dynamics due to the two processes together should be investigated to obtain the correct magnetic state after the action of a laser pulse.

In this Chapter, the results of Chapters 3 and 4 are applied to study a spin Larmor precession in an external magnetic field induced by circularly polarized light. It will be shown that the phase and amplitude of the induced oscillations are determined during the laser excitation. Therefore, the calculation of the

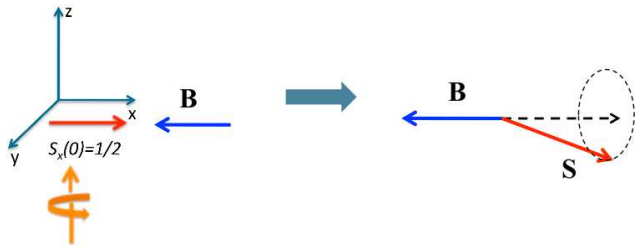

Figure 5.1: Spin 1/2 in an external magnetic field

time evolution of an electron spin during the action of a laser pulse is necessary to obtain the spin dynamics after it.

5.1 Single spin in an external magnetic field

The same system as in Section 3.3 is considered (see Fig. 5.1), but, additionally, an external magnetic field B applied in the $-x$ direction acts on the spin. It yields the splitting of the ground state s into two states $|x+\rangle$ and $|x-\rangle$ by the Zeeman interaction (see Fig. 5.2). The lowest energy state is $|x+\rangle$ with the spin pointing in the $+x$ direction and the energy $\epsilon_{x+} = \epsilon_{1s} - B/2$ (in atomic units). The state $|x-\rangle$ with the spin pointing in the $-x$ direction is with the energy $\epsilon_{x-} = \epsilon_{1s} + B/2$. The excited state is split into six levels by the spin orbit and Zeeman interactions (see Appendix C.3.1). The spin orbit coupling constant ζ_{soc} is 20 meV, which splits the $2p^{3/2}$ and $2p^{1/2}$ states by 30 meV in the absence of the magnetic field.

This system is excited by an ultrafast circularly polarized laser pulse propagating in the z direction. This pulse induces Raman transitions in the system with non-zero probability of a spin flip (see Chapter 3). This means that Raman transitions from the $|x+\rangle$ to the $|x-\rangle$ state are allowed (see Fig. 5.2). The new spin state after the excitation is the superposition of the states $|x+\rangle$ and $|x-\rangle$, resulting in the spin deviation from its initial alignment. This leads to the spin precession around the external magnetic field with the frequency of the Larmor precession $\omega_B = B$ (Fig. 5.1).

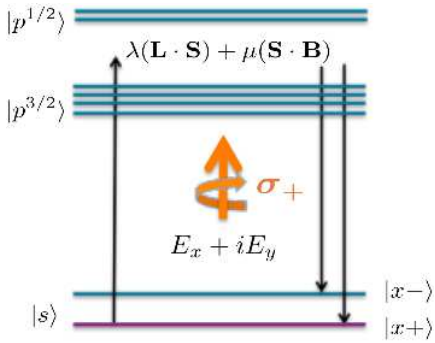

Figure 5.2: The energy level scheme of the system.

5.2 Spin equations of motion

It was shown in Section 4.3.1 that the effective spin Hamiltonian acting on the spin in the s state can be written as

$$\mathcal{H}_g = -\omega_B \hat{S}_x + f(t)\left(S_y\hat{S}_x - S_x\hat{S}_y\right) + g(t)\hat{S}_z + h(t)\hat{S}^2. \tag{5.1}$$

The equations of motion of the spin components of the s state are provided by the relation $i\langle S_\alpha\rangle' = \langle[S_\alpha, \mathcal{H}_g]\rangle$ ($\alpha = x,\, y,\, z$)

$$\begin{aligned} S_x' &= -f(t)S_xS_z - g(t)S_y \\ S_y' &= -f(t)S_yS_z + g(t)S_x + \omega S_z \\ S_z' &= f(t)(S_x^2 + S_y^2) - \omega S_y. \end{aligned} \tag{5.2}$$

The functions $f(t)$, $g(t)$ and $h(t)$ are time-dependent functions, which describe the action of the circularly polarized laser pulse. They are non-zero during the excitation, and zero after it. The functions $f(t)$ and $g(t)$, which enter Eq. 5.2, are connected to the second order wave function $\Psi_2 = \begin{pmatrix} (1/\sqrt{2})\psi_{21}(t) \\ (1/\sqrt{2})\psi_{22}(t) \end{pmatrix}$ via the relations

$$\begin{aligned} &f(t) = 2\,\mathrm{Re}\,(Y_2 - Y_1)\,, \quad g(t) = \mathrm{Im}\,(Y_2 - Y_1) \\ &Y_2 - Y_1 = \frac{2\left(V_-V_+' - V_+V_-'\right)}{V_+^2 e^{-i\omega_B t} - V_-^2 e^{i\omega_B t}} \\ &V_+ = 1 + \frac{\psi_{21}(t) + \psi_{22}(t)}{2}, \quad V_- = \frac{\psi_{21}(t) - \psi_{22}(t)}{2}. \end{aligned} \tag{5.3}$$

The second order wave function in the presence of the external magnetic field excited by a laser pulse with the electric field $\mathbf{E} = -(\mathbf{n}_x + i\mathbf{n}_y)\mathcal{E}f(t)\sin(\omega_0 t)$ are

$$\Psi_2(t) = \frac{1}{\sqrt{2}}\begin{pmatrix}\psi_{21}(t)\\ \psi_{22}(t)\end{pmatrix} = \frac{1}{\sqrt{2}}\left(\frac{\mathcal{E}}{\omega_0}\right)^2 \int_{-\infty}^{t} dt'\,\mathcal{U}(t')\begin{pmatrix}\sum_j |d_{\uparrow j}|^2 G_j(t')\\ \sum_j |d_{\downarrow j}|^2 G_j(t')\end{pmatrix}, \quad (5.4)$$

where

$$G_j(t') = e^{-i\Delta\omega_{0j}t'} f(t'/T)\cos(\omega_0 t') \int_{-\infty}^{t'} dt'' e^{i\Delta\omega_{0j}t''} e^{-i\omega_B t''/2} f(t''/T)\cos(\omega_0 t'') \quad (5.5)$$

and $\mathcal{U}(t) = e^{i\omega_B \hat{S}_x t} = \begin{pmatrix}\cos(\frac{\omega_B t}{2}) & -i\sin(\frac{\omega_B t}{2})\\ -i\sin(\frac{\omega_B t}{2}) & \cos(\frac{\omega_B t}{2})\end{pmatrix}$ is the time evolution operator due to the stationary magnetic field. The summation is over excited states j. $\Delta\omega_{0j} = \epsilon_{2p,j} - \epsilon_{1s}$, where ϵ_{1s} is the energy of the un-split $1s$ state, $\epsilon_{2p,j}$ are the energies of the excited states. $d_{\uparrow j}$ and $d_{\downarrow j}$ are the dipole matrix elements of the transitions from the states $|1s, S_z = +\frac{1}{2}\rangle$ and $|1s, S_z = -\frac{1}{2}\rangle$ to the state j.

The excited level, which is the p-state, is split into six states due to the spin orbit coupling and the Zeeman interaction (see Fig. 5.2). The wave functions of the excited states j, the dipole matrix elements $d_{\uparrow(\downarrow)j}$ of the transitions, and energies of the excited states $\epsilon_{2p,j}$ are calculated in Appendix C.3.1. It is also shown there that the spin reorientation is possible only in the presence of the spin-orbit coupling. The Zeeman interaction alone does not lead to the spin state change via the stimulated Raman scattering.

5.3 Time evolution of the spin vector

In this section, spin dynamics driven by the action of a circularly polarized laser pulse and different applied magnetic fields is calculated. Two applied magnetic fields with magnitudes of 7 T and 20 T are considered. Although the chosen magnetic fields are rather high, they are reasonable for the comparison with the experiments, studying the ultrafast IFE at a presence of an external magnetic field. The external magnetic fields up to 0.5 T are usually applied, but materials used there have gyromagnetic factor about ten times higher than that of a single electron spin[1] (*e. g.* see Refs. [10, 40, 41, 53]). Thus, the chosen magnitudes of the magnetic fields result in Larmor precession frequencies, which are relevant for experiments.

[1]The electron spin gyromagnetic ratio is 2.8 MHz/G=28 GHz/T.

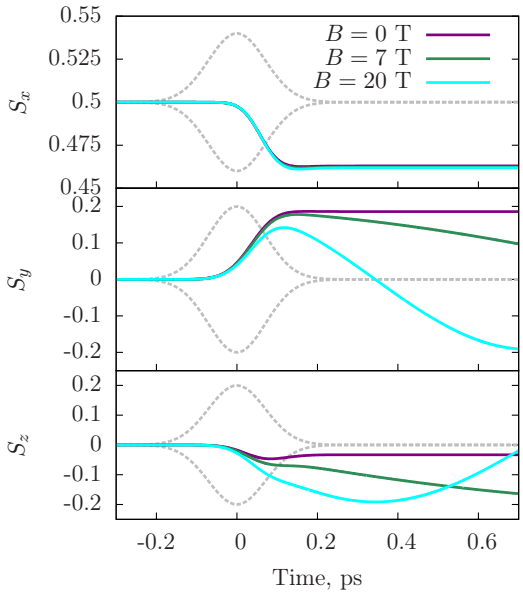

Figure 5.3: Time evolution of spin vector components due to the excitation at different applied magnetic fields in the x direction. The gray line represents the time evolution of the electric field amplitude. Laser pulse duration is 117 fs, detuning 0 meV.

The laser excitation is with the left-circularly polarized Gaussian shaped pulse with the duration $T_{\text{dr1}} = 117$ fs (spectral width 15 meV) and fluence $E_{\text{fl}} \approx 2$ mJ/cm^2 (see Section 3.1 for details). The laser central frequency ω_0 at zero detuning[2]. The magnetic field of 7 T results in the Larmor precession period T_{B7} of approximately 5 ps, $T_{B7}/T_{\text{dr1}} = 40$, and the splitting of the s state by 0.8 meV. The magnetic field of 20 T results in the Larmor precession period T_{B20} of approximately 1.7 ps, $T_{B20}/T_{\text{dr1}} = 15$, and the splitting of the s state by 2.7 meV.

The time evolution of the spin vector components S_x, S_y and S_z are shown on Fig. (5.3) at the two applied magnetic fields and zero magnetic field for a reference. The spin vector components at zero magnetic field will be referred to as the "reference values" $S_x^{(0)}$, $S_y^{(0)}$, $S_z^{(0)}$. Although the time evolution of the

[2]Detuning is defined as the difference between the laser central frequency and the energy between un-split $1s$ and $2p$ states: $\omega_0 - (\epsilon_{2p} - \epsilon_{1s})$.

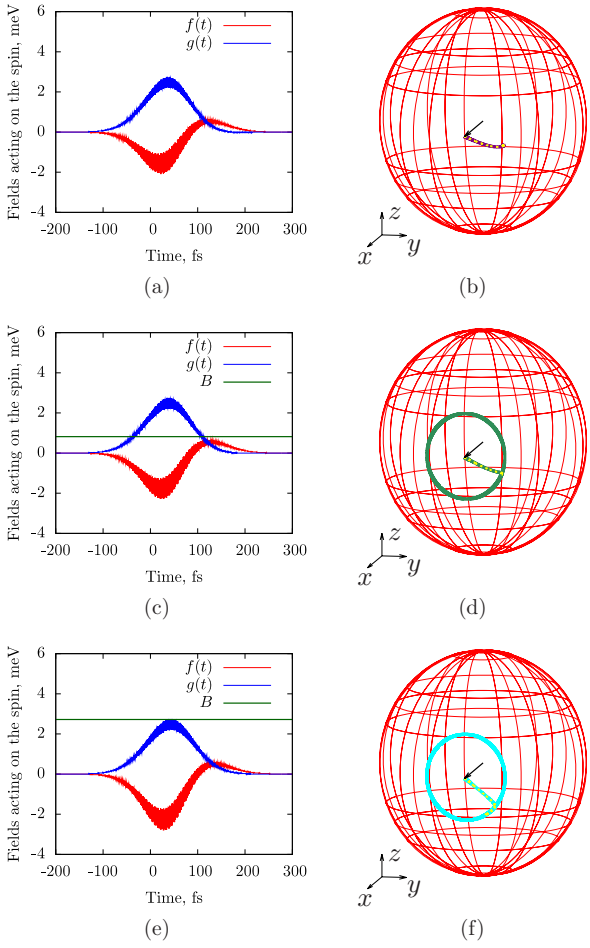

Figure 5.4: Left column: fields (in energy units) acting on the spin during the excitation. Right column: the corresponding time evolution of the spin vector on the Bloch sphere (note that these 3D plots have different meaning from Fig. 3.7 in Chapter 3, which depicts the *final* spin vector position depending on the *frequency*). The black arrow shows the initial alignment of spin. The two-color lines show the dynamics of the spin during the excitation, *i. e.* at $t < 200$ fs, the one-color lines show the dynamics of the spin after the excitation at $t > 200$ fs. The external magnetic fields are (a), (b) $B = 0$. (c), (d) $B = 7$ T. (e), (f) $B = 20$ T.

S_x component is almost not affected at the chosen conditions[3], the dynamics of the S_y and S_z components is affected by the external magnetic field during the excitation. S_y and S_z considerably deviate from the reference values at the time, when the electric field amplitude starts to be negligible (at the time $\tau_\mathrm{p} = 200$ fs).

Let us examine the error on the phase of the spin Larmor oscillation, which would be obtained, if one ignores the action of the magnetic field during the laser excitation. The spin oscillation around the magnetic field after the action of the laser pulse is described by the equations

$$\begin{aligned} S_x(t > \tau_\mathrm{p}) &= S_x(\tau_\mathrm{p}) \\ S_y(t > \tau_\mathrm{p}) &= S_y(\tau_\mathrm{p})\cos(\omega_B t) + S_z(\tau_\mathrm{p})\sin(\omega_B t) \\ S_z(t > \tau_\mathrm{p}) &= S_z(\tau_\mathrm{p})\cos(\omega_B t) - S_y(\tau_\mathrm{p})\sin(\omega_B t) \end{aligned} \tag{5.6}$$

If the spin motion due to the magnetic field during the excitation would be ignored, then the reference values $S_x^{(0)}$, $S_y^{(0)}$, $S_z^{(0)}$ would be substituted as the initial conditions for the equations of the spin oscillation: $S_{x,y,z}(\tau_\mathrm{p}) = S^0_{x,y,z}(\tau_\mathrm{p})$. This would lead to the phase disagreement with the exactly obtained time evolutions of 14° in the case of $B = 7$ T and 47° in the case of $B = 20$ T. Thus, the sudden approximation does not work correctly even if the oscillation period is about 50 times larger than the pulse duration. This statement is confirmed by the observation of Satoh *et al.* that models, which ignore the time-dependency of a laser pulse, are not sufficient to describe the initial stage of a magnetic precession [43].

Fig. 5.4 shows the fields acting on the spin in energy units (see Eq. (5.1)) and the corresponding spin vector movement in time, which are the 3D picture of the time evolutions shown on Fig. 5.3. The functions $f(t)$ and $g(t)$ arise from the excitation by the laser pulse. Although $f(t)$ and $g(t)$ depend on the magnetic field (see Eq. (5.3)), their modifications even due to the magnetic field of 20 T are negligible. It follows from Figs. 5.4c and e that $f(t)$ and $g(t)$ during the excitation are of the same order of magnitude as the Zeeman interaction.

Comparing Figs. 5.4b, d and f, it can be seen that the spin vector evolution during the excitation is modified by the external magnetic field. The spin moves almost always in the xy plane, when magnetic field is zero. However, its trajectory during the excitation is rotated by about 45° around the z axis, when $B = 20$ T. Furthermore, the spin trajectory starts to follow that of the Larmor oscillation even during the action of the laser pulse at $B = 20$ T (see Fig. 5.4f).

[3]It will be shown in the next section that this can be different at other conditions.

The amplitude of the spin precession is $A_S = \sqrt{S_y^2 + S_z^2} = \sqrt{1/4 - S_x^2}$. At the same time, it was shown in Section 3.3.2 that the spin-flip probability is given by $w_{\text{s-f}} = 1/2 - S_x$. Thus, the amplitude of the induced precessions of the single spin system is related to the spin-flip probability as $A_S = \sqrt{w_{\text{s-f}} - w_{\text{s-f}}^2}$. Since the spin-flip probability is proportional to the peak intensity squared, the amplitude of the induced precessions is linearly proportional to the peak intensity at low values of $w_{\text{s-f}}$, which agrees with the experimental observations [4].

5.4 Spectral dependence

The S_x component of the spin vector and, consequently, the amplitude of the induced precession A_S did not depend on the magnitude of the magnetic field at the laser pulse parameters chosen in the previous section. However, it is not always the case.

Figs. (5.5a and b) show the dependence of the amplitude on the detuning and the laser pulse spectral width at zero magnetic field[4] and $B = 20$ T. The spectral width $\Delta\omega_{\text{sw}}$ is varied between 5 meV and 35 meV, which corresponds for Gaussian-shaped pulses to the pulse durations between 365 fs and 54 fs. The amplitude of the electric field at every value of $\Delta\omega_{\text{sw}}$ is adjusted in such way that the value of $\mathcal{E}/\Delta\omega_{\text{sw}}$ is constant (see Section 3.3.2 for details).

Fig. 5.5c shows the difference between the amplitudes at $B = 0$ and $B = 20$ T, $\Delta A_S = A_S^{(B=0)} - A_S^{(B=20\text{T})}$, depending on the spectral width and laser frequency. The difference between the amplitudes is negligible at large spectral widths. However, it becomes noticeable at spectral widths lower than 10 meV, thereby the amplitude at zero magnetic field is higher than at $B = 20$ T.

This effect is due to the interplay between the laser pulse spectral width and the value of the Zeeman interaction. If the spectral width is about 30 meV, it is much higher than the Zeeman interaction, which is 2.72 meV. The values of transition amplitudes are not influenced by the detuning due to the Zeeman splitting of the s state (see Fig. 5.2). However, when the spectral width decreases to 10 meV or lower, it starts to be comparable with the Zeeman interaction. The difference between the initial $|x+\rangle$ and final $|x-\rangle$ state due to the Zeeman splitting becomes significant for the value of the transition amplitudes, which become reduced by the detuning.

Laser pulse parameters, at which the time evolution of S_x is considerably

[4]The value $A_S = \sqrt{1/4 - S_x^2(\tau_{\text{p}})}$ is referred to as an "amplitude" in the case of zero magnetic field for convenience.

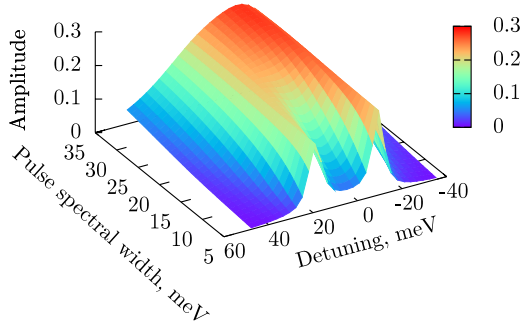

(a)

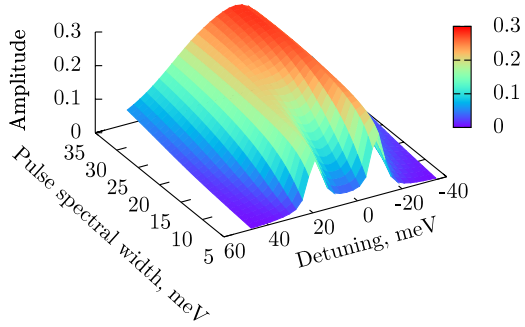

(b)

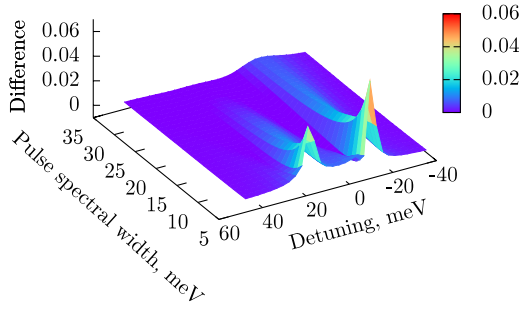

(c)

Figure 5.5: (a), (b) the dependence of the amplitude of the induced precession, $A_S = \sqrt{1/4 - S_x^2(\tau_\mathrm{p})}$, on the laser central frequency and spectral width at (a) $B = 0$; (b) $B = 20$ T. (c) The difference between the amplitudes shown on (a) and (b). Note that Fig. (3.4b) shows the dependence of the final spin-flip probability $w_{\text{s-f}}(\tau_\mathrm{p}) = 1/2 - S_x(\tau_\mathrm{p})$ on the same parameters.

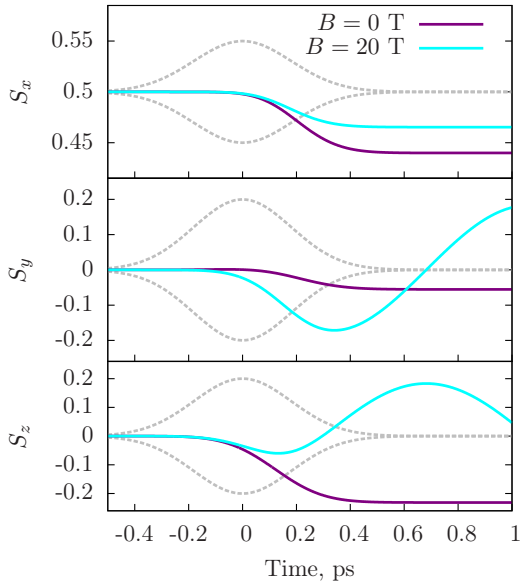

Figure 5.6: Time evolution of spin vector components due to the excitation at different applied magnetic fields in the x direction. The gray line represents the time evolution of the electric field amplitude. Laser pulse duration is 300 fs, detuning 10 meV.

affected by magnetic field of 20 T, are taken to compare the spin dynamics. Thus, a laser pulse with duration $T_{\mathrm{dr2}} = 300$ fs ($\Delta\omega_{\mathrm{sw}} = 6$ meV) and the central frequency of 10 meV detuning is taken. The pulse duration is by a factor 2.6 longer than in the previous case. The laser-induced spin dynamics at zero magnetic field and magnetic field of 20 T are compared. The period of the spin Larmor precession due to the magnetic field of 20 T is $T_{B20}/T_{\mathrm{dr2}} = 6$.

As expected, the time evolutions of all spin vector components S_x, S_y and S_z at magnetic field 20 T considerably deviate from the corresponding time evolutions at zero magnetic field during the action of the laser pulse (see Fig. 5.6). Fig. 5.7 shows the corresponding 3D picture of the spin vector trajectory and the fields acting on the spin in energy units. The functions $f(t)$ and $g(t)$ at $B = 20$ T are noticeably smaller than $f(t)$ and $g(t)$ at zero magnetic field. The considerable dependence of $f(t)$ and $g(t)$ on the magnetic field is due to the small laser pulse spectral width. Its value of 6 meV is comparable with the Zeeman interaction of about 3 meV and leads to the non-negligible

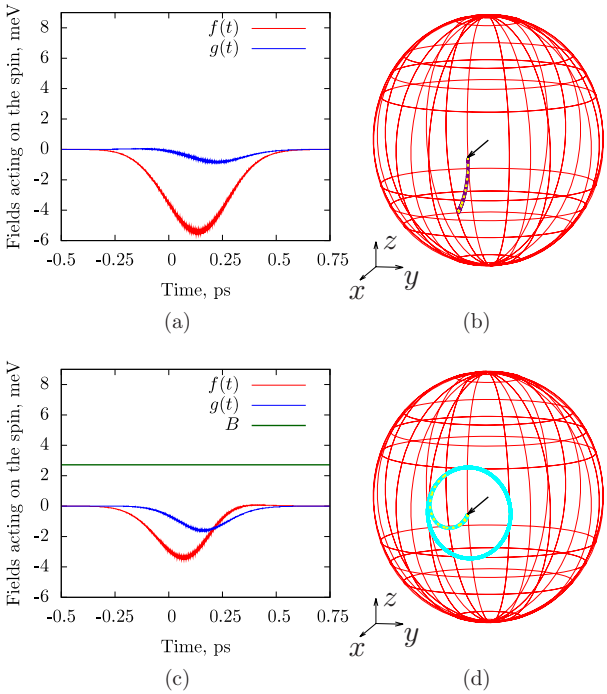

Figure 5.7: Left column: fields (in energy units) acting on the spin during the excitation. Right column: the corresponding time evolution of the spin vector on the Bloch sphere. The black arrow shows the initial alignment of spin. The two-color lines show the dynamics of the spin during the excitation, *i. e.* at $t < 200$ fs, the one-color lines show the dynamics of the spin after the excitation at $t > 200$ fs. The external magnetic fields are (a), (b) $B = 0$. (c), (d) $B = 20$ T.

dependence of the transition amplitudes on the magnetic field, resulting in the noticeable effect on the values of $f(t)$ and $g(t)$. This effect was negligible in the previous case, when the excitation was with the laser pulse of 117 fs duration (see Fig. 5.4a, c, e).

It can be noticed that the sign of the function $g(t)$ at the current laser pulse parameters (shown on Figs. 5.7a, c) is different from that in the previous case (shown on Fig. 5.4a, c, e). The spin trajectories triggered by the two laser pulses at zero magnetic field are also dissimilar (Figs. 5.7b and 5.4b). This difference is due to the different central frequencies of the laser pulse, which result in the different spin dynamics as was discussed in the Chapter 3 (see the discussion of Fig. (3.7)).

The further distinction from the situation in the previous section is that the spin vector trajectory is influenced much more by the magnetic field (see Fig. 5.7b, d). Now, the Larmor precession period is comparable with the laser pulse duration ($T_{B20}/T_{\mathrm{dr2}} = 6$), and the spin has enough time to rotate around the magnetic field during the excitation. However, the Larmor oscillation should not influence the dynamics of the S_x components and should not lead to the reduction of the amplitude A_S. Thus, the reduction of A_S results from the decrease of $f(t)$ due to the small spectral width of the laser pulse.

This statement can be checked by applying a laser pulse of the equal duration, but larger spectral width. A rectangular shaped laser pulse with the duration of 300 fs has the spectral width of 12 meV, which is two times longer than that of the Gaussian pulse of the same duration. Thus, the effect of the magnetic field on the amplitude A_S due to the action of the rectangular shaped laser pulse of the same duration and central frequency is calculated. The relative difference between the amplitudes at $B = 0$ and $B = 20$ T is[5] $\Delta A_S^{\mathrm{rec}} = 7\%$. The same value in the previous case, when the Gaussian shaped pulse with the same duration was applied, was $\Delta A_S^{\mathrm{Gauss}} = 26\%$. Thus, the values of the induced amplitudes are affected by an external magnetic field if a laser pulse spectral width is comparable with the Zeeman interaction. However, they are not necessary affected, if a laser pulse duration is comparable to a precession period.

[5]The relative difference is calculated as $\Delta A_S = \frac{A_S^{(B0)} - A_S^{(B20)}}{0.5(A_S^{(B0)} + A_S^{(B20)})} \times 100\%$, where $A_S^{(B0)}$ is the amplitude at zero magnetic field, $A_S^{(B20)}$ is the amplitude at the magnetic field of 20 T.

5.5 Conclusions

The interplay between the spin dynamics triggered by a laser pulse and an external magnetic field during the excitation is studied in this Chapter. It is shown that the magnetic field affects the spin dynamics during the action of a laser pulse even if the pulse duration is several tens times higher than the induced magnetic precession period. This results in the accumulation of the Larmor oscillation phase already during the excitation. This conclusion does not concern only Larmor precessions, but is general for any other types of induced oscillations [43].

The second effect is the decrease of the induced oscillation amplitude with the increase of the magnetic field. However, this effect becomes relevant, if the laser pulse spectral width is comparable with the Zeeman interaction. Namely, if the ratio of the laser pulse spectral width to the Zeeman interaction energy is less than five. Therefore, if the Zeeman interaction is rather large, laser pulses with large spectral width are more advantageous than laser pulses of the same duration, but smaller spectral width.

The effect of an applied magnetic field on the induced amplitude results from the dependence of transition amplitudes on the energies of involved system states. This leads to the dependence of the functions, representing the action of a laser pulse in the spin equations of motion, on an applied magnetic field. However, if a laser spectral width is much higher than the Zeeman interaction, then this dependence can be ignored.

Chapter 6

Modeling of the ultrafast inverse Faraday effect in magnetic crystals

The role of three local electron interactions for the IFE were studied in the previous Chapters. Namely, the spin-orbit coupling, the electron correlations within a given atom (Chapter 3) and Zeeman interaction (Chapter 5) were investigated. However, non-local interactions are also relevant for materials' magneto-optical properties [51]. Thus, interactions typical for a solid state, *i. e.* crystal field and exchange interactions, are considered in this Chapter.

It was shown in Chapter 3 that the presence of the spin-orbit coupling is necessary for the IFE, and the strength of the effect is determined by the magnitude of SOC. It will be shown in this Chapter that the IFE is also strongly affected by the crystal field interactions. Section 6.1 provides an example of an analysis of the IFE including both spin-orbit and crystal field interactions. This example demonstrates that the strength of the IFE strongly depends on the crystal field acting on an atom/ion.

Section 6.2 provides a method to simulate the magnetization dynamics in a magnetic material triggered by the ultrafast IFE. The mechanism of the excitation of magnetic precessions and induction of a magnetic moment in an easy plane antiferromagnet will be demonstrated. The study of the magnetization dynamics in an antiferromagnet is motivated by the observations of Satoh *et al.* in Ref. [43]. They showed that the IFE triggered terahertz spin oscillations in the compensated antiferromagnet NiO. These observations were quite unexpected, since they were against the suggestion that the IFE is possible only in a material with a non-zero magnetic moment [3]. According to this suggestion,

an effective magnetic field, induced by the IFE, has to produce a torque to a material's net magnetic moment to induce the precession of magnetization.

The phenomenological model of Ref. [124] indeed predicted the possibility of the ultrafast IFE in an antiferromagnet. However, this approach has several disadvantages for the interpretation of Satoh *et al.*'s experiment. First, the model is based on an assumption that the duration of a laser pulse is much shorter than the period of an induced spin precession. It was discussed in the previous Chapter that this approximation cannot be applied to describe laser-induced terahertz magnetic precessions. Second, the model considers the light excitation as an ultrashort magnetic pulse. Therefore, it does not provide the information about the dependence of the effect on laser pulse and material parameters.

The method described in Section 6.2, first, does not make any assumptions on the pulse duration and, thus, can be used for the interpretation of the subpicosecond magnetization dynamics. Second, the technique involves the analysis of material properties and thus provides the details about the dependence of the effect on a material structure.

6.1 Crystal field and spin-orbit coupling

6.1.1 Crystal field

Consider an ion in a crystalline environment. Additionally to the electron interactions of a free ion, there appear the Coulomb interactions between each electron and all the charges external to the ion [134, 135]. The crystal field potential due to the surrounding ions at the location of the k-th unpaired electron of the ion, is

$$V(\mathbf{r}_k) = \sum_j \frac{Z_j}{|\mathbf{R}_j - \mathbf{r}_k|}, \tag{6.1}$$

$\mathbf{R}_j$ and $\mathbf{r}_k$ are the positions of the j-th ligand ion and k-th unpaired electron. The center of the ion is taken as the origin, the summation is over all ligand ions in a crystal.

The complete treatment of the crystal field potential is quite complicated. But it can be simplified with the help of the crystal field theory, which treats the neighboring ions as point charges. In this case, the potential $V(\mathbf{r}_k)$ obeys the Laplace's equation and can be expanded in terms of the spherical harmonics Y_n^m with expansion coefficients A_n^m. Thus, the Hamiltonian describing the

crystal field acting on the ion is

$$\mathcal{H}_{\rm cr} = -\sum_{k=1}^{n_e} V(\mathbf{r}_k) = \sum_{n=0}^{\infty}\sum_{m=-n}^{n} A_n^m \sum_{k=1}^{n_e} |\mathbf{r}_k|^n Y_n^m(\theta_k, \phi_k), \tag{6.2}$$

n_e is the number of all unpaired electrons of the ion.

The Hamiltonian $\mathcal{H}_{\rm cr}$ can take a convenient form with the help of Steven's operator equivalent method [136]. According to this method, the Hamiltonian is first expressed in terms of the cartesian coordinates x, y and z. Then, applying that the matrix elements of the operators involving x, y and z are proportional to those of $\hat{L}_x$, $\hat{L}_y$ and $\hat{L}_z$ operators (or $\hat{J}_x$, $\hat{J}_y$ and $\hat{J}_z$), the spherical harmonics are expressed via $\hat{L}_x$, $\hat{L}_y$ and $\hat{L}_z$ operators (or $\hat{J}_x$, $\hat{J}_y$ and $\hat{J}_z$). For instance,

$$\sum_{k=1}^{n_e} Y_2^0 \propto \sum_{k=1}^{n_e}(3z_k^2 - \langle|\mathbf{r}_k|^2\rangle) \propto \langle r^2\rangle \left(3\hat{J}_z^2 - \hat{J}(\hat{J}+1)\right) = \langle r^2\rangle \mathcal{O}_2^0, \tag{6.3}$$

where r is the orbital radius. $\mathcal{O}_2^0$ is called the operator equivalent of Y_2^0. Thus, the crystal field Hamiltonian can be expressed via the operator equivalents $\mathcal{O}_n^m$, which are the L or J operators:

$$\mathcal{H}_{\rm cr} = \sum_{n=0}^{\infty}\sum_{m=-n}^{n} A_n^m \Theta_n \langle r^n\rangle \mathcal{O}_n^m = \sum_{n=0}^{\infty}\sum_{m=-n}^{n} B_n^m \mathcal{O}_n^m. \tag{6.4}$$

n can take values 2, 4, 6, because n cannot exceed $2L$ due to the orthogonality of the spherical harmonics. Odd numbers disappear for crystals with inversion symmetry. $n = 0$ gives an additive constant to the potential.

The operator equivalents $\mathcal{O}_n^m$ can be expressed by $\hat{L}_x$, $\hat{L}_y$ and $\hat{L}_z$ operators or $\hat{J}_x$, $\hat{J}_y$ and $\hat{J}_z$ depending on whether L or J is a good quantum number. For instance, the action of the crystal field on the $4f$ electrons in rare-earth-based solids is much weaker than the spin-orbit coupling [137]. The Hund's rules dominate the crystal field effects in this case, and the crystal field acts only within a given J-manifold. Thus, the crystal field Hamiltonian can be expressed via the J operators.

The situation is different for transition metal ions (particularly 3d-ions), for which crystal field effects are much larger than the spin-orbit coupling. J is not a good quantum number anymore, and the crystal field mixes states within a given (L, S) term. The crystal field Hamiltonian can be expressed via the L operators in this case.

The operator equivalents $\mathcal{O}_n^m$ are not always straightforwardly found as in (6.3), since the angular momentum operators do not commute. Fortunately, there are tables providing the operators $\mathcal{O}_n^m$ (e. g. in [138]).

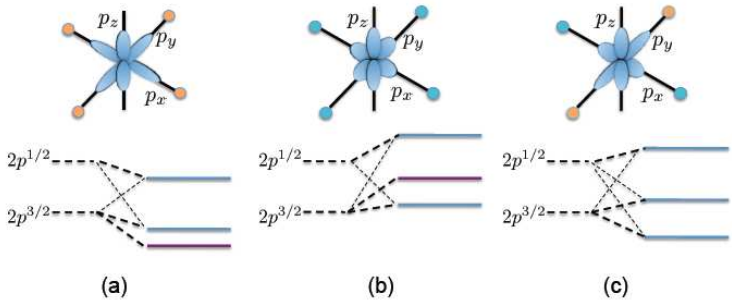

Figure 6.1: The energy level diagram of the $2p$ state split by $\mathcal{H}_0 = \zeta_{\text{soc}}\mathbf{L}\cdot\mathbf{S} + \mathcal{H}_{\text{cr}}$, where $\mathcal{H}_{\text{cr}}$ is (a) $-\frac{1}{3}\Delta\left(\mathcal{O}_2^0+2\right)$, (b) $+\frac{1}{3}\Delta\left(\mathcal{O}_2^0+2\right)$, (c)$\pm\Delta\mathcal{O}_2^2$. The bold dotted lines show the main origin of the level, the thick dotted line shows the admixture of the other level.

6.1.2 Effect of the crystal field on the IFE

It will be shown in this subsection, that the crystal field interaction is relevant for the IFE. This is demonstrated on a simple system in order to provide a clear example of the effect of the crystal field interaction. The chosen system corresponds to the case, when the crystal field interaction is expressed in terms of L operators.

The system similar to that in Section 3.3 is taken. It consists of an electron in the $1s$ state with spin aligned initially along the x axis. The excited state, which is the $2p$ state, is split by the spin-orbit interaction and the crystal field interaction, which was zero in Section 3.3. L is the good quantum number in this case, and the crystal field Hamiltonian is expressed in terms of L operators. The crystal field is of the same order of the spin-orbit coupling, and the corresponding Hamiltonians should be diagonalized together.

Three types of the crystal field interactions are considered. The first is determined by four equal positive point charges, each two of them are situated on the both sides of the x and y axis at equal distance (see Fig. 6.1a). The second is the same as the first, but the charges are negative (see Fig. 6.1b). The third crystal field is caused by two negative charges on the x axis, and two positive charges on the y axis situated at equal distance and with equal absolute values (see Fig. 6.1c).

The crystal field interaction splits the p state, but does not affect the s

state, which is spherically symmetric. However, it shifts the energy of the s state, since the electron interacts with the point charges. The degeneracy of the p orbitals is removed by the crystal field. The crystalline electric field is able to orient the electronic charge cloud into an energetically favorable direction [134]. For instance, the p_y orbital is stretched along the y axis, and p_x orbital is squeezed along the x axis in the third case (see Fig. 6.1c). The p_z orbital is unaffected in all three cases.

The crystal field Hamiltonians $\mathcal{H}_{\rm cr}^{(a)}$, $\mathcal{H}_{\rm cr}^{(b)}$ and $\mathcal{H}_{\rm cr}^{(c)}$ describing the crystal field on Fig. 6.1a, b, and c, and the corresponding energy splittings $\varepsilon_{x,y,z}$ of the orbitals $p_{x,y,z}$ at zero spin-orbit coupling are

$$\begin{aligned} &\mathcal{H}_{\rm cr}^{(a)} = -\Delta(\hat{L}^2 - \hat{L}_x^2 - \hat{L}_y^2) = -\frac{1}{3}\Delta\left(\mathcal{O}_2^0 + 2\right) \\ &\varepsilon_x = \varepsilon_y = -\Delta, \quad \varepsilon_z = 0 \end{aligned} \tag{6.5}$$

$$\begin{aligned} &\mathcal{H}_{\rm cr}^{(b)} = \Delta(\hat{L}^2 - \hat{L}_x^2 - \hat{L}_y^2) = \frac{1}{3}\Delta\left(\mathcal{O}_2^0 + 2\right) \\ &\varepsilon_x = \varepsilon_y = \Delta, \quad \varepsilon_z = 0 \end{aligned} \tag{6.6}$$

$$\begin{aligned} &\mathcal{H}_{\rm cr}^{(c)} = \Delta(\hat{L}_y^2 - \hat{L}_x^2) = -\Delta\mathcal{O}_2^2 \\ &\varepsilon_x = \Delta, \quad \varepsilon_y = -\Delta, \quad \varepsilon_z = 0, \end{aligned} \tag{6.7}$$

Since the wave functions at zero SOC are symmetric with respect to spin, the spin of the s state does not reorient after the Raman transitions via the p state (see Appendix C.3.2).

If the spin-orbit coupling is present in the system, the Hamiltonian acting on the p state is $\mathcal{H}_0 = \zeta_{\rm soc}\mathbf{L}\cdot\mathbf{S} + \mathcal{H}_{\rm cr}$. The p state is split into three levels, called Kramers doublets, with the wave functions of the form

$$\psi_{2p}^{\pm} = \alpha\left|m_L = \pm 1, m_S = \pm\frac{1}{2}\right\rangle + \beta\left|0, \mp\frac{1}{2}\right\rangle + \gamma\left|\mp 1, \pm\frac{1}{2}\right\rangle. \tag{6.8}$$

The presence of the doublet is the consequence of the Kramer's theorem, which says that the energy levels of systems with an odd total number of electrons (or other fermions) remain at least doubly degenerate in the presence of purely electric fields due to the time reversal symmetry.

The Hamiltonians $\mathcal{H}_0 = \zeta_{\rm soc}\mathbf{L}\cdot\mathbf{S} + \mathcal{H}_{\rm cr}^{(a,b,c)}$ are diagonalized in Appendix C.3.2 and the corresponding wave functions of the p state are obtained. Let us first consider the effect of the fields $\mathcal{H}_{\rm cr}^{(a)}$ and $\mathcal{H}_{\rm cr}^{(b)}$. The corresponding wave

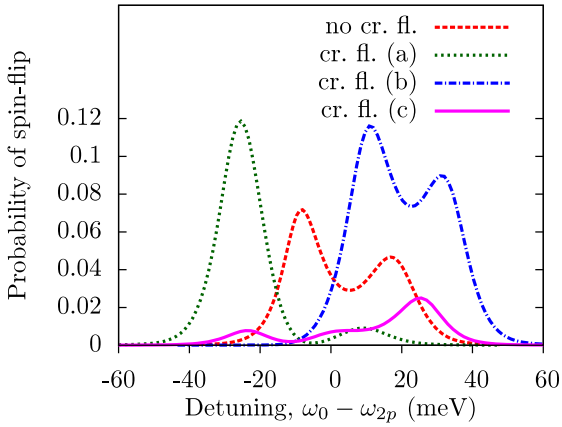

Figure 6.2: The final spin-flip probability depending on the detuning $\omega_0 - \omega_{2p}$ at the crystal fields (a), (b) and (c) with $\Delta = 20$ meV and without crystal field. $\zeta_{\text{soc}} = 20$ meV for all plots. The laser pulse parameters are the same as described in Chapter 3.

functions $\psi^{2p}_{k,\pm}$ of the three doublets obtain the form

$$\begin{aligned}
&\psi^{2p}_{1\pm} = \big|\pm 1, \pm 1/2\big\rangle \\
&\psi^{2p}_{2\pm} = \alpha_2\big|\pm 1, \mp 1/2\big\rangle + \beta_2|0, \pm 1/2\big\rangle \\
&\psi^{2p}_{3\pm} = \alpha_3\big|\pm 1, \mp 1/2\big\rangle + \beta_3|0, \pm 1/2\big\rangle \\
&|\alpha_2|^2 + |\alpha_3|^2 = 1, \quad |\alpha_{2,3}| = |\beta_{3,2}|,
\end{aligned} \tag{6.9}$$

It can be noticed, that the wave functions $\psi^{2p}_{1\pm}$ are of pure $2p^{3/2}$ origin (see Eq. (C.1.5) in Appendix C.1). Whereas, the wave functions of the level 2 are of $2p^{3/2}$ origin (corresponds to $2p^{3/2}$ at $\Delta = 0$) with the admixture of the wave functions of $2p^{1/2}$, and the level 3 is of $2p^{1/2}$ origin with the admixture of the wave functions of the $2p^{3/2}$.

The transitions from the s state induced by left-circularly polarized light are allowed only to the states with the projection $m_L = 1$. Thus, the transitions from the state with the spin-up component are allowed only to the level 1, the transitions of the state with the spin-down component are allowed to levels 2 and 3. The energy level diagrams for the case $\zeta_{\text{soc}} = \Delta$ are shown on Figs. 6.1a and b.

The IFE in the systems with the crystal fields (a) and (b) and zero crystal field are compared by studying the spin-flip probabilities. The dependencies

of the final spin-flip probability on the laser frequency are shown on Fig. 6.2. From the dependencies one can see that the IFE is higher in the systems with the two crystal fields compared to that at zero crystal field. This is due to the energy separation of the level 1 and level 2, which are degenerate without the crystal field. Their splitting provides the additional difference in the transition amplitudes for the spin-up and spin-down components, which is necessary for the IFE. Therefore, the spin-flip probability at laser frequencies in the vicinity of the levels 1 and 2 is higher than that at zero crystal field (the left peaks on the plots (a) and (b) on Fig. 6.2).

However, the spin-flip probability at the laser frequencies in the vicinity of the level 3 is lower at the crystal field (a) than that at zero crystal field (the right peak on the plot (a) on Fig. 6.2). The Raman transition amplitudes via the level 3 from the s state with the spin-down component are proportional to $|\alpha_3|^2$ (see Eq. (C.3.2.15)). The coefficient $|\alpha_3|$ is lowered due to the crystal field (a) resulting in the decrease of the spin-flip probability. However, $|\alpha_3|$ is increased due to the crystal field (b), therefore the spin-flip probability at frequencies in the vicinity of the level 3 is higher at the crystal field (b) than at zero crystal field (the right peak on the plot (b) on Fig. 6.2).

Let us now consider the crystal field (c). The wave functions of the three doublets of the excited state are

$$\psi_{2p}^{k\pm} = \alpha_k \left|\pm 1, \pm\frac{1}{2}\right\rangle + \beta_k \left|0, \mp\frac{1}{2}\right\rangle + \gamma_k \left|\mp 1, \pm\frac{1}{2}\right\rangle \qquad (6.10)$$
$$\alpha_k \neq 0, \quad \beta_k \neq 0, \quad \gamma_k \neq 0, \quad k = 1, 2, 3.$$

It is shown in Appendix C.3.2 that the energies of the levels and the transition amplitudes do not depend on the sign of Δ of the crystal field (c). The energy level diagrams for the case $\Delta = \pm\zeta_{\rm soc}$ are shown on Figs. 6.1c.

The transitions induced by the left-circularly polarized light are allowed for both spin components to every of the three levels. Therefore, the crystal field (c) increases the symmetry of the transitions for spin-up and spin-down. Thus, the IFE is decreased due to this crystal field (see Fig. 6.2). The situation by the crystal fields (a) and (b) is different, since they produced "additional" selection rules by forbidding transitions to the level 2 for the spin-up component.

The difference between the effects of the crystal fields (a) and (b), and (c) on the spin-flip probability can be understood by comparing their dependence

on the coefficients entering the doublets

$$w_{\text{s-f}}^{(a,b)}(t) \propto \left|\Gamma_1(t) - |\alpha_2^{(a,b)}|^2\Gamma_2(t) - (1 - |\alpha_2^{(a,b)}|^2)\Gamma_3(t)\right|^2 \tag{6.11}$$

$$w_{\text{s-f}}^{(c)}(t) =\propto \left|\sum_k^3 (|\alpha_k^{(c)}|^2 - |\gamma_k^{(c)}|^2)\Gamma_k(t)\right|^2,$$

where the functions $\Gamma_k(t)$ depend on the energies of the excited states. It can be noticed that the factors before $\Gamma_k(t)$ are higher for the crystal fields (a) and (b) than that for the crystal field (c).

These examples demonstrate that the crystal field interaction plays an important role for the strength of the IFE. Different types of a crystal field can lead either to increase or reduction of the effect. The analysis of the interplay of the crystal field effect and spin-orbit coupling in a material provides an idea about its effectiveness for the IFE. Such analysis is advantageous for a search among many possible structures for materials with the most strongest IFE, since this technique does not involve complicated electron structure calculations.

6.2 Dynamics of an easy plane antiferromagnet due to the ultrafast inverse Faraday effect

In this Section, the dynamics of two antiferromagnetically coupled sub-lattices in a crystal field environment induced by the ultrafast IFE is described. Applying the Weiss mean field theory for the exchange interaction [134] and assuming that atoms in the systems are excited coherently, the problem is reduced to two coupled systems each consisting of one atom.

The magnetic moment of each system changes due to the IFE, and so does the effective magnetic field caused by the exchange interaction, which acts on the other system. Therefore, the time evolutions of both systems depend on each other, and their dynamics has to be calculated simultaneously. The time evolution of the vectors $\mathbf{M}$ and $\mathbf{L}$, which are proportional to the ferromagnetic and antiferromagnetic vectors[1] will be derived.

The equations of motion for the components of vectors $\mathbf{M}$ and $\mathbf{L}$ will be obtained using the technique introduced in the Chapter 4. Thus, the momen-

[1]Ferromagnetic vector is the difference and antiferromagnetic vector is the sum of magnetic moments of sub-latices of an antiferromagnet/ferrimagnet.

tum operator, which provides the time evolutions of magnetic vectors induced by the ultrafast IFE, will be derived. It will be shown that the dynamics of the considered antiferromagnetic system during and after the excitation can be fully described by fifteen first order nonlinear differential equations. All details about the derivation and calculation of the introduced equations can be found in Appendix E.

6.2.1 Ground and excited states of two antiferromagnetically coupled sub-lattices

The antiferromagnet is treated in the framework of the Weiss mean field theory [134]. According to this theory, the quantum fluctuations can be neglected, and the exchange interaction between any two atoms is considered as the Zeeman interaction of the spin of each atom with the magnetic field, which is the spin average of the other atom. This means that the Hamiltonian $\mathcal{H}_{\mathrm{ex}12} = \mathcal{J}_{\mathrm{ex}0}\hat{S}_1 \cdot \hat{S}_2$ is substituted by $\mathcal{H}_{\mathrm{ex}} = \mathcal{J}_{\mathrm{ex}0}(\hat{S}_1\langle S_2\rangle + \langle S_1\rangle\hat{S}_2)$. With the assumption that the exchange interaction only with the next neighbor atoms is relevant, the Hamiltonian acting on atom i is expressed as

$$\mathcal{H}_{\mathrm{ex}(i)} = Z\mathcal{J}_{\mathrm{ex}0}\langle S_{\mathrm{nn}}\rangle\hat{S}_i, \tag{6.12}$$

Z is the number of the neighboring atoms, $\langle S_{\mathrm{nn}}\rangle$ is the average spin of a next neighbor atom. Using that the magnetic moment of an atom in the case of the LS-coupling is proportional to $g_J\mathbf{J} = \mathbf{L} + 2\mathbf{S}$ (g_J is the Landé factor), where $\mathbf{J} = \mathbf{L} + \mathbf{S}$, the exchange interaction acting on atom i can be expressed as

$$\mathcal{H}_{\mathrm{ex}(i)} = Z\mathcal{J}_{\mathrm{ex}0}(g_L - 1)^2\langle J_{\mathrm{nn}}\rangle\hat{J}_i. \tag{6.13}$$

The approximation is valid, when the fluctuations of the effective magnetic field $Z\langle J_{\mathrm{nn}}\rangle$ are small, which is true, when each spin has many nearest neighbors.

The chosen system consists of two equal sub-lattices coupled antiferromagnetically. Every atom belonging to the sub-lattice 1 is surrounded by Z atoms belonging to the sub-lattice 2 and vice versa. The exchange interaction acting on atoms belonging to the sub-lattices 1 and 2 can be written in the framework of the Weiss mean field theory as

$$\begin{aligned}\mathcal{H}_{\mathrm{ex}1} &= \mathcal{J}_{\mathrm{ex}}(J_{x2}\hat{J}_{x1} + J_{y2}\hat{J}_{y1} + J_{z2}\hat{J}_{z1}) \\ \mathcal{H}_{\mathrm{ex}2} &= \mathcal{J}_{\mathrm{ex}}(J_{x1}\hat{J}_{x2} + J_{y1}\hat{J}_{y2} + J_{z1}\hat{J}_{z2}),\end{aligned} \tag{6.14}$$

$\mathcal{J}_{\mathrm{ex}} = Z\mathcal{J}_{\mathrm{ex}0}(g_L - 1)^2$.

A crystal field with uniaxial symmetry in the z-direction acts on the systems. The spin-orbit coupling is assumed to be much larger than the crystal field, and the Hamiltonian can be expressed via the total momentum operators. In some cases, the term $B_2^0\mathcal{O}_2^0$ is sufficient to describe an uniaxial crystal field [134]. Thus the crystal field Hamiltonian $\mathcal{H}_{\rm cr} = B_2^0\mathcal{O}_2^0 = \Delta\left(3\hat{J}_z^2 - J^2\right)$.

It is assumed that the ground state of each atom in a system is characterized by a term with the total angular momentum J equal to 3/2. Thus, the total Hamiltonian acting on each atom is

$$\mathcal{H}_0 = \mathcal{H}_{\rm ex1} + \mathcal{H}_{\rm ex2} + \Delta\left(3\hat{J}_{z1}^2 - \frac{15}{4}\right) + \Delta\left(3\hat{J}_{z2}^2 - \frac{15}{4}\right). \tag{6.15}$$

The crystal field is a possible source of magnetic anisotropy, and the ground state alignment of the magnetic vectors are determined by the sign of Δ [134]. $\Delta > 0$ is taken, which makes the alignment of the magnetic moment along the z axis energetically unfavorable, and results in the xy plane being the easy plane. It is assumed that the neighboring terms are separated from the ground state by an energy, which is much larger than the spectral width of a laser pulse, which will be used for the excitation.

The initial direction of the magnetic vectors of the sub-lattices is chosen as the x axis. The energy of the system is the lowest, when the absolute values of J_{x1} and J_{x2} are the largest, but the vectors are antiparallel. Thus, the initial wave functions, which are spinors [2], have the form

$$\Psi_0^{(1)} = \begin{pmatrix} a \\ b \\ b \\ a \end{pmatrix},\ \Psi_0^{(2)} = \begin{pmatrix} a \\ -b \\ b \\ -a \end{pmatrix},\ \mathrm{Im}(a) = \mathrm{Im}(b) = 0,\ a > 0,\ b > 0. \tag{6.16}$$

It can be easily checked that $\langle\Psi_0^{(1)}|\hat{J}_{x1}|\Psi_0^{(1)}\rangle = -\langle\Psi_0^{(2)}|\hat{J}_{x2}|\Psi_0^{(2)}\rangle$, and $\langle\Psi_0^{(1,2)}|\hat{J}_{y1,2}|\Psi_0^{(1,2)}\rangle = 0$, $\langle\Psi_0^{(1,2)}|\hat{J}_{z1,2}|\Psi_0^{(1,2)}\rangle = 0$. The values of a and b depend on the ratio between the exchange interaction and the crystal field (see Appendix E.1). The crystal field interaction leads to partial quenching of the total magnetic moment, and the expectation values of the $\hat{J}_{x1,2}$ operators are smaller than $\pm 3/2$.

It is assumed, that the laser-induced Raman transitions of the atoms of each sub-lattice go via their excited states characterized by the term with $J = 5/2$. The other excited states, *e. g.* with $J = 3/2$ and $1/2$, are assumed to

[2] The k-th component of a spinor is the projection of the wave function on a state $|J_z = J - k\rangle$ (see Section 3.4 for details).

	$\lvert\mathrm{ex}, J_z = \pm\frac{5}{2}\rangle$	$\lvert\mathrm{ex}, J_z = \pm\frac{3}{2}\rangle$	$\lvert\mathrm{ex}, J_z = \pm\frac{1}{2}\rangle$
$\lvert\mathrm{g}, J_z = 3/2\rangle$	$-\sqrt{\frac{2}{3}}d_0$	0	0
$\lvert\mathrm{g}, J_z = 1/2\rangle$	0	$-\sqrt{\frac{1}{5}}d_0$	0
$\lvert\mathrm{g}, J_z = -1/2\rangle$	0	0	$-\sqrt{\frac{1}{10}}d_0$
$\lvert\mathrm{g}, J_z = -3/2\rangle$	0	0	$-\sqrt{\frac{1}{30}}d_0$

Table 6.1: The dipole matrix elements of the transitions from a ground state $|\mathrm{g}, J_z = M\rangle$ to an excited state $|\mathrm{ex}, J_z = M + 1\rangle$ for left-circularly polarized light.

be energetically inaccessible for the applied laser pulse. It is also assumed, that the exchange interaction between the sub-lattices negligibly affects the excited state. Thus, the Hamiltonian for each system is simply $\Delta_1 \left(3\hat{J}^2_{z1,2} - \hat{J}^2_{1,2}\right)$[3]. It is already diagonal and the eigenstates and energies of the excited state are

$$\begin{aligned} &|J_{z1,2} = \pm 5/2\rangle,\ \varepsilon_{\mathrm{ex}1} = \varepsilon_{\mathrm{ex}} + 10\Delta_1 \\ &|J_{z1,2} = \pm 3/2\rangle,\ \varepsilon_{\mathrm{ex}2} = \varepsilon_{\mathrm{ex}} + 2\Delta_1 \\ &|J_{z1,2} = \pm 1/2\rangle,\ \varepsilon_{\mathrm{ex}3} = \varepsilon_{\mathrm{ex}} - 8\Delta_1, \end{aligned} \tag{6.17}$$

$\varepsilon_{\mathrm{ex}} = 2$ meV is the energy of the excited state in the absence of the crystal field. The crystal field constant $\Delta_1 = 3$ meV is taken.

Let us examine the selection rules for the transitions from the ground state $|\mathrm{g}\rangle$ to the excited state $|\mathrm{ex}\rangle$ for an excitation by left-circularly polarized light. It was discussed in Section 3.4 that a dipole matrix element of a transition from a state with a total moment J and projection $J_z = m$ to a state with total moment $J + 1$ and $J_z = m + 1$ by $r_+ = (x + iy)/\sqrt{2}$ is [131]

$$\langle J+1\, m+1|r_+|J\, m\rangle = -\sqrt{\frac{(J+m+1)(J+m+2)}{(J+1)(2J+1)(2J+3)}}\,\langle J+1|r|J\rangle. \tag{6.18}$$

This relation is applied to obtain the dipole matrix elements shown in Table 6.1. d_0 is a reduced dipole matrix element: $d_0 = \langle \mathrm{ex}, J = 5/2|r|\mathrm{g}, J = 3/2\rangle$. $d_0 = 1$ a. u. is taken for simplicity.

[3]Note that the crystal field constant is not necessary the same as that of the ground state, since it depends on the orbital radius.

6.2.2 Equations of motion

The equations of motion, which describe the dynamics of the antiferromagnetic system induced by the ultrafast inverse Faraday effect, are introduced in this subsection. The IFE is triggered by a left-circularly polarized Gaussian-shaped laser pulse with the electric field

$$\mathbf{E} = -\frac{\mathbf{n}_x + i\mathbf{n}_y}{\sqrt{2}}\mathcal{E} f(t/T)\sin(\omega_0 t), \tag{6.19}$$

where $f(t/T) = e^{-t^2/T^2}/\sqrt{\pi^3}$. The pulse if of 117 fs duration (see Section 3.1 for details) with the peak intensity of 2×10^{10} W/cm^2 and the fluence 8 mJ/cm^2. The fluence of the pulse is chosen 4 times higher compared to the that used in the Chapter 3, because the electron interactions acting on the ground state of the current system are quite high and resist to the magnetic moment reorientation.

It is assumed that all atoms belonging to the same sub-lattice are excited coherently by a laser pulse. Thus, the dynamics of all atoms belonging to one sub-lattice can be simulated by one system. Therefore, the system 1 describes the dynamics of atoms belonging to the sub-lattice 1 and the system 2 - of atoms belonging to the sub-lattice 2. The dynamics of these systems is determined by the effective Hamiltonians $\mathcal{H}_{\text{ex1}} + \mathcal{H}_{\text{cr}}^{(1)} + \mathcal{H}_J^{(1)}$ and $\mathcal{H}_{\text{ex2}} + \mathcal{H}_{\text{cr}}^{(2)} + \mathcal{H}_J^{(2)}$, where

$$\begin{aligned}
\mathcal{H}_{\text{ex1}} &= \mathcal{J}_{\text{ex}}\left(J_{x2}\hat{J}_{x1} + J_{y2}\hat{J}_{y1} + J_{z2}\hat{J}_{z1}\right)\\
\mathcal{H}_{\text{ex2}} &= \mathcal{J}_{\text{ex}}\left(J_{x1}\hat{J}_{x2} + J_{y1}\hat{J}_{y2} + J_{z1}\hat{J}_{z2}\right),\\
\mathcal{H}_{\text{cr}}^{(1,2)} &= \Delta\left(\hat{J}_{z1,2}^2 + \frac{15}{4}\right).
\end{aligned}$$

It was shown in the Chapter 4 that the action of the IFE on a system characterized by the total momentum $J = 3/2$ can be written in the form of the momentum operator

$$\begin{aligned}
\mathcal{H}_J^{(1,2)} = &-\sum_a^4 \gamma_a^{(1,2)} n_a^{(1,2)} \\
&+ \frac{1}{2}\sum_{a,b}^4 \frac{1}{(p_a p_b)^2}\left(\nu_a^{(1,2)} - \nu_b^{(1,2)}\right)\left(n_{ab-}^{(1,2)}\hat{n}_{ab+}^{(1,2)} - n_{ab+}^{(1,2)}\hat{n}_{ab-}^{(1,2)}\right),
\end{aligned} \tag{6.20}$$

where $p_2 = p_3 = 1$, $p_1 = p_4 = \frac{\sqrt{3}}{2}$. $\hat{n}^{(1)}_{ab\pm}$ and $\hat{n}^{(2)}_{ab\pm}$ are J operators[4] acting on system 1 and 2 correspondingly. They can be expressed by a combination of $\hat{J}_{x1,2}$, $\hat{J}_{y1,2}$, $\hat{J}_{z1,2}$ and $\hat{J}^2_{1,2}$. These operators can be represented by 4×4 matrices, which elements are (indices 1 and 2 are omitted)

$$\begin{aligned}
&\text{If } b > a, \quad (n_{ab+})_{ab} = (n_{ab+})_{ba} = p_a p_b, \quad (n_{ab-})_{ab} = -ip_a p_b, \quad (n_{ab-})_{ba} = ip_a p_b, \\
&\text{If } a = b, \quad \hat{n}_{aa\pm} = \hat{n}_a, \quad (n_a)_{aa} = 1 \\
&(n_{ab\pm})_{cd} = 0, \text{ if } c \neq a,\ c \neq b,\ d \neq a,\ d \neq b \text{ or } a > b.
\end{aligned} \tag{6.21}$$

For example, $\hat{n}_{12+} = \begin{pmatrix} 0 & \frac{\sqrt{3}}{2} & 0 & 0 \\ \frac{\sqrt{3}}{2} & 0 & 0 & 0 \\ 0 & 0 & 0 & 0 \\ 0 & 0 & 0 & 0 \end{pmatrix}$, $\hat{n}_{12-} = \begin{pmatrix} 0 & -i\frac{\sqrt{3}}{2} & 0 & 0 \\ i\frac{\sqrt{3}}{2} & 0 & 0 & 0 \\ 0 & 0 & 0 & 0 \\ 0 & 0 & 0 & 0 \end{pmatrix}$. The usual momentum operators are connected to the operators $\hat{n}^{(1,2)}_{kl\pm}$ by

$$\begin{aligned}
\hat{J}_{x1,x2} &= \hat{n}^{(1,2)}_{12+} + \hat{n}^{(1,2)}_{23+} + \hat{n}^{(1,2)}_{34+} \\
\hat{J}_{y1,y2} &= \hat{n}^{(1,2)}_{12-} + \hat{n}^{(1,2)}_{23-} + \hat{n}^{(1,2)}_{34-} \\
\hat{J}_{z1,z2} &= \frac{3}{2}\hat{n}^{(1,2)}_1 + \frac{1}{2}\hat{n}^{(1,2)}_2 - \frac{1}{2}\hat{n}^{(1,2)}_3 - \frac{3}{2}\hat{n}^{(1,2)}_4 \\
\hat{J}^2_{1,2} &= \frac{15}{4}\left(\hat{n}^{(1,2)}_1 + \hat{n}^{(1,2)}_2 + \hat{n}^{(1,2)}_3 + \hat{n}^{(1,2)}_4\right).
\end{aligned} \tag{6.22}$$

$n^{(1,2)}_{kl\pm}$ are the expectation values of $\hat{n}^{(1,2)}_{kl\pm}$ operators: $n^{(1,2)}_{kl\pm} = \langle \Psi^{(1,2)}_{\mathrm{g}} | \hat{n}^{(1,2)}_{kl\pm} | \Psi^{(1,2)}_{\mathrm{g}} \rangle$. The coefficients $\nu^{(1,2)}_k$ and $\gamma^{(1,2)}_k$ will be given at the end of this subsection. It will be also shown there that $\nu^{(1)}_k = \nu^{(2)}_k = \nu$ and $\gamma^{(1)}_k = \gamma^{(2)}_k = \gamma$.

It is more convenient to consider the dynamics of vectors $\mathbf{M} = \mathbf{M}_1 + \mathbf{M}_2$ and $\mathbf{L} = \mathbf{M}_1 - \mathbf{M}_2$, where $M_{1,2} = (J_{x1,x2}, J_{y1,y2}, J_{z1,z2})$. The vectors $\mathbf{M}$ and $\mathbf{L}$ are proportional to ferromagnetic and antiferromagnetic vectors of the antiferromagnet. The equations of motion of the components M_α and L_α of the vectors $\mathbf{M}$ and $\mathbf{L}$ are given by the commutator with the effective Hamiltonian acting on the system:

$$\begin{aligned}
&iM'_\alpha = \langle [\hat{M}_\alpha, \mathcal{H}_0 + \mathcal{H}_J] \rangle, \ iL'_\alpha = \langle [\hat{L}_\alpha, \mathcal{H}_0 + \mathcal{H}_J] \rangle \\
&\mathcal{H}_0 = \mathcal{H}^{(1)}_0 + \mathcal{H}^{(2)}_0 = \left[\mathcal{H}^{(1)}_{\mathrm{cr}} + \mathcal{H}_{\mathrm{ex1}}\right] + \left[\mathcal{H}^{(2)}_{\mathrm{cr}} + \mathcal{H}_{\mathrm{ex2}}\right] \\
&\mathcal{H}_J = \mathcal{H}^{(1)}_J + \mathcal{H}^{(2)}_J,
\end{aligned} \tag{6.23}$$

where $\hat{M}_\alpha = \hat{J}_{\alpha 1} + \hat{J}_{\alpha 2}$ and $\hat{L} = \hat{J}_{\alpha 1} - \hat{J}_{\alpha 2}$.

[4]The operator $\mathcal{H}_J$ is expressed via operators $\hat{n}_{ab\pm}$ instead of $\hat{N}_{ab\pm}$ for convenience. They are related to each other by: if $a \neq b$ $\hat{n}_{ab\pm} = p_a p_b \hat{N}_{ab\pm}$, else $\hat{n}_{aa\pm} = \hat{n}_a = \hat{N}_a$.

The components $M_x(t)$, $M_y(t)$ and $L_z(t)$ are zero during and after the excitation for the following reason. First, it was shown in Chapter 4 that if two systems initially had equal z and opposite x and y components of magnetic vectors, then they would remain with equal z and opposite x and y components due to the dynamics induced by the IFE. Second, the exchange interaction has no effect on M_x and M_y, and also does not affects L_z, if $M_x = 0$ and $M_y = 0$ (see Appendix E for details). And finally, it holds for the crystal field $\mathcal{H}_{\rm cr}$ that if M_x and M_y are initially zero, they would remain zero. $\mathcal{H}_{\rm cr}$ has no effect on L_z. Therefore, all interaction acting on the systems demand that their x and y projections of the magnetic vectors are opposite, and z projections are equal, resulting in $M_x(t) = 0$, $M_y(t) = 0$ and $L_z(t) = 0$.

The equations of motion of the remaining components are

$$\begin{aligned}
M_x =& 0, \quad M_y = 0, \quad L_z = 0 \\
L'_x =& F_0(\nu_k, m_k) L_x + g(\gamma_k) L_y + F_{xy}(\nu_k, l_{12+}, l_{34+}) + G_{xy}(\gamma_k, l_{12-}, l_{34-}) \\
&+ 3\Delta(-2l_{12-} + 2l_{34-}) - \mathcal{J}_{\rm ex} L_y M_z \\
L'_y =& F_0(\nu_k, m_k) L_y - g(\gamma_k) L_x + F_{xy}(\nu_k, l_{12-}, l_{34-}) - G_{xy}(\gamma_k, l_{12+}, l_{34+}) \\
&+ 3\Delta(2l_{12+} - 2l_{34+}) + \mathcal{J}_{\rm ex} L_x M_z \\
M'_z =& F_0(\nu_k, m_k) M_z + F_z(\nu_k, m_k) M_z,
\end{aligned} \tag{6.24}$$

where $m_{kl\pm}$ and $l_{kl\pm}$ are the expectation values of the operators $\hat{m}_{kl\pm} = \hat{n}^{(1)}_{kl\pm} + \hat{n}^{(2)}_{kl\pm}$ and $\hat{l}_{kl\pm} = \hat{n}^{(1)}_{kl\pm} - \hat{n}^{(2)}_{kl\pm}$. The functions $F_0(\nu_k, m_k)$, $g(\gamma_k)$, $F_{xy}(\nu_k, l_{12\pm}, l_{34\pm})$, $G_{xy}(\gamma_k, l_{12\pm}, l_{34\pm})$ and $F_z(\nu_k, m_k)$ are defined in Appendix E.

The set of six equations is not sufficient to describe the dynamics of the whole system, because, apart from the six variables $M_{x,y,z}$ and $L_{x,y,z}$, the functions m_k and $l_{ab\pm}$ also enter Eq. (6.24). The time derivative of each expectation value, which enters (6.24), has to be found in order to obtain the complete set of the equations. The corresponding operators have to be commuted with the Hamiltonian, thereby new operators appear in the equations. Therefore, it is convenient to solve the equations of motion for the expectation values $m_{ab\pm}$ and $l_{ab\pm}$, and express $M_{x,y,z}$ and $L_{x,y,z}$ via these variables using

$$\begin{aligned}
\hat{L}_x &= \hat{l}_{12+} + \hat{l}_{23+} + \hat{l}_{34+} \\
\hat{L}_y &= \hat{l}_{12-} + \hat{l}_{23-} + \hat{l}_{34-} \\
\hat{M}_z &= \frac{3}{2}\hat{m}_1 + \frac{1}{2}\hat{m}_2 - \frac{1}{2}\hat{m}_3 - \frac{3}{4}\hat{m}_4.
\end{aligned} \tag{6.25}$$

The full set of the equations involves 16 variables: $l_{12\pm}$, $l_{23\pm}$, $l_{34\pm}$, $l_{14\pm}$,

$m_{13\pm}$, $m_{24\pm}$, m_1, m_2, m_3 and m_4, the equations of motion for which are

$$m'_{ab\pm} = \left(-\sum_{k=1}^{4} \nu_k m_k + \nu_a + \nu_b \right) m_{ab\pm} \pm (\gamma_a - \gamma_b) m_{ab\mp} - i\langle [\hat{m}_{ab\pm}, \mathcal{H}_0] \rangle$$
$$l'_{ab\pm} = \left(-\sum_{k=1}^{4} \nu_k m_k + \nu_a + \nu_b \right) l_{ab\pm} \pm (\gamma_a - \gamma_b) l_{ab\mp} - i\langle [\hat{l}_{ab\pm}, \mathcal{H}_0] \rangle. \quad (6.26)$$

The commutators of $\hat{m}_{ab\pm}$ and $\hat{l}_{ab\pm}$ with the Hamiltonian $\mathcal{H}_0$, which can be expressed as

$$\mathcal{H}_0 = \frac{\mathcal{J}_{\text{ex}}}{2} \left(-L_x \hat{L}_x - L_y \hat{L}_y + M_z \hat{M}_z \right) + 3\Delta \left(\frac{\hat{M}_z^2 + \hat{L}_z^2}{2} + \frac{\hat{J}_1^2 + \hat{J}_2^2}{3} \right), \quad (6.27)$$

are given in Table E.1 in Appendix E. All other variables are zero at any time: $m_{12\pm}(t) = 0$, $m_{23\pm}(t) = 0$, $m_{34\pm}(t) = 0$, $m_{14\pm}(t) = 0$, $l_{13\pm}(t) = 0$, $l_{24\pm}(t) = 0$ and $l_a(t) = 0$. Applying that $m_1 + m_2 + m_3 + m_4 = \sum_{a=1}^{4} n_a^{(1)} + \sum_{a=1}^{4} n_a^{(2)} = 2$, the system describing the dynamics of the antiferromagnet can be reduced to 15 first order differential equations.

Let us come back to the functions $\nu_k^{(1,2)}$ and $\gamma_k^{(1,2)}$. They depend on the properties of the excitation, energy levels of a system and dipole matrix elements of involved transitions. They should be equal for systems with equal electronic structure excited by the same laser pulse independent on the systems' initial states. However, the situation is more complicated in our case. The exchange part of the Hamiltonian $\mathcal{H}_0$ acting on the ground state manifold of atoms belonging to the sub-lattice 1 depends on the magnetic vector of the sub-lattice 2 and vice versa. The orientation and magnitude of the magnetic vectors of the sub-lattices are changing during the excitation. This means that $\nu_k^{(1)}$ and $\gamma_k^{(1)}$ of the IFE-momentum operator acting on the system 1 depend on the magnetic state of the system 2. $\nu_k^{(1)}$ and $\gamma_k^{(1)}$ at any time t during the excitation depend on the values of $J_{x2}(t)$, $J_{y2}(t)$ and $J_{z2}(t)$, and vice versa for $\nu_k^{(2)}$ and $\gamma_k^{(2)}$. However, the coefficients for both systems are indeed equal: $\nu_k^{(1)} = \nu_k^{(2)} = \nu$ and $\gamma_k^{(1)} = \gamma_k^{(2)} = \gamma$ due to symmetry considerations (see Appendix E.3.1). Therefore, the functions ν_k and γ_k need to be calculated only for one system.

The functions ν_k and γ_k are derived for the system 1. They are related to the vector $\mathcal{A}$, which contains the transition amplitudes from the states with different J_{z1} projections[5], by the relations $\nu_k = \text{Re}\,(Y_k)$ and $\gamma_k = \text{Im}\,(Y_k)$,

[5]See Section 4.1.1 and Eq. (E.2.5) for details.

where $Y_k = [\mathcal{U}\mathcal{A}']_k/[\mathcal{U}\mathcal{A}]_k$. $[\mathcal{U}\mathcal{A}']_k$ and $[\mathcal{U}\mathcal{A}]_k$ are the k-th elements of the vectors $\mathcal{U}\mathcal{A}'$ and $\mathcal{U}\mathcal{A}$.

$\mathcal{U}$ is the time evolution operator, which is related to the Hamiltonian $\mathcal{H}_0^{(1)} = \mathcal{H}_{\rm cr}^{(1)} + \mathcal{H}_{\rm ex1}$ by $i\mathcal{U} = \mathcal{H}_0^{(1)}\mathcal{U}$. $\mathcal{H}_0^{(1)}$ consists of two parts: the time-independent crystal field interaction $\mathcal{H}_{\rm cr}$ and exchange interaction part $\mathcal{H}_{\rm ex1}$, which depends on the magnetic vector of the sub-lattice 2:

$$\mathcal{H}_{\rm ex1}(t) = \mathcal{J}_{\rm ex}\left(-L_x(t)\hat{J}_{x1} - L_y(t)\hat{J}_{y1} + M_z(t)\hat{J}_{z1}\right)/2.$$

Thus, $\mathcal{H}_0^{(1)}$ is time-dependent and the time evolution operator cannot be written in the form of matrix exponential $\mathcal{U} \neq e^{-i\mathcal{H}_0^{(1)}t}$. The action of the operator $\mathcal{U}$ on a vector $\overline{\Psi}$ can be derived numerically with the procedure described in Appendix E.3.1. Note that since the time evolution operator $\mathcal{U}$ depends on $L_x(t)$, $L_y(t)$ and $M_z(t)$, the functions $\nu_k(t)$ and $\gamma_k(t)$ are also dependent on $L_x(t)$, $L_y(t)$ and $M_z(t)$.

The elements of $\mathcal{A}$ are obtained using Eqs. (A.2.9) and (A.2.11) and applying the selection rules for the excitation by left-circularly polarized light given in Table 6.1. The k-th element of $\mathcal{A}$ is

$$\text{if } P_{0k} \neq 0,\ \mathcal{A}_k = 1 - \mathcal{C}_k^{(1,2)}/P_{0k}^{(1,2)},\ \text{else } \mathcal{A}_k^{(1,2)} = 0, \tag{6.28}$$

where P_{0k} is the k-th element of the initial wave function $\Psi_{\rm g}^{(1)}(0)$ (see Eq. 6.16). $\mathcal{C}_k$ is the k-th element of the vector

$$\mathcal{C} = \mathcal{E}^2|d_0|^2\left[\int_{-\infty}^{t} dt'\,\mathcal{U}^{-1}(t')\right]\begin{pmatrix} \frac{2}{3}\hat{F}(t',\varepsilon_{\rm ex1})Q_1(t') \\ \frac{1}{5}\hat{F}(t',\varepsilon_{\rm ex2})Q_2(t') \\ \frac{1}{10}\hat{F}(t',\varepsilon_{\rm ex3})Q_3(t') \\ \frac{1}{30}\hat{F}(t',\varepsilon_{\rm ex3})Q_4(t') \end{pmatrix}, \quad Q(t) = \mathcal{U}(t)\Psi_{\rm g}^{(1)}(0). \tag{6.29}$$

The action of the operator $\hat{F}(t',\varepsilon_{{\rm ex}j})$ on $Q_k(t')$ is defined by

$$\begin{aligned}\hat{F}(t',\varepsilon_{{\rm ex}j})Q_k(t') =& f(t'/T)\cos(\omega_0 t')e^{-i\varepsilon_{{\rm ex}j}t'} \\ &\times \int_{-\infty}^{t''} dt''\, f(t''/T)\cos(\omega_0 t'')e^{i\varepsilon_{{\rm ex}j}t''}Q_k(t'').\end{aligned} \tag{6.30}$$

It was discussed in Chapter 4 that the inequality of the elements of the vector $\mathcal{A}$ makes the IFE possible. In our case, all four elements $\mathcal{A}_k$ are different. As in the previous systems, this is due to the SOC, which is responsible for different dipole matrix elements of the transitions from the states with different J_{z1} projections. The crystal field in the excited state enhances the diversity of the vector $\mathcal{A}$ elements, because it makes the factors $\varepsilon_{{\rm ex}j}$ entering $\mathcal{A}_k$ different.

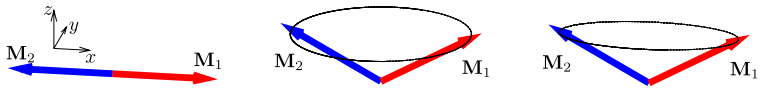

(a) Initial alignment (b) Circular mode (c) Elliptical mode

Figure 6.3: (a) The initial alignment of the magnetic vectors. (b) The circular mode. (c) The elliptical mode.

The calculation of the functions ν_k and γ_k can be simplified in some cases. As was discussed in Chapter 5, if the pump laser pulse spectral width $\Delta\omega_{\text{sw}}$ is much larger than the splitting of the ground state manifold, then the dependence of ν_k and γ_k on the time evolution operator $\mathcal{U}$ can be neglected. When this condition does not hold, the calculation still can be simplified in the case, then the laser pulse spectral width is much larger than the variation of the exchange interaction: $\Delta\omega_{\text{sw}} \gg |\mathcal{H}_{\text{ex1}}(t) - \mathcal{H}_{\text{ex1}}(t=0)|$. If this relation is true, then $\mathcal{H}_{\text{ex1}}$ can be assumed constant for the calculation of the functions ν_k and γ_k, and their dependence on $L_x(t)$, $L_y(t)$ and $M_z(t)$ can be ignored.

6.2.3 Results

It was shown in the previous subsection that the action of the ultrafast IFE on our system results in the rotation of the vector $\mathbf{L}$ and the induction of the vector $\mathbf{M}$, which was initially zero. Thereby, the components L_x, L_y and M_z change in time, while M_x, M_y and L_z remain zero. This means that the vectors $\mathbf{M}_1$ and $\mathbf{M}_2$, which are initially aligned antiparallel (see Fig. 6.3a), move in such way that their x and y projections remain opposite and z projections are equal (see Figs. 6.3b and c).

Figs. 6.4 and 6.5 show the dynamics of the vectors L_x, L_y and M_z and corresponding 3D picture of the vectors $\mathbf{M}_1$ and $\mathbf{M}_2$ during and after the excitation obtained by the numerical solution of the 15 differential equations 6.26. Five situations are considered: zero crystal field and the crystal field one order smaller than the exchange interaction (Figs.6.4a-d), exchange interaction $\approx$ crystal field (Figs.6.4e and f), and zero exchange and the exchange interaction one order smaller than the crystal field (Figs.6.5a-d).

As seen from Figs. 6.4 and 6.5, the M_z component changes only during the action of light. This is because the exchange interaction and the crystal field do not act on M_z (see Eq. 6.24). Thus, it changes only during the excitation and remains constant after it. However, all interactions act on L_x and L_y components. Thus, they are time-dependent during and after the excitation. Let us first look into their dynamics due to exchange interaction and crystal

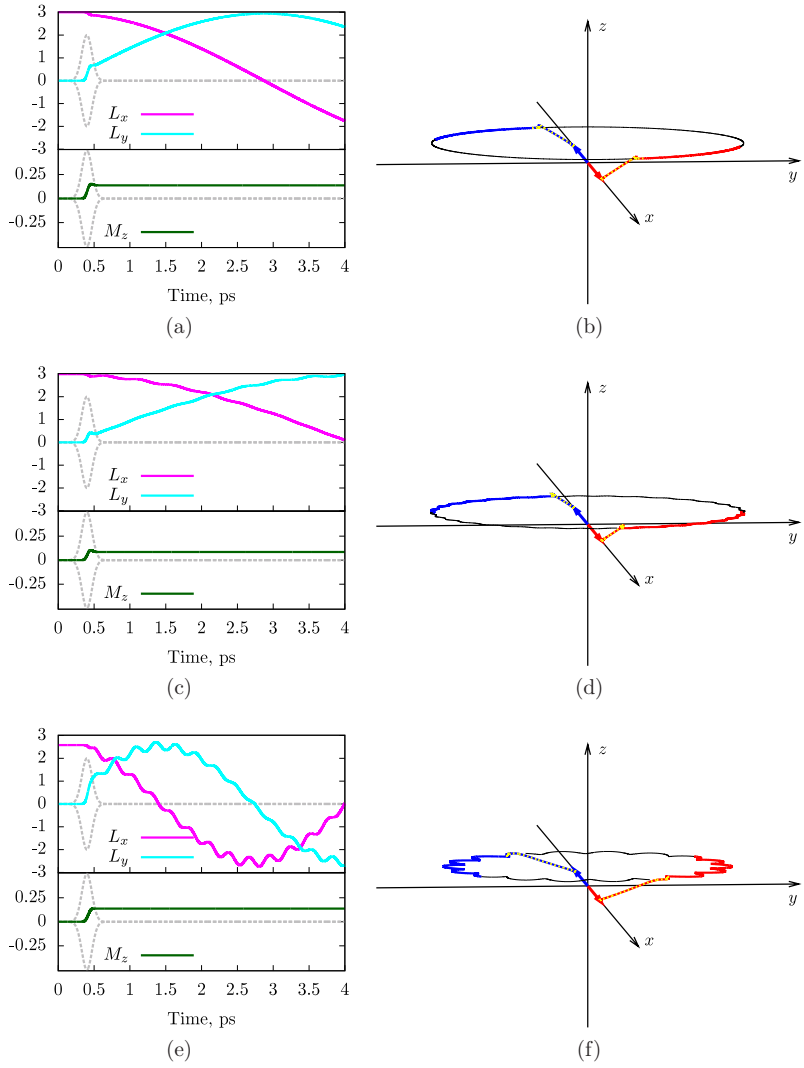

Figure 6.4: Left column: the time evolutions of L_x, L_y and M_z. Right column: The corresponding 3D-picture showing the time evolutions of the vectors $\mathbf{M}_1$ (in red) and $\mathbf{M}_2$ (in blue). Dotted yellow lines show the time evolutions of $\mathbf{M}_1$ and $\mathbf{M}_2$ during the excitation. $\mathcal{J}_{\text{ex}} = 3$ meV. The crystal field increases from up to down: (a), (b) $\Delta = 0$ meV; (c), (d) $\Delta = 0.2$ meV; (e),(f) $\Delta = 2$ meV.

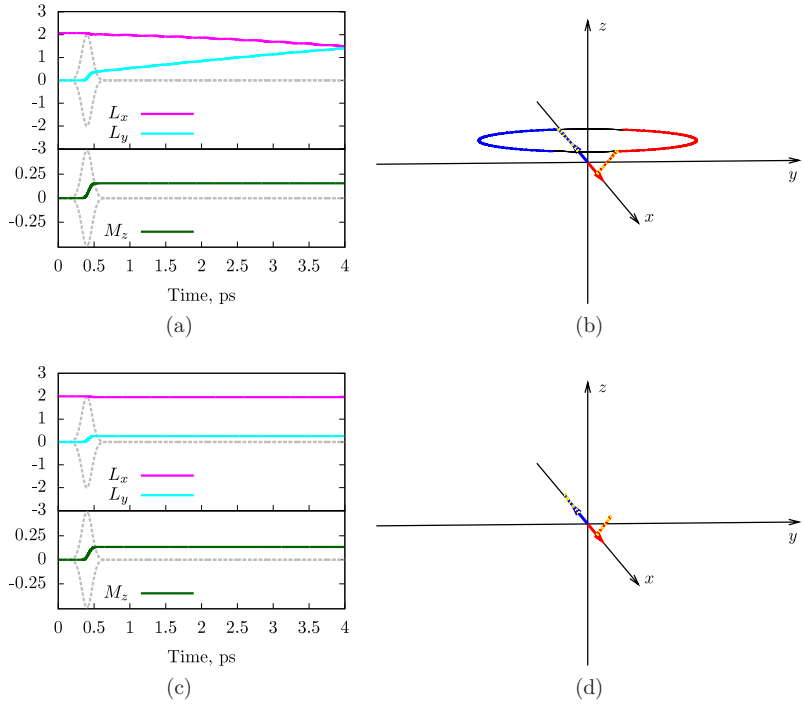

Figure 6.5: Left column: the time evolutions of L_x, L_y and M_z. Right column: The corresponding 3D-picture showing the time evolutions of the vectors $\mathbf{M}_1$ (in red) and $\mathbf{M}_2$ (in blue). Dotted yellow lines show the time evolutions of $\mathbf{M}_1$ and $\mathbf{M}_2$ during the excitation. $\Delta = 2$ meV. The exchange interaction decreases from up to down: (a), (b) $\mathcal{J}_{\text{ex}} = 0.3$ (c), (d) $\mathcal{J}_{\text{ex}} = 0$ meV.

field separately.

Zero crystal field

Assume that the crystal field acting on the ground state is much smaller than the exchange interaction. Let us examine, what changes for the system (6.24), which describes the dynamics of the vectors $\mathbf{M}$ and $\mathbf{L}$ during and after the action of the laser pulse. Although the crystal field term disappeared, the system (6.24) still includes the variables $\hat{l}_{12\pm}$, $\hat{l}_{34\pm}$ and $\hat{m}_a$ due to the excitation. The operators $\hat{l}_{ab\pm}$ and $\hat{m}_a$ have to be commuted with $\hat{L}_x$, $\hat{L}_y$ and $\hat{M}_z$, thereby, the new variables appear (see Table E.1). This again results in 15 equations,

describing the motion of the vectors $\mathbf{M}$ and $\mathbf{L}$ during the excitation.

The factors γ_k and ν_k, with which $l_{ab\pm}$ and m_a enter the system 6.24, are zero after the action of the laser pulse. Thus, no additional variables enter the system (6.24) after the excitation. Eq. (6.24) can be rewritten as

$$\begin{aligned} &M_z(t > \tau_\mathrm{p}) = M_{z0} = \mathrm{const},\ \omega_\mathcal{J} = \mathcal{J}_{ex} M_{z0} \\ &L_x' = -\omega_\mathcal{J} L_y \\ &L_y' = \omega_\mathcal{J} L_x \\ &L_z = M_x = M_y = 0. \end{aligned} \tag{6.31}$$

Thus, a circular rotation of the vectors $\mathbf{M}_1$ and $\mathbf{M}_2$ around the z axis with a frequency proportional to the value of M_z is excited by the IFE (see Figs. 6.3b and 6.4a, b).

Zero exchange interaction

Now, assume the reverse situation, when the exchange interaction is much weaker than the crystal field. The unperturbed Hamiltonian in this case is $\mathcal{H}_0 = \mathcal{H}_\mathrm{cr}^{(1)} + \mathcal{H}_\mathrm{cr}^{(2)}$. The Hamiltonians $\mathcal{H}_\mathrm{cr}^{(1,2)}$ do not depend on time and are diagonal. Therefore, the time evolution operators $\mathcal{U}^{(1,2)} = e^{-i\mathcal{H}_\mathrm{cr}^{(1,2)} t}$ are simply diagonal matrices, which considerably simplifies the calculation of the functions ν_k and γ_k.

The next simplification is that the system describing the dynamics of the vectors $\mathbf{M}$ and $\mathbf{L}$ can be reduced to nine equations. Additional variables do not appear, when the operators $\hat{l}_{ab\pm}$ and $\hat{m}_a$ are commuted with the crystal field Hamiltonian (see Table E.1). Thus, the dynamics during the excitation is described only by nine differential equations involving m_1, m_2, m_3, $l_{12\pm}$, $l_{23\pm}$, $l_{34\pm}$. After the excitation, the system is described by four differential equations. Its solution leads to

$$\begin{aligned} L_x &= A\cos(6\Delta t + \phi_A) + B\cos(6\Delta t - \phi_B) + C_x \\ L_y &= A\sin(6\Delta t + \phi_A) - B\sin(6\Delta t - \phi_B) + C_y \\ M_z &= \mathrm{const},\ M_x = M_y = 0 \end{aligned} \tag{6.32}$$

ϕ_A, ϕ_B, A, B, C_x and C_y are constants defined in Appendix E.4.2. These equations describe the elliptical rotation of the vectors $\mathbf{M}_1$ and $\mathbf{M}_2$ around the z axis (see Fig. 6.3c). However, this mode cannot be excited without the exchange interaction. It is shown in Appendix E.4.2 that the transitions are allowed only to the states with the same energy as the ground state in this case. Thus, although the components L_x, L_y and M_z are changed during the excitation, they do not precess (see Fig. 6.5c and d).

Exchange interaction and crystal field

It was shown in the previous subsection that the dynamics of the system after the excitation is described by 15 differential equations in the case, when both interaction are present. Both vectors **M** and **L** change during the action of the pulse. After the excitation, the vector **M** is constant and the vector **L** precesses.

The precession of the vector **L** is determined by circular and elliptical mode resulting in rather complicated trajectory (see Figs. 6.4c-f and 6.5a-b). This trajectory is described by 15 differential equations even after the excitation. This is due to the presence of the terms $3\Delta(\pm 2l_{12\pm} \mp 2l_{34\pm})$ in the system (6.24). The commutation of the operators $\hat{l}_{12\pm}$ and $\hat{l}_{34\pm}$ with $\mathcal{H}_0$ leads to appearance of new variables (see Table E.1).

Note, that the amplitude of the precession of the components L_x and L_y decreases with the increase of the crystal field (see Figs.6.4 and 6.5). It was discussed in Section 6.2.1 that the angular momentum is partly quenched due to the crystal field, and thus, the lengths of the vectors $\mathbf{M}_1$ and $\mathbf{M}_2$ are reduced. The final value of M_z is also different in all cases. This is because the value of the IFE and its dependence on laser pulse frequency are strongly affected by the internal interactions acting on the magnetic moment as was shown in Section 6.1.2.

It should be noted that the dynamics obtained for our system is slightly different to that induced in NiO by Satoh *et al.* in Ref. [43]. Satoh *et al.* observed the oscillations of both ferromagnetic and antiferromagnetic vectors. However, the precession of only antiferromagnetic vector is excited in our case. The precession of the ferromagnetic vector was not invoked, because the laser pulse propagating along the crystal field axis was applied.

To sum up, it was shown that the dynamics of the easy plane antiferromagnet during the excitation can be fully described by a system of 15 first-order differential equations. The mechanism of the induction of the net magnetic moment and triggering of the precession of the antiferromagnetic vector of an easy plane antiferromagnet was demonstrated.

The developed technique to study the magnetization dynamics induced by the ultrafast IFE, can be applied to other materials, which are not necessary antiferromagnetic. The equations of motion introduced in this Thesis can be used as a link to derive a macroscopic description of the ultrafast IFE from the microscopic one provided here.

Chapter 7

Conclusions and Outlook

A theoretical basis for the description of the inverse Faraday effect (IFE) triggered by subpicosecond laser pulses was developed in this Thesis. First, we have shown that the classical interpretation of the IFE as the generation of an effective magnetic field during the action of laser light cannot be applied to describe the novel ultrafast experiments. This interpretation works for magnetization dynamics *during* the action of a stationary excitation for a time, which is enough for a quasi-equilibrium to settle. However, the ultrafast IFE is a different process, which acts as follows. The stimulated Raman scattering, which takes place for a time much smaller than any system relaxation times, brings the system away from its ground magnetic state. This excites a magnetic precession, which lasts for times much longer than the laser pulse duration.

The expression for the time evolution of induced magnetization during the ultrafast excitation was derived by the solution of the time-dependent Schrödinger equation. The dependence of the induced magnetization on laser pulse electric field, which we obtained, is different from the classical one, but approaches it at long time scales. We showed that the final value of the induced magnetization is determined by the laser pulse spectral width and the integral of the pulse electric field over time in the ultrafast case.

We demonstrated that a circularly polarized laser pulse can induce magnetic changes in a system only if the spin-orbit coupling is present in a system. In this case, the spin symmetry for transition probabilities is broken and the Raman transitions to a new magnetic state are allowed. The crystal field structure plays also an important role for the IFE and can either enhance or reduce it. However, the IFE is not possible in the presence of a crystal field alone.

The Heisenberg representation for the ultrafast inverse Faraday effect was derived from the Schrödinger picture. Thus, an operator acting on a total an-

gular momentum, the components of which depend on transition dipole matrix elements and laser pulse electric field, was deduced. The purpose of this work was to derive how circularly polarized light couples to total angular momentum components individually. The momentum operator allows to separate the motion of a magnetic vector due to the action of light from that induced by other fields acting on a magnetic system. Furthermore, it provides the equations of motion of magnetic vector components during the excitation, which smoothly merge the equations of motion after the action of a laser pulse.

First, these equations of motion were applied to describe the laser-induced Larmor precession of a single spin in an external magnetic field. It was demonstrated that the external magnetic field can strongly influence the spin dynamics during the action of a laser pulse. Thus, we demonstrated that the sudden approximation is not sufficient to describe the laser induced magnetic precessions, the periods of which are even several tens times longer than the laser pulse duration.

Finally, the equations of motion were applied to describe the dynamics of a compensated easy plane antiferromagnet with an uniaxial crystal structure. We obtained that the action of the ultrafast IFE in this system leads to the induction of the net magnetic moment and excitation of an antiferromagnetic vector precession.

We have several suggestions how the work performed in this Thesis can be applied and extended for a further study of ultrafast laser induced phenomena.

1) We showed that the approximations of the classical theory of the IFE derived for the stationary excitation are not applicable for the ultrafast case. This also should be true for classical theories of other magneto-optical effects. Thus, we suggest that the similar study should be performed for other effects, especially for (direct) Faraday or Kerr effect, which are used for the measurement of magnetization.

2) The developed method to describe the dynamics induced in magnetic crystals by the ultrafast IFE is general and can be applied for magnetization dynamics in real materials. Thus, it can be used either for the interpretation of experiments which are already done or to suggest new ones.

3) We provided several examples how the selection rules, which determine the transition probabilities, depend on the electron interactions. They demonstrate how the analysis of the effectiveness of the IFE in an electron system can be performed. Thus, it can be used for the comparison of the IFE strength in various materials.

4) The dependence of the induced magnetization on the laser pulse properties, which is derived here, can be employed for the manipulation of magne-

tization dynamics by adjusting laser pulse parameters.

5) Finally, the momentum operator can be used as a link to derive a macroscopic description of the ultrafast IFE.

Appendix A

The solution of the time-dependent Schrödinger equation

A.1 The solution of the time-dependent Schrödinger equation by iterations

The time-dependent Schrödinger equation, which describes the time evolution of a wave function of an electron system due to a perturbation $\hat{V}$, is

$$\Psi'(t) = (\mathcal{H}_0 + \hat{V})\Psi(t). \tag{A.1.1}$$

$\mathcal{H}_0$ is the unperturbed Hamiltonian of the system. An electronic system in the absence of the perturbation $\hat{V}$ is described by the Hamiltonian $\mathcal{H}_0$

$$\mathcal{H}_0 = \sum_\alpha \mathbf{p}_\alpha^2/2 + \mathcal{V}_{\text{int}}. \tag{A.1.2}$$

$\mathbf{p}_\alpha$ is the momentum of an electron, $\mathcal{V}_{\text{int}}$ is the sum of the kinetic energy of nuclei, the interaction energy between electrons and nuclei and mutual Coulomb energy of the electrons and nuclei. The interactions, which are important for effects on the spin of the electrons, such as the spin-orbit- and Zeeman interactions, must be also included to $\mathcal{V}_{\text{int}}$. The summation is over all electrons in the system.

In order to solve the equation, one makes an *Ansatz* that

$$\Psi(t) = \mathcal{U}(\Psi_0 + \Psi_1(t) + \Psi_2(t) + \ldots), \tag{A.1.3}$$

where $\mathcal{U}$ is the time evolution operator, which by definition fulfills the equation $i\mathcal{U}' = \mathcal{H}_0\mathcal{U}$, $\Psi_0 = \Psi(0)$ and Ψ_n are some time-dependent functions.

Combining the Eq. (A.1.1) and the property of the time evolution operator $\mathcal{U}$, one obtains

$$\begin{aligned}(\mathcal{H}_0 + \hat{V})\Psi(t) &= i(\mathcal{U}(\Psi_0 + \Psi_1 + \Psi_2 + \ldots))' \\ &= \mathcal{U}(i\Psi_1' + i\Psi_2' + \ldots) + \mathcal{H}_0\mathcal{U}(\Psi_0 + \Psi_1 + \Psi_2 + \ldots)\end{aligned} \tag{A.1.4}$$

Subtraction of the term $\mathcal{H}_0\Psi(t)$ from both sides leads to

$$\hat{V}\Psi(t) = \mathcal{U}(i\Psi_1' + i\Psi_2' + \ldots), \tag{A.1.5}$$

and multiplication of both sides by the inverse operator $\mathcal{U}^{-1}$ results in

$$\mathcal{U}^{-1}\hat{V}\mathcal{U}(\Psi_0 + \Psi_1 + \Psi_2 + \ldots) = (i\Psi_1' + i\Psi_2' + \ldots). \tag{A.1.6}$$

Thus, the Eq. (A.1.1) can be solve iteratively, calculating the series of integrals

$$\Psi_{n+1} = -i\int_{-\infty}^{t} \mathcal{U}^{-1}\hat{V}\mathcal{U}\Psi_n, \quad n = 0\ldots\infty. \tag{A.1.7}$$

If Hamiltonian $\mathcal{H}_0$ does not change in time, the time evolution operator $\mathcal{U}$ equals to the matrix exponent $e^{-i\mathcal{H}_0 t}$, and Eq. A.1.3 turns to

$$\begin{aligned}\Psi(t) = e^{-i\mathcal{H}_0 t} \Bigg(&\Psi_0 - i\int_{-\infty}^{t} dt'\, e^{i\mathcal{H}_0 t'}\hat{V}e^{-i\mathcal{H}_0 t'}\Psi_0 \\ &- \int_{-\infty}^{t} dt'\, e^{i\mathcal{H}_0 t'}\hat{V}e^{-i\mathcal{H}_0 t'}\int_{-\infty}^{t'} dt''\, e^{i\mathcal{H}_0 t''}\hat{V}e^{-i\mathcal{H}_0 t''}\Psi_0 + \ldots\Bigg).\end{aligned} \tag{A.1.8}$$

A.2 Excitation by light

In the case of excitation by light, the perturbation is determined by the electric field $\mathbf{E}$ and dipole moment of the system $\mathbf{d}$: $\hat{V} = -\mathbf{d}\cdot\mathbf{E}$. The action of a laser pulse with a frequency ω_0 and an electric field $\mathbf{E}$

$$\mathbf{E} = \mathbf{n}\mathcal{E}f(t/T - \mathbf{r}/(cT))\sin(\omega_0 t). \tag{A.2.1}$$

on an electronic system with the spatial extend much smaller than the wavelength $\lambda_0 = c/\omega_0$ is considered. $\mathcal{E}$ is the amplitude of the electric field, $\mathbf{n}$ is perpendicular to the direction of propagation and the function $f(t/T)$ describes the time-dependence of the amplitude of the electric field.

The electric field is related to the vector potential [130]

$$\mathbf{E} = -\frac{1}{c}\mathbf{A}'. \tag{A.2.2}$$

The vector potential obeys the wave equation

$$\Delta\mathbf{A} = \left(\frac{\partial}{c\partial t}\right)^2 \mathbf{A} = \frac{1}{c^2}\mathbf{A}'' \quad ; \quad \nabla\mathbf{A} = 0. \tag{A.2.3}$$

The spatial extent of the wave train, cT, has to be large compared to the wavelength λ_0 to ensure that $\mathbf{A}$ fulfills Eq. (A.2.3).

If the momentum operator in Eq. (A.1.2) is replaced by $\mathbf{p} - \mathbf{A}/c$, the Hamiltonian acting on the wave function of the system $\Psi(t)$ is

$$\begin{aligned}\mathcal{H}_0 + \hat{V} &= \frac{1}{2}\left(\mathbf{p}_\alpha - \frac{\mathbf{A}}{c}\right)^2 + \mathcal{V}_{\text{int}} \\ &= \mathcal{H}_0 - \frac{1}{c}\mathbf{A}\sum_\alpha \mathbf{p}_\alpha + \frac{1}{2c^2}\mathbf{A}^2\end{aligned} \tag{A.2.4}$$

The term $\mathbf{A}^2/2c^2$ will be shown to be not relevant for further considerations. Thus, $\hat{V} = -\mathbf{A}\sum_\alpha \mathbf{p}_\alpha/c = -\hat{Q}/c$ is substituted to the Eq. A.1.8

$$\begin{aligned}\Psi(t) = e^{-i\mathcal{H}_0 t}\Bigg(&\Psi_0 + \frac{i}{c}\int_{-\infty}^{t} dt'\, e^{i\mathcal{H}_0 t'}\hat{Q}e^{-i\mathcal{H}_0 t'}\Psi_0 \\ &+ \frac{1}{c^2}\int_{-\infty}^{t} dt'\, e^{i\mathcal{H}_0 t'}\hat{Q}e^{-i\mathcal{H}_0 t'}\int_{-\infty}^{t'} dt''\, e^{i\mathcal{H}_0 t''}\hat{Q}e^{-i\mathcal{H}_0 t''}\Psi_0 + \ldots\Bigg).\end{aligned} \tag{A.2.5}$$

The second term of the expansion in the brackets describes the transitions from the ground state having the energy ε_i to any possible excited states ϕ_j having the energy ε_j[1], *i. e.* the absorption. The third term describes the transitions from the ground state to possible intermediate states ϕ_j, and from the intermediate states to final states ϕ_f having the energy ε_f. This term is responsible for the stimulated Raman scattering. The further terms are of higher order of the inverse speed of light $1/c$, and can be ignored.

$$\begin{aligned}\Psi(t) = e^{-i\mathcal{H}_0 t}\Bigg(&\Psi_0 + \frac{i}{c}\sum_j |\phi_j\rangle\int_{-\infty}^{t} dt'\, e^{i(\varepsilon_j-\varepsilon_i)t'}\langle\phi_j|\hat{Q}|\Psi_0\rangle \\ &+ \frac{1}{c^2}\sum_{jf}|\phi_f\rangle\int_{-\infty}^{t} dt' e^{i(\varepsilon_f-\varepsilon_j)t'}\,\langle\phi_f|\hat{Q}|\phi_j\rangle\int_{-\infty}^{t'} dt''\, e^{i(\varepsilon_j-\varepsilon_i)t''}\langle\phi_j|\hat{Q}|\Psi_0\rangle + \ldots\Bigg).\end{aligned} \tag{A.2.6}$$

[1] An electronic system with a discrete spectrum is considered.

Replacing the matrix element of the momentum operator by the dipole operator $\mathcal{D} = \sum_\alpha \mathbf{r}_\alpha$ with the relation $i\sum_\alpha \mathbf{p}_\alpha = [\mathcal{D}, \mathcal{H}_0]$, one obtains

$$\Psi(t) = e^{-i\mathcal{H}_0 t}\left(\Psi_0 + \Psi_1(t) + \Psi_2(t)\right), \tag{A.2.7}$$

$$\Psi_1(t) = \sum_j d_{ij}\Gamma_j^{(1)}(t)|\phi_j\rangle \tag{A.2.8}$$

$$\Psi_2(t) = \sum_{jf} d_{ij}d_{jf}\Gamma_{jf}^{(2)}(t)|\phi_f\rangle \tag{A.2.9}$$

where $d_{nm} = \langle\phi_m|\mathbf{n}\mathcal{D}|\phi_n\rangle$ are the dipole matrix elements of the transitions from the states n to m, where $\{n, m\} \in \{i, j, f\}$. The functions $\Gamma_j^{(1)}(t)$ and $\Gamma_{jf}^{(2)}(t)$ are

$$\Gamma_j^{(1)}(t) = i(\varepsilon_j - \varepsilon_i)\int_{-\infty}^{t} dt'\, e^{i(\varepsilon_j-\varepsilon_i)t'}P(t'), \tag{A.2.10}$$

$$\Gamma_{jf}^{(2)}(t) = (\varepsilon_f - \varepsilon_j)(\varepsilon_j - \varepsilon_i)\int_{-\infty}^{t} dt' e^{i(\varepsilon_f-\varepsilon_j)t'}P(t')\int_{-\infty}^{t'} dt''\, e^{i(\varepsilon_j-\varepsilon_i)t''}P(t''), \tag{A.2.11}$$

where $P(t) = (\mathcal{E}/\omega_0)f(t/T)\cos(\omega_0 t)$.

The term $\mathbf{A}^2/2c^2$ in Hamiltonian (A.2.4) is ignored for the following reason. If it is substituted to the integral (A.2.6), then

$$-i\int_{-\infty}^{t} dt' e^{i(\varepsilon_f-\varepsilon_i)t'}\langle\phi_f|\frac{1}{2c^2}\mathbf{A}^2|\Psi_0\rangle = \tag{A.2.12}$$

$$= -\frac{i}{4c^2}\int_{-\infty}^{t} dt' P(t)^2 e^{i(\varepsilon_f-\varepsilon_i)t'}\langle\phi_f|1+\cos(2\omega_0 t)|\Psi_0\rangle.$$

The transition matrix element is diagonal in the electronic states and does not give rise to any transitions.

A.3 The solutions for particular cases

The integrals entering the expression for the second order wave function (Eqs. A.2.9 and A.2.11) are solved numerically by the Gauss integration method. Thereby, the values of the integrals are calculated in 10^4 time points and averaged over every five time point. This precision is necessary due to the strongly oscillating factor $\cos(\omega_0 t)$. The analytical expressions of the functions $\Gamma_{jf}^{(2)}(t)$ (Eq. A.2.9) are given below for two laser pulse shapes, which will be used in the Thesis, in order to provide an idea about the time-dependence of the second order wave function.

A.3.1 For Gaussian-shaped laser pulses

In this subsection, the solution of Eq. (A.1.8) is derived for the case, when the function $f(t/T)$, which describes the time-dependence of the amplitude of the electric field $\mathbf{E}$ (see Eq. (A.2.1)), is a Gaussian function: $f(t/T) = e^{-t^2/T^2}/\sqrt{\pi^3}$.

$$\Gamma_j^{(1)}(t) = \frac{i\mathcal{E}}{\omega_0}\int_{-\infty}^{t} dt' e^{i(\varepsilon_j-\varepsilon_i)t'}\cos(\omega_0 t)e^{-t^2/T^2}. \tag{A.3.1.1}$$

With the solution of the Fourier integral [139]

$$\int_{-\infty}^{s} ds' e^{iw_\pm s'}e^{-s'^2} = \frac{\sqrt{\pi}}{2}e^{-\frac{w_\pm^2}{4}}\,\mathrm{erfc}(\frac{i}{2}w_\pm - s), \tag{A.3.1.2}$$

and replacing s by t/T and $w_\pm$ by $T(\varepsilon_f - \varepsilon_i \pm \omega_0)$, one obtains the time-dependence of $\Gamma_f^{(1)}(t)$

$$\begin{aligned}\Gamma_j^{(1)}(t) = &\frac{\mathcal{E}T(\varepsilon_j-\varepsilon_i)}{2\pi\omega_0}\times\\ &\times\left[e^{-\frac{\left(T\left(\omega_{ij}+\omega_0\right)\right)^2}{4}}\,\mathrm{erfc}\left(\frac{i}{2}T\left(\omega_{ij}+\omega_0\right)-\frac{t}{T}\right)+\right.\\ &\left.+\,e^{-\frac{\left(T\left(\omega_{ij}-\omega_0\right)\right)^2}{4}}\,\mathrm{erfc}\left(\frac{i}{2}T\left(\omega_{ij}-\omega_0\right)-\frac{t}{T}\right)\right].\end{aligned} \tag{A.3.1.3}$$

with $\omega_{ij} = \varepsilon_j - \varepsilon_i$. The second order wave function does not have an analytical expression

$$\begin{aligned}\Gamma_{jf}^{(2)}(t) = &\frac{2(\varepsilon_f-\varepsilon_j)(\varepsilon_j-\varepsilon_i)}{\sqrt{\pi}}\left(\frac{\mathcal{E}T}{2\pi\omega_0}\right)^2\times\\ &\times\int_{-\infty}^{t/T} ds'\left[e^{i(\varepsilon_f-\varepsilon_j)Ts'}\cos(\omega_0 Ts')e^{-s'^2}\right.\\ &\times\left[e^{-\frac{\left(T\left(\omega_{ij}+\omega_0\right)\right)^2}{4}}\,\mathrm{erfc}\left(\frac{i}{2}T\left(\omega_{ij}+\omega_0\right)-s'\right)+\right.\\ &\left.\left.+\,e^{-\frac{\left(T\left(\omega_{ij}-\omega_0\right)\right)^2}{4}}\,\mathrm{erfc}\left(\frac{i}{2}T\left(\omega_{ij}-\omega_0\right)-s'\right)\right]\right].\end{aligned} \tag{A.3.1.4}$$

A.3.2 For rectangular shaped laser pulses

This time the excitation with a laser pulse with a rectangular shape is considered. Namely, $f(t/T)$ is defined as

$$\begin{aligned} &\text{If } t \notin [-T/2, T/2], \text{ then} \quad f(t/T) = 0, \\ &\text{if } t \in [-T/2, T/2], \text{ then} \quad f(t/T) = 1. \end{aligned} \tag{A.3.2.1}$$

$$\Gamma_j^{(1)} = \frac{i\mathcal{E}(\varepsilon_j - \varepsilon_i)}{\omega_0} \int_{-T/2}^{t} \cos(\omega_0 t') e^{i\omega_{ij} t'} dt' \tag{A.3.2.2}$$

$$\begin{aligned} \Gamma_{jf}^{(2)} =& (\varepsilon_j - \varepsilon_i)(\varepsilon_f - \varepsilon_j) \left(\frac{\mathcal{E}}{\omega_0}\right)^2 \times \\ &\times \int_{-T/2}^{t} \cos(\omega_0 t') e^{i\omega_{jf} t'} dt' \int_{-T/2}^{t'} \cos(\omega_0 t'') e^{i\omega_{ij} t''} dt'' \end{aligned} \tag{A.3.2.3}$$

Since $\Gamma_j^{(1)}$ and $\Gamma_{jf}^{(2)}$ are integrals, they can be expressed by the following functions $F^{(1,2)}(t)$

$$\begin{aligned} &\text{If } t < -T/2, \text{ then} \quad \Gamma_{j(f)}^{(1,2)} = 0, \\ &\text{if } t \in [-T/2, T/2], \text{ then} \quad \Gamma_{j(f)}^{(1,2)} = a^{(1,2)} \left(F^{(1,2)}(t) - F^{(1,2)}(-T/2)\right), \\ &\text{if } t > T/2, \text{ then} \quad \Gamma_{j(f)}^{(1,2)} = a^{(1,2)} F^{(1,2)}(T/2) \\ &a^{(1)} = \frac{i\mathcal{E}(\varepsilon_j - \varepsilon_i)}{\omega_0} \\ &a^{(2)} = (\varepsilon_j - \varepsilon_i)(\varepsilon_f - \varepsilon_j) \left(\frac{\mathcal{E}}{\omega_0}\right)^2 \end{aligned} \tag{A.3.2.4}$$

The functions $F^{(1)}(t)$ and $F^{(2)}(t)$ are

$$F^{(1)}(t) = -\frac{i}{2} \left(\frac{e^{i(\omega_{ij} + \omega_0)t}}{\omega_{ij} + \omega_0} + \frac{e^{i(\omega_{ij} - \omega_0)t}}{\omega_{ij} - \omega_0} \right) \tag{A.3.2.5}$$

$$\begin{aligned} F^{(2)}(t) = \frac{1}{\omega_{ij}^2 - \omega_0^2} \Bigg[& -\frac{e^{i\omega_{if} t}}{2} \frac{\omega_{ij}}{\omega_{if}} \\ & + \frac{e^{-i\omega_{ij} T/2}}{4} \left(\frac{e^{i(\omega_{jf} + \omega_0)t}}{\omega_{jf} + \omega_0} + \frac{e^{i(\omega_{jf} - \omega_0)t}}{\omega_{jf} - \omega_0} \right) \\ & \times \left(e^{i(\omega_0 - \omega_{ij})T/2} (\omega_0 + \omega_{ij}) + e^{-i(\omega_0 + \omega_{ij})T/2} (\omega_0 - \omega_{ij}) \right) \\ & - \frac{1}{4} \left(\frac{\omega_{ij} - \omega_0}{\omega_{if} + 2\omega_0} e^{i(\omega_{if} + 2\omega_0)t} + \frac{\omega_{ij} + \omega_0}{\omega_{if} - 2\omega_0} e^{i(\omega_{if} - 2\omega_0)t} \right) \Bigg] \end{aligned} \tag{A.3.2.6}$$

After the excitation finishes, the functions $\Gamma_j^{(1)}$ and $\Gamma_{jf}^{(2)}$ are constant and have the following values

$$\Gamma_j^{(1)}(T/2) = a^{(1)} \left(\frac{\sin(\frac{i(\omega_{ij}+\omega_0)T}{2})}{\omega_{ij}+\omega_0} + \frac{\sin(\frac{i(\omega_{ij}-\omega_0)T}{2})}{\omega_{ij}-\omega_0} \right) \tag{A.3.2.7}$$

$$\Gamma_{jf}^{(2)}(T/2) = a^{(2)} \Bigg[-\frac{i\omega_{ij}}{\omega_{ij}^2-\omega_0^2} \frac{\sin(\frac{\omega_{if}T}{2})}{\omega_{if}} + \tag{A.3.2.8}$$

$$\frac{i}{2} \left(\frac{e^{-i(\omega_{ij}-\omega_0)T/2}}{(\omega_{ij}-\omega_0)} + \frac{e^{-i(\omega_{ij}+\omega_0)T/2}}{(\omega_{ij}+\omega_0)} \right) \left(\frac{\sin(\frac{(\omega_{jf}+\omega_0)T}{2})}{(\omega_{jf}+\omega_0)} + \frac{\sin(\frac{(\omega_{jf}-\omega_0)T}{2})}{(\omega_{jf}-\omega_0)} \right)$$

$$- \frac{i}{4} \left(\frac{1}{\omega_{ij}+\omega_0} \frac{\sin(\frac{(\omega_{if}+2\omega_0)T}{2})}{\omega_{if}+2\omega_0} + \frac{1}{\omega_{ij}-\omega_0} \frac{\sin(\frac{(\omega_{if}-2\omega_0)T}{2})}{\omega_{if}-2\omega_0} \right) \Bigg]$$

Appendix B

Laser pulse characteristics

The electric and magnetic fields of a laser pulse

$$\begin{aligned}\mathbf{E} &= \mathcal{E} f(t/T)\sin(\mathbf{q}_0\mathbf{r} - \omega_0 t)\mathbf{n} \\ \mathbf{H} &= -H f(t/T)\sin(\mathbf{q}_0\mathbf{r} - \omega_0 t)\mathbf{q}_0 \times \mathbf{n},\end{aligned} \tag{B.1}$$

where $\mathbf{q}_0 = (\omega_0/c)\mathbf{e}_0$, where e_0 is the direction of propagation, give equal contributions to the energy

$$\begin{aligned}E_p =& \frac{1}{8\pi}\int d^3\mathbf{r}\, 2\left[\mathcal{E} f(t/T)\sin(\mathbf{q}_0\mathbf{r} - \omega_0 t)\right]^2 = \\ =& \frac{\mathcal{E}^2 c}{8\pi}\int d^2\mathbf{r}\int_{-\infty}^{\infty} dt\, f^2(t/T).\end{aligned} \tag{B.2}$$

The laser pulse fluence is the energy per square S

$$E_{\text{fl}} = \frac{dE_p}{dS} = \frac{\mathcal{E}^2 c}{8\pi}\int_{-\infty}^{\infty} dt\, f^2(t/T). \tag{B.3}$$

The laser pulse intensity is the energy per square S and per time

$$I = \frac{dE_p}{dSdt} = \frac{\mathcal{E}^2 c}{8\pi} f^2(t/T). \tag{B.4}$$

The spectral density is related to the Fourier transform of electric field amplitude as

$$S(\omega) = |\mathcal{F}[E(t)]|^2 = \frac{1}{2\pi}\left|\mathcal{E}\int_{-\infty}^{\infty} f(t/T)\cos(\omega_0 t)e^{-i\omega t}dt\right|^2. \tag{B.5}$$

B.1 Gaussian pulse

If the time dependence of the electric field is given by

$$f(t/T) = e^{-t^2/T^2}, \tag{B.1.1}$$

then the pulse fluence is

$$E_{\mathrm{fl}} = \left(\frac{\mathcal{E}^2 c}{8\pi}\right) \frac{T\sqrt{\pi}}{\sqrt{2}}. \tag{B.1.2}$$

The pulse duration T_{dr} is the FWHM of intensity, thus

$$T_{\mathrm{dr}} = \sqrt{2\ln 2}\, T. \tag{B.1.3}$$

The spectral density is

$$\begin{aligned} S(\omega) =& \frac{\mathcal{E}^2}{2\pi} \left| \int_{-\infty}^{\infty} e^{-t^2/T^2} \cos(\omega_0 t) e^{-i\omega t} dt \right|^2 \\ =& \left(\frac{\mathcal{E}^2 T^2}{2\pi}\right) \frac{\pi}{4} \left(e^{-(\omega_0-\omega)^2 T^2/4} + e^{-(\omega_0+\omega)^2 T^2/4} \right)^2 \\ \approx& \left(\frac{\mathcal{E}T}{\sqrt{2\pi}}\right)^2 \frac{\pi}{4} e^{-(\omega_0-\omega)^2 T^2/2} \end{aligned} \tag{B.1.4}$$

The spectral width is the FWHM of the spectral density $\Delta\omega = \frac{2\sqrt{2\ln 2}}{T} = \frac{4\ln 2}{T_{\mathrm{dr}}}$.

B.2 Rectangular pulse

If the time dependence of the electric field is given by

$$\begin{aligned} f(t/T) &= 1 \text{ at } t \in [-T/2, T/2], \\ f(t/T) &= 0 \text{ at } t \notin [-T/2, T/2], \end{aligned} \tag{B.2.1}$$

then the pulse fluence is

$$E_{\mathrm{fl}} = \left(\frac{\mathcal{E}^2 c}{8\pi}\right) T. \tag{B.2.2}$$

The pulse duration is simply $T_{\mathrm{dr}} = T$. The spectral density is

$$\begin{aligned} S(\omega) =& \frac{\mathcal{E}^2}{2\pi} \left| \int_{-T/2}^{T/2} \cos(\omega_0 t) e^{-i\omega t} dt \right|^2 \\ \approx& \left(\frac{\mathcal{E}T}{\sqrt{2\pi}}\right)^2 \left| \frac{\sin((\omega_0-\omega)T/2)}{(\omega_0-\omega)T} \right|^2 \end{aligned} \tag{B.2.3}$$

The spectral width is $\Delta\omega \approx 5.6/T_{\mathrm{dr}}$.

B.3 Triangular pulse

If the time dependence of the electric field is given by

$$\begin{aligned} f(t/T) &= (t/T+1)/2 \text{ at } t \in [-T,T], \\ f(t/T) &= 0 \text{ at } t \notin [-T,T], \end{aligned} \tag{B.3.1}$$

then the pulse fluence is

$$E_{\text{fl}} = \left(\frac{\mathcal{E}^2 c}{8\pi}\right)\frac{2T}{3}. \tag{B.3.2}$$

The pulse duration is $T_{\text{dr}} = T/\sqrt{2}$. The spectral density is

$$\begin{aligned} S(\omega) =& \frac{\mathcal{E}^2}{2\pi}\left|\frac{1}{2}\int_{-T}^{T}(t/T+1)\cos(\omega_0 t)e^{-i\omega t}dt\right|^2 \\ \approx& \frac{\mathcal{E}^2}{2\pi}T^2\left|\frac{1}{i(\omega_0-\omega)T}\left(e^{i(\omega_0-\omega)T} - \frac{\sin((\omega_0-\omega)T)}{(\omega_0-\omega)T}\right)\right|^2 \\ \approx& \left(\frac{\mathcal{E}T}{\sqrt{2\pi}}\right)^2 \frac{1}{(\omega_0-\omega)^2T^2}\left(1 - \frac{\sin(2(\omega_0-\omega)T)}{(\omega_0-\omega)T} + \frac{\sin^2((\omega_0-\omega)T)}{(\omega_0-\omega)^2T^2}\right). \end{aligned} \tag{B.3.3}$$

$S(\omega_0) = 1$. The spectral width $\Delta\omega \approx 3.5/T = 2.47/T_{\text{dr}}$.

Appendix C

Single spin

C.1 The calculation of the second order wave function in the hydrogen atom-like system

In order to derive the dipole matrix elements, one has first to recall the wave functions of levels in a hydrogen atom [131]. The wave functions of the $1s$ state are

$$\Psi^{1s}_{jj_z} = R_{1s}\psi_{jj_z}, \tag{C.1.1}$$

$j = 1/2$ is the total orbital momentum, $j_z = \pm 1/2$ is the projection of the momentum on the z direction, $R_{1s} = 2e^{-r}$ is the radial part and ψ_{jj_z} is the spherical part.

$$\psi_{1/2,\pm 1/2} = Y_{00}\chi_{\pm}, \tag{C.1.2}$$

$Y_{00} = Y_{l=0,m_l=0} = \sqrt{\frac{1}{4\pi}}$ is the spherical harmonic function and $\chi_{\pm}$ are the spinor functions: $\chi_+ = \binom{1}{0}$, $\chi_- = \binom{0}{1}$.

The wave functions of the $2p$ state have the form

$$\Psi^{2p}_{jj_z} = R_{2p}\psi_{jj_z} \tag{C.1.3}$$

with the radial function $R_{2p} = \frac{1}{2\sqrt{6}} r e^{-r/2}$. The functions ψ_{jj_z} are found by the diagonalization of the Hamiltonian $\mathcal{H}_{\mathrm{SOC}} = -\zeta_{\mathrm{soc}}\mathbf{S}\cdot\mathbf{L}$, which can be repre-

sented as

$$\left(\begin{array}{c|cccccc} & Y_{11}\chi_+ & Y_{11}\chi_- & Y_{10}\chi_+ & Y_{10}\chi_- & Y_{1-1}\chi_+ & Y_{1-1}\chi_- \\ \hline Y_{11}\chi_+ & -\frac{\zeta_{\rm soc}}{2} & 0 & 0 & 0 & 0 & 0 \\ Y_{11}\chi_- & 0 & \frac{\zeta_{\rm soc}}{2} & -\frac{\zeta_{\rm soc}}{\sqrt{2}} & 0 & 0 & 0 \\ Y_{10}\chi_+ & 0 & -\frac{\zeta_{\rm soc}}{\sqrt{2}} & 0 & 0 & 0 & 0 \\ Y_{10}\chi_- & 0 & 0 & 0 & 0 & -\frac{\zeta_{\rm soc}}{\sqrt{2}} & 0 \\ Y_{1-1}\chi_+ & 0 & 0 & 0 & -\frac{\zeta_{\rm soc}}{\sqrt{2}} & \frac{\zeta_{\rm soc}}{2} & 0 \\ Y_{1-1}\chi_- & 0 & 0 & 0 & 0 & 0 & -\frac{\zeta_{\rm soc}}{2} \end{array}\right) \tag{C.1.4}$$

The eigenfunctions of this Hamiltonian with the energy $-\zeta_{\rm soc}/2$ are

$$\begin{aligned} \psi_{3/2,3/2} &= Y_{11}\chi_+ \\ \psi_{3/2,1/2} &= \sqrt{\frac{2}{3}}Y_{10}\chi_+ + \sqrt{\frac{1}{3}}Y_{11}\chi_- \\ \psi_{3/2,-1/2} &= \sqrt{\frac{2}{3}}Y_{10}\chi_- + \sqrt{\frac{1}{3}}Y_{1-1}\chi_+ \\ \psi_{3/2,-3/2} &= Y_{1-1}\chi_- \end{aligned} \tag{C.1.5}$$

and the eigenfunctions with the energy $\zeta_{\rm soc}$ are

$$\begin{aligned} \psi_{1/2,1/2} &= \sqrt{\frac{1}{3}}Y_{10}\chi_+ - \sqrt{\frac{2}{3}}Y_{11}\chi_- \\ \psi_{1/2,-1/2} &= \sqrt{\frac{1}{3}}Y_{10}\chi_- - \sqrt{\frac{2}{3}}Y_{1-1}\chi_+. \end{aligned} \tag{C.1.6}$$

Y_{lm} are the spherical harmonics

$$\begin{aligned} Y_{10} &= \sqrt{\frac{3}{4\pi}}\frac{z}{r} \\ Y_{11} &= \sqrt{\frac{3}{8\pi}}\frac{y-ix}{r} \\ Y_{1-1} &= \sqrt{\frac{3}{8\pi}}\frac{y+ix}{r}. \end{aligned} \tag{C.1.7}$$

The dipole matrix elements of the transitions from the $1s$ to $2p$ state are $\int d^3r \Psi^{2p*}_{j'j'_z}\, \mathbf{n}\mathcal{D}\, \Psi^{1s}_{jj_z}$. It is assumed, that the spin is initially in the x direction.

It means that the ground state wave-function is

$$\Psi_0 = Y_{00}R_{1s} \cdot \frac{1}{\sqrt{2}}(\chi_+ + \chi_-) \tag{C.1.8}$$

Therefore, the dipole matrix elements of transitions from the ground state to the excited states in the system are

$$\int d^3r \Psi^{2p*}_{jj_z} \frac{x+iy}{\sqrt{2}} \Psi_0 = \tag{C.1.9}$$
$$= \int d^3r R_{2p} \psi^*_{jj_z} \frac{x+iy}{\sqrt{2}} Y_{00} R_{1s} \frac{1}{\sqrt{2}}(\chi_+ + \chi_-)$$

The spinors, entering the integrals, obey the relations $\chi^*_\pm \chi_\mp = 0$, $\chi^*_\pm \chi_\pm = 1$. Examining the wave functions of the $2p$ state (Eq. (C.1.5)), one can see that there are three types of integrals entering (C.1.9)

$$\int d^3r Y^*_{11} R_{2p} \frac{x+iy}{\sqrt{2}} Y_{00} R_{1s} = \tag{C.1.10}$$
$$= \int d^3r \frac{1}{\sqrt{2}} \frac{1}{2\sqrt{6}} r e^{-r/2} \sqrt{\frac{3}{8\pi}} \frac{y+ix}{r} (x+iy) \sqrt{\frac{1}{4\pi}} 2e^{-r} =$$
$$= -i\frac{2^{15/2}}{3^5} = d_0$$
$$\int d^3r Y^*_{10} R_{2p} \frac{x+iy}{\sqrt{2}} Y_{00} R_{1s} \propto \int d^3r\, z(x+iy) = 0 \tag{C.1.11}$$
$$\int d^3r Y^*_{1-1} R_{2p} \frac{x+iy}{\sqrt{2}} Y_{00} R_{1s} \propto \int d^3r (y-ix)(x+iy) =$$
$$= -i \int d^3r (x^2 - y^2) = 0. \tag{C.1.12}$$

Therefore, there are only three nonzero dipole matrix elements of the transitions from the ground state to the excited states induced by circularly polarized laser light:

$$d_{01} \quad = \int d^3r \Psi^{2p*}_{3/2,3/2} \frac{x+iy}{\sqrt{2}} \Psi_0 = \tag{C.1.13}$$
$$= \frac{1}{\sqrt{2}} \int d^3r \Psi^{2p*}_{3/2,3/2} \frac{x+iy}{\sqrt{2}} \Psi^{1s}_{1/2,1/2} = \frac{1}{\sqrt{2}} d_0;$$

the other to $\{2p, j = 3/2, j_z = 1/2\}$:

$$d_{02} \quad = \int d^3r \Psi^{2p*}_{3/2,1/2} \frac{x+iy}{\sqrt{2}} \Psi_0 = \tag{C.1.14}$$
$$= \frac{1}{\sqrt{2}} \int d^3r \Psi^{2p*}_{3/2,1/2} \frac{x+iy}{\sqrt{2}} \Psi^{1s}_{1/2,-1/2} = \frac{1}{\sqrt{2}} \sqrt{\frac{1}{3}} d_0;$$

and to $\{2p, j = 1/2, j_z = 1/2\}$:

$$\begin{aligned} d_{03} &= \int d^3r \Psi^{2p\,*}_{1/2,1/2} \frac{x+iy}{\sqrt{2}} \Psi_0 = \\ &= \frac{1}{\sqrt{2}} \int d^3r \Psi^{2p\,*}_{1/2,1/2} \frac{x+iy}{\sqrt{2}} \Psi^{1s}_{1/2,-1/2} = -\frac{1}{\sqrt{2}} \sqrt{\frac{2}{3}} d_0. \end{aligned} \tag{C.1.15}$$

Likewise, there are three allowed transitions from the exited states back to the $1s$ state:

1) to the spin-up state from the $\{2p, j = 3/2, j_z = 3/2\}$ state with the dipole matrix element $d_{10} = d_0^*$,

2) to the spin-down state from $\{2p, j = 3/2, j_z = 1/2\}$ with $d_{20} = \sqrt{1/3} \cdot d_0^*$ and

3) to the spin-down state from $\{2p, j = 1/2, j_z = 1/2\}$ with $d_{30} = -\sqrt{2/3} \cdot d_0^*$.

The time-dependent parts $\Gamma^{(2)}(t)$, which enter Eq. (3.9), depend on the energies of initial, intermediate and final states. Since it is assumed that the SOC in the system is considerable and the $2p$ state is split, two functions $\Gamma^{(2)}(t)$ can be distinguished: the one for the transitions to the excited states with $j = 3/2$, designated as $\Gamma^{(2)}_{3/2}(t)$, and for $j = 1/2$, designated as $\Gamma^{(2)}_{1/2}(t)$. Applying Eq. (3.9) to the system, one obtains the second order wave-function, which describes the stimulated Raman scattering process

$$\begin{aligned} \Psi_2(t) = \quad & d_{01} d_{10} \Gamma^{(2)}_{3/2}(t) \Psi^{1s}_{1/2} + d_{02} d_{20} \Gamma^{(2)}_{3/2}(t) \Psi^{1s}_{-1/2} + \\ & + d_{03} d_{30} \Gamma^{(2)}_{1/2}(t) \Psi^{1s}_{-1/2} = \\ = \quad & \frac{1}{\sqrt{2}} \left(|d_0|^2 \Gamma^{(2)}_{3/2}(t) \chi_+ + \frac{1}{3} |d_0|^2 \Gamma^{(2)}_{3/2}(t) \chi_- + \right. \\ & \left. + \frac{2}{3} |d_0|^2 \Gamma^{(2)}_{1/2}(t) \chi_- \right) Y_{00} R_{1s} = \\ = \quad & \frac{|d_0|^2}{\sqrt{2}} \begin{pmatrix} \Gamma^{(2)}_{3/2}(t) \\ \frac{1}{3} \Gamma^{(2)}_{3/2}(t) + \frac{2}{3} \Gamma^{(2)}_{1/2}(t) \end{pmatrix} Y_{00} R_{1s}. \end{aligned} \tag{C.1.16}$$

C.2 The effect of linear polarized light

If the light was linear, there would be no spin-rotation in the system. For example, for linear light in the x direction, the integrals entering (C.1.9) are

$$\begin{aligned}
&\int d^3r Y_{11}^* R_{2p} x Y_{00} R_{1s} = \\
&= \int d^3r \frac{1}{\sqrt{6}} \sqrt{\frac{1}{4\pi}} r e^{-3r/2} \sqrt{\frac{3}{8\pi}} \frac{y+ix}{r}\, x = i d_x \\
&\int d^3r Y_{10}^* R_{2p} x Y_{00} R_{1s} \propto \int d^3r\, zx = 0 \\
&\int d^3r Y_{1-1}^* R_{2p} x Y_{00} R_{1s} = \\
&= \int d^3r \frac{1}{\sqrt{6}} \sqrt{\frac{1}{4\pi}} r e^{-3r/2} \sqrt{\frac{3}{8\pi}} \frac{y-ix}{r}\, x = -i d_x.
\end{aligned} \tag{C.2.1}$$

And the second order wave function in the case of linear light would be

$$\begin{aligned}
\Psi_2^{\ln}(t) &= \frac{|d_x|^2}{\sqrt{2}} \begin{pmatrix} \Gamma^{(2)}_{3/2}(t) + \frac{1}{3}\,\Gamma^{(2)}_{3/2}(t) - \frac{2}{3}\,\Gamma^{(2)}_{1/2}(t) \\ \Gamma^{(2)}_{3/2}(t) + \frac{1}{3}\,\Gamma^{(2)}_{3/2}(t) - \frac{2}{3}\,\Gamma^{(2)}_{1/2}(t) \end{pmatrix} Y_{00} R_{1s} = \\
&= |d_x|^2 \left(\frac{4}{3}\,\Gamma^{(2)}_{3/2}(t) - \frac{2}{3}\,\Gamma^{(2)}_{1/2}(t) \right) Y_{00} R_{1s} \begin{pmatrix} \frac{1}{\sqrt{2}} \\ \frac{1}{\sqrt{2}} \end{pmatrix}.
\end{aligned} \tag{C.2.2}$$

The spinor of the function would always correspond to the alignment of the spin in the x direction and no rotation could be observed. It can be easily reproduced for linear light in any direction.

C.3 Spin-orbit coupling and an external field

C.3.1 Spin-orbit coupling and Zeeman interaction

In this Section, the effect of spin orbit coupling determined by the term $\zeta_{\text{soc}}\mathbf{L}\cdot\mathbf{S}$ together with an external magnetic field determined by the term $\frac{1}{2}\mathbf{B}\cdot(2\mathbf{S}+\mathbf{L})$ on the hydrogen atom-like system is studied. Magnetic filed pointing in the $-x$ direction is considered. Thus, the Hamiltonian is

$$\mathcal{H}_0 = -\frac{B}{2}(2\hat{S}_x + \hat{L}_x) - \zeta_{\text{soc}}\mathbf{L}\cdot\mathbf{S} \tag{C.3.1.1}$$

The effect of $\mathcal{H}_0$ on the s state is trivial. SOC does not affect s state, and the state is split only due to the Zeeman interaction by energy $\Delta\varepsilon = B$ into

two levels with wave functions

$$\Psi^{1s}_{x\pm} = R_{1s}Y_{00}(\chi_+ \pm \chi_-)/\sqrt{2} \text{ with energy } \varepsilon_{0x\pm} = \varepsilon_{1s} \pm B/2. \qquad \text{(C.3.1.2)}$$

On has to diagonalize the following Hamiltonian containing both SOC and Zeeman terms in order to obtain the splitting of $2p$-state:

$$\left(\begin{array}{c|cccccc} & Y_{11}\chi_+ & Y_{11}\chi_- & Y_{10}\chi_+ & Y_{10}\chi_- & Y_{1-1}\chi_+ & Y_{1-1}\chi_- \\ \hline Y_{11}\chi_+ & -\frac{\zeta_{\rm soc}}{2} & -\frac{B}{2} & -\frac{B}{2\sqrt{2}} & 0 & 0 & 0 \\ Y_{11}\chi_- & -\frac{B}{2} & \frac{\zeta_{\rm soc}}{2} & -\frac{\zeta_{\rm soc}}{\sqrt{2}} & -\frac{B}{2\sqrt{2}} & 0 & 0 \\ Y_{10}\chi_+ & -\frac{B}{2\sqrt{2}} & -\frac{\zeta_{\rm soc}}{\sqrt{2}} & 0 & -\frac{B}{2} & -\frac{B}{2\sqrt{2}} & 0 \\ Y_{10}\chi_- & 0 & -\frac{B}{2\sqrt{2}} & -\frac{B}{2} & 0 & -\frac{\zeta_{\rm soc}}{\sqrt{2}} & -\frac{B}{2\sqrt{2}} \\ Y_{1-1}\chi_+ & 0 & 0 & -\frac{B}{2\sqrt{2}} & -\frac{\zeta_{\rm soc}}{\sqrt{2}} & \frac{\zeta_{\rm soc}}{2} & -\frac{B}{2} \\ Y_{1-1}\chi_- & 0 & 0 & 0 & -\frac{B}{2\sqrt{2}} & -\frac{B}{2} & -\frac{\zeta_{\rm soc}}{2} \end{array}\right). \qquad \text{(C.3.1.3)}$$

It has six eigenvectors and eigenenergies. The eigenenergies are $\varepsilon_{k_\pm} = \varepsilon_{2p,k_\pm} + E_{k_\pm}$, $k_+ = 1,2,3$, $k_- = 4,5,6$. E_{k_+} are the solutions of the equation

$$E^3_{k_+} + \frac{B}{2}E^2_{k_+} - \left(\frac{3\zeta^2_{\rm soc}}{4} + \frac{B\zeta_{\rm soc}}{2} + \frac{B^2}{2}\right)E_{k_+} + \left(-\frac{\zeta^3_{\rm soc}}{4} + \frac{\zeta_{\rm soc}B^2}{4} - \frac{3\zeta^2_{\rm soc}B}{8}\right) = 0, \qquad \text{(C.3.1.4)}$$

and E_{k_-} are the solutions of the equation

$$E^3_{k_-} - \frac{B}{2}E^2_{k_-} - \left(\frac{3\zeta^2_{\rm soc}}{4} - \frac{B\zeta_{\rm soc}}{2} + \frac{B^2}{2}\right)E_{k_-} + \left(-\frac{\zeta^3_{\rm soc}}{4} + \frac{\zeta_{\rm soc}B^2}{4} + \frac{3\zeta^2_{\rm soc}B}{8}\right) = 0, \qquad \text{(C.3.1.5)}$$

Thus, $2p$ state is split energetically into six levels with wave functions

$$\begin{aligned}\Psi^{2p}_{k_\pm} = R_{2p}\Big[&\alpha_{k_\pm}\big(Y_{11}\chi_+ \pm Y_{1-1}\chi_-\big) \\ &+ \beta_{k_\pm}\big(Y_{11}\chi_- \pm Y_{1-1}\chi_+\big) + \gamma_{k_\pm}\big(Y_{10}\chi_+ \pm Y_{10}\chi_-\big)\Big],\end{aligned} \qquad \text{(C.3.1.6)}$$

where (if $\zeta_{\rm soc} \neq 0$ and $B \neq 0$)

$$\alpha_{k_\pm} = \frac{B\left(\frac{5}{8}\zeta_{\rm soc} - \frac{3}{4}E_{k_\pm}\right)}{\mathcal{N}_{k_\pm}\left(E_{k_\pm} + \frac{1}{2}\zeta_{\rm soc}\right)}, \quad \beta_{k_\pm} = \frac{E_{k_\pm} + \frac{B}{4} - \frac{\zeta_{\rm soc}}{2}}{\mathcal{N}_{k_\pm}}, \quad \gamma_{k_\pm} = \frac{E_{k_\pm} - \frac{3}{2}\zeta_{\rm soc} - \frac{B}{2}}{\sqrt{2}\mathcal{N}_{k_\pm}}, \qquad \text{(C.3.1.7)}$$

$\mathcal{N}_{k_\pm}$ is the normalisation factor, which provides $|\alpha_{k_\pm}|^2+|\beta_{k_\pm}|^2+|\gamma_{k_\pm}|^2=1$. If $\zeta_{\rm soc}=0$, $B\neq 0$, then

$$\begin{aligned}
&\alpha_{1,6}=\frac{1}{2\sqrt{2}}, \quad \beta_{1,6}=\frac{1}{2\sqrt{2}}, \quad \gamma_{1,6}=-\frac{1}{2}, \quad \varepsilon_{k_{1,6}}=\varepsilon_{2p}\\
&\alpha_{2,5}=\frac{1}{2}, \quad \beta_{2,5}=-\frac{1}{2}, \quad \gamma_{2,5}=0, \quad \varepsilon_{k_{2,5}}=\varepsilon_{2p}\pm B/2\\
&\alpha_{3,4}=\frac{1}{2\sqrt{2}}, \quad \beta_{3,4}=\frac{1}{2\sqrt{2}}, \quad \gamma_{3,4}=\frac{1}{2}, \quad \varepsilon_{k_{3,4}}=\varepsilon_{2p}\mp B
\end{aligned} \tag{C.3.1.8}$$

If spin is initially aligned along the magnetic field, *e. g.* in the $+x$ direction, then the initial wave function is $\Psi_0^{1s}=R_{1s}Y_{00}\begin{pmatrix}1/\sqrt{2}\\1/\sqrt{2}\end{pmatrix}$. And the second order wave function of this system excited by left-circularly polarized light is (see Eq. (A.2.9))

$$\begin{aligned}
\Psi_2(t)=&\int_{-\infty}^{t}dt\,\mathcal{U}\begin{pmatrix}\sum_{k\pm}|\alpha_{k_\pm}|^2G_{k\pm}(t)\\ \sum_{k\pm}|\beta_{k_\pm}|^2G_{k\pm}(t)\end{pmatrix}, \qquad (C.3.1.9)\\
=&\frac{1}{2}\int_{-\infty}^{t}dt\sum_{k\pm}G_{k\pm}(t)\left[\left(|\alpha_{k_\pm}|^2+|\beta_{k_\pm}|^2\right)\begin{pmatrix}1\\1\end{pmatrix}e^{-iHt/2}\right.\\
&\left.+\left(|\alpha_{k_\pm}|^2-|\beta_{k_\pm}|^2\right)\begin{pmatrix}1\\-1\end{pmatrix}e^{iHt/2}\right],
\end{aligned}$$

The functions $G_{k\pm}$ depend on the $k_\pm$-th energy of the excited state, and $\mathcal{U}=e^{i\omega\hat{S}_x t}=\begin{pmatrix}\cos(\frac{\omega t}{2}) & -i\sin(\frac{\omega t}{2})\\ -i\sin(\frac{\omega t}{2}) & \cos(\frac{\omega t}{2})\end{pmatrix}$ is the time evolution operator, which obeys the condition $\mathcal{H}_0\mathcal{U}=i\mathcal{U}'$. If $\zeta_{\rm soc}\neq 0$, then $|\alpha_{k_\pm}|^2\neq|\beta_{k_\pm}|^2$, and $\Psi_2(t)$ is not proportional to Ψ_0^{1s}, thus, the spin is rotated. But if $\zeta_{\rm soc}=0$, then $|\alpha_{k_\pm}|^2=|\beta_{k_\pm}|^2$ for any $k_\pm$, and $\Psi_2(t)\propto\Psi_0$. Thus, the spin is rotated after Raman transitions only if $\zeta_{\rm soc}\neq 0$.

C.3.2 Spin-orbit coupling and crystal field

If there are negative charges situated on the y-axis and positive charges situated on the x-axis, then the Hamiltonian acting on the system can be written as

$$\mathcal{H}_0=-\Delta(\hat{L}_y^2-\hat{L}_x^2)-\zeta_{\rm soc}\mathbf{L}\cdot\mathbf{S}, \quad \Delta>0. \tag{C.3.2.1}$$

This Hamiltonian does not affect the wave functions and energy of the s state, but leads to the splitting of the p state. Using that

$$\hat{L}_x^2=\begin{pmatrix}1/2 & 0 & 1/2\\ 0 & 1 & 0\\ 1/2 & 0 & 1/2\end{pmatrix}, \quad \hat{L}_y^2=\begin{pmatrix}1/2 & 0 & -1/2\\ 0 & 1 & 0\\ -1/2 & 0 & 1/2\end{pmatrix}, \tag{C.3.2.2}$$

the Hamiltonian acting on the p state can be expressed in the matrix form as

$$\left(\begin{array}{c|cccccc} & Y_{11}\chi_+ & Y_{11}\chi_- & Y_{10}\chi_+ & Y_{10}\chi_- & Y_{1-1}\chi_+ & Y_{1-1}\chi_- \\ \hline Y_{11}\chi_+ & -\zeta_{\rm soc}/2 & 0 & 0 & 0 & \Delta & 0 \\ Y_{11}\chi_- & 0 & \zeta_{\rm soc}/2 & -\zeta_{\rm soc}/\sqrt{2} & 0 & 0 & \Delta \\ Y_{10}\chi_+ & 0 & -\zeta_{\rm soc}/\sqrt{2} & 0 & 0 & 0 & 0 \\ Y_{10}\chi_- & 0 & 0 & 0 & 0 & -\zeta_{\rm soc}/\sqrt{2} & 0 \\ Y_{1-1}\chi_+ & \Delta & 0 & 0 & -\zeta_{\rm soc}/\sqrt{2} & \zeta_{\rm soc}/2 & 0 \\ Y_{1-1}\chi_- & 0 & \Delta & 0 & 0 & 0 & -\zeta_{\rm soc}/2 \end{array}\right). \tag{C.3.2.3}$$

This Hamiltonian obtains three eigen-energies $\epsilon_{2p,k} = \epsilon_{2p} + E_k$, $k = 1, 2, 3$, E_k are the solutions of the equation

$$E_k^3 - E_k(\Delta^2 + 3\zeta_{\rm soc}^2/4) - \zeta_{\rm soc}^3/4 = 0 \tag{C.3.2.4}$$

Each eigenvalue corresponds to two eigenvectors

$$\psi_{k1}^{2p} = \begin{pmatrix} \frac{\Delta}{E_k+\zeta_{\rm soc}/2} \\ 0 \\ 0 \\ -\frac{\zeta_{\rm soc}}{\sqrt{2}E_k} \\ 1 \\ 0 \end{pmatrix} \text{ and } \psi_{k2}^{2p} = \begin{pmatrix} 0 \\ 1 \\ -\frac{\zeta_{\rm soc}}{\sqrt{2}E_k} \\ 0 \\ 0 \\ \frac{\Delta}{E_k+\zeta_{\rm soc}/2} \end{pmatrix} \tag{C.3.2.5}$$

Thus, the $2p$ state is split energetically into three levels, which are twice degenerate, with the wave functions

$$\begin{aligned} \psi_{k1}^{2p} &= \alpha_k Y_{11}\chi_+ + \beta_k Y_{10}\chi_- + \gamma_k Y_{1-1}\chi_+ \\ \psi_{k2}^{2p} &= \alpha_k Y_{1-1}\chi_- + \beta_k Y_{10}\chi_+ + \gamma_k Y_{11}\chi_- \end{aligned} \tag{C.3.2.6}$$

$\alpha_{k_\pm} = \frac{\Delta}{(E_k+\zeta_{\rm soc}/2)\mathcal{N}_{k_\pm}}$, $\beta_{k_\pm} = -\frac{\zeta_{\rm soc}}{\sqrt{2}E_k\mathcal{N}_{k_\pm}}$, $\gamma_{k_\pm} = \frac{1}{\mathcal{N}_{k_\pm}}$, $\mathcal{N}_{k_\pm} = |\psi_{k1}^{2p}| = |\psi_{k2}^{2p}|$.

Eq. (C.3.2.6) is correct only if $\zeta_{\rm soc} \neq 0$. If $\zeta_{\rm soc} = 0$, then the wave functions are

$$\begin{aligned} \psi_{1(1,2)}^{2p} &= Y_{10}\chi_\pm, \text{ with the energy } \epsilon_{2p,k} = \epsilon_{2p} \\ \psi_{2(1,2)}^{2p} &= \frac{Y_{11}\chi_\pm + Y_{1-1}\chi_\pm}{\sqrt{2}}, \text{ with the energy } \epsilon_{2p,k} = \epsilon_{2p} + \Delta \\ \psi_{3(1,2)}^{2p} &= \frac{Y_{11}\chi_\pm - Y_{1-1}\chi_\pm}{\sqrt{2}}, \text{ with the energy } \epsilon_{2p,k} = \epsilon_{2p} - \Delta \end{aligned} \tag{C.3.2.7}$$

If the system was initially in the state with the wave function $\Psi_0 \propto \binom{q}{r}$, $|q|^2 + |r|^2 = 1$, and was excited by a left-circular polarized light, then by the selection rules

$$\Psi_2(t) = \begin{pmatrix} q\sum_k |\alpha_k|^2 \Gamma_k(t) \\ r\sum_k |\gamma_k|^2 \Gamma_k(t) \end{pmatrix} \not\propto \Psi_0^{1s}, \text{ if } \zeta_{\text{soc}} \neq 0$$
$$\Psi_2(t) = \begin{pmatrix} q\,(\frac{\Gamma_2(t)}{2} + \frac{\Gamma_3(t)}{2}) \\ r\,(\frac{\Gamma_2(t)}{2} + \frac{\Gamma_3(t)}{2}) \end{pmatrix} \propto \Psi_0^{1s}, \text{ if } \zeta_{\text{soc}} = 0, \tag{C.3.2.8}$$

where the $\Gamma_k = \Gamma^{(2)}_{1s,2pk}$ depend on the k-th energy of the excited state (see Eq. (A.2.11)). Since it depends on the coefficient $|\alpha_k|^2$, which does not depend on the sign of Δ, the effect is independent on the sign of Δ in this case. The spin-flip probability is

$$w_{\text{s-f}}(t) = \frac{|\langle \Psi_2(t)| \, {}^{r}_{-q} \rangle|^2}{|\Psi_0 + \Psi_2(t)|^2} = |qr|^2 \frac{|\sum_k (|\alpha_k|^2 - |\gamma_k|^2)\Gamma_k|^2}{|\Psi_0 + \Psi_2(t)|^2}. \tag{C.3.2.9}$$

If there are positive (negative) charges on both x and y axis, then the Hamiltonian acting on the system can be written as

$$\mathcal{H}_0 = -\Delta((1 - \hat{L}_x^2) + (1 - \hat{L}_y^2)) - \zeta_{\text{soc}} \mathbf{L} \cdot \mathbf{S}, \tag{C.3.2.10}$$

where $\Delta > 0$ for the positive charges, $\Delta < 0$ for the negative charges. The Hamiltonian acting on the p state in the matrix form is

$$\left(\begin{array}{c|cccccc} & Y_{11}\chi_+ & Y_{11}\chi_- & Y_{10}\chi_+ & Y_{10}\chi_- & Y_{1-1}\chi_+ & Y_{1-1}\chi_- \\ \hline Y_{11}\chi_+ & -\frac{\zeta_{\text{soc}}}{2} - \Delta & 0 & 0 & 0 & 0 & 0 \\ Y_{11}\chi_- & 0 & \frac{\zeta_{\text{soc}}}{2} - \Delta & \frac{\zeta_{\text{soc}}}{\sqrt{2}} & 0 & 0 & 0 \\ Y_{10}\chi_+ & 0 & -\frac{\zeta_{\text{soc}}}{\sqrt{2}} & 0 & 0 & 0 & 0 \\ Y_{10}\chi_- & 0 & 0 & 0 & 0 & -\frac{\zeta_{\text{soc}}}{\sqrt{2}} & 0 \\ Y_{1-1}\chi_+ & 0 & 0 & 0 & -\frac{\zeta_{\text{soc}}}{\sqrt{2}} & \frac{\zeta_{\text{soc}}}{2} - \Delta & 0 \\ Y_{1-1}\chi_- & 0 & 0 & 0 & 0 & 0 & -\frac{\zeta_{\text{soc}}}{2} - \Delta \end{array}\right). \tag{C.3.2.11}$$

The $2p$ state is split energetically into three levels, which are twice degenerate. The wave functions are

$$\psi_{11}^{2p} = Y_{11}\chi_+, \quad \psi_{12} = Y_{1-1}\chi_-$$
$$\psi_{21,31}^{2p} = \alpha_{2,3} Y_{11}\chi_- + \beta_{2,3} Y_{10}\chi_+ \tag{C.3.2.12}$$
$$\psi_{22,32}^{2p} = \alpha_{2,3} Y_{1-1}\chi_+ + \beta_{2,3} Y_{10}\chi_-,$$

the corresponding energies are $\epsilon_{2p,k} = \epsilon_{2p} + E_k$, where

$$E_1 = -\zeta_{\rm soc}/2 - \Delta, \quad E_{2,3} = \frac{\zeta_{\rm soc} - 2\Delta \pm \sqrt{4\Delta^2 - 4\Delta\zeta_{\rm soc} + 9\zeta_{\rm soc}^2}}{4} \tag{C.3.2.13}$$
$$\alpha_{2,3} = \frac{\sqrt{2}E_{2,3}}{\sqrt{2E_{2,3}^2 + \zeta_{\rm soc}^2}}, \quad \beta_{2,3} = -\frac{\zeta_{\rm soc}}{\sqrt{2E_{2,3}^2 + \zeta_{\rm soc}^2}}, \quad \zeta_{\rm soc} \neq 0.$$

It should hold that $|\alpha_2|^2 + |\alpha_3|^2 = 1$, and $|\beta_2|^2 + |\beta_3|^2 = 1$, At the same time, the normalization of the wave function requires $|\alpha_{2,3}|^2 + |\beta_{2,3}|^2 = 1$. Thus, $|\beta_2| = |\alpha_3|$, $|\beta_3| = |\alpha_2|$.

If $\zeta_{\rm soc} = 0$, the $2p$ state is split energetically into two levels, one of which is twice degenerate, and another fourfold degenerate

$$\psi_{11,12}^{2p} = Y_{10}\chi_{\pm}, \text{ with the energy } \epsilon_{2p,1} = \epsilon_{2p} \tag{C.3.2.14}$$
$$\psi_{21,22}^{2p} = Y_{11}\chi_{\pm}, \quad \psi_{23,24}^{2p} = Y_{1-1}\chi_{\pm}, \text{ with the energy } \epsilon_{2p,1} = \epsilon_{2p} - \Delta$$

If the system was initially in the state with the wave function $\Psi_0 \propto \binom{q}{r}$, $|q|^2 + |r|^2 = 1$, and was excited by a left-circular polarized light, then by the selection rules

$$\Psi_2(t) = \begin{pmatrix} q\,\Gamma_1(t) \\ r\left(|\alpha_2|^2\Gamma_2(t) + |\alpha_3|^2\Gamma_3(t)\right) \end{pmatrix} \not\propto \Psi_0^{1s}, \text{ if } \zeta_{\rm soc} \neq 0$$
$$\Psi_2(t) = \begin{pmatrix} q\,\Gamma_2(t) \\ r\,\Gamma_2(t) \end{pmatrix} \propto \Psi_0^{1s}, \text{ if } \zeta_{\rm soc} = 0, \tag{C.3.2.15}$$

where the Γ_k depend on the k-th energy of the excited state. Thus, the spin of $1s$ state is reoriented only if $\zeta_{\rm soc} \neq 0$ in both cases. The spin-flip probability is

$$w_{\text{s-f}}(t) = \frac{|\langle\Psi_2(t)|\,{}^{r}_{-q}\rangle|^2}{|\Psi_0 + \Psi_2(t)|^2} = |qr|^2\frac{|\Gamma_1 - |\alpha_2|^2\Gamma_2 - |\alpha_3|^2\Gamma_3|^2}{|\Psi_0 + \Psi_2(t)|^2} \tag{C.3.2.16}$$

Appendix D

Momentum operator

The operator $\mathcal{H}_J$, which should describe the action of circularly polarized light due to the ultrafast IFE on the ground state manifold, will be derived. It should yield the time dependence of magnetic states via a Schrödinger equation.

$$i\Psi_g' = [\mathcal{H}_0 + \mathcal{H}_J]\Psi_g, \tag{D.1}$$

where $\mathcal{H}_0$ includes all internal and external fields acting on the ground state apart from the light.

It was shown in Chapter 2 that the wave function of the ground state manifold of a system perturbed by a laser pulse via the stimulated Raman scattering process is $\Psi_g(t) = \mathcal{U}(t)\Psi_{02}(t)$, where $\Psi_{02}(t) = \big(\Psi_0 + \Psi_2(t)\big)/|\Psi_0 + \Psi_2(t)|$. $\mathcal{U}$ is the time evolution operator, which obeys the equation $\mathcal{H}_0\mathcal{U} = i\mathcal{U}'$. Ψ_0 is the wave function of the initial state: $\Psi_g(0) = \Psi_0$, $\Psi_2(t)$ is the second order wave function (see Eq. 2.37).

The initial wave function Ψ_0 of the system is a spinor, which can be expressed as

$$\Psi_0 = \begin{pmatrix} P_{01} \\ P_{02} \\ \vdots \\ P_{0n} \end{pmatrix}, \tag{D.2}$$

where $n = 2J + 1$, J is total momentum and P_{0k} is the k-th projection of J on the z axis, $\sum_k |P_{0k}|^2 = 1$.

The action of a circularly polarized laser pulse propagating in the z direction is considered. k-th spinor element of the second order wave function Ψ_{02} is proportional to the dipole moments $\langle e|\mathbf{x} \pm i\mathbf{y}|\Psi_{0k}\rangle$, where e is an excited state (see Chapter 3). Thus, the k-th element of Ψ_{02} is proportional to P_{0k}

multiplied by some time-dependent factor $A_k(t)e^{i\phi_k(t)}$, and

$$\Psi_g = \mathcal{U}\left[\frac{1}{\mathcal{N}(t)}\begin{pmatrix} A_1(t)e^{i\phi_1(t)}P_{01} \\ \vdots \\ A_k(t)e^{i\phi_k(t)}P_{0k} \\ \vdots \end{pmatrix}\right] = \begin{pmatrix} P_1(t) \\ \vdots \\ P_k(t) \\ \vdots \end{pmatrix}, \tag{D.3}$$

$P_{0k} = P_k(0)$, $A_k(0)e^{i\phi(0)} = 1$, $\mathcal{N}^2 = \sum_k |P_{0k}|^2|A_k|^2$.

D.1 The operator in case $\mathcal{U} = \mathbf{1}$

The operator is derived first for the case, that there is no field except light which acts on the magnetic momentum of the ground state: $\mathcal{U} = \mathbf{1}$, $\mathcal{H}_J\Psi_g = i\,\Psi_g'$ and $\Psi_g = \Psi_{02}$. The operator $\mathcal{H}_J^0$ is defined by the equation $\mathcal{H}_J^0\Psi_{02} = i\,\Psi_{02}'$. If $\mathcal{U} = \mathbf{1}$, $\mathcal{H}_J = \mathcal{H}_J^0$

If the magnetic momentum of a system is parallel to the laser pulse propagation direction, then it is not rotated (see Chapter 3). Thus, if $\Psi_0 = \begin{pmatrix} 0 \\ \vdots \\ P_k \\ \vdots \end{pmatrix}$, there $|P_k| = 1$, then the momentum operator acts only on the i-th component of the wave function, so that the other magnetic components do not become populated: $\mathcal{H}_J^0\Psi_g = \frac{1}{\mathcal{N}(t)}\begin{pmatrix} 0 \\ \vdots \\ A_k(t)e^{i\phi_k(t)} \\ \vdots \end{pmatrix}$. The function Ψ_g is normalized to unity, $|\Psi_g| = 1$, and $\Psi_g = e^{i\phi_k(t)}\Psi_0$. Thus, the diagonal elements of the operator $\mathcal{H}_J$ are $(\mathcal{H}_J^0)_{kk} = -\phi_k'(t)$.

The other components of the operator $\mathcal{H}_J^0$ are found first for the simplest case, when $J = S = 1/2$. The initial wave function corresponding to spin aligned in an arbitrary direction is $\Psi_0 = \binom{P_{01}}{P_{02}}$, $|P_{01}|^2 + |P_{02}|^2 = 1$. The operator $\mathcal{H}_J$ is a hermitian 2×2 matrix

$$\mathcal{H}_J^0 = \begin{pmatrix} -\phi_1'(t) & c(t) \\ c^*(t) & -\phi_2'(t). \end{pmatrix} \tag{D.1.1}$$

The action of this operator on Ψ_g results in

$$\mathcal{H}_J^0\Psi_g = \begin{pmatrix} -\phi_1'P_1 + cP_2 \\ c^*P_1 - \phi_2'P_2 \end{pmatrix} \tag{D.1.2}$$

And on the other hand, $\mathcal{H}_J^0 \Psi_g = i\Psi_g'$. The differentiation of Ψ_g leads to

$$
\begin{aligned}
i\Psi_g' &= \begin{pmatrix} i\left(\frac{A_1}{\mathcal{N}}\right)' e^{i\phi_1} P_{01} - \phi_1' e^{i\phi_1} \frac{A_1}{\mathcal{N}} P_{01} \\ i\left(\frac{A_2}{\mathcal{N}}\right)' e^{i\phi_k} P_{02} - \phi_2' e^{i\phi_2} \frac{A_2}{\mathcal{N}} P_{02} \end{pmatrix} = \begin{pmatrix} i\left(\left(\frac{A_1}{\mathcal{N}}\right)' / \frac{A_1}{\mathcal{N}}\right) P_1 - \phi_1' P_1 \\ i\left(\left(\frac{A_2}{\mathcal{N}}\right)' / \frac{A_2}{\mathcal{N}}\right) P_2 - \phi_2' P_2 \end{pmatrix} \\
&= \begin{pmatrix} i\left(\frac{A_1'}{A_1} - \frac{(\mathcal{N}^2)'}{2\mathcal{N}^2}\right) P_1 - \phi_1' P_1 \\ i\left(\frac{A_2'}{A_2} - \frac{(\mathcal{N}^2)'}{2\mathcal{N}^2}\right) P_2 - \phi_2' P_2 \end{pmatrix} = \begin{pmatrix} i\left(\frac{A_1'}{A_1} - |P_1|^2 \frac{A_1'}{A_1} - |P_2|^2 \frac{A_2'}{A_2}\right) P_1 - \phi_1' P_1 \\ i\left(\frac{A_2'}{A_2} - |P_1|^2 \frac{A_1'}{A_1} - |P_2|^2 \frac{A_2'}{A_2}\right) P_2 - \phi_2' P_2 \end{pmatrix} \\
&= \begin{pmatrix} i\left(\frac{A_1'}{A_1} - \frac{A_2'}{A_2}\right) P_1 P_2^* P_2 - \phi_1' P_1 \\ i\left(\frac{A_2'}{A_2} - \frac{A_1'}{A_1}\right) P_2 P_1^* P_1 - \phi_2' P_2 \end{pmatrix}
\end{aligned} \tag{D.1.3}
$$

Thus, the operator in the case $J = 1/2$ is

$$
\mathcal{H}_J^0 = \begin{pmatrix} -\phi_1'(t) & iP_1 P_2^* \left(\frac{A_1'}{A_1} - \frac{A_2'}{A_2}\right) \\ iP_1^* P_2 \left(\frac{A_2'}{A_2} - \frac{A_1'}{A_1}\right) & -\phi_2'(t) \end{pmatrix}. \tag{D.1.4}
$$

The operator can be conveniently expressed via the operators

$$
\begin{aligned}
\hat{N}_{12+} &= \begin{pmatrix} 0 & 1 \\ 1 & 0 \end{pmatrix} = 2\hat{S}_x, \quad \hat{N}_{12-} = \begin{pmatrix} 0 & -i \\ i & 0 \end{pmatrix} = 2\hat{S}_y \\
\hat{N}_1 &= \begin{pmatrix} 1 & 0 \\ 0 & 0 \end{pmatrix} = \frac{2}{3}\hat{S}^2 + \hat{S}_z, \quad \hat{N}_2 = \begin{pmatrix} 0 & 0 \\ 0 & 1 \end{pmatrix} = \frac{2}{3}\hat{S}^2 - \hat{S}_z
\end{aligned} \tag{D.1.5}
$$

It can be noticed that

$$
P_1 P_2^* = \langle P_g | \frac{\hat{N}_{12+} - i\hat{N}_{12-}}{2} | P_g \rangle. \tag{D.1.6}
$$

Thus, the operator can be expressed as

$$
\mathcal{H}_J^0 = -\sum_k \gamma_k \hat{N}_k + \frac{1}{2} \sum_{k,l} (\nu_k - \nu_l) \big(N_{kl-} \hat{N}_{kl+} - N_{kl+} \hat{N}_{kl-} \big), \tag{D.1.7}
$$

where $\{k, l\} \in \{1, 2\}$, $\gamma_k = \phi_k'$, $\nu_k = \frac{A_k'}{A_k}$.

It can be checked that the general form of the operator is

$$
\mathcal{H}_J = \begin{pmatrix} \ddots & & & & \\ & -\gamma_k & \cdots & iP_k P_l^* (\nu_k - \nu_l) & \cdots \\ & \vdots & \ddots & & \\ & iP_k^* P_l (\nu_l - \nu_k) & & & \\ & \vdots & & & \end{pmatrix}, \tag{D.1.8}
$$

finding the k-th element of a spinor, which is the result of the action of $\mathcal{H}_J$ on Ψ_g,

$$\begin{aligned}
(\mathcal{H}^0_J\Psi_g)_k &= -\phi'_k P_k + i\sum_{l,l\neq k} P_l\left[P_k P_l^*\left(\frac{A'_k}{A_k}-\frac{A'_l}{A_l}\right)\right]\\
&= -\phi'_k P_k + iP_k\left[\frac{A'_k}{A_k}\sum_{l,l\neq k}|P_l|^2 - \sum_l |P_l|^2\frac{A'_l}{A_l}\right]\\
&= -\phi'_k P_k + iP_k\left[\frac{A'_k}{A_k}(1-|P_k|^2) - \sum_{l,l\neq k}|P_l|^2\frac{A'_l}{A_l}\right]\\
&= -\phi'_k P_k + iP_k\left[\frac{A'_k}{A_k} - \sum_l |P_l|^2\frac{A'_l}{A_l}\right]\\
&= -\phi'_k P_k + iP_k\left[\frac{A'_k}{A_k} - \sum_l \frac{|P_{0l}|^2 A_l A'_l}{\mathcal{N}^2}\right]\\
&= -\phi'_k P_k + iP_k\left[\frac{A'_k}{A_k} - \frac{(\mathcal{N}^2)'}{2\mathcal{N}^2}\right]\\
&= -\phi'_k P_k + iP_k\left(\frac{A_k}{\mathcal{N}}\right)'\Big/\left(\frac{A_k}{\mathcal{N}}\right)\\
&= \left(-\phi'_k + i\frac{|P_k|'}{|P_k|}\right)P_k = iP'_k.
\end{aligned} \tag{D.1.9}$$

Thus, $\mathcal{H}^0_J\Psi_g = i\Psi'_g$.

The operator $\mathcal{H}_J$ can be expressed via the operators $\hat{N}_{kl\pm}$, which can be represented by matrices with the elements

$$\begin{aligned}
&(N_{kl+})_{kl} = (N_{kl+})_{lk} = 1,\ l \geq k\\
&(N_{kl-})_{kl} = -i, \quad (N_{kl-})_{lk} = i,\ l > k\\
&\hat{N}_k = \hat{N}_{kk+}, \quad (N_{kk+})_{kk} = 1\\
&(N_{kl\pm})_{mn} = 0, \text{ if } m \neq k,\ m \neq l,\ n \neq k,\ n \neq l \text{ or } l < k.
\end{aligned} \tag{D.1.10}$$

Thereby, the expression (D.1.7) is general for any $n = 2J+1$

$$\mathcal{H}^0_J = -\sum_k^n \gamma_k \hat{N}_k + \frac{1}{2}\sum_{k,l}^n (\nu_k - \nu_l)\big(N_{kl-}\hat{N}_{kl+} - N_{kl+}\hat{N}_{kl-}\big). \tag{D.1.11}$$

D.2 The general form of the operator

The wave function of the ground state in the case of $\mathcal{U} \neq \mathbf{1}$ can be expressed as

$$\Psi_g = \mathcal{U}\left[\frac{1}{\mathcal{N}(t)}\begin{pmatrix} A_1(t)e^{i\phi_1(t)}P_{01} \\ \vdots \\ A_k(t)e^{i\phi_k(t)}P_{0k} \\ \vdots \end{pmatrix}\right] = \frac{1}{\mathcal{N}(t)}\begin{pmatrix} \vdots \\ B_k(t)P_{0k} \\ \vdots \end{pmatrix} = \begin{pmatrix} P_1(t) \\ \vdots \\ P_k(t) \\ \vdots \end{pmatrix}, \tag{D.2.1}$$

where $\begin{pmatrix} \vdots \\ B_k(t) \\ \vdots \end{pmatrix} = \mathcal{U}\begin{pmatrix} \vdots \\ A_k(t)e^{i\phi_k} \\ \vdots \end{pmatrix} = \mathcal{U}\mathcal{A}$. Substituting Ψ_g instead of Ψ_{02} into the relation $\mathcal{H}_J^0\Psi_{02} = i\Psi'_{02}$ with $\mathcal{H}_J^0$ being

$$\mathcal{H}_J^0 = -\sum \mathrm{Im}\left(\frac{B'_k}{B_k}\right)\hat{N}_k + \frac{1}{2}\sum \mathrm{Re}\left(\frac{B'_k}{B_k} - \frac{B'_l}{B_l}\right)\left(N_{kl-}\hat{N}_{kl+} - N_{kl+}\hat{N}_{kl-}\right). \tag{D.2.2}$$

Using that

$$\begin{pmatrix} \vdots \\ B'_k(t) \\ \vdots \end{pmatrix} = \mathcal{U}'\begin{pmatrix} \vdots \\ A_k(t)e^{i\phi_k} \\ \vdots \end{pmatrix} + \mathcal{U}\begin{pmatrix} \vdots \\ (A_k(t)e^{i\phi_k})' \\ \vdots \end{pmatrix} = -i\mathcal{H}_0\frac{\Psi_g}{\mathcal{N}} + \mathcal{U}\mathcal{A}',$$

$\mathcal{H}_J^0$ can be separated into two parts $\mathcal{H}_J^0 = \overline{\mathcal{H}_0} + \overline{\mathcal{H}_J}$.

$$\begin{aligned}
\overline{\mathcal{H}_J} = &-\sum \mathrm{Im}\left(\frac{[\mathcal{U}\mathcal{A}']_k}{[\mathcal{U}\mathcal{A}]_k}\right)\hat{N}_k \\
&+\frac{1}{2}\sum \mathrm{Re}\left(\frac{[\mathcal{U}\mathcal{A}']_k}{[\mathcal{U}A]_k} - \frac{[\mathcal{U}\mathcal{A}']_l}{[\mathcal{U}\mathcal{A}]_l}\right)\left(N_{kl-}\hat{N}_{kl+} - N_{kl+}\hat{N}_{kl-}\right) \\
\overline{\mathcal{H}_0} = &\sum \mathrm{Im}\left(\frac{[i\mathcal{H}_0\Psi_g]_k}{P_k}\right)\hat{N}_k \\
&-\frac{1}{2}\sum \mathrm{Re}\left(\frac{i[\mathcal{H}_0\Psi_g]_k}{P_k} - \frac{i[\mathcal{H}_0\Psi_g]_l}{P_l}\right)\left(N_{kl-}\hat{N}_{kl+} - N_{kl+}\hat{N}_{kl-}\right)
\end{aligned}$$

The k-th element of $\overline{\mathcal{H}_0}\Psi_g$ is

$$\begin{aligned}[\overline{\mathcal{H}_0}\Psi_g]_k &= +\operatorname{Im}(i[\mathcal{H}_0\Psi_g]_k) - i\operatorname{Re}(i[\mathcal{H}_0\Psi_g]_k)\sum_{l\neq k}|P_l|^2 + \\ &P_k\sum_{l\neq k}|P_l|^2\operatorname{Re}\left(\frac{i[\mathcal{H}_0\Psi_g]_l}{P_l}\right) \\ &= \operatorname{Re}([\mathcal{H}_0\Psi_g]_k) + i\operatorname{Im}([\mathcal{H}_0\Psi_g]_k) - i\sum_l \operatorname{Im}(P_l^*[\mathcal{H}_0\Psi_g]_l) \\ &= [\mathcal{H}_0\Psi_g]_k - i\operatorname{Im}\left([\Psi_g^*\mathcal{H}_0\Psi_g]_l\right) = [\mathcal{H}_0\Psi_g]_k,\end{aligned}$$

therefore $\overline{\mathcal{H}_0} = \mathcal{H}_0$. At the same time $\mathcal{H}_g\Psi_g = [\mathcal{H}_0 + \mathcal{H}_J]\Psi_g = i\Psi_g'$, where $\mathcal{H}_g$ is the Hamiltonian acting on the ground state. Thus, the general form of $\mathcal{H}_J$ in the case of any $\mathcal{U}$ is

$$\mathcal{H}_J = -\sum_k^n \gamma_k\hat{N}_k + \frac{1}{2}\sum_{k,l}^n(\nu_k - \nu_l)\left(N_{kl-}\hat{N}_{kl+} - N_{kl+}\hat{N}_{kl-}\right) \tag{D.2.3}$$

$$\nu_k = \operatorname{Re}(Y_k), \quad \gamma_k = \operatorname{Im}(Y_k), \quad Y_k = [\mathcal{U}\mathcal{A}']_k/[\mathcal{U}A]_k. \tag{D.2.4}$$

D.3 Commutator with the momentum operator

In this section, it is shown that the equations of motion of the expectation values of $\hat{N}_{kl\pm}$ operators are given by

$$N'_{kl\pm} = (\mathcal{F} + \nu_k + \nu_l)N_{kl\pm} \pm (\gamma_k - \gamma_l)N_{kl\mp}, \tag{D.3.1}$$

where $\mathcal{F} = -2\sum_i \nu_i N_i$. For example, if $J = 3/2$, then

$$\begin{aligned}\hat{N}_{12+} &= \begin{pmatrix}0&1&0&0\\1&0&0&0\\0&0&0&0\\0&0&0&0\end{pmatrix}, \quad \hat{N}_{12-} = \begin{pmatrix}0&-i&0&0\\i&0&0&0\\0&0&0&0\\0&0&0&0\end{pmatrix}, \\ \mathcal{F} &= -2(\nu_1 N_1 + \nu_2 N_2 + \nu_3 N_3 + \nu_4 N_4) \\ &= -2\left(\nu_1|P_1|^2 + \nu_2|P_2|^2 + \nu_3|P_3|^2 + \nu_4|P_4|^2\right)\end{aligned} \tag{D.3.2}$$

The equations of motion for their expectation values are

$$\begin{aligned}N'_{12+} &= (\mathcal{F} + \nu_1 + \nu_2)N_{12+} + (\gamma_1 - \gamma_2)N_{12-} \\ N'_{12-} &= (\mathcal{F} + \nu_1 + \nu_2)N_{12-} - (\gamma_1 - \gamma_2)N_{12+}\end{aligned} \tag{D.3.3}$$

$J_{x,y,z}$ can be expressed via $\hat{N}_{kl\pm}$ operators

$$\begin{aligned}\hat{J}_x &= \frac{\sqrt{3}}{2}\hat{N}_{12+} + \hat{N}_{23+} + \frac{\sqrt{3}}{2}\hat{N}_{34+} \\ \hat{J}_y &= \frac{\sqrt{3}}{2}\hat{N}_{12-} + \hat{N}_{23-} + \frac{\sqrt{3}}{2}\hat{N}_{34-} \\ \hat{J}_z &= \frac{3}{2}\hat{N}_1 + \frac{1}{2}\hat{N}_2 - \frac{1}{2}\hat{N}_3 - \frac{3}{2}\hat{N}_4\end{aligned} \tag{D.3.4}$$

The equations of motion of the expectation values of the operator $\hat{N}_{kl\pm}$ in the Heisenberg picture is given by

$$N'_{kl\pm} = -i\langle[\hat{N}_{kl\pm}, \mathcal{H}_J]\rangle \tag{D.3.5}$$

The commutators of the $\hat{N}_{kl\pm}$ operators are found with diagonal, H_d, and non-diagonal part, H_n, of the operator $\mathcal{H}_J = \hat{H}_d + \hat{H}_n$ separately. The elements of $\hat{N}_{kl\pm}$, $\hat{H}_{d,n}$, $\hat{N}_{kl\pm}\hat{H}_{d,n}$, $\hat{H}_{d,n}\hat{N}_{kl\pm}$ and $[\hat{N}_{kl\pm}, \hat{H}_{d,n}]$ are designated as n_{kl}, $h_{kl}^{(d,n)}$, $p_{kl}^{(d,n)}$, $q_{kl}^{(d,n)}$ and $l_{kl}^{(d,n)}$ correspondingly.

1) Commutation of $\hat{N}_{kl\pm}$ with the diagonal part $\hat{H}_d$ ($h_{aa}^{(d)} \neq 0$, $h_{ab}^{(d)} = 0$, if $a \neq b$)

$$\begin{aligned}&p_{ab}^{(d)} = \sum_c n_{ac}h_{cb}^{(d)} = n_{ab}h_{bb}^{(d)}, \\ &q_{ab}^{(d)} = \sum_c h_{ac}^{(d)}n_{cb} = n_{ab}h_{aa}^{(d)}, \\ &l_{ab}^{(d)} = p_{ab}^{(d)} - q_{ab}^{(d)} = n_{ab}h_{bb}^{(d)} - n_{ab}h_{aa}^{(d)} = n_{ab}(h_{bb}^{(d)} - h_{aa}^{(d)}), \\ &l_{kl}^{(d)} = n_{kl}(\gamma_l - \gamma_k), \quad l_{lk}^{(d)} = -n_{lk}(\gamma_l - \gamma_k), \quad l_{ab}^{(d)} = 0, \text{ if } \{a,b\} \notin \{k,l\} \\ &[\hat{N}_{kl\pm}, \hat{H}_d] = \pm i(\gamma_k - \gamma_l)\hat{N}_{kl\mp}\end{aligned} \tag{D.3.6}$$

2) Commutation of $\hat{N}_{kl\pm}$ with the non-diagonal part $\hat{H}_n$ ($h_{aa}^{(n)} = 0$, $h_{ab}^{(n)} \neq 0$, if $a \neq b$)

$$\begin{aligned}&p_{ka}^{(n)} = n_{kl}h_{la}^{(n)}, \quad p_{la}^{(n)} = n_{lk}h_{ka}^{(n)}, \quad p_{ba}^{(n)} = 0, \text{ if } b \neq k, l \\ &q_{ak}^{(n)} = n_{lk}h_{al}^{(n)}, \quad q_{al}^{(n)} = n_{kl}h_{ak}^{(n)}, \quad q_{ab}^{(n)} = 0, \text{ if } b \neq k, l.\end{aligned} \tag{D.3.7}$$

The expectation value of $[\hat{N}_{kl\pm}, \hat{H}_n]$ equals to $\sum_{ab} P_a^* P_b l_{ab}^{(n)}$, P_i are defined in

Eq. (D.3),

$$\begin{aligned}
\sum_{ab} P_a^* P_b l_{ab}^{(n)} &= \sum_a P_k^* P_a n_{kl} h_{la}^{(n)} + P_l^* P_a n_{lk} h_{ka}^{(n)} - P_a^* P_l n_{kl} h_{ak}^{(n)} - P_a^* P_k n_{lk} h_{al}^{(n)} \\
&= i \sum_a P_k^* P_l |P_a|^2 (\nu_l - \nu_a) n_{kl} + P_l^* P_k |P_a|^2 (\nu_k - \nu_a) n_{lk} - \\
&\qquad P_k^* P_l (\nu_a - \nu_k) n_{kl} - P_l^* P_k |P_a|^2 (\nu_a - \nu_l) n_{lk} \qquad \text{(D.3.8)} \\
&= i \sum_a \left[-2|P_a|^2 \nu_a + |P_a|^2 (\nu_k + \nu_l) \right] \left[P_k^* P_l n_{kl} + P_l^* P_k n_{lk} \right] \\
&= i \left[-2 \left(\sum_a |P_a|^2 \nu_a \right) + (\nu_k + \nu_l) \right] N_{kl\pm}.
\end{aligned}$$

The relation $\sum_a |P_a|^2 = 1$, which is due to the normalization of the wave function, is used.

Appendix E

Dynamics of an easy plane antiferromagnet

E.1 Ground and excited states

A system of two antiferromagnetically coupled sub-lattices is considered in the framework of the Weiss mean field theory. The exchange interaction $\mathcal{H}_{\mathrm{ex1(2)}}$ acting on each atom belonging to sub-lattice 1(2) can be written according to the theory as (see Section 6.2.1)

$$\begin{aligned}\mathcal{H}_{\mathrm{ex1}} &= \mathcal{J}_{\mathrm{ex}}(J_{x2}\hat{J}_{x1} + J_{y2}\hat{J}_{y1} + J_{z2}\hat{J}_{z1}) \\ \mathcal{H}_{\mathrm{ex2}} &= \mathcal{J}_{\mathrm{ex}}(J_{x1}\hat{J}_{x2} + J_{y1}\hat{J}_{y2} + J_{z1}\hat{J}_{z2}),\end{aligned} \tag{E.1.1}$$

The total magnetic momentum J of each atom in the ground state is equal to 3/2. An uniaxial crystal field in the z-direction is acting on the system additionally to the exchange interaction. The spin-orbit coupling is assumed to be much larger than the crystal field and exchange interaction, thus, the Hamiltonian can be expressed via the total momentum operators. The total Hamiltonian acting on each atom belonging to sub-lattice 1 or 2 is

$$\mathcal{H}_0 = \mathcal{H}_{\mathrm{ex1}} + \mathcal{H}_{\mathrm{ex2}} + \Delta\left(3\hat{J}_{z1}^2 - \frac{15}{4}\right) + \Delta\left(3\hat{J}_{z2}^2 - \frac{15}{4}\right). \tag{E.1.2}$$

Δ is the value of the crystal field. $\Delta > 0$ is taken, thus, the xy plane is the easy plane. The initial direction of the magnetic vectors of the sub-lattices is defined as the x axis.

The energy and the wave function of the energetically lowest state of the sub-lattices 1 are found by diagonalization of the Hamiltonian, which includes

the crystal field interaction and the effective field in the x direction caused by the exchange interaction with the system 2

$$\mathcal{H}_{0(\text{eff})} = \Delta\left(3\hat{J}_{z1}^2 - \frac{15}{4}\right) + (\mathcal{J}_{\text{ex}}J_{x2})\hat{J}_{x1}, \tag{E.1.3}$$

J_{x2} is the expectation value of the magnetic momentum in the x direction of the system 2. The ground state of the system is the state with the lowest energy, *i. e.* the state, where the lengths of the magnetic vectors $|J_{x1}|$ and $|J_{x2}|$ are the largest, but the vectors are antiparallel $J_{x1} = -J_{x2}$. It can take values of $\pm\frac{3}{2}$ and $\pm\frac{1}{2}$ in the absence of the crystal field. However, the magnetic momentum is partly quenched due to the crystal field. The actual value of J_{x2} depends also on the magnetic momentum of the system 1, therefore, it is not known.

An iteration procedure is applied to find the correct expectation values of the quenched magnetic momenta. We would like to determine the state with the largest and opposite values of J_{x1} and J_{x2}. Therefore, the largest negative eigenvalue of J_{x2}, namely $-3/2$, in the absence of the crystal field is taken for the first step. Then, the effective field in the x direction is defined as $\mathcal{J}_0 = -\frac{3}{2}\mathcal{J}_{\text{ex}}$, and the eigenfunctions of the Hamiltonian are determined

$$\begin{aligned}\mathcal{H}_{0(\text{eff})} &= \Delta\left(3J_{z1}^2 - \frac{15}{4}\right) + \mathcal{J}_0\hat{J}_{x1} \\ &= \begin{pmatrix} 3\Delta & \frac{\sqrt{3}}{2}\mathcal{J}_0 & 0 & 0 \\ \frac{\sqrt{3}}{2}\mathcal{J}_0 & -3\Delta & \mathcal{J}_0 & 0 \\ 0 & \mathcal{J}_0 & -3\Delta & \frac{\sqrt{3}}{2}\mathcal{J}_0 \\ 0 & 0 & \frac{\sqrt{3}}{2}\mathcal{J}_0 & 3\Delta \end{pmatrix}.\end{aligned} \tag{E.1.4}$$

It has four possible eigenvectors and eigenvalues:

$$\begin{aligned}E_{\text{s1,s2}}^{(1)} &= -\frac{\mathcal{J}_0}{2} \pm \sqrt{\mathcal{J}_0^2 + 3\Delta\mathcal{J}_0 + 9\Delta^2}, \\ E_{\text{s3,s4}}^{(1)} &= \frac{\mathcal{J}_0}{2} \pm \sqrt{\mathcal{J}_0^2 - 3\Delta\mathcal{J}_0 + 9\Delta^2}\end{aligned} \tag{E.1.5}$$

$$\Psi_{\text{s1,s2}}^{(1)} = \begin{pmatrix} 1 \\ \frac{E_{\text{s1,s2}}-3\Delta}{\frac{\sqrt{3}}{2}\mathcal{J}_0} \\ -\frac{E_{\text{s1,s2}}-3\Delta}{\frac{\sqrt{3}}{2}\mathcal{J}_0} \\ -1 \end{pmatrix}, \quad \Psi_{\text{s3,s4}}^{(1)} = \begin{pmatrix} 1 \\ \frac{E_{\text{s3,s4}}-3\Delta}{\frac{\sqrt{3}}{2}\mathcal{J}_0} \\ \frac{E_{\text{s3,s4}}-3\Delta}{\frac{\sqrt{3}}{2}\mathcal{J}_0} \\ 1 \end{pmatrix} \tag{E.1.6}$$

The expectation values of the x projection of the magnetic momentum of the system 1 are calculated with the resulting wave-functions $J_{x1} =$

$\langle\Psi_{si}^{(1)}|\hat{J}_x|\Psi_{si}^{(1)}\rangle$ (i stays for 1, 2, 3 or 4). The largest positive value of J_{x1} is substituted to $\mathcal{J}_0 = J_{x1}\mathcal{J}_{\rm ex}$ and the eigenfunctions of the system 2 with the Hamiltonian

$$\mathcal{H}_{0(\rm eff)} = \Delta\left(3\hat{J}_{z2}^2 - \frac{15}{4}\right) + \mathcal{J}_0\hat{J}_{x2} \tag{E.1.7}$$

are calculated.

The new values of J_{x2} are found with the new eigenfunctions and the procedure with the system 1 is repeated taking $\mathcal{J}_0 = J_{x2}\mathcal{J}_{\rm ex}$, where J_{x2} is the largest negative value. J_{x1} and J_{x2} converge to certain values, which differ only by a sign, after about 20 loops. According to Eq. (E.1.6) the wave functions, describing the magnetic vectors aligned in the x direction, having equal length, but anti-parallel aligned, have the form

$$\Psi_0^{(1)} = \begin{pmatrix} a \\ b \\ b \\ a \end{pmatrix},\ \Psi_0^{(2)} = \begin{pmatrix} a \\ -b \\ b \\ -a \end{pmatrix},\ \mathrm{Im}(a) = \mathrm{Im}(b) = 0,\ a > 0,\ b > 0. \tag{E.1.8}$$

The corresponding expectation values of the J projections are

$$\begin{aligned} &J_{x1} = \sqrt{3}ab \pm 2b^2 + \sqrt{3}ab,\ J_{x2} = -\sqrt{3}ab - 2b^2 - \sqrt{3}ab \\ &J_{z1,2} = \frac{3}{2}|a|^2 + \frac{1}{2}|b|^2 - \frac{1}{2}|b^2| - \frac{3}{2}|a|^2 = 0 \\ &J_{y1,2} = \pm\sqrt{3}\,\mathrm{Re}(a)\,\mathrm{Im}(b) \pm 2\,\mathrm{Re}(b)\,\mathrm{Im}(b) \pm \sqrt{3}\,\mathrm{Re}(b)\,\mathrm{Im}(a) = 0, \end{aligned} \tag{E.1.9}$$

It is assumed, that each system is excited by a circular polarized laser pulse tuned in the vicinity of an excited state with the total magnetic momentum is $J = 5/2$. The other excited states with $J = 3/2$ and $1/2$ are assumed to be separated from the state with $J = 5/2$ by the energy, which is much larger than the pulse spectral width. It is assumed that this state is not influenced by the exchange interaction with the other sub-lattice. Thus, the Hamiltonians acting on the excited states of systems 1 and 2 are simply $\Delta\left(3\hat{J}_{z1,2}^2 - \hat{J}_{1,2}^2\right)$. They are already diagonal and the eigenstates and energies of the excited state are

$$\begin{aligned} &|J_{z1,2} = \pm 5/2\rangle,\ \varepsilon_{\rm ex1} = \varepsilon_{\rm ex} + 10\Delta \\ &|J_{z1,2} = \pm 3/2\rangle,\ \varepsilon_{\rm ex2} = \varepsilon_{\rm ex} + 2\Delta \\ &|J_{z1,2} = \pm 1/2\rangle,\ \varepsilon_{\rm ex3} = \varepsilon_{\rm ex} - 8\Delta, \end{aligned} \tag{E.1.10}$$

$\varepsilon_{\rm ex}$ is the energy of the state in the absence of the crystal field, the index 1 and 2 is omitted.

E.2 Time evolution due to the IFE

It was shown in Chapter 4 that the action of the IFE on the system with the wave function, describing the ground-state manifold

$$\Psi_g(t) = \begin{pmatrix} P_1(t) \\ P_2(t) \\ P_3(t) \\ P_4(t) \end{pmatrix} \tag{E.2.1}$$

can be represented by the operator

$$\mathcal{H}_J = \begin{pmatrix} -\gamma_1 & i(\nu_1-\nu_2)P_1P_2^* & i(\nu_1-\nu_3)P_1P_3^* & i(\nu_1-\nu_4)P_1P_4^* \\ i(\nu_2-\nu_1)P_2P_1^* & -\gamma_2 & i(\nu_2-\nu_3)P_2P_3^* & i(\nu_2-\nu_4)P_2P_3^* \\ i(\nu_3-\nu_1)P_3P_1^* & i(\nu_3-\nu_2)P_3P_2^* & -\gamma_3 & i(\nu_3-\nu_4)P_3P_4^* \\ i(\nu_4-\nu_1)P_4P_1^* & i(\nu_4-\nu_2)P_4P_2^* & i(\nu_4-\nu_3)P_4P_3^* & -\gamma_4 \end{pmatrix} \tag{E.2.2}$$

$$= -\sum_a^4 \gamma_a n_a + \frac{1}{2}\sum_{a,b}^4 \frac{1}{(p_a p_b)^2}\,(\nu_a-\nu_b)(n_{ab-}\hat{n}_{ab+} - n_{ab+}\hat{n}_{ab-})\,,$$

The operators $\hat{n}_{ab\pm}$ are total momentum operators, which can be expressed by a combination $\hat{J}_x$, $\hat{J}_y$, $\hat{J}_z$ and $\hat{J}^2$. These operators can be represented by 4×4 matrices with elements

$$\begin{aligned} &\text{If } a<b, \quad (n_{ab+})_{ab} = (n_{ab+})_{ba} = p_a p_b, \quad (n_{ab-})_{ab} = -ip_a p_b, \quad (n_{ab-})_{ba} = ip_a p_b, \\ &\text{if } a=b, \quad \hat{n}_{aa\pm} = \hat{n}_a, \quad (n_a)_{aa} = 1 \\ &(n_{ab\pm})_{cd} = 0, \text{ if } c\neq a,\ c\neq b,\ d\neq a,\ d\neq b, \text{ or } a>b \end{aligned} \tag{E.2.3}$$

$$p_2 = p_3 = 1, \quad p_1 = p_4 = \frac{\sqrt{3}}{2}.$$

For example, $\hat{n}_{12+} = \begin{pmatrix} 0 & \frac{\sqrt{3}}{2} & 0 & 0 \\ \frac{\sqrt{3}}{2} & 0 & 0 & 0 \\ 0 & 0 & 0 & 0 \\ 0 & 0 & 0 & 0 \end{pmatrix}$, $\hat{n}_{12-} = \begin{pmatrix} 0 & -i\frac{\sqrt{3}}{2} & 0 & 0 \\ i\frac{\sqrt{3}}{2} & 0 & 0 & 0 \\ 0 & 0 & 0 & 0 \\ 0 & 0 & 0 & 0 \end{pmatrix}$. Note, that $\hat{n}_{ab\pm}$ are used instead of the operators $\hat{N}_{ab\pm}$ (see in Eq. (D.1.10)) for convenience. $\hat{N}_{ab\pm}$ are connected to the operators $\hat{n}_{ab\pm}$ by the coefficients p_a and p_b. The operators $\hat{J}_{x,y,z}$ can be represented via $\hat{n}_{ab\pm}$ by

$$\begin{aligned} \hat{J}_x &= \hat{n}_{12+} + \hat{n}_{23+} + \hat{n}_{34+} \\ \hat{J}_y &= \hat{n}_{12-} + \hat{n}_{23-} + \hat{n}_{34-} \\ \hat{J}_z &= \frac{3}{2}\hat{n}_1 + \frac{1}{2}\hat{n}_2 - \frac{1}{2}\hat{n}_3 - \frac{3}{2}\hat{n}_4. \end{aligned} \tag{E.2.4}$$

$\nu_a = \mathrm{Re}\,(Y_a)$, $\gamma_a = \mathrm{Im}\,(Y_a)$, $Y_a = [\mathcal{U}\mathcal{A}']_a/[\mathcal{U}\mathcal{A}]_a$, where $\mathcal{U}$ is the time evolution operator, which acts on the ground state manifold. $\mathcal{A}$ is defined by

$$\Psi_g(t) = \mathcal{U}\mathcal{A}^T\Psi_g(0)/\mathcal{N}(t), \quad \mathcal{N}(t) = |\Psi_g(t)|. \tag{E.2.5}$$

According to Eqs. (A.1.7) and (D.2.1) the a-th element of $\mathcal{A}$ is

$$\mathcal{A}_a = 1 - \mathcal{C}_a/P_{0a}, \text{ if } P_{0a} \neq 0; \text{ else } \mathcal{A}_a = 0, \tag{E.2.6}$$

where $P_{0a} = P_a(0)$, $\mathcal{C}_a$ is the a-th element of the vector obtained by the action of the operator in brackets on the initial wave function

$$\mathcal{C} = -\left[\sum_j^3 \int_{-\infty}^{t} dt' \mathcal{U}^{-1}\hat{V}e^{-i\varepsilon_{\mathrm{ex}j}t}\int_{-\infty}^{t'} dt'' e^{i\varepsilon_{\mathrm{ex}j}t}\hat{V}\mathcal{U}\right]\begin{pmatrix} P_{01} \\ P_{02} \\ P_{03} \\ P_{04} \end{pmatrix}, \tag{E.2.7}$$

the summation is over the excited states j. If the system 1 or 2 is excited by a laser pulse with electric field

$$\mathbf{E} = \frac{\mathbf{n}_x + i\mathbf{n}_y}{\sqrt{2}}\mathcal{E}\cdot f(t/T)\sin(\omega_0 t), \tag{E.2.8}$$

then using the results of Appendix A.2 and applying the selection rules for the excitation by left-circularly polarized light (see Table 6.1), the vector $\mathcal{C}$ can be expressed as

$$\mathcal{C} = \mathcal{E}^2|d_0|^2\left[\int_{-\infty}^{t} dt' \mathcal{U}^{-1}\right]\begin{pmatrix} \frac{2}{3}\hat{F}(t',\varepsilon_{\mathrm{ex}1})Q_1(t') \\ \frac{1}{5}\hat{F}(t',\varepsilon_{\mathrm{ex}2})Q_2(t') \\ \frac{1}{10}\hat{F}(t',\varepsilon_{\mathrm{ex}3})Q_3(t') \\ \frac{1}{30}\hat{F}(t',\varepsilon_{\mathrm{ex}3})Q_4(t') \end{pmatrix}, \tag{E.2.9}$$

where $d_0 = \langle \mathrm{ex}, J = 5/2|r|\mathrm{g}, J = 3/2\rangle$, the vector $Q(t)$ equals to $\mathcal{U}(t)\Psi_{\mathrm{g}}(0)$, and the action of the operator $\hat{F}(t',\varepsilon_{\mathrm{ex}j})$ on $Q_k(t')$ is defined by

$$\begin{aligned}\hat{F}(t',\varepsilon_{\mathrm{ex}j})Q_k(t') =& f(t'/T)\cos(\omega_0 t')e^{-i\varepsilon_{\mathrm{ex}j}t'} \\ &\times \int_{-\infty}^{t''} dt'' f(t''/T)\cos(\omega_0 t'')e^{i\varepsilon_{\mathrm{ex}j}t''}Q_k(t'')\end{aligned} \tag{E.2.10}$$

The factor $(\varepsilon_k - \varepsilon_i)(\varepsilon_f - \varepsilon_k)/\omega_0^2$ should also enter the integral (E.2.10), where ε_i and ε_f are the energies of the initial and final states. However, it is applied that $|\varepsilon_k - \varepsilon_{i,f}| - \omega_0 \ll \omega_0$, because detuning is at most of order 10^{-2} meV and ω_0 is several meV. Thus, $(\varepsilon_k - \varepsilon_i)/\omega_0 \approx 1$, $(\varepsilon_f - \varepsilon_k)/\omega_0 \approx -1$, and the factor simply equal to -1 is taken.

E.3 Equations of motion

The formalism below is derived under the assumption that all atoms belonging to one sub-lattice are excited coherently by a laser pulse. In this case, the problem can be reduced to two systems, each consisting of one atom: the system 1 of the atom from the sub-lattice 1 and the system 2 of the atom from the sub-lattice 2. The dynamics of atom 1 and 2 are determined by the effective Hamiltonians $\mathcal{H}_0^{(1)} + \mathcal{H}_J^{(1)}$ and $\mathcal{H}_0^{(2)} + \mathcal{H}_J^{(2)}$, where

$$
\begin{aligned}
&\mathcal{H}_0^{(1)} = \mathcal{H}_{\text{ex1}} + \mathcal{H}_{\text{cr}}^{(1)},\ \mathcal{H}_0^{(2)} = \mathcal{H}_{\text{ex2}} + \mathcal{H}_{\text{cr}}^{(2)} \\
&\mathcal{H}_{\text{ex1}} = \mathcal{J}_{\text{ex}}(J_{x2}\hat{J}_{x1} + J_{y2}\hat{J}_{y1} + J_{z2}\hat{J}_{z1}) \\
&\mathcal{H}_{\text{ex2}} = \mathcal{J}_{\text{ex}}(J_{x1}\hat{J}_{x2} + J_{y1}\hat{J}_{y2} + J_{z1}\hat{J}_{z2}), \\
&\mathcal{H}_{\text{cr}}^{(1,2)} = \Delta(\hat{J}_{z1,2}^2 + \frac{15}{4}) \\
&\mathcal{H}_J^{(1,2)} = -\sum_a^4 \gamma_a^{(1,2)} n_a^{(1,2)} \\
&\qquad + \frac{1}{2}\sum_{a,b}^4 \frac{1}{(p_a p_b)^2}\left(\nu_a^{(1,2)} - \nu_b^{(1,2)}\right)\left(n_{ab-}^{(1,2)}\hat{n}_{ab+}^{(1,2)} - n_{ab+}^{(1,2)}\hat{n}_{ab-}^{(1,2)}\right).
\end{aligned}
\tag{E.3.1}
$$

The operators $\hat{n}_{ab\pm}^{(1)}$ $\hat{n}_{ab\pm}^{(2)}$ act on system 1 and 2, correspondingly.

The functions $\nu_a^{(1,2)}$ and $\gamma_a^{(1,2)}$ entering the operators $\mathcal{H}_J^{(1)}$ and $\mathcal{H}_J^{(2)}$ should be equal, if they act on the equal systems: $\nu_a^{(1)} = \nu_a^{(2)}$, $\gamma_a^{(1)} = \gamma_a^{(2)}$. However, the situation is complicated by the dependence of $\nu_a^{(1,2)}$ and $\gamma_a^{(1,2)}$ on the time evolution operator $\mathcal{U}$, which is different for both systems, since the Hamiltonians $\mathcal{H}_{\text{ex1}}$ and $\mathcal{H}_{\text{ex2}}$ are not equal. Fortunately, as it will be shown later they are equal anyway. Thus, ν_a and γ_a equal for both systems are taken.

The equations of motion of $J_{x1,x2}$, $J_{y1,y2}$ and $J_{z1,z2}$ are given by $iJ'_{\alpha1,\alpha2} = \langle[\mathcal{H}_0 + \mathcal{H}_J^{(1)} + \mathcal{H}_J^{(2)}, \hat{J}_{\alpha1,\alpha2}]\rangle$. Applying that the equations of motions of $n_{ab\pm}^{(1,2)}$ due to the momentum operator describing the IFE are (see Eq. (4.19))

$$
n_{ab\pm}^{(1,2)\prime} = (\mathcal{F} + \nu_a^{(1,2)} + \nu_b^{(1,2)})n_{ab\pm}^{(1,2)} \pm (\gamma_a - \gamma_b)n_{ab\mp}^{(1,2)}, \tag{E.3.2}
$$

and using Eq. (E.2.4), the equations of motion of $J_{x,y,z1,2}$ during the excitation

can be found

$$\begin{aligned}
J'_{x1,2} =& F_1(\nu_k, n_k^{(1,2)})J_{x1,2} + g_1 J_{y1,2} + f_1 n_{12+}^{(1,2)} + f_2 n_{34+}^{(1,2)} + g_2 n_{12-}^{(1,2)} + g_3 n_{34-}^{(1,2)} \\
&\pm \mathcal{J}_{\rm ex}(J_{z1}J_{y2} - J_{y1}J_{z2}) + 3\Delta(-2n_{12-}^{(1,2)} + 2n_{34-}^{(1,2)}) \qquad \text{(E.3.3)} \\
J'_{y1,2} =& F_1(\nu_k, n_k^{(1,2)})J_{y1,2} - g_1 J_{x1,2} + f_1 n_{12-}^{(1,2)} + f_2 n_{34-}^{(1,2)} - g_2 n_{12+}^{(1,2)} - g_3 n_{34+}^{(1,2)} \\
&\pm \mathcal{J}_{\rm ex}(-J_{z1}J_{x2} + J_{x1}J_{z2}) + 3\Delta(2n_{12+}^{(1,2)} - 2n_{34+}^{(1,2)}) \\
J'_{z1,2} =& F_1(\nu_k, n_k^{(1,2)})J_{z1,2} + f_3 + f_4 n_1^{(1,2)} + f_5 n_4^{(1,2)} \\
&\pm \mathcal{J}_{\rm ex}(J_{y1}J_{x2} - J_{x1}J_{y2}).
\end{aligned}$$

The following substitutions are used

$$\begin{aligned}
& g_1(t) = (\gamma_2 - \gamma_3), \quad g_2(t) = (\gamma_1 - 2\gamma_2 + \gamma_3), \quad g_3(t) = (-\gamma_2 + 2\gamma_3 - \gamma_4) \\
& f_1(t) = \nu_1 - \nu_3, \quad f_2(t) = \nu_4 - \nu_2, \quad f_3(t) = \frac{\nu_2 - \nu_3}{2} \\
& f_4(t) = 3\nu_1 - 2\nu_2 - \nu_3, \quad f_5(t) = \nu_2 + 2\nu_3 - 3\nu_4 \qquad \text{(E.3.4)} \\
& \mathcal{F}(\nu_k, n_k^{(1,2)}) = -2(\nu_1 n_1^{(1,2)} + \nu_2 n_2^{(1,2)} + \nu_3 n_3^{(1,2)} + \nu_4 n_4^{(1,2)}) \\
& F_1(\nu_k, n_k^{(1,2)}) = (\mathcal{F}(\nu_k, n_k^{(1,2)}) + \nu_2 + \nu_3).
\end{aligned}$$

It is more convenient to consider the equations of motion of the components of vectors $\mathbf{M} = \mathbf{M}_1 + \mathbf{M}_2$ and $\mathbf{L} = \mathbf{M}_1 - \mathbf{M}_2$, where $\mathbf{M}_{1,2} = (J_{x1,2}, J_{y1,2}, J_{z1,2})$. It is easy to show that $M'_x = 0$ and $M'_y = 0$ as follows. The dynamics of the vector $\mathbf{M}$ is determined by three interactions acting on the systems 1 and 2: the exchange interaction, the interaction with light via the IFE and the crystal field interaction. It is shown below that each of the three interactions lead to $M'_x = 0$ and $M'_y = 0$.

It can be easily seen that the exchange interaction does not influence $\mathbf{M}$ at all: $[\hat{J}_{x,y,z1} + \hat{J}_{x,y,z2}, \mathcal{H}_{\rm ex1} + \mathcal{H}_{\rm ex2}] = 0$. It was shown in Section 4.3.2 that if two systems were initially aligned in such way that their z projections were equal and x and y projections were opposite, then these relations would remain for the dynamics induced by the IFE. It means that if $L_z(0) = 0$, $M_x(0) = 0$ and $M_y(0) = 0$, then $L_z(t) = 0$, $M_x(t) = 0$ and $M_y(t) = 0$ due to the IFE. The conditions are fulfilled and $M'_x = 0$ and $M'_y = 0$.

And finally, let us write the equations of motion for $\mathbf{M}$ due to the crystal

field only:

$$\begin{aligned} M_x' =& 6\Delta(-m_{12-} + m_{34-}) \\ M_y' =& 6\Delta(m_{12+} - m_{34+}) \\ m_{12+}' =& -6\Delta\, m_{12-}, \quad m_{12-}' = 6\Delta\, m_{12+} \\ m_{34+}' =& 6\Delta\, m_{34-}, \quad m_{34-}' = -6\Delta\, m_{34+} \\ M_z' =& 0, \end{aligned} \tag{E.3.5}$$

where $m_{ab\pm} = n^{(1)}_{ab\pm} + n^{(2)}_{ab\pm}$. The initial conditions of these equations are $m_{12\pm}(0) = 0$, $m_{34\pm}(0) = 0$, $M_x(0) = 0$, $M_y(0) = 0$. Therefore, $M_x' = 0$ and $M_y' = 0$.

Thus, all three interactions lead to $M_x' = 0$ and $M_y' = 0$. Therefore, the differential equations for the components of the vectors $\mathbf{M}$ and $\mathbf{L}$ are

$$\begin{aligned} M_x' =& 0 \\ M_y' =& 0 \\ M_z' =& F_0(\nu_a, m_a)M_z + \frac{1}{2}\mathcal{F}(\nu_a, l_a)L_z + F_z(\nu_a, m_a) \\ L_x' =& F_0(\nu_k, m_k)L_x + \frac{1}{2}\mathcal{F}(\nu_k, l_k)M_x + g(\gamma_a)L_y \\ &+ F_{xy}(\nu_k, l_{12+}, l_{34+}) + G_{xy}(\gamma_k, l_{12-}, l_{34-}) \\ &+ 3\Delta(-2l_{12-} + 2l_{34-}) + \mathcal{J}_{\rm ex}(L_zM_y - M_zL_y) \\ L_y' =& F_0(\nu_k, m_k)L_y + \frac{1}{2}\mathcal{F}(\nu_a, l_a)M_y - g(\gamma_a)L_x \\ &+ F_{xy}(\nu_k, l_{12-}, l_{34-}) - G_{xy}(\gamma_k, l_{12+}, l_{34+}) \\ &+ 3\Delta(2l_{12+} - 2l_{34+}) + \mathcal{J}_{\rm ex}(L_xM_z - M_xL_z) \\ L_z' =& F_0(\nu_k, m_k)L_z + \frac{1}{2}\mathcal{F}(\nu_k, l_k)M_z + f_4l_1 + f_5l_4 \\ &+ \mathcal{J}_{\rm ex}(L_yM_x - L_xM_y). \end{aligned} \tag{E.3.6}$$

The substitutions applied:

$$\begin{aligned} F_0(\nu_k, m_k) &= \frac{1}{2}F(\nu_k, m_k) + \nu_2 + \nu_3 \\ F_{xy}(\nu_k, l_{12\pm}, l_{34\pm}) &= f_1l_{12\pm} + f_2l_{34\pm} \\ F_z(\nu_k, m_k) &= f_3 + f_4m_1 + f_5m_4 \\ G_{xy}(\gamma_k, l_{12\pm}, l_{34\pm}) &= g_2l_{12\pm} + g_3l_{34\pm} \\ g(\gamma_k) &= g_1 \end{aligned}$$

The variables $m_{ab\pm}$ and $l_{ab\pm}$ are the expectation values of the operators

$$\hat{m}_{ab\pm} = \hat{n}^{(1)}_{ab\pm} + \hat{n}^{(2)}_{ab\pm}, \quad \hat{l}_{ab\pm} = \hat{n}^{(1)}_{ab\pm} - \hat{n}^{(2)}_{ab\pm}. \tag{E.3.7}$$

Since $M_x(0) = 0$, $M_y(0) = 0$, they remain zero: $M_x(t) = 0$, $M_y(t) = 0$. Substituting these relations to the equation for L'_z, one obtains that its exchange part $\mathcal{J}_{\rm ex}(L_yM_x - L_xM_y)$ equals to zero. Thus, the dynamics of L_z is determined by the IFE only, which leads to $L_z(t) = 0$, as was discussed above. It will be also shown below that $l_k = 0$. Thus, the equations of motions are

$$\begin{aligned}
M_x =& 0, \quad M_y = 0, \quad L_z = 0 \\
M'_z =& F_0(\nu_a, m_a)M_z + F_z(\nu_a, m_a) \\
L'_x =& F_0(\nu_a, m_a)L_x + g(\gamma_a)L_y + F_{xy}(\nu_a, l_{12+}, l_{34+}) + G(\gamma_a, l_{12-}, l_{34-}) \\
&+ 3\Delta(-2l_{12-} + 2l_{34-}) - \mathcal{J}_{\rm ex}M_zL_y \\
L'_y =& F_0(\nu_a, m_a)L_y - g(\gamma_a)L_x + F_{xy}(\nu_a, l_{12-}, l_{34-}) - G(\gamma_a, l_{12+}, l_{34+}) \\
&+ 3\Delta(2l_{12+} - 2l_{34+}) + \mathcal{J}_{\rm ex}L_xM_z
\end{aligned} \tag{E.3.8}$$

The set of six equations is not sufficient to describe the dynamics of the whole system, because, apart from the six variables $M_{x,y,z}$ and $L_{x,y,z}$, the functions m_k and $l_{ab\pm}$ also enter Eq. (E.3.9). The time derivative of each expectation value, which enters (E.3.9), has to be found in order to obtain the complete set of the equations. The corresponding operators have to be commuted with the Hamiltonian, thereby new operators appear in the equations. Therefore, it is convenient to solve the equations of motion for the expectation values $m_{ab\pm}$ and $l_{ab\pm}$, and express $M_{x,y,z}$ and $L_{x,y,z}$ via these variables using Eqs. (E.2.4) and (E.3.7).

The full set of the equations involves 16 variables: $l_{12\pm}$, $l_{23\pm}$, $l_{34\pm}$, $l_{14\pm}$, $m_{13\pm}$, $m_{24\pm}$, m_1, m_2, m_3 and m_4. Applying that $\sum_k m_k = \sum_k n^{(1)} + \sum_k n^{(2)} = 2$, the system can be reduced to 15 equations. The other variables are zero at any time: $m_{12\pm}(t) = 0$, $m_{23\pm}(t) = 0$, $m_{34\pm}(t) = 0$, $m_{14\pm}(t) = 0$, $l_{13\pm}(t) = 0$, $l_{24\pm}(t) = 0$ and $l_a(t) = 0$. The proof for that is given for the dynamics due to the IFE only. However, it can be done for the dynamics due to all interactions together analogically. First, let us write the equation of motion for l_a using Eqs. (E.3.2) and (E.3.7)

$$\begin{aligned}
l'_a &= \left(\frac{1}{2}\mathcal{F}(\nu_a, m_a) + 2\nu_a\right) l_a + \frac{1}{2}\mathcal{F}(\nu_a, l_a)m_{ab\pm} \\
&= \left(\frac{1}{2}\mathcal{F}(\nu_a, m_a) + 2\nu_a\right) l_a - \left(\sum_k \nu_k l_k\right) m_{ab\pm}.
\end{aligned} \tag{E.3.9}$$

It can be easily seen that $l_a(t) = 0$ due to the initial conditions $l_k(0) = 0$. Thus, the equations of motion for the remained variables can be written as

$$m'_{ab\pm} = \left(\frac{1}{2}\mathcal{F}(\nu_a, m_a) + \nu_a + \nu_b\right) m_{ab\pm} \pm (\gamma_a - \gamma_b) m_{ab\mp} \tag{E.3.10}$$
$$l'_{ab\pm} = \left(\frac{1}{2}\mathcal{F}(\nu_a, m_a) + \nu_a + \nu_b\right) l_{ab\pm} \pm (\gamma_a - \gamma_b) l_{ab\mp}.$$

It follows from these equations that all variables $m_{ab\pm}(t)$ and $l_{ab\pm}(t)$, which initial conditions are $m_{ab\pm}(0) = 0$ and $l_{ab\pm}(0) = 0$, remain zero.

Thus, the dynamics of the system can be described by 15 first order differential equations of the form

$$m'_{ab\pm} = \left(\frac{1}{2}\mathcal{F}(\nu_a, m_a) + \nu_a + \nu_b\right) m_{ab\pm} \pm (\gamma_a - \gamma_b) m_{ab\mp} - i\langle[\hat{m}_{ab\pm}, \mathcal{H}_0]\rangle \tag{E.3.11}$$
$$l'_{ab\pm} = \left(\frac{1}{2}\mathcal{F}(\nu_a, m_a) + \nu_a + \nu_b\right) l_{ab\pm} \pm (\gamma_a - \gamma_b) l_{ab\mp} - i\langle[\hat{l}_{ab\pm}, \mathcal{H}_0]\rangle.$$

where the Hamiltonian $\mathcal{H}_0 = \mathcal{H}_0^{(1)} + \mathcal{H}_0^{(2)}$ can be written as

$$\mathcal{H}_0 = \frac{\mathcal{J}_{\text{ex}}}{2}\left(-L_x\hat{L}_x - L_y\hat{L}_y + M_z\hat{M}_z\right) + 3\Delta\left(\frac{\hat{M}_z^2 + \hat{L}_z^2}{2} + \frac{\hat{J}_1^2 + \hat{J}_2^2}{3}\right), \tag{E.3.12}$$

where

$$\begin{aligned}
\hat{L}_x &= \hat{J}_{x1} - \hat{J}_{x2} = \hat{l}_{12+} + \hat{l}_{23+} + \hat{l}_{34+} \\
\hat{L}_y &= \hat{J}_{y1} - \hat{J}_{y2} = \hat{l}_{12-} + \hat{l}_{23-} + \hat{l}_{34-} \\
\hat{M}_z &= \hat{J}_{z1} + \hat{J}_{z2} = \frac{3}{2}\hat{m}_1 + \frac{1}{2}\hat{m}_2 - \frac{1}{2}\hat{m}_3 - \frac{3}{2}\hat{m}_4.
\end{aligned} \tag{E.3.13}$$

These equations are solved numerically using fourth-order Runge-Kutta method [140].

Table E.1 shows the time derivatives of all involved variables $m_{ab\pm}$ and $l_{ab\pm}$ and corresponding expressions for $-i\langle[\hat{m}_{ab\pm}, \hat{O}]\rangle$ and $-i\langle[\hat{l}_{ab\pm}, \hat{O}]\rangle$, where $\hat{O}$ denotes the operators entering $\mathcal{H}_0$: $\hat{L}_x$, $\hat{L}_y$, $\hat{M}_z$ and $(\hat{M}_z^2 + \hat{L}_z^2)/2$. For instance, it follows from Eqs. (E.3.11) and Table E.1 that

$$\begin{aligned}
l'_{12+} = &\left(\frac{1}{2}\mathcal{F}(\nu_a, m_a) + \nu_1 + \nu_2\right) l_{12+} + (\gamma_1 - \gamma_2) l_{12-} \\
&- \frac{\mathcal{J}_{\text{ex}}}{2}\left[L_x m_{13-} + L_y\left(\frac{3}{2}m_1 - \frac{3}{2}m_2 - m_{13+}\right) + M_z l_{12-}\right] - 6\Delta l_{12-}.
\end{aligned} \tag{E.3.14}$$

	$\hat{L}_x$	$\hat{L}_y$	$\hat{M}_z$	$\frac{\hat{M}_z^2+\hat{L}_z^2}{2}$
l'_{12+}	m_{13-}	$\frac{3}{2}m_1 - \frac{3}{2}m_2 - m_{13+}$	$-l_{12-}$	$-2l_{12-}$
l'_{12-}	$-\frac{3}{2}m_1 + \frac{3}{2}m_2 - m_{13+}$	$-m_{13-}$	l_{12+}	$2l_{12+}$
l'_{23+}	$-m_{13-} + m_{24-}$	$2m_2 - 2m_3$ $+m_{13+} - m_{24+}$	$-l_{23-}$	0
l'_{23-}	$-2m_2 + 2m_3$ $+m_{13+} - m_{24+}$	$m_{13-} - m_{24-}$	l_{23+}	0
l'_{34+}	$-m_{24-}$	$\frac{3}{2}m_3 - \frac{3}{2}m_4 + m_{24+}$	$-l_{34-}$	$2l_{34-}$
l'_{34-}	$-\frac{3}{2}m_3 + \frac{3}{2}m_4 + m_{24+}$	m_{24-}	l_{34+}	$-2l_{34+}$
l'_{14+}	$\frac{3}{4}(m_{13-} - m_{24-})$	$\frac{3}{4}(m_{13+} - m_{24+})$	$-3l_{14-}$	0
l'_{14-}	$\frac{3}{4}(-m_{13+} + m_{24+})$	$\frac{3}{4}(m_{13-} - m_{24-})$	$3l_{14-}$	0
m'_{13+}	$l_{12-} + l_{14-} - \frac{3}{4}l_{23-}$	$l_{12+} - l_{14+} - \frac{3}{4}l_{23+}$	$-2m_{13-}$	$-2m_{13-}$
m'_{13-}	$-l_{12+} - l_{14+} + \frac{3}{4}l_{23+}$	$l_{12-} - l_{14-} - \frac{3}{4}l_{23-}$	$2m_{13+}$	$2m_{13+}$
m'_{24+}	$\frac{3}{4}l_{23-} - l_{14-} - l_{34-}$	$l_{14+} + \frac{3}{4}l_{23+} - l_{34+}$	$-2m_{24-}$	$2m_{24-}$
m'_{24-}	$-\frac{3}{4}l_{23+} + l_{14+} + l_{34+}$	$l_{14-} + \frac{3}{4}l_{23-} - l_{34-}$	$2m_{24+}$	$-2m_{24+}$
m'_1	l_{12-}	$-l_{12+}$	0	0
m'_2	$l_{23-} - l_{12-}$	$-l_{23+} + l_{12+}$	0	0
m'_3	$-l_{23-} + l_{34-}$	$l_{23+} - l_{34+}$	0	0
m'_4	$-l_{34-}$	l_{34+}	0	0

Table E.1: First column: k', which is equal to $-i\langle[\hat{k}, \mathcal{H}_0 + \mathcal{H}_J]\rangle$, where $\hat{k}$ is $\hat{l}_{ab\pm}$ or $\hat{m}_{ab\pm}$. Four left columns: $-i\langle[\hat{k}, \hat{O}]\rangle$, where $\hat{O}$ denotes the operators entering $\mathcal{H}_0$: $\hat{L}_x$, $\hat{L}_y$, $\hat{M}_z$ and $\hat{M}_z^2$.

E.3.1 Functions ν_a and γ_a.

It is shown in this subsection that $\nu_a^{(1)} = \nu_a^{(2)}$ and $\gamma_a^{(1)} = \gamma_a^{(2)}$. These functions depend on the operator $\mathcal{U}$ (see Eq. D.2.4), the time evolution operator defined by $\mathcal{H}_0\mathcal{U} = i\mathcal{U}'$. According to Eqs. (E.1.1) and (E.1.2), the Hamiltonian $\mathcal{H}_0$ consists of two parts: the one describing the crystal field, which is time-independent, and the one describing the exchange interaction, which depends on the expectation values $J_{x,y,z1,2}$. $J_{x,y,z1,2}$ change in time due to the action of the ultrafast IFE. This means, that the Hamiltonian is time-dependent and the time evolution operator cannot be written in the from of the matrix exponential: $\mathcal{U} \neq e^{-i\mathcal{H}_0 t}$. Therefore, it is calculated numerically.

In order to calculate the action of the time evolution operator $\mathcal{U}$, one has to

use that by definition $\mathcal{U}(t_0,0)\overline{\Psi}(t_0)$ is the solution $\widetilde{\Psi}(t_0)$ of the time-dependent Schrödinger equation $i\widetilde{\Psi}' = \mathcal{H}_0\widetilde{\Psi}$ at time t_0 with the boundary conditions $\widetilde{\Psi}(0) = \overline{\Psi}(t_0)$. The following equations have to be solved to find the action of the operator $\mathcal{U}$ on the wave functions $\Psi^{(1,2)}$ belonging to the system and 1 and 2

$$\begin{aligned} i(\Psi^{(1)})'(t') &= (\mathcal{J}_{\text{ex}}(J_{x2}\hat{J}_{x1} + J_{y2}\hat{J}_{y1} + J_{z2}\hat{J}_{z1}) + \Delta(3\hat{J}_{z1}^2 - \hat{J}_1^2))\Psi^{(1)}(t') \\ i(\Psi^{(2)})'(t') &= (\mathcal{J}_{\text{ex}}(J_{x1}\hat{J}_{x2} + J_{y1}\hat{J}_{y2} + J_{z1}\hat{J}_{z2}) + \Delta(3\hat{J}_{z2}^2 - \hat{J}_2^2))\Psi^{(2)}(t'). \end{aligned} \tag{E.3.1.1}$$

Therefore, the functions $\nu_a^{(1,2)}(t)$ and $\gamma_a^{(1,2)}(t)$ should be calculated at every time step using the new values of $J_{x,y,z1,2}$, while solving the differential equations of motion. The differential equations E.3.1.1 are solved numerically using the Euler method [140].

Applying $J_{x1,y1} = -J_{x2,y2}$ and $J_{z1} = J_{z2}$ to $\mathcal{H}_0$, it can be shown that if the action of the Hamiltonian $\mathcal{H}_0$ on a vector of the following form is $\mathcal{H}_0 \begin{pmatrix} a \\ b \\ c \\ d \end{pmatrix} = \begin{pmatrix} a_h \\ b_h \\ c_h \\ d_h \end{pmatrix}$, then $\mathcal{H}_0 \begin{pmatrix} a \\ -b \\ c \\ -d \end{pmatrix} = \begin{pmatrix} a_h \\ -b_h \\ c_h \\ -d_h \end{pmatrix}$. Thus, the same is true for the operators $\mathcal{U}$ and $\mathcal{U}^{-1}$: if $\mathcal{U}^{(-1)} \begin{pmatrix} a \\ b \\ c \\ d \end{pmatrix} = \begin{pmatrix} a_1 \\ b_1 \\ c_1 \\ d_1 \end{pmatrix}$, then $\mathcal{U}^{(-1)} \begin{pmatrix} a \\ -b \\ c \\ -d \end{pmatrix} = \begin{pmatrix} a_1 \\ -b_1 \\ c_1 \\ -d_1, \end{pmatrix}$. Applying this condition to Eqs. (E.2.7) and (E.2.6), it can be easily shown that $\nu_a^{(1)} = \nu_a^{(2)}$ and $\gamma_a^{(1)} = \gamma_a^{(2)}$, which is consistent with the initial assumption. However, it still has to be accounted that functions $\nu_a(t)$ and $\gamma_a(t)$ depend on the values of $L_x(t)$, $L_y(t)$ and $M_z(t)$.

E.4 Results

E.4.1 Zero crystal field

Assume that the crystal field is zero. Although the operators $\hat{l}_{ab\pm}$ and $\hat{m}_{ab\pm}$ do not have to be commuted with the crystal field Hamiltonian, the system of the equations describing the motion of the vectors **M** and **L** during the excitation

still cannot be reduced. It was discussed in Section 4.3.2 that this system should contain nine equations involving the variables m_1, m_2, m_3, $l_{12\pm}$, $l_{23\pm}$, $l_{34\pm}$. When the corresponding operators are commuted with $\hat{L}_x$, $\hat{L}_y$ and $\hat{M}_z$, new variables appear (see Table E.1) expanding the system to 15 equations. However, the system involves only three variables L_x, L_y and M_z after the excitation has finished (see Eq. E.3.9)

$$\begin{aligned} L'_x &= -\omega_{\mathcal{J}} L_y \\ L'_y &= \omega_{\mathcal{J}} L_x \\ M_z(t > \tau_{\rm p}) &= M_{z0} = \text{const} \\ \omega_{\mathcal{J}} &= \mathcal{J}_{ex} M_{z0}. \end{aligned} \tag{E.4.1.1}$$

These equations describe the circular rotation of $\mathbf{M}_1$ and $\mathbf{M}_2$ around the z axis with the frequency proportional to the value of M_z, which is constant after the excitation.

E.4.2 Zero exchange interaction

Assume that the exchange interaction is negligibly small, but the crystal field is considerable. The unperturbed Hamiltonian in this case is $\mathcal{H}_0 = \mathcal{H}_{\rm cr}^{(1,2)} = \Delta\left(3J_{z1,2}^2 - 15/4\right)$. The Hamiltonians $\mathcal{H}_{\rm cr}^{(1,2)}$ do not depend on time and are diagonal. Therefore, the time evolution operator is simply $\mathcal{U} = e^{-i\mathcal{H}_{\rm cr}t}$, which is a diagonal matrix.

The next simplification is that the system of the equations can be reduced by the fact that the operators $\hat{l}_{ab\pm}$ and $\hat{m}_{ab\pm}$ do not have to be commuted with $\hat{L}_x$, $\hat{L}_y$ and $\hat{M}_z$. Therefore, in order to describe the motion of the vectors $\mathbf{L}$ and $\mathbf{M}$ during the excitation, one needs only nine equations for the variables m_1, m_2, m_3, $l_{12\pm}$, $l_{23\pm}$, $l_{34\pm}$.

Let us look into the dynamics of the $\mathbf{M}$ and $\mathbf{L}$ vectors after the time $\tau_{\rm p}$, when the excitation has finished. The functions $\gamma_a(t > \tau_{\rm p})$ and $\nu_a(t > \tau_{\rm p})$ are zero, thus, the equations of motion after the action of the laser pulse are

$$\begin{aligned} l'_{23\pm} &= 0 \quad m'_k = 0 \\ l'_{12+} &= -6\Delta\, l_{12-}, \quad l'_{12-} = 6\Delta\, l_{12+} \\ l'_{34+} &= 6\Delta\, l_{34-}, \quad l'_{34-} = -6\Delta\, l_{34+} \end{aligned} \tag{E.4.2.1}$$

These equations can be easily solved

$$\begin{aligned}
&l_{23\pm} = \text{const} \quad m_k = \text{const} \\
&l_{12+}(t) = A_{12}\cos(6\Delta t + \phi_{12}) \\
&l_{12-}(t) = A_{12}\sin(6\Delta t + \phi_{12}) \\
&l_{34+}(t) = A_{34}\cos(6\Delta t - \phi_{34}) \\
&l_{34-}(t) = -A_{34}\sin(6\Delta t - \phi_{34}) \\
&l_{ab+}(0) + il_{ab-}(0) = A_{ab}e^{i\phi_{ab}},\ A_{ab} = |l_{ab+}(0) + il_{ab-}(0)|
\end{aligned} \tag{E.4.2.2}$$

Thus, the dynamics of the vectors $\mathbf{L}$ and $\mathbf{M}$ is given by the equations

$$\begin{aligned}
&L_x = A_{12}\cos(6\Delta t + \phi_{12}) + A_{34}\cos(6\Delta t - \phi_{34}) + C_x \\
&L_y = A_{12}\sin(6\Delta t + \phi_{12}) - A_{34}\sin(6\Delta t - \phi_{34}) + C_y \\
&C_x = l_{23+}(\tau_\mathrm{p}) = \text{const},\ C_y = l_{23-}(\tau_\mathrm{p}) = \text{const} \\
&M_x = M_y = 0,\ M_z = \text{const}
\end{aligned} \tag{E.4.2.3}$$

These equations describe the elliptical rotation of the vector $\mathbf{L}$ around the z-axis with a constant z-component.

The elliptical mode cannot be excited in this system without the exchange interaction. It can be easily obtained that the initial states in the case of Hamiltonian $\mathcal{H}_\mathrm{cr} = \Delta\,(3J_z^2 - 15/4)$ are

$$\Psi_0^{(1)} = \begin{pmatrix} 0 \\ \frac{1}{\sqrt{2}} \\ \frac{1}{\sqrt{2}} \\ 0 \end{pmatrix},\ \Psi_0^{(2)} = \begin{pmatrix} 0 \\ -\frac{1}{\sqrt{2}} \\ \frac{1}{\sqrt{2}} \\ 0 \end{pmatrix}. \tag{E.4.2.4}$$

Writing the equations of motions for the variables $l_{12\pm}$ and $l_{34\pm}$

$$\begin{aligned}
l'_{12\pm} =&(\mathcal{F}(\nu_k, m_k) + \nu_1 + \nu_2)l_{12\pm} \pm (\gamma_1 - \gamma_2)l_{12\mp} \mp 6\Delta l_{12\mp} \\
l'_{34\pm} =&(\mathcal{F}(\nu_k, m_k) + \nu_3 + \nu_4)l_{34\pm} \pm (\gamma_3 - \gamma_4)l_{34\mp} \mp 6\Delta l_{34\mp}
\end{aligned} \tag{E.4.2.5}$$

and applying the boundary conditions $l_{12\pm}(0) = l_{34\pm}(0) = 0$, it can be easily seen that $l'_{12\pm}(t) = l'_{34\pm}(t) = 0$. Thus, the system of the equations, which describes the dynamics of the system during the excitation can be further reduced to five equations involving the variables m_1, m_2, m_3 and $n_{23\pm}$.

The variables $l_{12\pm}$ and $l_{34\pm}$ are zero at any time, and the motion of L_x and L_y is determined only by $l_{23\pm}$: $L_x(t) = l_{12+}(t) + l_{23+}(t) + l_{34+}(t) = l_{23+}(t)$ and $L_y(t) = l_{12-}(t) + l_{23-}(t) + l_{34-}(t) = l_{23-}(t)$. Since operators $\hat{l}_{23\pm}$ commute

with the crystal field Hamiltonian (see Table (E.1)), $l_{23\pm}(t > \tau_{\mathrm{p}})$ are constant after the excitation. Thus, L_x and L_y do not change after the excitation. In the terms of energy, this means that the Raman transitions to states with different energy are not allowed in the absence of the exchange interaction in our system. The elliptical mode can be excited in the presence of the exchange interaction, because the boundary conditions of Eq. (E.4.2.5) are different.

Bibliography

[1] Hartree, D. R. *Mathematical Proceedings of the Cambridge Philosophical Society* **24**, 89–110 0 (1928).

[2] Atomic units from Wikipedia,
`http://en.wikipedia.org/wiki/Atomic_units`.

[3] Kimel, A., Kirilyuk, A., and Rasing, T. *Laser and Photonics Reviews* **1**(3), 275–287 (2007).

[4] Kirilyuk, A., Kimel, A. V., and Rasing, T. *Rev. Mod. Phys.* **82**, 2731–2784 Sep (2010).

[5] Tudosa, I., Stamm, C., Kashuba, A. B., King, F., Siegmann, H. C., Stöhr, J., Ju, G., Lu, B., and Weller, D. *Nature* **428**, 831–833 April (2004).

[6] Güdde, J., Conrad, U., Jähnke, V., Hohlfeld, J., and Matthias, E. *Phys. Rev. B* **59**, R6608–R6611 Mar (1999).

[7] Beaurepaire, E., Merle, J.-C., Daunois, A., and Bigot, J.-Y. *Phys. Rev. Lett.* **76**, 4250–4253 May (1996).

[8] van Kampen, M., Jozsa, C., Kohlhepp, J. T., LeClair, P., Lagae, L., de Jonge, W. J. M., and Koopmans, B. *Phys. Rev. Lett.* **88**, 227201 May (2002).

[9] Kimel, A. V., Kirilyuk, A., Usachev, P. A., Pisarev, R. V., Balbashov, A. M., and Rasing, T. *Nature* **435**(7042), 655–657 May (2005).

[10] Kalashnikova, A. M., Kimel, A. V., Pisarev, R. V., Gridnev, V. N., Usachev, P. A., Kirilyuk, A., and Rasing, T. *Phys. Rev. B* **78**, 104301 Sep (2008).

[11] Kimel, A., Kirilyuk, A., Tsvetkov, A., Pisarev, R., and Rasing, T. *Nature* **429**(6994), 850–3 (2004).

[12] Ju, G., Hohlfeld, J., Bergman, B., van de Veerdonk, R. J. M., Mryasov, O. N., Kim, J.-Y., Wu, X., Weller, D., and Koopmans, B. *Phys. Rev. Lett.* **93**, 197403 Nov (2004).

[13] Bigot, J.-Y. *Comptes Rendus de l'Academie des Sciences - Series IV - Physics* **2**(10), 1483 – 1504 (2001).

[14] Cinchetti, M., Sánchez Albaneda, M., Hoffmann, D., Roth, T., Wüstenberg, J.-P., Krauß, M., Andreyev, O., Schneider, H. C., Bauer, M., and Aeschlimann, M. *Phys. Rev. Lett.* **97**, 177201 Oct (2006).

[15] Stamm, C., Kachel, T., Pontius, N., Mitzner, R., Quast, T., Holldack, K., Khan, S., Lupulescu, C., Aziz, E. F., Wietstruk, M., Durr, H. A., and Eberhardt, W. *Nature Materials* **6**(10), 740–743 August (2007).

[16] Malinowski, G., Dalla, Rietjens, J. H. H., Paluskar, P. V., Huijink, R., Swagten, H. J. M., and Koopmans, B. *Nat Phys* **4**(11), 855–858 November (2008).

[17] Bigot, J.-Y., Vomir, M., and Beaurepaire, E. *Nature Physics* **5**(7), 515–520 May (2009).

[18] Koopmans, B., Malinowski, G., Dalla Longa, F., Steiauf, D., Fähnle, M., Roth, T., Cinchetti, M., and Aeschlimann, M. *Nat Mater* **9**(3), 259–65 (2010).

[19] Zhang, G. and Hübner, W. *Applied Physics B: Lasers and Optics* **68**, 495–499 (1999).

[20] Hübner, W. and Zhang, G. *Journal of Magnetism and Magnetic Materials* **189**(1), 101 – 105 (1998).

[21] Hübner, W. and Zhang, G. P. *Phys. Rev. B* **58**, R5920–R5923 Sep (1998).

[22] Koopmans, B., Ruigrok, J. J. M., Longa, F. D., and de Jonge, W. J. M. *Phys. Rev. Lett.* **95**, 267207 Dec (2005).

[23] Battiato, M., Carva, K., and Oppeneer, P. M. *Phys. Rev. Lett.* **105**, 027203 Jul (2010).

[24] Zhang, G. P., Hübner, W., Lefkidis, G., Bai, Y., and George, T. F. *Nature Physics* **5**(7), 499–502 June (2009).

[25] Bovensiepen, U. *Nature Physics* **5**, 461–463 (2009).

[26] Carva, K., Battiato, M., and Oppeneer, P. M. *Nature Physics* **7**(9), 665–665 (2011). Letter.

[27] Zhang, G. P., Hübner, W., Lefkidis, G., Bai, Y., and George, T. F. *Nature Physics* **7**(9), 665–666 (2011). Letter.

[28] Vonesch, H. and Bigot, J.-Y. *arXiv:1201.0166v1 [cond-mat.str-el]* (2011).

[29] Koopmans, B., van Kampen, M., Kohlhepp, J. T., and de Jonge, W. J. M. *Phys. Rev. Lett.* **85**, 844–847 Jul (2000).

[30] Guidoni, L., Beaurepaire, E., and Bigot, J.-Y. *Phys. Rev. Lett.* **89**, 017401 Jun (2002).

[31] Woodford, S. R., Bringer, A., and Blugel, S. *Journal of Applied Physics* **101**, 053912 Mar (2007).

[32] Pitaevskii, L. P. *Sov. Phys. JETP* **12**, 1008–1013 (1961).

[33] Shen, Y. *The principles of nonlinear optics*. Wiley classics library. Wiley-Interscience, (2003).

[34] Kimel, A. V., Kirilyuk, A., Hansteen, F., Pisarev, R. V., and Rasing, T. *Journal of Physics: Condensed Matter* **19**(4), 043201 (2007).

[35] Pershan, P. S., van der Ziel, J. P., and Malmstrom, L. D. *Phys. Rev.* **143**, 574–583 Mar (1966).

[36] van der Ziel, J. P., Pershan, P. S., and Malmstrom, L. D. *Phys. Rev. Lett.* **15**, 190–193 Aug (1965).

[37] Kimel, A. V., Stanciu, C. D., Usachev, P. A., Pisarev, R. V., Gridnev, V. N., Kirilyuk, A., and Rasing, T. *Phys. Rev. B* **74**, 060403 Aug (2006).

[38] de Jong, J. A., Kimel, A. V., Pisarev, R. V., Kirilyuk, A., and Rasing, T. *Phys. Rev. B* **84**, 104421 Sep (2011).

[39] Kimel, A. V., Ivanov, B. A., Pisarev, R. V., Usachev, P. A., Kirilyuk, A., and Rasing, T. *Nature Physics* **5**(10), 727–731 August (2009).

[40] Reid, A. H. M., Kimel, A. V., Kirilyuk, A., Gregg, J. F., and Rasing, T. *Phys. Rev. B* **81**, 104404 Mar (2010).

[41] Jin, Z., Ma, H., Wang, L., Ma, G., Guo, F., and Chen, J. *Applied Physics Letters* **96**(20), 201108 May (2010).

[42] Jin, Z., Ma, H., Li, D., Ma, G., Wang, M., , and Zhao, C. *Journal of Applied Physics* **109**(7), 073109 April (2011).

[43] Satoh, T., Cho, S.-J., Iida, R., Shimura, T., Kuroda, K., Ueda, H., Ueda, Y., Ivanov, B. A., Nori, F., and Fiebig, M. *Phys. Rev. Lett.* **105**, 077402 Aug (2010).

[44] Satoh, T., Cho, S.-J., Shimura, T., Kuroda, K., Ueda, H., Ueda, Y., and Fiebig, M. *J. Opt. Soc. Am. B* **27**(7), 1421–1424 Jul (2010).

[45] Nishitani, J., Kozuki, K., Nagashima, T., and Hangyo, M. *Applied Physics Letters* **96**(22), 221906 –221906–3 may (2010).

[46] Li, J., Higuchi, T., Kanda, N., Konishi, K., Tikhodeev, S. G., and Kuwata-Gonokami, M. *Opt. Express* **19**(23), 22550–22556 Nov (2011).

[47] Kanda, N., Higuchi, T., Shimizu, H., Konishi, K., Yoshioka, K., and Kuwata-Gonokami, M. *Nat Commun* **2**, 362 (2011).

[48] Kampfrath, T., Sell, A., Klatt, G., Pashkin, A., Mährlein, S., Dekorsy, T., Wolf, M., Fiebig, M., Leitenstorfer, A., and Huber, R. *Nature Photonics* **5**, 31–34 (2011).

[49] Nishitani, J., Nagashima, T., and Hangyo, M. *Phys. Rev. B* **85**, 174439 May (2012).

[50] Reid, A. H. M., Kimel, A. V., Kirilyuk, A., Gregg, J. F., and Rasing, T. *Phys. Rev. Lett.* **105**, 107402 Sep (2010).

[51] Zvezdin, A. and Kotov, V. *Modern Magnetooptics and Magnetooptical Materials Materials*. Studies in condensed matter physics. Institute of Physics Pub., (1997).

[52] Hansteen, F., Kimel, A., Kirilyuk, A., and Rasing, T. *Phys. Rev. Lett.* **95**, 047402 Jul (2005).

[53] Hansteen, F., Kimel, A., Kirilyuk, A., and Rasing, T. *Phys. Rev. B* **73**, 014421 Jan (2006).

[54] Makino, T., Liu, F., Yamasaki, T., Kozuka, Y., Ueno, K., Tsukazaki, A., Fukumura, T., Kong, Y., and Kawasaki, M. *Phys. Rev. B* **86**, 064403 Aug (2012).

[55] Liu, F., Makino, T., Yamasaki, T., Ueno, K., Tsukazaki, A., Fukumura, T., Kong, Y., and Kawasaki, M. *Phys. Rev. Lett.* **108**, 257401 Jun (2012).

[56] Stanciu, C. D., Hansteen, F., Kimel, A. V., Kirilyuk, A., Tsukamoto, A., Itoh, A., and Rasing, T. *Phys. Rev. Lett.* **99**, 047601 Jul (2007).

[57] Rasing, T., Kirilyuk, A., Kimel, A. V., Stanciu, C. D., Hansteen, F., Itoh, A., and Tsukamoto, A. (2007).

[58] Vahaplar, K., Kalashnikova, A. M., Kimel, A. V., Hinzke, D., Nowak, U., Chantrell, R., Tsukamoto, A., Itoh, A., Kirilyuk, A., and Rasing, T. *Phys. Rev. Lett.* **103**, 117201 Sep (2009).

[59] Radu, I., Vahaplar, K., Stamm, C., Kachel, T., Pontius, N., Dürr, H. A., Ostler, T. A., Barker, J., Evans, R. F. L., Chantrell, R. W., Tsukamoto, A., Itoh, A., Kirilyuk, A., Rasing, T., and Kimel, A. V. *Nature* **472**(7342), 205–208 March (2011).

[60] Steil, D., Alebrand, S., Hassdenteufel, A., Cinchetti, M., and Aeschlimann, M. *Phys. Rev. B* **84**, 224408 Dec (2011).

[61] Alebrand, S., Hassdenteufel, A., Steil, D., Cinchetti, M., and Aeschlimann, M. *Phys. Rev. B* **85**, 092401 Mar (2012).

[62] Khorsand, A. R., Savoini, M., Kirilyuk, A., Kimel, A. V., Tsukamoto, A., Itoh, A., and Rasing, T. *Phys. Rev. Lett.* **108**, 127205 Mar (2012).

[63] Vahaplar, K., Kalashnikova, A. M., Kimel, A. V., Gerlach, S., Hinzke, D., Nowak, U., Chantrell, R., Tsukamoto, A., Itoh, A., Kirilyuk, A., and Rasing, T. *Phys. Rev. B* **85**, 104402 Mar (2012).

[64] Mentink, J. H., Hellsvik, J., Afanasiev, D. V., Ivanov, B. A., Kirilyuk, A., Kimel, A. V., Eriksson, O., Katsnelson, M. I., and Rasing, T. *Phys. Rev. Lett.* **108**, 057202 Jan (2012).

[65] Ostler, T. A., Barker, J., Evans, R. F. L., Chantrell, R. W., Atxitia, U., Chubykalo-Fesenko, O., El Moussaoui, S., Le Guyader, L., Mengotti, E., Heyderman, L. J., Nolting, F., Tsukamoto, A., Itoh, A., Afanasiev, D.,

Ivanov, B. A., Kalashnikova, A. M., Vahaplar, K., Mentink, J., Kirilyuk, A., Rasing, T., and Kimel, A. V. *Nat Commun* **3**, 666 (2012).

[66] de Jong, J. A., Razdolski, I., Kalashnikova, A. M., Pisarev, R. V., Balbashov, A. M., Kirilyuk, A., Rasing, T., and Kimel, A. V. *Phys. Rev. Lett.* **108**, 157601 Apr (2012).

[67] Terui, Y., Satoh, T., Moriya, R., Ivanov, B. A., Ando, K., Saitoh, E., Shimura, T., and Kuroda, K. *arXiv:1107.2457v1* Jul (2011).

[68] Kajiwara, Y., Harii, K., Takahashi, S., Ohe, J., Uchida, K., Mizuguchi, M., Umezawa, H., Kawai, H., Ando, K., Takanashi, K., Maekawa, S., and Saitoh, E. *Nature* **464**(7286), 262–6 (2010).

[69] Satoh, T., Terui, Y., Moriya, R., Ivanov, B. A., Ando, K., Saitoh, E., Shimura, T., and Kuroda, K. *Nature Photonics (advance online publication)* (2012).

[70] Lefkidis, G., Zhang, G. P., and Hübner, W. *Phys. Rev. Lett.* **103**, 217401 Nov (2009).

[71] Woodford, S. R. *Phys. Rev. B* **79**, 212412 Jun (2009).

[72] Boeglin, C., Beaurepaire, E., Halte, V., Lopez-Flores, V., Stamm, C., Pontius, N., Durr, H. A., and Bigot, J. Y. *Nature* **465**(7297), 458–461 May (2010).

[73] Liu, R.-B., Yao, W., and Sham, L. *Advances in Physics* **59**(5), 703–802 (2010).

[74] Slavcheva, G. and Roussignol, P. *Optical Generation and Control of Quantum Coherence in Semiconductor Nanostructures*. NanoScience and Technology. Springer, (2010).

[75] Greilich, A., Yakovlev, D. R., Shabaev, A., Efros, A. L., Yugova, I. A., Oulton, R., Stavarache, V., Reuter, D., Wieck, A., and Bayer, M. *Science* **313**(5785), 341–345 (2006).

[76] Tischler, J. G., Bracker, A. S., Gammon, D., and Park, D. *Phys. Rev. B* **66**, 081310 Aug (2002).

[77] Imamoglu, A., Awschalom, D. D., Burkard, G., DiVincenzo, D. P., Loss, D., Sherwin, M., and Small, A. *Phys. Rev. Lett.* **83**, 4204–4207 Nov (1999).

[78] Economou, S. E. and Reinecke, T. L. *Phys. Rev. Lett.* **99**, 217401 Nov (2007).

[79] Economou, S. E., Sham, L. J., Wu, Y., and Steel, D. G. *Phys. Rev. B* **74**, 205415 Nov (2006).

[80] Chen, P., Piermarocchi, C., Sham, L. J., Gammon, D., and Steel, D. G. *Phys. Rev. B* **69**, 075320 Feb (2004).

[81] Clark, S. M., Fu, K.-M. C., Ladd, T. D., and Yamamoto, Y. *Phys. Rev. Lett.* **99**, 040501 Jul (2007).

[82] Yao, W., Liu, R.-B., and Sham, L. J. *Journal of Applied Physics* **101**, 081721 (2007).

[83] Xu, X., Sun, B., Berman, P. R., Steel, D. G., Bracker, A. S., Gammon, D., and Sham, L. J. *Science* **317**(5840), 929–932 (2007).

[84] Gupta, J. A., Knobel, R., Samarth, N., and Awschalom, D. D. *Science* **292**(5526), 2458–2461 (2001).

[85] Dutt, M. V. G., Cheng, J., Li, B., Xu, X., Li, X., Berman, P. R., Steel, D. G., Bracker, A. S., Gammon, D., Economou, S. E., Liu, R.-B., and Sham, L. J. *Phys. Rev. Lett.* **94**, 227403 Jun (2005).

[86] Wu, Y., Kim, E. D., Xu, X., Cheng, J., Steel, D. G., Bracker, A. S., Gammon, D., Economou, S. E., and Sham, L. J. *Phys. Rev. Lett.* **99**, 097402 Aug (2007).

[87] Unold, T., Mueller, K., Lienau, C., Elsaesser, T., and Wieck, A. D. *Phys. Rev. Lett.* **92**, 157401 Apr (2004).

[88] Gurudev Dutt, M. V., Cheng, J., Wu, Y., Xu, X., Steel, D. G., Bracker, A. S., Gammon, D., Economou, S. E., Liu, R.-B., and Sham, L. J. *Phys. Rev. B* **74**, 125306 Sep (2006).

[89] Ramsay, A. J., Boyle, S. J., Kolodka, R. S., Oliveira, J. B. B., Skiba-Szymanska, J., Liu, H. Y., Hopkinson, M., Fox, A. M., and Skolnick, M. S. *Phys. Rev. Lett.* **100**, 197401 May (2008).

[90] Berezovsky, J., Mikkelsen, M. H., Gywat, O., Stoltz, N. G., Coldren, L. A., and Awschalom, D. D. *Science* **314**(5807), 1916–1920 (2006).

[91] Berezovsky, J., Mikkelsen, M. H., Stoltz, N. G., Coldren, L. A., and Awschalom, D. D. *Science* **320**(5874), 349–352 (2008).

[92] Press, D., Ladd, T. D., Zhang, B., and Yamamoto, Y. *Nature* **456**, 218–221 November (2008).

[93] Kodriano, Y., Schwartz, I., Poem, E., Benny, Y., Presman, R., Truong, T. A., Petroff, P. M., and Gershoni, D. *Phys. Rev. B* **85**, 241304 Jun (2012).

[94] Greilich, A., Economou, S. E., Spatzek, S., Yakovlev, D. R., Reuter, D., Wieck, A. D., Reinecke, T. L., and Bayer, M. *Nature Physics* **5**(4), 262–266 March (2009).

[95] Kim, E. D., Truex, K., Xu, X., Sun, B., Steel, D. G., Bracker, A. S., Gammon, D., and Sham, L. J. *Phys. Rev. Lett.* **104**, 167401 Apr (2010).

[96] De Greve, K., McMahon, P. L., Press, D., Ladd, T. D., Bisping, D., Schneider, C., Kamp, M., Worschech, L., Hofling, S., Forchel, A., and Yamamoto, Y. *Nat Phys* **7**(11), 872–878 November (2011).

[97] Hawkins, P. E., Malinovskaya, S. A., and Malinovsky, V. S. *Physica Scripta* **2012**(T147), 014013 (2012).

[98] Xu, X., Wu, Y., Sun, B., Huang, Q., Cheng, J., Steel, D. G., Bracker, A. S., Gammon, D., Emary, C., and Sham, L. J. *Phys. Rev. Lett.* **99**, 097401 Aug (2007).

[99] Atatüre, M., Dreiser, J., Badolato, A., Hgele, A., Karrai, K., and Imamoglu, A. *Science* **312**(5773), 551–553 (2006).

[100] Bayer, M., Ortner, G., Stern, O., Kuther, A., Gorbunov, A. A., Forchel, A., Hawrylak, P., Fafard, S., Hinzer, K., Reinecke, T. L., Walck, S. N., Reithmaier, J. P., Klopf, F., and Schäfer, F. *Phys. Rev. B* **65**, 195315 May (2002).

[101] Yugova, I. A., Greilich, A., Zhukov, E. A., Yakovlev, D. R., Bayer, M., Reuter, D., and Wieck, A. D. *Phys. Rev. B* **75**, 195325 May (2007).

[102] Greilich, A., Spatzek, S., Yugova, I. A., Akimov, I. A., Yakovlev, D. R., Efros, A. L., Reuter, D., Wieck, A. D., and Bayer, M. *Phys. Rev. B* **79**, 201305 May (2009).

[103] Hahn, E. L. *Phys. Rev.* **80**, 580–594 Nov (1950).

[104] Press, D., Greve, K. D., McMahon, P. L., Ladd, T. D., Friess, B., Schneider, C., Kamp, M., Höfling, S., Forchel, A., and Yamamoto, Y. *Nature Photonics* **4**, 367–370 April (2010).

[105] Shen, Y., Goebel, A. M., and Wang, H. *Phys. Rev. B* **75**, 045341 Jan (2007).

[106] Carter, S. G., Chen, Z., and Cundiff, S. T. *Phys. Rev. B* **76**, 201308 Nov (2007).

[107] Phelps, C., Sweeney, T., Cox, R. T., and Wang, H. *Phys. Rev. Lett.* **102**, 237402 Jun (2009).

[108] Reiter, D. E., Kuhn, T., and Axt, V. M. *Phys. Rev. B* **85**, 045308 Jan (2012).

[109] Reiter, D. E., Kuhn, T., and Axt, V. M. *Phys. Rev. Lett.* **102**, 177403 Apr (2009).

[110] Jelezko, F., Gaebel, T., Popa, I., Gruber, A., and Wrachtrup, J. *Phys. Rev. Lett.* **92**, 076401 Feb (2004).

[111] Buckley, B. B., Fuchs, G. D., Bassett, L. C., and Awschalom, D. D. *Science* **330**(6008), 1212–1215 (2010).

[112] Robledo, L., Elzerman, J., Jundt, G., Atature, M., Hogele, A., Falt, S., and Imamoglu, A. *Science* **320**(5877), 772–775 May (2008).

[113] Greilich, A., Carter, S. G., Kim, D., Bracker, A. S., and Gammon, D. *Nature Photonics* **5**, 702–708 September (2011).

[114] Kim, D., Carter, S. G., Greilich, A., Bracker, A. S., and Gammon, D. *Nature Physics* **7**, 223–229 December (2010).

[115] Elzerman, J. M., Weiss, K. M., Miguel-Sanchez, J., and Imamoğlu, A. *Phys. Rev. Lett.* **107**, 017401 Jun (2011).

[116] Landau, L. and Lifshitz, E. *Electrodynamics of continuous media*. Teoreticheskaja fizika. Pergamon Press, (1960).

[117] Pershan, P. S. *Phys. Rev.* **130**, 919–929 May (1963).

[118] Van Vleck, J. H. and Hebb, M. H. *Phys. Rev.* **46**, 17–32 Jul (1934).

[119] Landau, L. and Lifshitz, E. *Quantum Electrodynamics*. Course of Theoretical Physics, Vol. 4. Pergamon Press, (1982).

[120] In *The Physics of Thin Film Optical Spectra*, volume 44 of *Springer Series in Surface Sciences*, 187–198. Springer Berlin Heidelberg (2005).

[121] Popova, D., Bringer, A., and Blügel, S. *Phys. Rev. B* **84**, 214421 Dec (2011).

[122] Iida, R., Satoh, T., Shimura, T., Kuroda, K., Ivanov, B. A., Tokunaga, Y., and Tokura, Y. *Phys. Rev. B* **84**, 064402 Aug (2011).

[123] Perroni, C. A. and Liebsch, A. *Phys. Rev. B* **74**, 134430 Oct (2006).

[124] Galkin, A. and Ivanov, B. *JETP Letters* **88**, 249–253 (2008).

[125] Gridnev, V. N. *Phys. Rev. B* **77**, 094426 Mar (2008).

[126] Abramowitz, M. and Stegun, I. A. *Handbook of Mathematical Functions with Formulas, Graphs, and Mathematical Tables*. Dover Publications, New York, (1964).

[127] Wood, D., Remeika, J., and Kolb, E. *Journal of Applied Physics* **41**(13), 5315–5322 (1970). cited By (since 1996) 14.

[128] Newman, R. and Chrenko, R. M. *Phys. Rev.* **114**, 1507–1513 Jun (1959).

[129] Popova, D., Bringer, A., and Blügel, S. *Phys. Rev. B* **85**, 094419 Mar (2012).

[130] Loudon, R. *The quantum theory of light*. Oxford science publications. Clarendon Press, (1983).

[131] Landau, L. and Lifshitz, E. *Quantum mechanics, non-relativistic theory*. A-W series in advanced physics. Pergamon Press, (1958).

[132] Ralchenko, Y., Kramida, A. E., Reader, J., and Team, N. A. (2010). [Online]. Available: http://physics.nist.gov/asd. National Institute of Standards and Technology, Gaithersburg, MD.

[133] Mikhaylovskiy, R. V., Hendry, E., and Kruglyak, V. V. *Phys. Rev. B* **86**, 100405 Sep (2012).

[134] Buschow, K. and de Boer, F. *Physics of Magnetism and Magnetic Materials*. Focus on biotechnology. Springer, (2003).

[135] White, R. M. *Quantum theory of magnetism [by] Robert M. White*. McGraw-Hill New York, (1970).

[136] Stevens, K. W. H. *Proceedings of the Physical Society. Section A* **65**(3), 209 (1952).

[137] Fazekas, P. *Lecture Notes on Electron Correlation and Magnetism*. Series in Modern Condensed Matter Physics. World Scientific, (1999).

[138] Hutchings, M. volume 16 of *Solid State Physics*, 227 – 273. Academic Press (1964).

[139] Gradshteyn, I. S. and Ryzhik, I. M. *Table of Integrals, Series, and Products, Fifth Edition*. Academic Press, 5th edition, January (1994).

[140] Hildebrand, F. *Introduction to Numerical Analysis: Second Edition*. Dover Books on Advanced Mathematics. McGraw-Hill, (1956).

Acknowledgments

First of all, I would like to thank my supervisor Andreas Bringer for his great support during my PhD work. He was very helpful and was always ready to answer my questions. The discussions with him were extremely useful and helped to considerably upgrade not only this work, but also myself as a researcher.

I would like to thank Stefan Blügel, the director of the Institute of Quantum Theory of Materials, for giving me opportunity to to make my PhD work at Jülich Research Center. I thank him for being very motivating and supportive and giving me many valuable advices.

I would like to thank Prof. David DiVincenzo, who agreed to be the second referee of this thesis.

I am grateful to Marie-Curie training network FANTOMAS for the financial support of this work. I am grateful to the organizers of the project for assembling numerous project meetings and workshops, which were highly productive. I also thank all members of the project for many valuable discussions.

I thank the members of Prof. Theo Rasing's group at Radboud University in Nijmegen, especially, Alexey Kimel and Andrey Kirilyuk for worthwhile discussions during my visits to Nijmegen.

I am grateful to Ute Winkler, the assistant of Stefan Blügel, for being very helpful and competent, making the solution of any administrative problem much more simple. I would like to thank Josef Heinen and Dorothea Henkel for saving all data from my laptop, when it got broken. Thanks to them, I saved at least several weeks, which I would need to restore the data.

I would like to thank Prof. Boris Mavrin, the supervisor of my Diploma thesis at the Institute of Spectroscopy in Russia. I learned a lot from him, and work with him inspired me to continue doing science.

I am grateful to all members of Quantum Theory of Materials Group at Peter Grünberg Institute for a very nice and friendly atmosphere in the Group.

I would like to express my gratitude to my parents, who always believe in me and encourage to move forward. I thank Evgeny for his support and help, as well as all my friends for making my stay in Jülich enjoyable and happy.

Band / Volume 69
Magnetic Oxide Heterostructures: EuO on Cubic Oxides and on Silicon
C. Caspers (2013), xiii, 153 pp
ISBN: 978-3-89336-891-4

Band / Volume 70
Femtosecond Spin Dynamics in Magnetic Multilayers Employing High Harmonics of Laser Radiation
D. Rudolf (2013), vi, 121 pp
ISBN: 978-3-89336-894-5

Band / Volume 71
Development and application of a massively parallel KKR Green function method for large scale systems
A. R. Thieß (2013), ii, 173 pp
ISBN: 978-3-89336-906-5

Band / Volume 72
Conformational Dynamics of Calmodulin and Ribosome-Nascent Chain Complexes Studied by Time-Resolved Fluorescence Anisotropy
P. Lamprou (2013), 182 pp
ISBN: 978-3-89336-907-2

Band / Volume 73
Stereoselective synthesis of vicinal diols with enzymatic cascade reactions
J. Kulig (2013), XV, 177 pp
ISBN: 978-3-89336-911-9

Band / Volume 74
Computing Solids
Models, ab-initio methods and supercomputing
Lecture Notes of the 45th IFF Spring School 2014
March 10 – 21, 2014 Jülich, Germany
ed. by S. Blügel, N. Helbig, V. Meden, D. Wortmann (2014), ca. 1000 pp
ISBN: 978-3-89336-912-6

Band / Volume 75
Aberrationskorrigierte Photoemissionsmikroskopie an magnetischen Systemen: Von statischer Charakterisierung zu zeitaufgelöster Abbildung
F. Nickel (2013), x, 99 pp
ISBN: 978-3-89336-913-3

Band / Volume 76
Temperature-Induced Metamagnetic Transition and Domain Structures of Single-Crystalline FeRh Thin Films on MgO(100)
X. Zhou (2013), xi, 104 pp
ISBN: 978-3-89336-919-5

Band / Volume 77
Interplay between Magnetism and Superconductivity in Iron Based High Temperature Superconductors
S. Price (2013), 196 pp
ISBN: 978-3-89336-921-8

Band / Volume 78
Magnetoresistance and transport in carbon nanotube-based devices
C. Morgan (2013), viii, 131 pp
ISBN: 978-3-89336-926-3

Band / Volume 79
Development of a relativistic full-potential first-principles multiple scattering Green function method applied to complex magnetic textures of nano structures at surfaces
D. Bauer (2014), 193 pp
ISBN: 978-3-89336-934-8

Band / Volume 80
Identifizierung von artifiziellen Liganden eines in Nanodiscs inkorporierten integralen Membranproteins
M. Pavlidou (2014), 106 pp
ISBN: 978-3-89336-942-3

Band / Volume 81
Interdomain Functional Dynamics of Phosphoglycerate Kinase Studied by Single-Molecule FRET
M. Gabba (2014), v, 179 pp
ISBN: 978-3-89336-943-0

Band / Volume 82
Silizium Nanoribbon Feld-Effekt Transistoren zur Kopplung an elektroaktive Zellen
M. Jansen (2014), xvi, 181 pp
ISBN: 978-3-89336-944-7

Band / Volume 83
Microscopic description of the inverse Faraday effect at subpicosecond time scales
D. Popova (2014), 183 pp
ISBN: 978-3-89336-962-1

Schlüsseltechnologien / Key Technologies
Band / Volume 83
ISBN 978-3-89336-962-1